

# Variational quantum algorithm for measurement extraction from the Navier-Stokes, Einstein, Maxwell, Boussinesq-type, Lin-Tsien, Camassa-Holm, Drinfeld-Sokolov-Wilson, and Hunter-Saxton equations

Pete Rigas \*

## Abstract

Classical-quantum hybrid algorithms have recently garnered significant attention, which are characterized by combining quantum and classical computing protocols to obtain readout from quantum circuits of interest. Recent progress due to Lubasch et al in a 2019 paper provides readout for solutions to the Schrodinger and Inviscid Burgers equations, by making use of a new variational quantum algorithm (VQA) which determines the ground state of a cost function expressed with a superposition of expectation values and variational parameters. In the following, we analyze additional computational prospects in which the VQA can reliably produce solutions to other PDEs that are comparable to solutions that have been previously realized classically, which are characterized with noiseless quantum simulations. To determine the range of nonlinearities that the algorithm can process for other IVPs, we study several PDEs, first beginning with the Navier-Stokes equations and progressing to other equations underlying physical phenomena ranging from electromagnetism, gravitation, and wave propagation, from simulations of the Einstein, Boussinesq-type, Lin-Tsien, Camassa-Holm, Drinfeld-Sokolov-Wilson (DSW), and Hunter-Saxton equations. To formulate optimization routines that the VQA undergoes for numerical approximations of solutions that are obtained as readout from quantum circuits, cost functions corresponding to each PDE are provided in the supplementary section after which simulations results from hundreds of ZGR-QFT ansatze are generated. With such an ensemble of ansatze that we perform numerical experiments upon through time-evolution of quantum states corresponding to solution approximations of a PDE, we can readily compare different initial states of the solution across different PDEs that the VQA can effectively approximate, and establish rough comparisons between computational complexity of optimizing different cost functions. To quantify VQA performance for approximating solutions, we automate evaluation of our quantum circuits with the open source Cirq and QSimCirq platforms, which respectively prepare, and update, the state vector corresponding to a PDE solution state throughout the number of time steps in the evolution. To determine whether barren plateaus when optimizing for the ground state can be avoided, we also execute gradient-based, stochastic, and constrained, optimization procedures, which are compared with the performance of deterministic optimizers on a case-by-case basis.

**Keywords:** Quantum computation, variational quantum algorithms, variational quantum computing, quantum simulation, hybrid quantum algorithms, parameter shift rule, quantum embedding, gradient-based optimization, Nevergrad optimizer, Neighborhood algorithm, Particle-swarm, Competitive Particle-swarm, sequential least squares, Scipy optimizer, QSimCirq simulator, solution state vector, ansatz, measurement extraction, quantum circuit readout, time evolution

## 1 Introduction

### 1.1 Overview

The variational quantum algorithm (VQA) has attracted wide attention from several computational disciplines in physics, chemistry and materials science [12], with recent studies demonstrating how optimizers for such algorithms can be improved and parametrized for entanglement [17,18], robust

---

\*McMahon Lab, Cornell University

encoding in molecules for chemistry computations [1], various implementations for linear algebra problems [16,20], variance minimization [27], and the construction of quantum Gibbs states [3]. To further contribute to rapid developments, Lubasch et al in [11] introduce a new VQA which can be applied to solve nonlinear problems arising from various PDEs through specifications on quantum circuits, including an optimized quantum nonlinear processing unit (QNPU) for treating nonlinearities of the equation that is being solved for efficiently, in addition to randomly chosen variational parameters  $\lambda, \lambda_0$  which parametrize a cost function  $\mathcal{C}$  that is classically minimized. In turn, quantum registers prepared in circuits of polynomial depth not only require exponentially fewer parameters, but also provide ripe opportunity for the algorithm to be applied to several other nonlinear problems, some of which are presented in this article, including computational fluid dynamics problems raised by solutions to the Navier-Stokes equations, approximation of the gravitational field on different forms of matter raised by the stress-energy tensor of the Einstein field equations, distribution of electric and magnetic field interactions raised by the Maxwell equations, and wave interference, to provide a few examples.

To briefly expound upon the setting of [11], a variational quantum algorithm is applied to NLS and to the inviscid Burger’s equation, with MPS ansatzes of polynomial bond dimension [13,14]. Such ansatzes are advantageous for quantum computation in their ability to be represented as a product of isometric matrices which can be physically interpreted as the wave function of possible states for the solution to a PDE, after which variational states for the solution are time evolved. In comparison to cost functions obtained for NLS and the Burger’s equations, the Navier-Stokes cost function, and cost functions for other PDEs provided in the Supplementary section of this paper, involve a more complicated superposition of quantum states; for example, the Navier-Stokes cost function also includes parameters that are directly proportional to the time step and inversely proportional to the Reynolds number, in addition to several other expectation terms resulting from quantum states that are acted upon by differential operators which are represented with Adder and Adder dagger operators, while the cost function for the Einstein equations involves expectation terms dependent upon the metric and stress energy tensors.

For each PDE, we derive the cost function, as a result obtaining a superposition of quantum states parameterized in nonlinearities of the equation. To implement outstanding steps of the VQA, classical, stochastic, gradient-based, and constrained, optimization routines are implemented in order to determine circuit arrangements for which the VQA is capable of generating solutions to nonlinear problems for different classes of classically prepared initial data with the ZGR-QFT ansatz. Modifications to the general requirements imposed on quantum circuits in [11] are provided, following the derivation and presentation of all simulation results in the Supplementary Section, in which quantum circuits for the simulating the time evolution of PDEs considered in this article are achieved with QNPUs composed of a significantly higher number of input and output ports.

To apply this hybrid algorithm, and others, for studying nonlinearities and related behaviors of nonlinear problems, it is necessary to construct quantum circuits for approximating nonlinearities with expectation values, in addition to variational parameters that are modified throughout the optimization procedure as the algorithm is executed to obtain approximations of analytical solutions to a PDE of interest. For initial exploration of the Hilbert space before the VQA further time evolves the quantum state corresponding to the PDE solution, ansatzes, including the shallow layered ansatz obtained through a series of several rotation, and entanglement, operations, as well as computation of Fourier coefficients, provide additional performance metrics.

For running the algorithm with nonlinearities besides those which are discussed in [11], it is important to not only determine optimal circuit constructions that reduce noise in unitary gate operations for potential future applications of the VQA [10,15,23], but also the range of time steps that the optimizer must take to arrive to a ground state in order for approximations of the solution to be convergent. Specifically, in one case, nonlinearities that the VQA processes for obtaining solutions to the Navier-Stokes equations are simulated with quantum circuits with readout values from expectations taken between operators denoted with  $\hat{Q}$ , in addition to the pressure  $\rho$  exerted on direction of fluid flow in the system. To this end, quantum circuits for simulating time evolution of Navier-Stokes solutions are of shallow depth, permitting for readout from quantum circuits for nonlinearities of the Navier-Stokes cost function with the open-source Python Cirq package, as with the other 7 PDEs that are examined in the Supplementary Section. Notably, the primary difficulties

in applying the hybrid variational quantum algorithm to the Navier-Stokes equations, versus other PDEs of interest, is apparent through the QNPU construction for expectation terms from each cost function, which widely vary depending upon the order of spatial derivatives that are taken of the solution appearing in the equation, the initial conditions of the ansatz from which the optimization routine begins, the number of time steps, optimizer, amongst several other factors.

## 1.2 Paper organization

We present results from quantum circuits to compute all expectation values for each PDE. Beyond this starting point, within the framework of [11], we formulate applications in different nonlinear problems. The quantum circuits provided in the last Supplementary section demonstrate the sequence of unitary operations from which the quantum-classical computational loop is executed, in which individual plots for approximations of PDE solutions exhibit, generally, strong agreement with solutions that can be classically predicted, either from analytically known exact solutions, or from solution approximations provided from classical numerical schemes, that have been previously realized in the literature from the list of references provided both for the Introduction and Supplementary sections. From well-established representations of quantum networks as sequences of unitary transformations that are applied to qubits initialized in the 0 state at the beginning of time evolution [19], we obtain quantum readout through adaptations of the VQA of [11] with ZGR-QFT ansatzes that are classically simulable in polynomial time. From quantum circuit representations of expectation values expressed as a superposition from each cost function, the quantum operators corresponding to the first and second derivatives require that we introduce circuit representations for Adder, and Adder dagger, operators for processing quantum computations for time evolution.

From the QNPUs provided in quantum circuits used in [11] for solutions to two PDEs, the total number of qubits that are to be time evolved in a quantum circuit is indicative of the total runtime of each time evolution step for optimizing to the ground state of the cost function. To account for complexity posed by the Navier-Stokes cost function, and cost functions for other PDEs, in addition to several other computationally related challenges, ranging from those associated with vanishing gradients of the cost function to ansatz construction [11], expressibility of parametrizations for quantum circuits [17], qubit quality and stable quantum representations of solutions to PDE IVPs, data compression in machine learning for classification tasks, error mitigation, error correcting codes, and noise and complexity growth [2,6], different forms of ansatzes for the equations will be studied and qualitatively compared. To systematically characterize the coverage of the Hilbert space that we expect from such quantum simulations, we sample entries from a state wavefunction, from which comparisons with classical solution approximations can be established.

To ensure that the VQA robustly performs across different parameters that can be continuously adjusted for in the quantum circuit model, we generate a broad ensemble of quantum states for direct comparison with classically known exact solutions to each PDE, some of which are provided at the beginning of the Supplementary Section before the derivation of each cost function, and corresponding simulation results.

## 1.3 Acknowledgments

The author would like to thank Peter McMahon for suggesting a direction for the project, in addition to Abhi Sarma for extremely informative discussions surrounding implementation of ansatzes for the initial state of solutions, assisting with troubleshooting of quantum circuit construction in Cirq and the related Qsim package that is also utilized for generating noiseless quantum simulation, discussion of motivations for compiling the VQA for other nonlinear problems, parameter shift rule for each cost function differentiation that is derived in the supplementary section, gradient-based optimization, and possible future research directions with quantum machine learning, and Yilian Liu for discussions of applications of the VQA with other papers in the literature.

## 2 References

- [1] Albert, V., Covey, J. & Preskill, J. Robust Encoding of a Qubit in a Molecule. *Phys Rev* **10** 031050 (2020).
- [2] Brandao, F. et al. Models of quantum complexity growth. arXiv: 1912.04297 (2019).
- [3] Chowdhury, A., Low, G.H. & Wiebe, N. A Variational Quantum Algorithm for Preparing Quantum Gibbs States. arXiv: 2002.00055 (2020).
- [4] Eremenko, A. Spectral Theorems for Hermitian and Unitary Matrices. *Lecture Notes*.
- [5] Faist, P. et al. Continuous symmetries and approximate quantum error correction. arXiv: 1902.07714 (2019).
- [6] Gidney, C., Eker, M. How to factor 2048 bit RSA integers in 8 hours using 20 million noisy qubits. arXiv: 1905.09749 (2019).
- [7] Hadfield, S., Wang, Z., O’Gorman, B., Rieffel, E., Venturelli, D. & biswas, R. From the Quantum Approximate Optoimization Algorithm to a Quantum Alternating Operator Ansatz. *Quantum Optimization Theory, Algorithms, and Applications* **34** 12.2 (2019).
- [8] Iverson, J. & Preskill. J. Coherence in logical quantum channels. *New Journal of Physics* **22** 073066 (2020).
- [9] Kandala, A., et al. Harware-efficient Variational Quantum Eigensolver for Small Molecules and Quantum Magnets. *Nature* **549** 242 (2017).
- [10] Kim, I., Swingle, B. Robust entanglement renormalization on a noisy quantum computer. arXiv: 1711.07500 (2017).
- [11] Lubasch, M., et al. Variational quantum algorithms for nonlinear problems. *Phys Rev* **101** 010301 (2020).
- [12] McClean, J.R. et al. The theory of variational hybrid quantum-classical algorithms. *New J. Phys.* **18** 023023 (2016).
- [13] Orus, R. A Practical Introduction to Tensor Networks: Matrix Product States and Projected Entangled Pair States. *Annals of Physics* **349** 117-158 (2014).
- [14] Perez-Garcia, D., Verstraete, F., Wolf, M.M. & Cirac, J.I. Matrix Product State Representations. *Quantum Inf. Comput.* **7** 401 (2007).
- [15] Peruzzo, A., et al. A variational eigenvalue solver on a quantum processor. *Nature Communications* **5** 4213 (2014).
- [16] Preskill. J. Quantum computing in the NISQ era and beyond. *Quantum* **2**(79) (2018).
- [17] Sim, S., Johnson, P. & Aspuru-Guzik, A. Expressibility and entangling capability of parametrized quantum circuits for hybrid quantum-classical algorithms. *Advanced Quantum Technologies* **2**(12) (2019).
- [18] Sung, K., et al. Using models to improve optimizers for variational quantum algorithms. *Quantum Science and Technology* **5**(4) (2020).
- [19] Vedral, V., Barenco, A. & Ekert, A. Quantum Networks for Elementary Arithmetic Operations. *ArXiv*: quant-phy/9511018.

- [20] Xu, X. et al. Variational algorithms for linear algebra. arXiv:1909.03898 (2019).
- [21] Zhang, D.B., Zhan-Hao, Y. & Yin, T. Variational quantum eigensolvers by variance minimization. arXiv: 2006. 15781 (2020).
- [22] Thapliyal, H., Munoz-Coreas, E., Varun, T.S.S. & Humble, T.S. *Quantum Circuit Designs of Integer Division Optimizing T-count and T-depth*. arXiv:1809.09732 (2018).
- [23] Zhuang, Q., Preskill, J. & Jiang, L. Distributed quantum sensing enhanced by continuous-variable error correction. *New Journal of Physics* **22** (2020).
- [24] Abughalia, M.A. On the mathematical solution of the 2D Navier Stokes equations for different geometries. *Advances in Fluid Mechanics* **39** 2006.

# Contents

<b>1</b>	<b>Introduction</b>	<b>1</b>
1.1	Overview . . . . .	1
1.2	Paper organization . . . . .	3
1.3	Acknowledgments . . . . .	3
<b>2</b>	<b>References</b>	<b>4</b>
<b>3</b>	<b>Supplemental materials</b>	<b>7</b>
3.1	Earlier studies of exact solutions to the Navier-Stokes, Einstein, Maxwell, Lin-Tsien, and other PDEs . . . . .	7
3.2	Quantum circuit architecture . . . . .	7
<b>4</b>	<b>Supplementary section organization</b>	<b>8</b>
4.1	PDE library . . . . .	8
4.2	Cost function derivations for simulating optimization to the quantum ground state . .	9
4.3	Navier-Stokes equations . . . . .	9
4.3.1	Couette flow from the Navier-Stokes equations without a pressure gradient . .	13
4.4	Einstein field equations . . . . .	14
4.5	Maxwell equations . . . . .	41
4.6	Boussinesq type equation . . . . .	55
4.7	Lin-Tsien equation . . . . .	64
4.8	Camassa-Holm equation . . . . .	71
4.9	Drinfeld-Sokolov-Wilson equations . . . . .	113
4.10	Hunter-Saxton equation . . . . .	117
<b>5</b>	<b>Supplementary materials references</b>	<b>122</b>

### 3 Supplemental materials

#### 3.1 Earlier studies of exact solutions to the Navier-Stokes, Einstein, Maxwell, Lin-Tsien, and other PDEs

Previous works have investigated several different aspects of the Navier-Stokes equations, whether it be the domain over which solutions are obtained, specific assumptions of the behavior of the pressure gradient under translations and rotations and over discretizations of varying composition [21], each of which can impact the velocity profile that classically realized algorithms have predicted arise in time-dependent trajectories of fluids in two, and three, dimensional space. In higher dimensional cases beyond those considered in the two-dimensional plane, past works have studied the regularity structure of Navier-Stokes solutions, in addition to a stochastic formulation in which solutions for the Navier-Stokes equations driven by space time white noise were provided, through construction of Gaussian invariant measures and fixed point mappings [13,21].

On the other hand, efforts have also been made to prove analytical solutions for typically found pressure distributions to the equations as given in [16], in which usual procedures transform the PDE system to an ODE system from which standard separation of variables techniques yield solutions under specific circumstances and initial conditions. Under the expected initial conditions, solutions for the velocity components of Navier-Stokes in two or three dimensions exponentially decay with respect to time, in one case. From characteristics of such solutions and other closely related aspects of the Navier-Stokes equations, authors in previous works have observed that conservation laws of the system for other quantities, whether it be helicity, 2D entrophy or total vorticity of the trajectory, allow for numerical methods that are capable of simulating the pressure distribution across three dimensional objects including a square cylinder [9], sharing connections to desirable quantities which can be physically interpreted as the drag and drift forces on an airplane wing throughout a flight. For computation of aerodynamic pressure exerted upon an airplane wing, velocity profiles of fluids and gases must be approximated from components of the Navier-Stokes equations, which can yield a reconstruction of a two or three-dimensional vector field. Relatedly, the authors of [11] provide formulations of the Navier-Stokes and Stokes equations for incompressible fluid flow, while the authors of [2] avoid finite differencing of the equations altogether, still obtaining solutions, however, with unknown pressure as initial conditions, in directly opposition to the assumptions imposed on solutions to the Navier-Stokes equations obtained from the procedure in [16].

For other nonlinear problems, observations stemming primarily from Riemannian geometry and connections to Ricci curvature inform the structure of the stress-energy tensor for several different numerical studies of the Einstein equation, in which the authors of [3] establish variational principles allowing for arguments involving the covariant derivative, as symmetry of the Ricci curvature tensor with a damped Laplacian is formalized. Plots in the upcoming subsections of this Supplementary Section exhibit plots of solutions to Navier-Stokes for the  $x$  and  $y$  components of the velocity solution, and furthermore, comparisons of the performance of different ZGR-QFT anstzae in the coverage of the Hilbert space. For remaining PDEs of interest, references for exact solutions similarly exist, allowing for comparisons of the performance of the VQA, upon comparing to exact solutions [1,5,6,9].

#### 3.2 Quantum circuit architecture

Before executing gates of the QNPU, to trace output of control qubits in the circuit we illustrate the number of initialized  $|0\rangle$  states required for the execution of the variational algorithm from [13], in which qubits before being time evolved to the QNPU must be appropriately manipulated. For nonlinearities of the Navier-Stokes equations, executing nonlinearities raised by the cost function for the QNPU alone requires that we include additional qubits so that all expectation values from the superposition in the cost function can be added, and multiplied, together with a sufficient number of ancilla qubits. Moreover, we appropriately situate the input ports into the QNPU from previous gate operations in the circuit following the  $|0\rangle$  state initialization, allowing us to perform circuit simulations on a variable number of target qubits that are specifically determined for each PDE.

The Navier-Stokes QNPU processes target qubits following previous gate operations, which contain an Adder, for computing the resulting quantum state which approximates the quantum ground state following the time step magnitude of the evolution. To accommodate the circuit construction

so that all gates reflect the capability of the algorithm to be applied to other nonlinear equations, we incorporate standard variational parameters  $\lambda$  over which the cost function is optimized. For different cost functions, the computational cost of operations associated with approximating  $C(\lambda, \lambda_0)$  include scalar multiplication involving the variational parameter  $\lambda_0$  with itself, multiplication for various expectation values that are dependent on the pressure, and spatial geometry of the lattice over which the solution is approximated, with the scalar variational parameter product  $\tilde{\lambda}_0 \left(\frac{\tau}{h}\right)^2$ , and  $\left(\frac{\tau}{\rho h}\right)^2$ , as appearing in the Navier-Stokes cost function. Other fundamental constants, whether Newton’s gravitation constant or the permittivity of free space, parametrize the quantum circuit and QNPU of other PDEs, which respectively appear in cost functions provided for the Einstein and Maxwell equations. Besides computing such expectation value, additional computations must be dealt with by isolating all accompanying prefactors for each expectation value, including  $-\frac{\tau}{h}\lambda_0^*\tilde{\lambda}_0$ ,  $\frac{\tau}{\rho h}\lambda_0^*$ , and  $-\frac{1}{\rho}\left(\frac{\tau}{h}\right)^2\tilde{\lambda}_0$ , respectively, which is achieved by forming a quantum superposition for the cost function before different optimizers, time step magnitude, initial conditions, and ansatzes are implemented. Finally, when forming the quantum superposition encoding the ground state, additional ancilla for the control ports (CPs) to the QNPU are immediately accounted for by Cirq when the resultant state is approximated when sampling from the solution state vector prepared with QSimCirq. In the following circuit diagrams provided in the last section of the Supplementary materials, we establish all such specifications on the ancilla within the computational basis, and provide similarly related quantum circuit arrangements that were implemented in the cost function optimization for other nonlinear PDEs besides the previously solved PDEs. We gather results by reading off expectation values from the each cost function, and afterwards provide quantum simulation results for approximations of several solutions.

For Navier-Stokes quantum circuits, we stipulate that the control ports preceding the QNPU are acted upon an ancilla block of polynomial depth for operations associated with adding expectation values together, which in the case for other PDEs holds for QNPU with more IPs. With exception to the topmost control qubits which undergo a Hadamard gate before entering the QNPU through their respective IPs, additional ancilla within the QNPU are allotted for constructing the quantum superposition for the ground state at each time step of the evolution. With the quantum Fourier Transform (QFT), quantum network representations for dividing scalars can be achieved by loading the divisor and dividend into quantum registers, with the scheme being applicable to computations involving each expectation term. After each expectation is individually computed, the resulting superposition state is uniquely parametrized for each PDE. Before qubits are time evolved into the QNPU, for each cost function the ancilla block on the topmost layer, designated in blue, contains an arbitrary number of control qubits, each of which undergoes a Hadamard test, while additional ancilla qubits are responsible for any other computations when time evolving each target qubit represented in the quantum circuit.

Besides the QNPU block which treats nonlinearities of each PDE from expectation terms in the cost function, the H + Readout block applies the Hadamard gate to each ancilla after the QNPU and reads out values produced in qubits of the circuit that are time-evolved with an application of  $\hat{\sigma}_z$ . Furthermore, it is important to carefully keep track of the total number of control qubits associated with addition or multiplication on the quantum computer from the prefactors that have been previously identified. In light of rearrangements of each  $\mathcal{C}$  beginning for the Navier-Stokes equations in *Section 4.2*, the "Clifford + T" gate family is applied to individually load divisors, in which components of the superposition state dividend are loaded into each CP, after which a certain number of time steps are combined with expectation values for QNPU IPs. Outside of the QNPU, results of quantum computation for the cost function are terminated for the ancilla, and other qubits of the wavefunction, are readout from the H + Readout block.

## 4 Supplementary section organization

### 4.1 PDE library

To substantially enlarge the spectrum of nonlinearities that quantum simulators can process, we make use of the Google open source platform Cirq to simulate wavefunctions for solutions to various PDEs. From the following PDE library consisting of the following 8 PDEs, under specified initial conditions

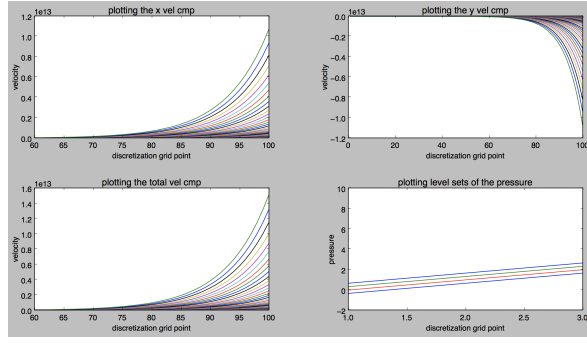


Figure 1: *Plots of Navier-Stokes solutions.* For exact solutions to Navier-Stokes, the  $x$  component of the velocity satisfies  $v_x = A \exp\left[\frac{c}{\nu(\alpha^2+\beta^2)(\alpha x+\beta y)}\right] + B$ , while the  $y$  component of the velocity satisfies  $v_y = \frac{1}{\beta} \left[ c - \alpha B - \alpha A \exp\left[\frac{c}{\nu(\alpha^2+\beta^2)(\alpha x+\beta y)}\right] \right]$  for real  $\alpha, \beta$ .

we simulate iterations of the quantum-classical hybrid algorithm for approximating previously studied classically solutions. To exhibit wide applicability of the Lubasch et al VQA, plots of solutions to each equation are provided following the cost function derivation. Quantum circuit diagrams after the cost function presented in the following sections provide an overlay of the sequence of unitary transformations which are performed on qubits in each step of time evolution before each cost function  $\mathcal{C}$  is optimized, in several conditions.

## 4.2 Cost function derivations for simulating optimization to the quantum ground state

The cost functions corresponding to each quantum circuit diagram are separately derived. We collect all expectation values from relevant terms appearing in the statement of each PDE, and impose initial conditions on the time evolution with different ZGR-QFT ansatze across hundreds of simulations. Initially we prepare each qubit in the 0 state and furthermore, examine the  $\hat{U}_j(\lambda)$  gates, where  $j$  runs over the number of qubits for each cost function  $\mathcal{C}$ . A subset of the expectation terms from each cost function are represented in the QNPU for measurement of components of the analytical solution, from which further discussion is devoted towards quantum circuit architecture with Figures in the last Supplementary Section.

## 4.3 Navier-Stokes equations

### Cost function derivation

To quantify time evolution forwards at the initial state and after an increment, we introduce the states  $\Psi$  and  $\tilde{\Psi}$ . To avoid confusion with the operator  $\hat{Q}$  in the cost function, below, the Navier-Stokes cost function is of the form,

$$\mathcal{C}^{p,x}(\lambda, \lambda_0) = (\lambda_0^{C^{p,x}})^2 + \left(\frac{\tau}{h}\right)^2 (\tilde{\lambda}_0^{C^{p,x}})^2 + \left(\frac{\tau}{\rho h}\right)^2 + 2 \operatorname{Re} \left\{ -\frac{\tau}{h} \lambda_0^* \tilde{\lambda}_0 \langle \Psi | \hat{Q} | \tilde{\Psi} \rangle + \frac{\tau}{\rho h} \lambda_0 \langle \Psi | \nabla_x | p \rangle - \dots \right. \\ \left. \frac{1}{\rho} \left(\frac{\tau}{h}\right)^2 \tilde{\lambda}_0 \langle p | \nabla_x^\dagger \hat{Q} | \tilde{\Psi} \rangle \right\},$$

which is readily obtained upon collection of terms from the expansion of  $\| |\tilde{\Psi}\rangle - \frac{\tau}{h} \hat{Q} |\Psi\rangle + \frac{\tau}{\rho h} \nabla_x p(t) \|^2$  after rearrangement, in which we make use of the straightforward identities for discrete approximations of derivatives in the Navier-Stokes equations after finite differencing, which are,

$$\hat{Q}|\Psi\rangle = \langle\Psi|\hat{Q}^\dagger \quad ,$$

by virtue of Hermiticity being preserved. Next, the Euler method is applied to obtain  $\mathcal{C}$  for variational state preparation, in order to determine ground states in the optimization landscape. From the Navier-Stokes cost function, we identify variational states that are to be prepared when the algorithm from [13] is ran. Specifically, the operator  $\hat{Q}$  in  $\mathcal{C}$  emerges from finite differencing the Navier-Stokes equations and isolating for the time increment of the state of the solution  $f$  forwards in time by an increment  $\tau$ , and takes the form, with  $\mathbf{1}$  as the identity operator,

$$\hat{Q} \equiv \frac{\hbar}{\tau} ( \mathbf{1} - |\Psi\rangle \nabla_x - v \nabla_y + v \Delta_x + v \Delta_y ) \quad ,$$

where in  $\hat{Q}$  above,

$$\begin{aligned} \nabla_x &= \frac{1}{\Delta x} ( A_x - \mathbf{1} ) \quad , \quad \nabla_y = \frac{1}{\Delta y} ( A_y - \mathbf{1} ) \quad , \\ \Delta_x &= \frac{1}{(\Delta x)^2} ( A_x^\dagger - 2 \mathbf{1} + A_x ) \quad \text{and} \quad \Delta_y = \frac{1}{(\Delta y)^2} ( A_y^\dagger - 2 \mathbf{1} + A_y ) \quad . \end{aligned}$$

We will make use of this procedure to study nonlinearities of the Euler and Poisson equations, in which quantum circuit architecture for computing expectation terms of the cost function above is executed for other PDEs with modifications to the QNPU and CP. After further discussion of the circuit outputs from the variational algorithm for Navier-Stokes, such modifications to the QNPU for the Euler and Poisson equations are valuable for analyzing computational bases with respect to nonlinear behaviors of inviscid flow, amongst other types of time evolution.

From the definition of  $\hat{Q}$ , we observe that the second and third expectations can be rewritten as,

$$\begin{aligned} \langle\Psi|\hat{Q}|\tilde{\Psi}\rangle &\equiv \langle\Psi|\left(\frac{\hbar}{\tau} (\mathbf{1} - |\Psi\rangle \nabla_x - v \nabla_y + v \Delta_x + v \Delta_y)\right)|\tilde{\Psi}\rangle \\ &\quad \Updownarrow \\ \langle\Psi|\frac{\hbar}{\tau}|\tilde{\Psi}\rangle &+ ( - \langle\Psi|\frac{\hbar}{\tau}(|\Psi\rangle)|\tilde{\Psi}\rangle ) + ( - \langle\Psi|\frac{\hbar}{\tau}v|\tilde{\Psi}\rangle ) + \langle\Psi|\frac{\hbar}{\tau}(v\Delta_x)|\tilde{\Psi}\rangle + \langle\Psi|\frac{\hbar}{\tau}(v\Delta_y)|\tilde{\Psi}\rangle \\ &\quad \Updownarrow \\ \frac{\hbar}{\tau} &(\langle\Psi|\tilde{\Psi}\rangle + ( - \langle\Psi|(|\Psi\rangle)|\tilde{\Psi}\rangle ) + ( - \langle\Psi|v|\tilde{\Psi}\rangle ) + \langle\Psi|v\Delta_x|\tilde{\Psi}\rangle + \dots \\ &\quad \langle\Psi|v\Delta_y|\tilde{\Psi}\rangle) \quad , \end{aligned}$$

which amounts to computing the summation of expectations above, with the final resultant multiplied by  $\frac{\hbar}{\tau}$  corresponding to the second term. As for the third term, we can similarly expand by making use of the definition of  $\hat{Q}$ , hence obtaining,

$$\begin{aligned}
p \nabla_x^\dagger \hat{Q} |\tilde{\Psi}\rangle &\equiv p \nabla_x^\dagger \left( \frac{\hbar}{\tau} (\mathbf{1} - |\Psi\rangle \nabla_x - v \nabla_y + v \Delta_x + v \Delta_y) \right) |\tilde{\Psi}\rangle \\
&\Downarrow \\
p \frac{\hbar}{\tau} \nabla_x^\dagger |\tilde{\Psi}\rangle + \left( - p \frac{\hbar}{\tau} \nabla_x^\dagger (|\Psi\rangle) \nabla_x |\tilde{\Psi}\rangle \right) + \left( - p \frac{\hbar}{\tau} \nabla_x^\dagger v \nabla_y |\tilde{\Psi}\rangle \right) + p \frac{\hbar v \Delta_x}{\tau} |\tilde{\Psi}\rangle + \dots \\
&\qquad\qquad\qquad p \frac{\hbar v \Delta_y}{\tau} |\tilde{\Psi}\rangle \\
&\Downarrow \\
\frac{\hbar}{\tau} \left( p \nabla_x^\dagger |\tilde{\Psi}\rangle + \left( - p \nabla_x^\dagger (|\Psi\rangle) \nabla_x |\tilde{\Psi}\rangle \right) + \left( - p \nabla_x^\dagger v \nabla_y |\tilde{\Psi}\rangle \right) + p v \Delta_x |\tilde{\Psi}\rangle + \dots \right. \\
&\qquad\qquad\qquad \left. p v \Delta_y |\tilde{\Psi}\rangle \right),
\end{aligned}$$

allowing for further rearrangements from respective collection of like terms in  $v$ ,  $|f(t)\rangle$ ,  $v\Delta_x$  and  $v\Delta_y$ , between the second and third expectation terms, giving

$$\frac{\hbar}{\tau} \left( - p v + \nabla_x^\dagger v \nabla_x \right) |\tilde{\Psi}\rangle ,$$

for  $|v(t)\rangle$ , while,

$$\frac{\hbar}{\tau} \left( - p (|\Psi\rangle + \nabla_x^\dagger |\Psi\rangle \nabla_x) |\tilde{\Psi}\rangle \right) ,$$

for  $|f(t)\rangle$ . Also, the remaining two terms dependent on  $v$  and  $p$  take the form,

$$\frac{2\hbar}{\tau} \left( p v \Delta_x |\tilde{\Psi}\rangle + \langle \Psi | v \Delta_y | \tilde{\Psi} \rangle \right) .$$

Hence applying linearity of expectation where appropriate in turn gives a cost function of the form, from the superposition,

$$\begin{aligned}
\lambda_0^2 + \left( \frac{\tau}{\hbar} \right)^2 \tilde{\lambda}_0^2 + \left( \frac{\tau}{\rho \hbar} \right)^2 + \frac{2\hbar}{\tau} \operatorname{Re} \left\{ \langle \Psi | \tilde{\Psi} \rangle + p \nabla_x^\dagger |\tilde{\Psi}\rangle - \langle \Psi | v \tilde{\Psi} \rangle + \dots \right. \\
\qquad\qquad\qquad p \nabla_x^\dagger v \nabla_x |\tilde{\Psi}\rangle - \dots \\
\qquad\qquad\qquad p (|\Psi\rangle + \nabla_x^\dagger |\Psi\rangle \nabla_x) |\tilde{\Psi}\rangle + \dots \\
\qquad\qquad\qquad \left. 2(p v \Delta_x |\tilde{\Psi}\rangle + \langle \Psi | v \Delta_y | \tilde{\Psi} \rangle) \right\} ,
\end{aligned}$$

which can be rearranged more explicitly, through substitution in terms with  $\nabla_x$ ,  $\nabla_y$ ,  $\Delta_x$  and  $\Delta_y$ , for the second term taken under  $\operatorname{Re}$ ,

$$p \nabla_x^\dagger |\tilde{\Psi}\rangle = \frac{p}{\Delta x} (A_x^\dagger - \mathbf{1}) |\tilde{\Psi}\rangle ,$$

and similarly for the third and fourth terms taken under  $\operatorname{Re}$ ,

$$\langle \Psi | v | \tilde{\Psi} \rangle + p \nabla_x^\dagger v \nabla_x | \tilde{\Psi} \rangle \equiv \langle \Psi | v | \tilde{\Psi} \rangle + \frac{p}{(\Delta x)^2} (\{A_x^\dagger - \mathbf{1}\} v \{A_x - \mathbf{1}\}) | \tilde{\Psi} \rangle .$$

For the fourth term taken under Re, we get

$$p (|\Psi\rangle + \nabla_x^\dagger |\Psi\rangle \nabla_x) | \tilde{\Psi} \rangle \equiv \frac{p}{(\Delta x)^2} (|\Psi\rangle + \{A_x^\dagger - \mathbf{1}\} |\Psi\rangle \{A_x - \mathbf{1}\}) | \tilde{\Psi} \rangle .$$

Finally, from the fourth term multiplied by two,

$$p v \Delta_x | \tilde{\Psi} \rangle + \langle \Psi | v \Delta_y | \tilde{\Psi} \rangle \equiv \frac{p}{(\Delta x)^2} v (A_x^\dagger - 2 \mathbf{1} + A_x) | \tilde{\Psi} \rangle + \langle \Psi | \frac{v}{(\Delta x)^2} (A_y^\dagger - 2 \mathbf{1} + A_y) | \tilde{\Psi} \rangle ,$$

from which we collect all rearrangements, in turn obtaining a cost function of the form from like terms,

$$\begin{aligned} & \lambda_0^2 + \left(\frac{\tau}{h}\right)^2 \tilde{\lambda}_0^2 + \left(\frac{\tau}{\rho h}\right)^2 + \frac{2h}{\tau} \operatorname{Re} \left\{ \langle \Psi | \tilde{\Psi} \rangle + \frac{p}{\Delta x} (A_x^\dagger - \mathbf{1}) | \tilde{\Psi} \rangle + \langle \Psi | v | \tilde{\Psi} \rangle - \dots \right. \\ & \frac{p}{(\Delta x)^2} (\{A_x^\dagger - \mathbf{1}\} v \{A_x - \mathbf{1}\}) | \tilde{\Psi} \rangle - \frac{p}{(\Delta x)^2} (|\Psi\rangle + \{A_x^\dagger - \mathbf{1}\} |\Psi\rangle \{A_x - \mathbf{1}\}) | \tilde{\Psi} \rangle + \dots \\ & \left. 2 \left( \frac{p}{(\Delta x)^2} v (A_x^\dagger - 2 \mathbf{1} + A_x) | \tilde{\Psi} \rangle + \frac{v}{(\Delta x)^2} \langle \Psi | (A_y^\dagger - 2 \mathbf{1} + A_y) | \tilde{\Psi} \rangle \right) \right\} , \end{aligned}$$

from which rearranging fifth expectation term under Re gives, by making use of the identity  $|f(t)\rangle = \lambda_0 |\Psi\rangle$ , which is related to the time evolved quantum state which satisfies  $|f(t+\tau)\rangle = \tilde{\lambda}_0 |\tilde{\Psi}\rangle$  for variational states,

$$\begin{aligned} \frac{p}{(\Delta x)^3} (\{\tilde{\lambda}_0 | \tilde{\Psi} \rangle + \{A_x^\dagger - \mathbf{1}\} \{\tilde{\lambda}_0 | \tilde{\Psi} \rangle\} \{A_x - \mathbf{1}\}) | \tilde{\Psi} \rangle & \equiv \left( \frac{p}{\Delta x} \{\tilde{\lambda}_0 | \tilde{\Psi} \rangle \right) + \frac{p}{(\Delta x)^2} \{A_x^\dagger - \mathbf{1}\} \times \dots \\ & \{\tilde{\lambda}_0 | \tilde{\Psi} \rangle\} (A_x - \mathbf{1}) | \tilde{\Psi} \rangle \\ & \updownarrow \\ \frac{p}{\Delta x} \{\tilde{\lambda}_0 | \tilde{\Psi} \rangle | \tilde{\Psi} \rangle + \frac{p}{(\Delta x)^2} \{A_x^\dagger - \mathbf{1}\} \{\tilde{\lambda}_0 | \tilde{\Psi} \rangle\} (A_x - \mathbf{1}) | \tilde{\Psi} \rangle , & \end{aligned}$$

which yields the desired cost function for Navier-Stokes below after substituting in for variational states for the solution to the Navier-Stokes equations, yielding,

$$\begin{aligned} \mathcal{C}^{p,x}(\lambda, \lambda_0^{C^{p,x}}) & = (\lambda_0^{C^{p,x}})^2 + \left(\frac{\tau}{h}\right)^2 (\tilde{\lambda}_0^{C^{p,x}})^2 + \left(\frac{\tau}{\rho h}\right)^2 + \frac{2h}{\tau} \operatorname{Re} \left\{ \langle \Psi | \tilde{\Psi} \rangle + \frac{p}{\Delta x} (A_x^\dagger - \mathbf{1}) | \tilde{\Psi} \rangle + \dots \right. \\ & \langle \Psi | v | \tilde{\Psi} \rangle - \dots \\ & \frac{p}{(\Delta x)^2} (\{A_x^\dagger - \mathbf{1}\} v \{A_x - \mathbf{1}\}) | \tilde{\Psi} \rangle - p \{\tilde{\lambda}_0 | \tilde{\Psi} \rangle\} | \tilde{\Psi} \rangle - \dots \\ & \frac{p}{(\Delta x)^2} \{A_x^\dagger - \mathbf{1}\} \{\tilde{\lambda}_0 | \tilde{\Psi} \rangle\} \{A_x - \mathbf{1}\} | \tilde{\Psi} \rangle + \dots \\ & \left. 2 \left( \frac{p}{(\Delta x)^2} v (A_x^\dagger - 2 \mathbf{1} + A_x) | \tilde{\Psi} \rangle + \dots \langle \Psi | \frac{v}{(\Delta x)^2} (A_y^\dagger - 2 \mathbf{1} + A_y) | \tilde{\Psi} \rangle \right) \right\} \end{aligned}$$

$$\begin{aligned}
\boxed{\mathcal{C}^{p,x}(\lambda, \lambda_0^{C^{p,x}})} &= (\lambda_0^{C^{p,x}})^2 + \left(\frac{\tau}{h}\right)^2 (\tilde{\lambda}_0^{C^{p,x}})^2 + \left(\frac{\tau}{\rho h}\right)^2 + \frac{2h}{\tau} \text{Re} \left\{ \langle \Psi | \tilde{\Psi} \rangle + \frac{p}{\Delta x} A_x^\dagger | \tilde{\Psi} \rangle - \dots \right. \\
&\quad \left. \frac{p}{\Delta x} | \tilde{\Psi} \rangle + \dots \right. \\
&\quad \langle \Psi | v | \tilde{\Psi} \rangle - \frac{p}{(\Delta x)^2} v A_x^\dagger A_x | \tilde{\Psi} \rangle - \frac{p}{(\Delta x)^2} v A_x^\dagger | \tilde{\Psi} \rangle - \dots \\
&\quad \frac{p}{(\Delta x)^2} v A_x | \tilde{\Psi} \rangle + \frac{p}{(\Delta x)^2} v | \tilde{\Psi} \rangle - p \tilde{\lambda}_0 \langle \tilde{\Psi} | \tilde{\Psi} \rangle - \dots \\
&\quad \frac{p}{(\Delta x)^2} \tilde{\lambda}_0 \langle \tilde{\Psi} | A_x^\dagger A_x | \tilde{\Psi} \rangle - \frac{2p}{(\Delta x)^2} \tilde{\lambda}_0 \langle \tilde{\Psi} | A_x^\dagger | \tilde{\Psi} \rangle + \dots \\
&\quad \frac{p}{(\Delta x)^2} \tilde{\lambda}_0 \langle \tilde{\Psi} | \tilde{\Psi} \rangle + \frac{2p}{(\Delta x)^2} v A_x^\dagger | \tilde{\Psi} \rangle - \frac{4p}{(\Delta x)^2} v | \tilde{\Psi} \rangle + \dots \\
&\quad \left. \frac{2p}{(\Delta x)^2} v A_x | \tilde{\Psi} \rangle + \frac{v}{(\Delta x)^2} \langle \tilde{\Psi} | A_y^\dagger | \tilde{\Psi} \rangle - \frac{2v}{(\Delta x)^2} \langle \tilde{\Psi} | \tilde{\Psi} \rangle + \dots \right\} , \\
&\quad \frac{v}{(\Delta x)^2} \langle \Psi | A_y | \tilde{\Psi} \rangle \left. \right\} ,
\end{aligned}$$

for the  $x$  component of the solution.

As one modification to the Lubasch et al variational algorithm, another cost function must be introduced within the QNPU which has expectation terms dependent on the other component of the solution which appears in the Navier-Stokes equations. We denote this additional cost function as  $\mathcal{C}^y(\lambda, \lambda_0)$ . The quantum circuit diagram for Navier-Stokes illustrates the expectation terms from this cost function for only one component of the solution. To accommodate expectation terms associated with the remaining cost function  $\mathcal{C}^y$  for the one, or two, more velocity components of the solution, we prepare additional quantum states for manipulation. To obtain additional cost functions for quantum simulation, we follow similar procedures used to obtain the first Navier-Stokes cost function, instead for different instances of pressure distributions.<sup>1</sup>

To this end, we introduce several cases to further study the computations associated with different pressure dependent expectation terms arising in expectation values of the Navier-Stokes cost function. If the pressure distribution is uniform, in the simplest case each pressure dependent term amounts to the expectation with a quantity that is uniformly constant over the domain. In more realistic cases in which the pressure distribution at every point of the domain is not precisely the same, the variational state  $|p(t + \tau)\rangle$  after  $|p(t)\rangle$  is time evolved forwards requires additional specification of how the pressure distribution varies with the interior of the domain in which the Navier-Stokes solution is obtained. We introduce classes of admissible pressure distributions for the Navier-Stokes equations in the following cases. In the cases below, we discuss how the pressure distribution would be prepared and computed on the quantum computer for one coordinate, from which computations for the remaining component easily follow by repeating the procedure with additional cost functions for more velocity components.

#### 4.3.1 Couette flow from the Navier-Stokes equations without a pressure gradient

Under a pressure distribution with no magnitude at every point on the domain over which readout for Navier-Stokes is produced, the cost function simplifies to the following. We cross off an expectation value if it is dependent on the pressure  $p$ , yielding the distribution,

<sup>1</sup>Further remarks will also shed light upon determining ground states for the Navier-Stokes cost function in different pressure distributions, and how convergence to the ground state is dependent upon the time evolution step number and magnitude.

$$c^{C,x}(\lambda, \lambda_0^{C,x}) = (\lambda_0^{C,x})^2 + \left(\frac{\tau}{h}\right)^2 \tilde{\lambda}_0^2 + \left(\frac{\tau}{\rho h}\right)^2 + \frac{2h}{\tau} \operatorname{Re} \left\{ \langle \Psi | | \tilde{\Psi} \rangle + \langle \Psi | v | \tilde{\Psi} \rangle - \dots \right. \\ \left. 2v \langle \Psi | A_x^\dagger - 2\mathbf{1} + A_x | \tilde{\Psi} \rangle \right\},$$

for the cost function of the  $x$  component of the solution under no pressure gradient.

#### 4.4 Einstein field equations

##### Cost function derivation

To isolate components of the metric component necessary for the description of trajectories in space-time, we recall that the statement of the field equations with a vanishing cosmological constant  $\Delta$  takes the form,

$$\mathcal{R}_{\mu\nu} - Rg_{\mu\nu} = \frac{8\pi G}{c^4} T_{\mu\nu} \\ \Downarrow \\ \frac{\partial \Gamma_{jm}^i}{\partial x^k} - \frac{\partial \Gamma_{jk}^i}{\partial x^m} + \Gamma_{rk}^i \Gamma_{jm}^r - \Gamma_{rm}^i \Gamma_{jk}^r - Rg_{\mu\nu} = \frac{8\pi G}{c^4} T_{\mu\nu},$$

where the Ricci curvature terms on the left hand side of the field equations are expressed from commutators of Christoffel symbols and their derivatives, from which further rearrangement into second order partial derivatives of the metric tensor implies,

$$\frac{1}{2} \left( \frac{\partial^2 g_{jm}}{\partial x^i \partial x^n} - \frac{\partial^2 g_{nj}}{\partial x^i \partial x^m} - \frac{\partial^2 g_{im}}{\partial x^j \partial x^n} + \frac{\partial^2 g_{ni}}{\partial x^j \partial x^m} \right) - Rg_{\mu\nu} = \frac{8\pi G}{c^4} T_{\mu\nu} \\ \frac{1}{2} \left( \underbrace{\left\{ \frac{\partial}{\partial x^i} \frac{\partial}{\partial x^n} g_{jm} - \frac{\partial}{\partial x^i} \frac{\partial}{\partial x^m} g_{nj} \right\}}_{\mathbf{1}} \right. \\ \left. - \underbrace{\left\{ \frac{\partial}{\partial x^j} \frac{\partial}{\partial x^n} g_{im} - \frac{\partial}{\partial x^j} \frac{\partial}{\partial x^m} g_{ni} \right\}}_{\mathbf{2}} \right) - Rg_{\mu\nu} = \frac{8\pi G}{c^4} T_{\mu\nu} \\ \star \qquad \qquad \qquad \star\star$$

Proceeding further, the operators designated **1**, **2**, **3** and **4**, on the right hand side are respectively equivalent to the quantities  $\star$  and  $\star\star$  below, each of which are scaled in products of differences about any degree of freedom,

$$\frac{\partial}{\partial x^i} \left( \frac{\partial}{\partial x^n} - \frac{\partial}{\partial x^m} \right) \equiv (\Delta_i)^{-1} (A_i - 1) \left( \frac{A_n - 1}{\Delta_n} - \frac{A_m - 1}{\Delta_m} \right) \\ \Downarrow \\ \frac{1}{\Delta_i \Delta_n} (A_i - 1) (A_n - 1) - \frac{1}{\Delta_i \Delta_m} (A_i - 1) (A_m - 1) \\ \Downarrow \\ \underbrace{\frac{1}{\Delta_i \Delta_n} \{A_i A_n - A_i - A_n + 1\}}_{\mathbf{1}} - \underbrace{\frac{1}{\Delta_i \Delta_m} \{A_i A_m - A_i - A_m + 1\}}_{\mathbf{2}},$$

and,

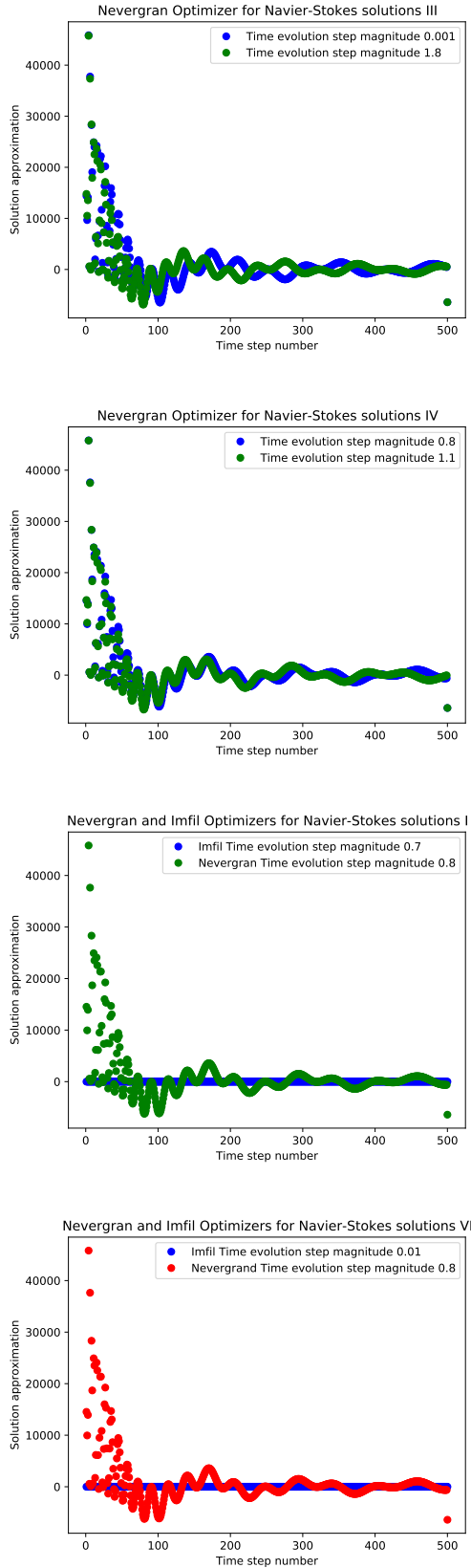


Figure 2: *Plots of Navier-Stokes solutions for Couette flow.* In the variational quantum simulations above, solution points to the Navier-Stokes equations in the absence of pressure gradients are colored in blue, green, or red. From the curvature of solutions curves that are optimized with Nevergran or Scipy Imfil optimizers, the Nevergran optimizer exhibits optimal performance in capturing the behavior of the quantum state encoding the Navier-Stokes solution as the solution relaxes to the steady-state velocity.

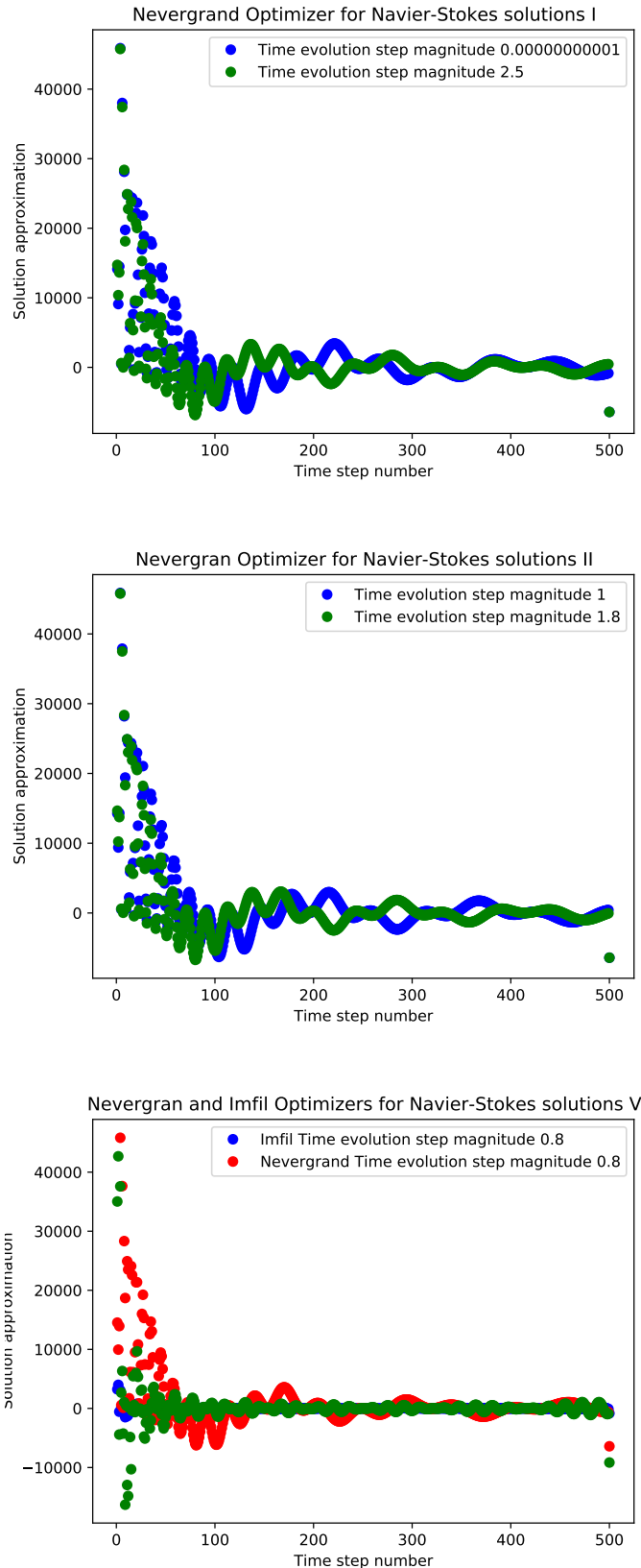


Figure 3: *Additional plots of Navier-Stokes solutions for Couette flow.* Under the Nevergran optimizer, solutions to the Navier-Stokes equation for Couette flow relax to the steady-state velocity, after which the solution continues to fluctuate. In the third plot, a direct comparison of the Navier-Stokes solutions obtained from the Imfil and Nevergran optimizers exhibits that solution approximations provided by Nevergran optimizer fluctuate significantly less often below the solution axis than solution approximations provided by the Imfil optimizer do.

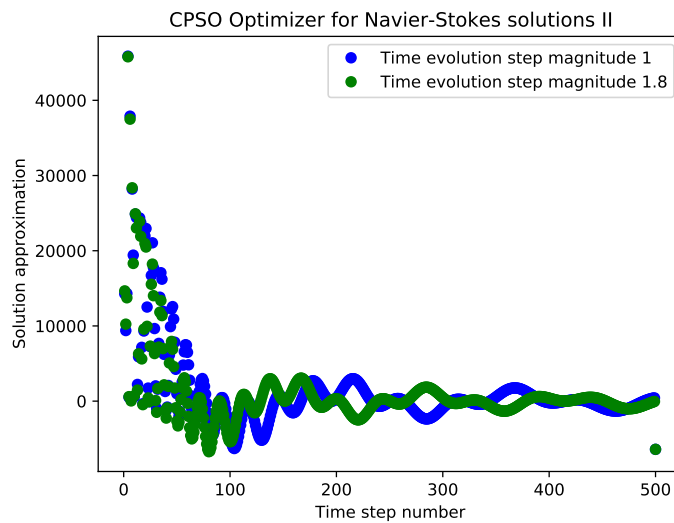
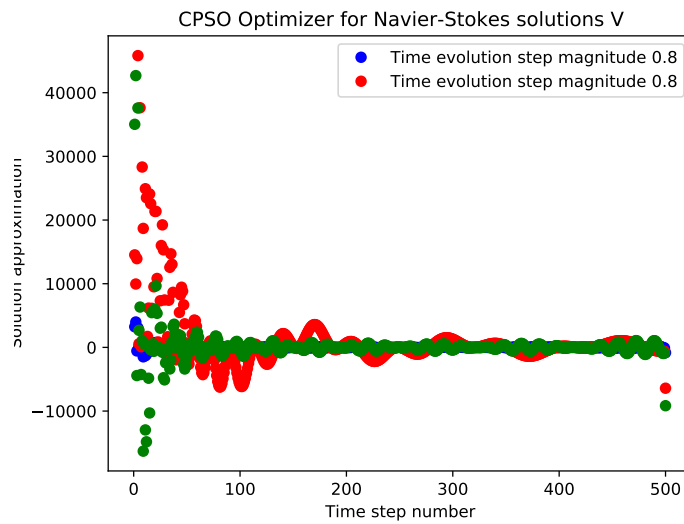


Figure 4: *Plots of Navier-Stokes solutions obtained with stochastic optimizers CPSO, AND CMAES.* Under stochastic optimizers, solution approximations to Navier-Stokes Couette flow fluctuate more significantly below and above the solution axis, as do approximations produced by the Imfil optimizer provided in the previous figure.

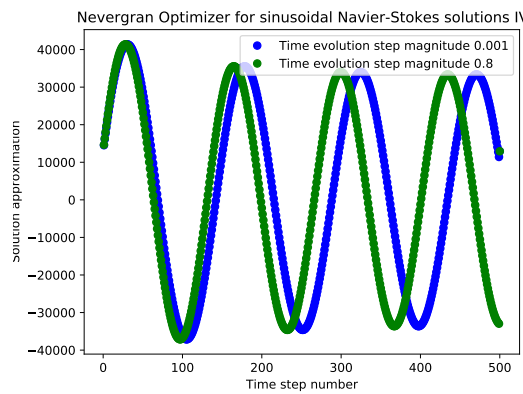
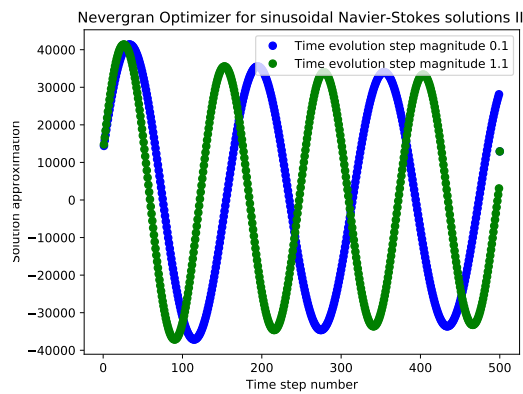
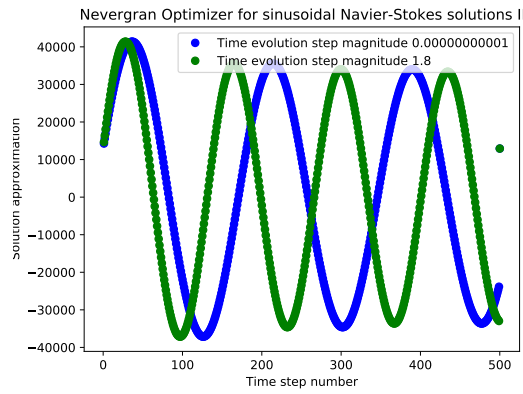
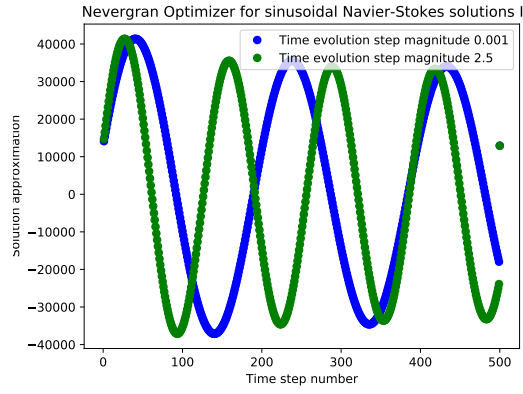
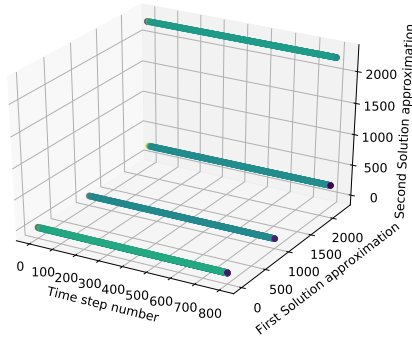
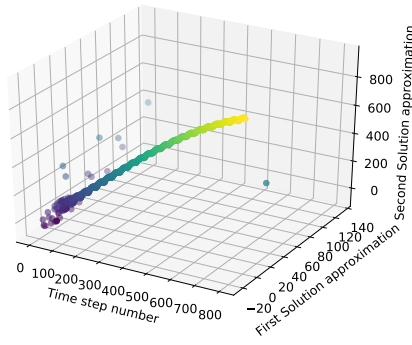


Figure 5: *Plots of Navier-Stokes sinusoidal solutions.* By comparison with exact analytical solutions obtained from Picard iterates, solution approximations obtained from readout of the variational quantum algorithm produces approximations of analytically known sinusoidal solutions.

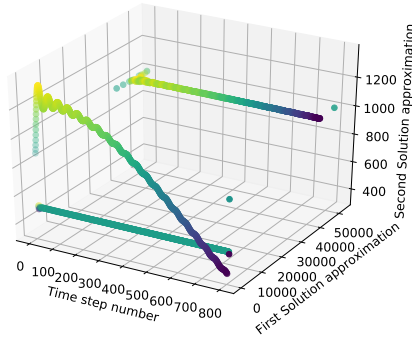
Stochastic NA Optimizer for Navier-Stokes Solutions



Stochastic NA Optimizer for Navier-Stokes Solutions



Stochastic NA Optimizer for Navier-Stokes Solutions



Stochastic NA Optimizer for Navier-Stokes Solutions

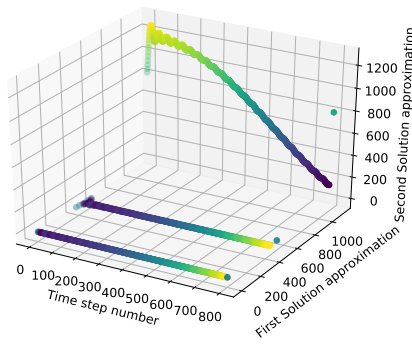
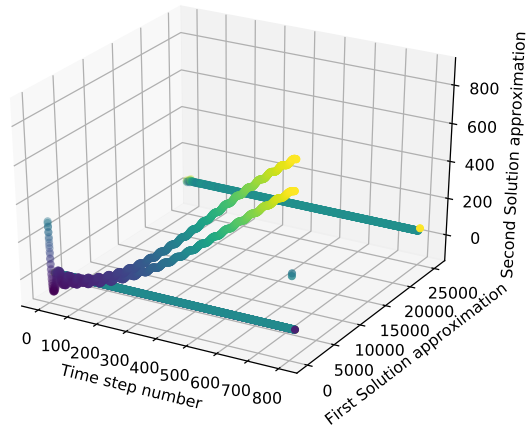
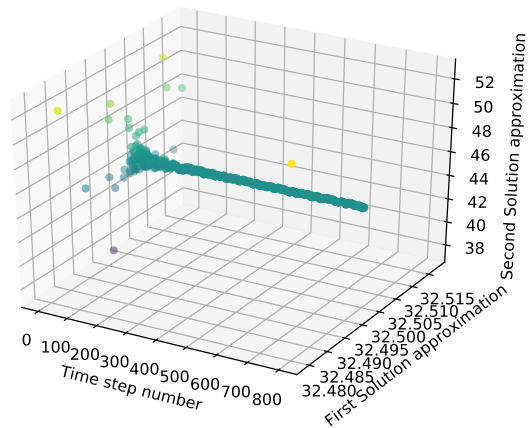


Figure 6: *Plots of two-dimensional Navier-Stokes solutions obtained with stochastic optimizers. Previous methods with stochastic optimizers from one-dimensional solutions were similarly implemented for two components of motion.*

Stochastic NA Optimizer for Navier-Stokes Solutions



Stochastic NA Optimizer for Navier-Stokes Solutions



Stochastic NA Optimizer for Navier-Stokes solutions

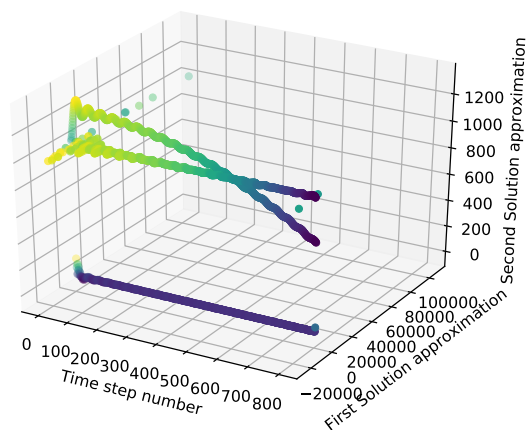
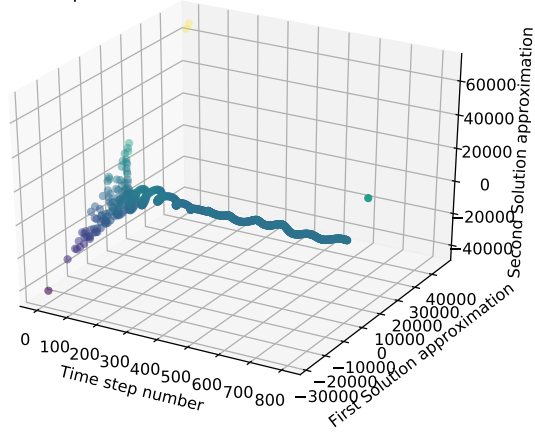
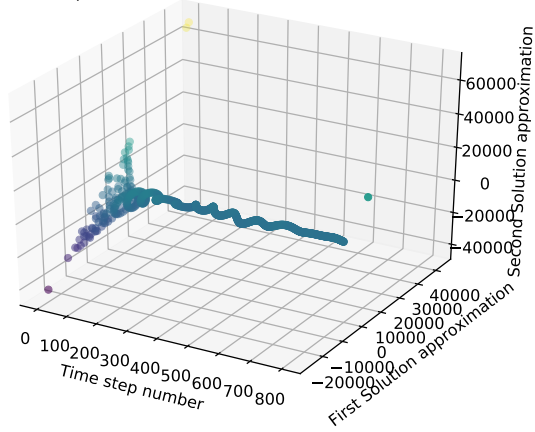


Figure 7: Plots of two-dimensional Navier-Stokes solutions obtained with stochastic optimizers. Previous methods with stochastic optimizers from one-dimensional solutions were similarly implemented for two components of motion.

NA Optimizer for Navier-Stokes solutions III



NA Optimizer for Navier-Stokes solutions II



NA Optimizer for Navier-Stokes solutions III

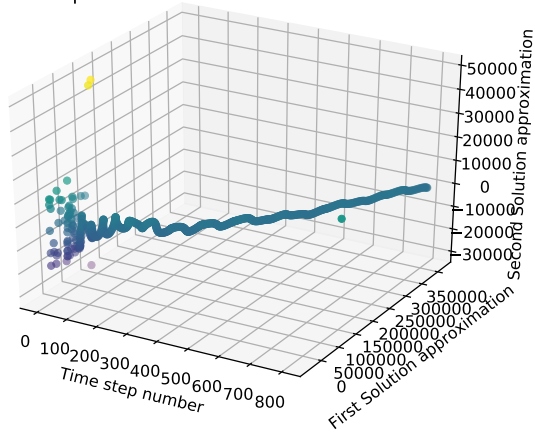
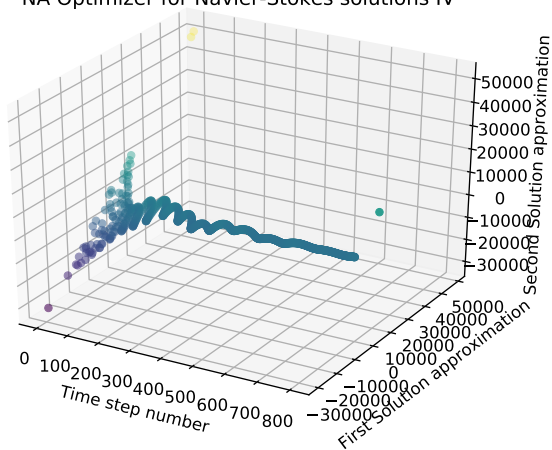
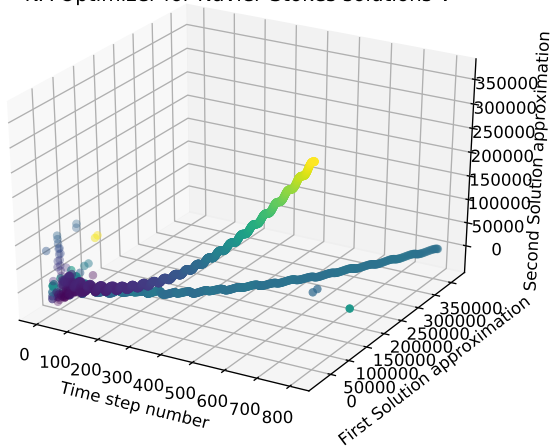


Figure 8: *Plots of two-dimensional Navier-Stokes solutions obtained with stochastic optimizers. Previous methods with stochastic optimizers from one-dimensional solutions were similarly implemented for two components of motion.*

NA Optimizer for Navier-Stokes solutions IV



NA Optimizer for Navier-Stokes solutions V



NA Optimizer for Navier-Stokes solutions I

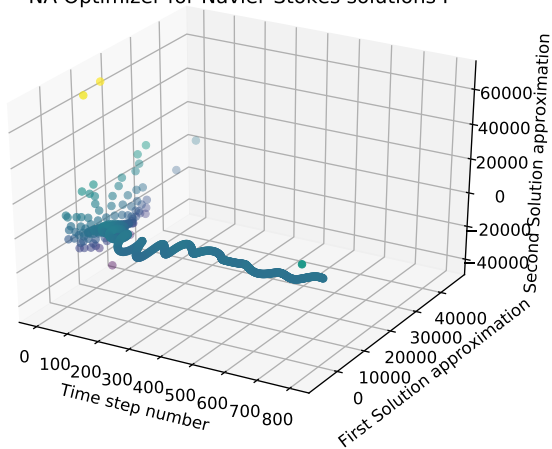
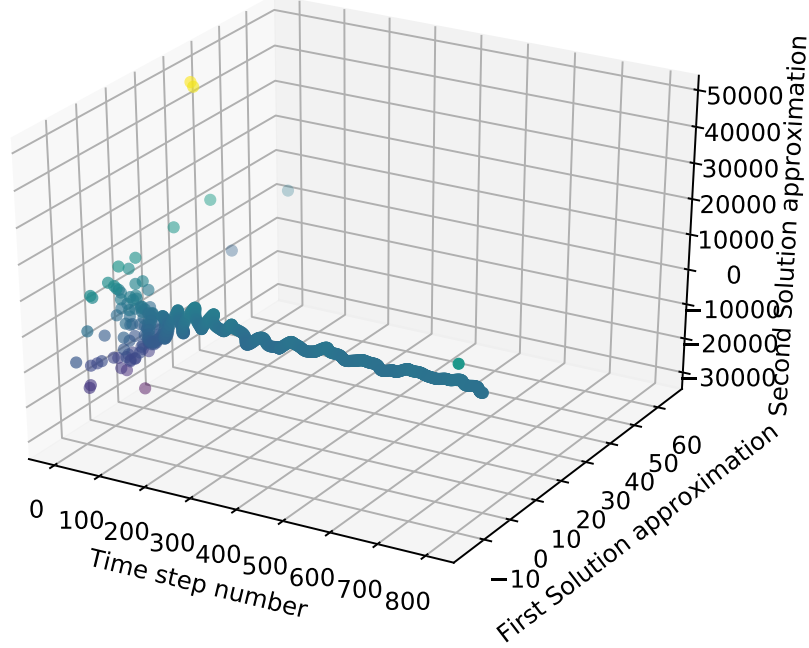


Figure 9: *Plots of two-dimensional Navier-Stokes solutions obtained with stochastic optimizers. Previous methods with stochastic optimizers from one-dimensional solutions were similarly implemented for two components of motion.*

NA Optimizer for Navier-Stokes solutions I



NA Optimizer for Navier-Stokes solutions VI

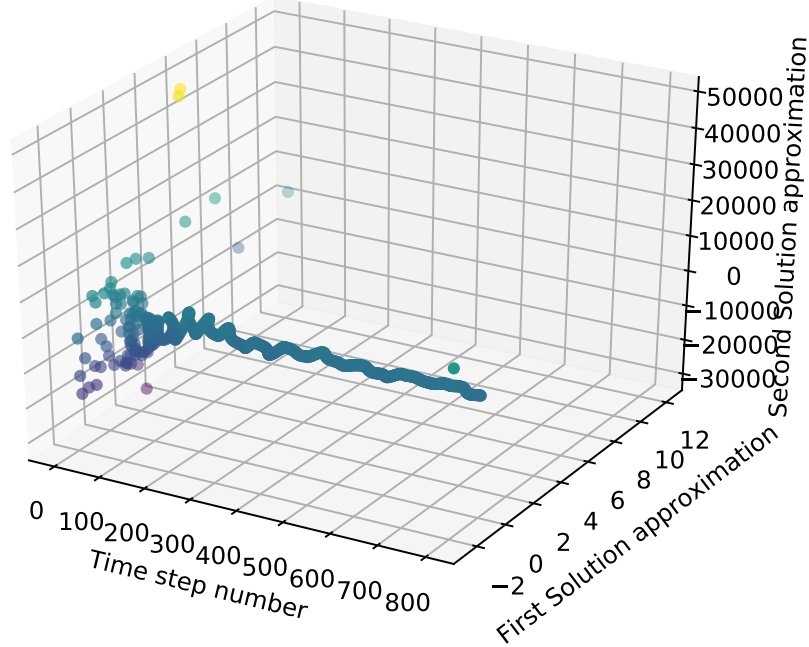


Figure 10: *Plots of two-dimensional Navier-Stokes solutions obtained with stochastic optimizers. Previous methods with stochastic optimizers from one-dimensional solutions were similarly implemented for two components of motion.*

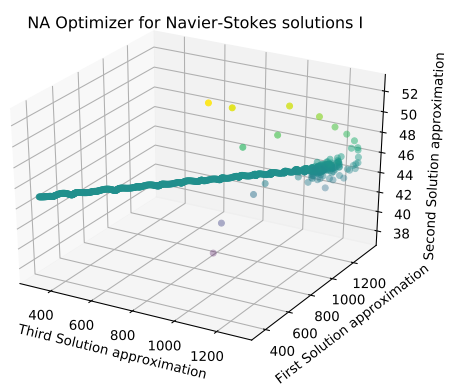
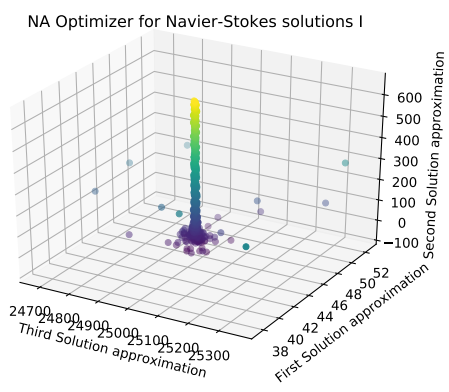
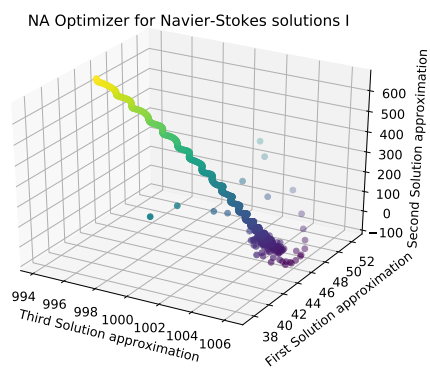


Figure 11: *Plots of three-dimensional Navier-Stokes solutions obtained with stochastic optimizers. Previous methods with stochastic optimizers from one-dimensional solutions were similarly implemented for three components of motion.*

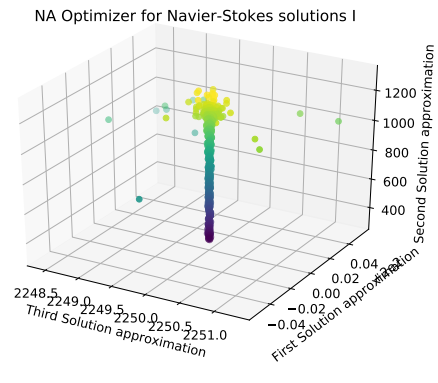
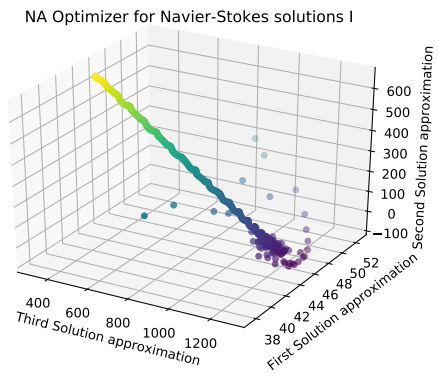
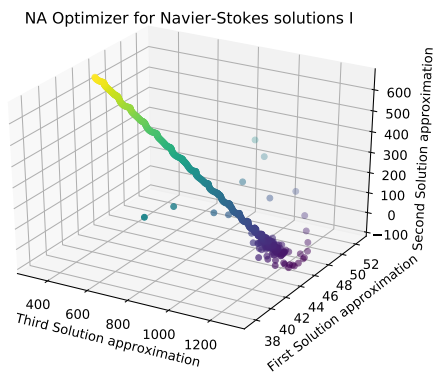
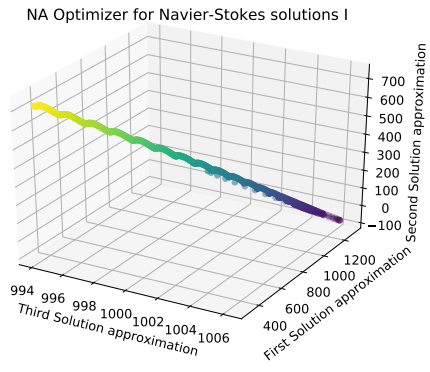


Figure 12: *Plots of three-dimensional Navier-Stokes solutions obtained with stochastic optimizers.* Previous methods with stochastic optimizers from one-dimensional solutions were similarly implemented for three components of motion.

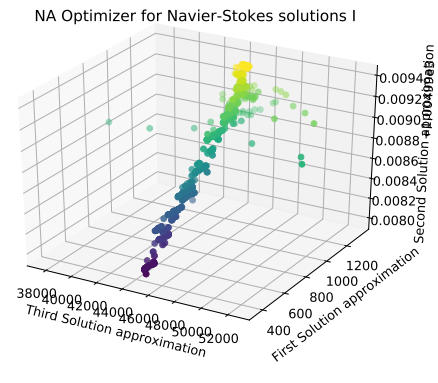
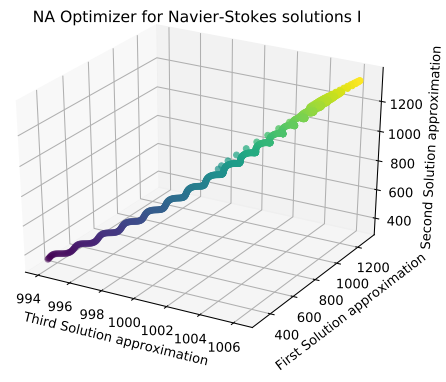
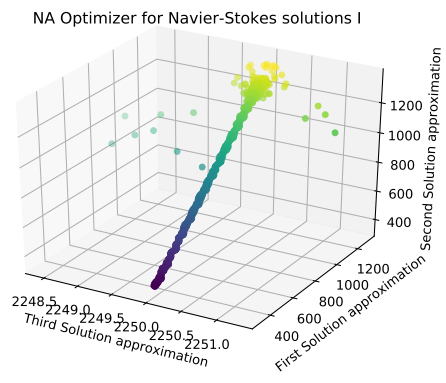
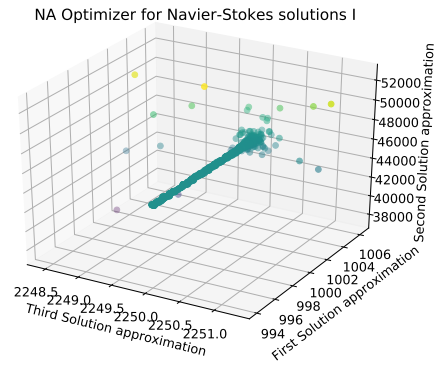


Figure 13: *Plots of three-dimensional Navier-Stokes solutions obtained with stochastic optimizers.* Previous methods with stochastic optimizers from one-dimensional solutions were similarly implemented for three components of motion.

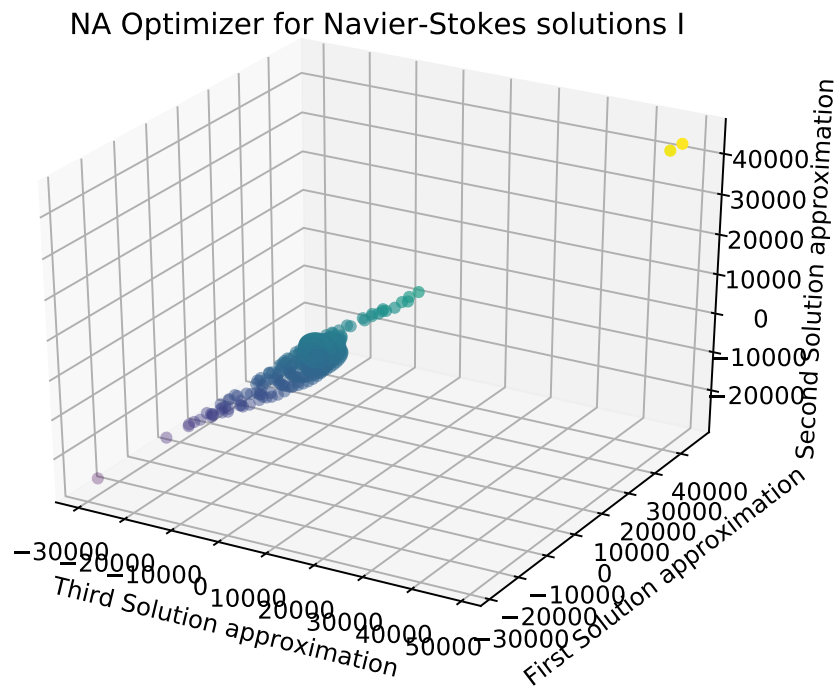
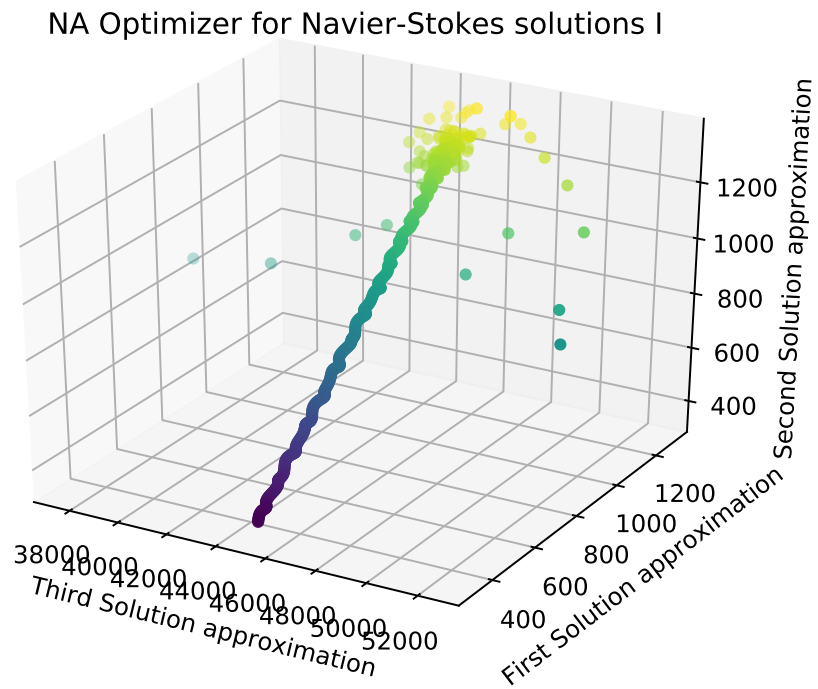


Figure 14: *Plots of three-dimensional Navier-Stokes solutions obtained with stochastic optimizers. Previous methods with stochastic optimizers from one-dimensional solutions were similarly implemented for three components of motion.*

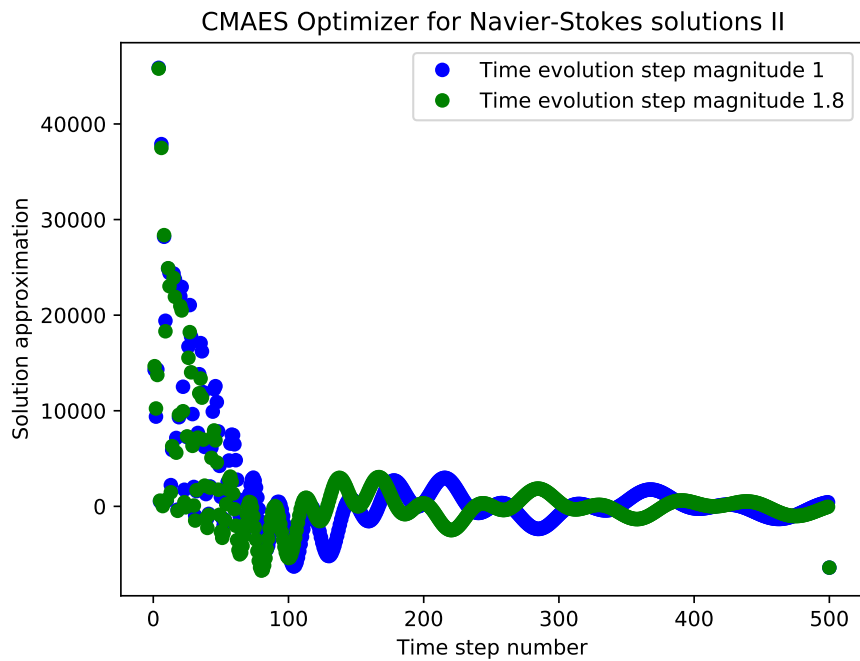
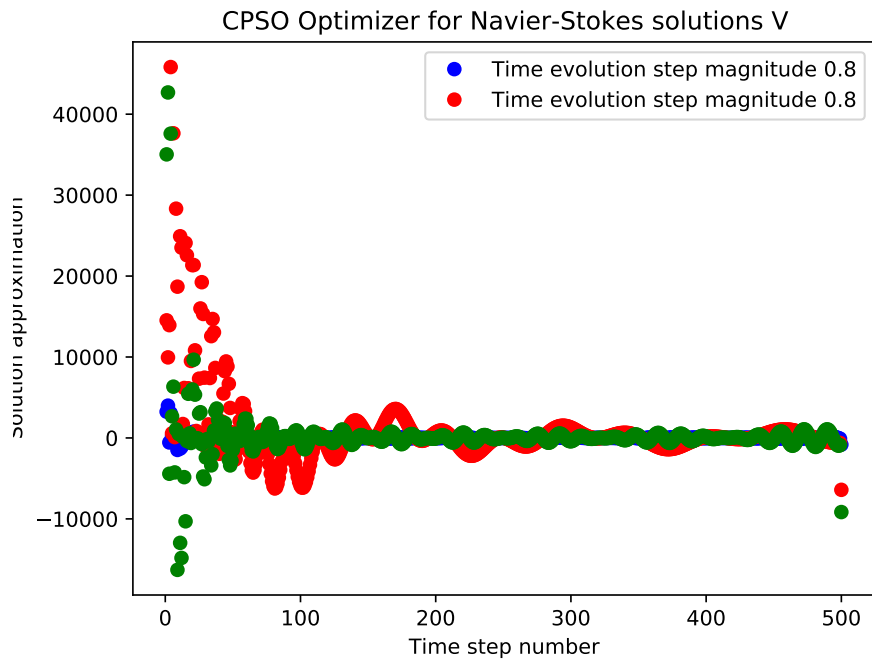


Figure 15: Additional plots of Navier-Stokes solutions obtained with stochastic optimizers *CPSO* and *CMAES*. Under stochastic optimizers, solution approximations to Navier-Stokes Couette flow obtained with the *CPSO* optimizer fluctuate more significantly below and above the solution axis, as do approximations produced by the *Imfil* optimizer provided in the previous figure. In the second figure provided, the solution approximations to Navier-Stokes with the *CMAES* optimizer provides more accurate solutions for Couette flow which fluctuate significantly less before time step 100.

$$\begin{aligned}
\frac{\partial}{\partial x^j} \left( \frac{\partial}{\partial x^n} - \frac{\partial}{\partial x^m} \right) &\equiv (\Delta_j)^{-1} (A_j - \mathbf{1}) \left( \frac{A_n - \mathbf{1}}{\Delta_n} - \frac{A_m - \mathbf{1}}{\Delta_m} \right) \\
&\Downarrow \\
\frac{1}{\Delta_j \Delta_n} (A_j - \mathbf{1}) (A_n - \mathbf{1}) - \frac{1}{\Delta_j \Delta_m} (A_j - \mathbf{1}) (A_m - \mathbf{1}) \\
&\Downarrow \\
\underbrace{\frac{1}{\Delta_j \Delta_n} \{A_j A_n - A_j - A_n + \mathbf{1}\}}_{\mathbf{3}} - \underbrace{\frac{1}{\Delta_j \Delta_m} \{A_j A_m - A_j - A_m + \mathbf{1}\}}_{\mathbf{4}} .
\end{aligned}$$

The resulting operator superposition of the leftmost term on the right hand side of the field equations, which is itself a superposition of two components of the metric tensor, takes the form,<sup>2</sup>,

$$\begin{aligned}
\mathbf{1} |g_{jm}\rangle - \mathbf{2} |g_{nj}\rangle &\equiv \frac{1}{\Delta_i \Delta_n} (A_i A_n - A_i - A_n + \mathbf{1}) |g_{jm}\rangle - \frac{1}{\Delta_i \Delta_m} (A_i A_m - A_i - A_m + \mathbf{1}) |g_{nj}\rangle \\
&\Downarrow \\
\frac{1}{\Delta_i \Delta_n} (A_i A_n |g_{jm}\rangle - A_i |g_{jm}\rangle - A_n |g_{jm}\rangle + |g_{jm}\rangle) - \frac{1}{\Delta_i \Delta_m} (A_i A_m |g_{nj}\rangle - A_i |g_{nj}\rangle - A_m |g_{nj}\rangle + |g_{nj}\rangle) \\
&\Downarrow \\
\underbrace{\frac{A_i}{\Delta_i} \left( \frac{A_n}{\Delta_n} |g_{jm}\rangle - \frac{A_m}{\Delta_m} |g_{nj}\rangle \right) - \frac{A_i}{\Delta_i} \left( \frac{|g_{jm}\rangle}{\Delta_n} - \frac{|g_{nj}\rangle}{\Delta_m} \right) - \frac{A_n}{\Delta_i \Delta_n} |g_{jm}\rangle + \frac{A_m}{\Delta_i \Delta_m} |g_{nj}\rangle}_{\star} + \dots \\
\underbrace{\frac{|g_{jm}\rangle}{\Delta_i \Delta_n} - \frac{|g_{nj}\rangle}{\Delta_i \Delta_m}}_{\star} ,
\end{aligned}$$

where the superposition given in the ultimate equality is equivalent to  $\star$ , for components of  $g$ , in addition to,

$$\begin{aligned}
\mathbf{3} |g_{im}\rangle - \mathbf{4} |g_{ni}\rangle &\equiv \frac{1}{\Delta_j \Delta_n} (A_j A_n - A_j - A_n + \mathbf{1}) |g_{im}\rangle - \frac{1}{\Delta_j \Delta_m} (A_j A_m - A_j - A_m + \mathbf{1}) |g_{ni}\rangle \\
&\Downarrow \\
\frac{A_j A_n}{\Delta_j \Delta_n} |g_{im}\rangle - \frac{A_j}{\Delta_j \Delta_n} |g_{im}\rangle - \frac{A_n}{\Delta_j \Delta_n} |g_{im}\rangle + \frac{|g_{im}\rangle}{\Delta_j \Delta_n} - \frac{A_j A_m}{\Delta_j \Delta_m} |g_{ni}\rangle + \dots \\
A_j |g_{ni}\rangle + A_m |g_{ni}\rangle - |g_{ni}\rangle \\
&\Downarrow \\
\underbrace{\frac{A_j}{\Delta_j} \left( \frac{A_n}{\Delta_n} |g_{im}\rangle - \frac{A_m}{\Delta_m} |g_{ni}\rangle \right) - \frac{A_j}{\Delta_j} \left( \frac{|g_{im}\rangle}{\Delta_n} - \frac{|g_{ni}\rangle}{\Delta_m} \right) - \frac{A_n}{\Delta_j \Delta_n} |g_{im}\rangle}_{\star\star} + \dots \\
\underbrace{\frac{A_m}{\Delta_j \Delta_n} |g_{ni}\rangle + \frac{|g_{im}\rangle}{\Delta_j \Delta_n} - \frac{|g_{ni}\rangle}{\Delta_j \Delta_m}}_{\star\star} ,
\end{aligned}$$

<sup>2</sup>With abuse of notation, set  $g_{jm} \equiv |g_{jm}\rangle$  for the quantum state prepared corresponding to each component of the metric tensor, and  $T_{\mu\nu} \equiv |T_{\mu\nu}\rangle$ .

which is equivalent to  $\star\star$ . Consolidating terms from each superposition of quantum states yields,

$$\frac{A_i}{\Delta_i} \left( \frac{A_n}{\Delta_n} |g_{jm}\rangle - \frac{A_m}{\Delta_m} |g_{nj}\rangle \right) - \frac{A_i}{\Delta_i} \left( \frac{|g_{jm}\rangle}{\Delta_n} - \frac{|g_{nj}\rangle}{\Delta_m} \right) - \frac{A_n}{\Delta_n} \left( \frac{|g_{jm}\rangle}{\Delta_i} + \frac{|g_{im}\rangle}{\Delta_j} \right) + \frac{A_m}{\Delta_m} \left( \frac{|g_{nj}\rangle}{\Delta_i} - \frac{|g_{ni}\rangle}{\Delta_j} \right) + \dots \\ \frac{1}{\Delta_i} \left( \frac{|g_{jm}\rangle}{\Delta_n} - \frac{|g_{nj}\rangle}{\Delta_m} \right),$$

for the first 6 terms, and

$$\frac{A_j}{\Delta_j} \left( \frac{A_n}{\Delta_n} |g_{im}\rangle - \frac{A_m}{\Delta_m} |g_{ni}\rangle \right) - \frac{A_j}{\Delta_j} \left( \frac{|g_{im}\rangle}{\Delta_n} - \frac{|g_{ni}\rangle}{\Delta_m} \right) + \frac{1}{\Delta_j} \left( \frac{|g_{im}\rangle}{\Delta_n} - \frac{|g_{ni}\rangle}{\Delta_m} \right),$$

for the remaining 4 terms. Altogether, the terms on the right hand side of the field equations which are not first or second derivatives of components of the metric tensor either yield spatial derivatives of the time-evolved variational state for the metric tensor, or time-evolved spatial derivatives of the variational state. From the superposition, as in the derivation of the previous cost function we isolate variational states associated with metric tensor components, with the following decomposition, dependent on the order to which the metric tensor is differentiated,

$$\underbrace{\frac{A_i}{\Delta_i} \left( \frac{A_n}{\Delta_n} |g_{jm}\rangle - \frac{A_m}{\Delta_m} |g_{nj}\rangle \right) + \frac{A_j}{\Delta_j} \left( \frac{A_n}{\Delta_n} |g_{im}\rangle - \frac{A_m}{\Delta_m} |g_{ni}\rangle \right)}_{\text{Second order terms}} - \underbrace{\frac{A_i}{\Delta_i} \left( \frac{|g_{jm}\rangle}{\Delta_n} - \frac{|g_{nj}\rangle}{\Delta_m} \right) + \frac{A_j}{\Delta_j} \left( \frac{|g_{im}\rangle}{\Delta_n} - \dots \right)}_{\text{First order terms}} \\ \underbrace{\frac{|g_{ni}\rangle}{\Delta_m} - \frac{A_n}{\Delta_n} \left( \frac{|g_{jm}\rangle}{\Delta_i} + \frac{|g_{im}\rangle}{\Delta_j} \right)}_{\text{First order terms}} + \\ \underbrace{\frac{A_m}{\Delta_m} \left( \frac{|g_{nj}\rangle}{\Delta_i} - \frac{|g_{ni}\rangle}{\Delta_j} \right)}_{\text{First order terms}} = \frac{8\pi G}{c^4} |T_{\mu\nu}\rangle - \underbrace{\left( \frac{|g_{jm}\rangle}{\Delta_i \Delta_n} - \frac{|g_{nj}\rangle}{\Delta_i \Delta_m} - \frac{|g_{im}\rangle}{\Delta_j \Delta_n} + \frac{|g_{ni}\rangle}{\Delta_j \Delta_m} - R |g_{\mu\nu}\rangle \right)}_{\text{Zeroth order terms}}.$$

From components  $jm$ ,  $nj$ ,  $im$  and  $ni$  of  $g$ , the variational state time-evolved forwards by  $\tau$  can be read off as follows. From the first component of the metric tensor, the second order derivative terms from the partial derivative operators for the  $jm$  component of the metric tensor is given by the superposition,

$$\frac{A_i A_n}{\Delta_i \Delta_n} |g_{jm}\rangle - \frac{A_i}{\Delta_i \Delta_n} |g_{jm}\rangle - \frac{A_n}{\Delta_n \Delta_i} |g_{jm}\rangle = \frac{8\pi G}{c^4} |T_{\mu\nu}\rangle - \frac{|g_{jm}\rangle}{\Delta_i \Delta_n},$$

which is suitably scaled in the  $i$  and  $n$  degrees of freedom, while the remaining equalities for other possible components of the metric tensor either alternate in sign between components of the solution and the stress-energy tensor,

$$\mp \frac{A_i A_m}{\Delta_i \Delta_m} |g_{nj}\rangle \pm \frac{A_i}{\Delta_i \Delta_m} |g_{nj}\rangle \pm \frac{A_m}{\Delta_m \Delta_i} |g_{nj}\rangle = \frac{8\pi G}{c^4} |T_{\mu\nu}\rangle \pm \frac{|g_{nj}\rangle}{\Delta_i \Delta_m}.$$

From the relationship between the variational states, and spatial derivatives of variational states for the metric tensor, the time evolved variational state for the solution to the field equations takes the form,

$$|\widetilde{g}\rangle = -\frac{8\pi G\Delta_i\Delta_n}{c^4} |T_{\mu\nu}\rangle + |g_{jm}\rangle + A_i |\widetilde{g_{jm}}\rangle - A_i |g_{jm}\rangle ,$$

corresponding to the  $jm$  metric tensor component, in which  $(g_{jm})_\tau$  represents the variational state for the solution evolved forwards by  $\tau$ , and  $g_{jm}$  represents the variational state before the time evolution step. The resulting quantum state whose ground state is to be determined from the cost function takes the following form after expansion,

$$\begin{aligned} \mathcal{C}^E(\lambda, \lambda_0^E) &= \left\| |\widetilde{g_{jm}}\rangle - |g_{jm}\rangle \right\|^2 \\ &\Downarrow \\ &= \left\| -\frac{8\pi G\Delta_i\Delta_n}{c^4} |T_{\mu\nu}\rangle + A_i |\widetilde{g_{jm}}\rangle - A_i |g_{jm}\rangle \right\|^2 \\ &\Downarrow \\ &= (\lambda_0^E)^2 + \text{Re} \left\{ \langle T_{\mu\nu} | \left( \frac{8\pi G\Delta_i\Delta_n}{c^4} \right)^2 |T_{\mu\nu}\rangle + (A_i |\widetilde{g_{jm}}\rangle - A_i |g_{jm}\rangle)^2 + \dots \right. \\ &\quad \left. 2 \left( \frac{8\pi G\Delta_i\Delta_n}{c^4} \right) |T_{\mu\nu}\rangle (A_i |\widetilde{g_{jm}}\rangle - A_i |g_{jm}\rangle) \right\} \\ &\Downarrow \\ &= (\lambda_0^E)^2 + 2 \text{Re} \left\{ \langle g_{jm} | A_i^\dagger A_i |\widetilde{g_{jm}}\rangle - \left( \frac{8\pi G\Delta_i\Delta_n}{c^4} \right) (2 |T_{\mu\nu}\rangle \{A_i |g_{jm}\rangle - 2 A_i |\widetilde{g_{jm}}\rangle) \right\} - \frac{8\pi G\Delta_i\Delta_n}{c^4} \left. \right\} \\ &\Downarrow \\ \boxed{\mathcal{C}^E(\lambda, \lambda_0^E)} &= (\lambda_0^E)^2 + \text{Re} \left\{ \langle g_{jm} | A_i^\dagger A_i |\widetilde{g_{jm}}\rangle - \frac{16\pi G\Delta_i\Delta_n}{c^4} \langle \widetilde{g_{jm}} | A_i^\dagger |T_{\mu\nu}\rangle + \dots \right. \\ &\quad \left. \frac{16\pi G\Delta_i\Delta_n}{c^4} \langle \widetilde{g_{jm}} | A_i^\dagger |T_{\mu\nu}\rangle - \left( \frac{8\pi G\Delta_i\Delta_n}{c^4} \right)^2 \right\} , \end{aligned}$$

in which we denote the quantum state for the metric tensor, and the time evolved state of the quantum solution representative, respectively with  $(g_{jm}) \equiv |g_{jm}\rangle$ , and  $(g_{jm})_\tau \equiv |\widetilde{g_{jm}}\rangle$ . As a result, the square of the norm between the time evolved variational state and the preceding state takes the form above. To numerically simulate solutions in the space-time manifold, we present several of the incarnations below for the stress energy tensor.

- *Point particle test.* The expression of the stress energy tensor for the gravitational pull exerted upon a single microscopic body in space-time is,

$$T_{\mu\nu} \equiv \frac{m v_\mu(t) v_\nu(t)}{\sqrt{1 - \left(\frac{v}{c}\right)^2}} \left| x - x(t) \right| ,$$

where  $m$  is the mass of the test particle traveling at velocity  $v$  with trajectory  $x(t)$ , and  $v_\mu$  and  $v_\nu$  are the velocity vectors for  $\mu, \nu \in \{0, 1, 2, 3\}$ . Under this assumption, the resulting cost function is,

$$\boxed{\mathcal{C}_p^E(\lambda, \lambda_0^E)} = \left( \lambda_0^E \right)^2 + 2 \operatorname{Re} \left\{ \langle g_{jm} | A_i^\dagger A_i | \widetilde{g_{jm}} \rangle - 2 \frac{8\pi G \Delta_i \Delta_n}{c^4} \frac{m v_\mu(t) v_\nu(t)}{\sqrt{1 - (v/c)^2}} \left| x - x(t) \right| \times \dots \right. \\ \left. A_i | g_{jm} \rangle + 2 \frac{8\pi G \Delta_i \Delta_n}{c^4} \frac{m v_\mu(t) v_\nu(t)}{\sqrt{1 - (v/c)^2}} \left| x - x(t) \right| A_i | \widetilde{g_{jm}} \rangle - \dots \right. \\ \left. \left( \frac{8\pi G \Delta_i \Delta_n}{c^4} \right)^2 \right\} .$$

- Equilibrium fluid test. In thermodynamic equilibrium, the stress-energy tensor is,

$$T_{\mu\nu} \equiv \left( \rho + \frac{p}{c^2} \right) u_\mu u_\nu + p \left( \frac{1}{g_{\mu\nu}} \right) ,$$

where  $\rho$  is the mass-energy density,  $p$  the hydrostatic pressure,  $u_\mu$  and  $u_\nu$  are the four velocities of the equilibrium fluid, implying that the cost function is,

$$\boxed{\mathcal{C}_f^E(\lambda, \lambda_0^E)} \equiv \left( \lambda_0^E \right)^2 + 2 \operatorname{Re} \left\{ \langle g_{jm} | A_i^\dagger A_i | \widetilde{g_{jm}} \rangle - 2 \frac{8\pi G \Delta_i \Delta_n}{c^4} \times \dots \right. \\ \left( \rho + \frac{p}{c^2} \right) u_\mu u_\nu A_i | g_{jm} \rangle + p \left( \frac{1}{|g_{\mu\nu}|} \right) A_i | g_{jm} \rangle + 2 \frac{8\pi G \Delta_i \Delta_n}{c^4} \times \dots \\ \left( \rho + \frac{p}{c^2} \right) u_\mu u_\nu A_i | \widetilde{g_{jm}} \rangle + p \left( \frac{1}{|g_{\mu\nu}|} \right) A_i | \widetilde{g_{jm}} \rangle - \dots \\ \left. \left( \frac{8\pi G \Delta_i \Delta_n}{c^4} \right)^2 \right\} .$$

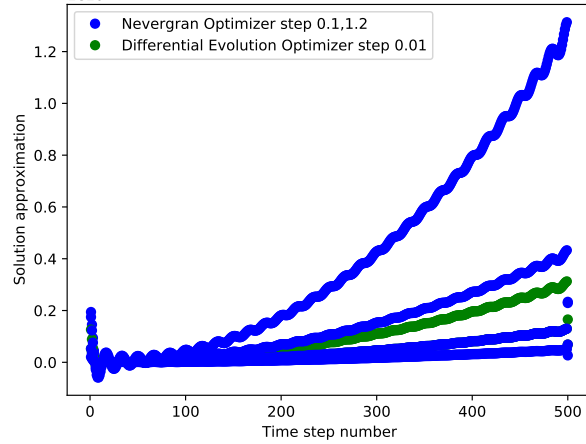
- Electromagnetic field tensor. For an electromagnetic field  $\mathcal{E}$ , the corresponding stress-energy tensor is,

$$T_{\mu\nu} \equiv \frac{1}{\mu_0} \left( F_{\mu\alpha} g^{\alpha\beta} F_{\nu\beta} - \frac{1}{4} g_{\mu\nu} F^{\delta\gamma} F_{\delta\gamma} \right) ,$$

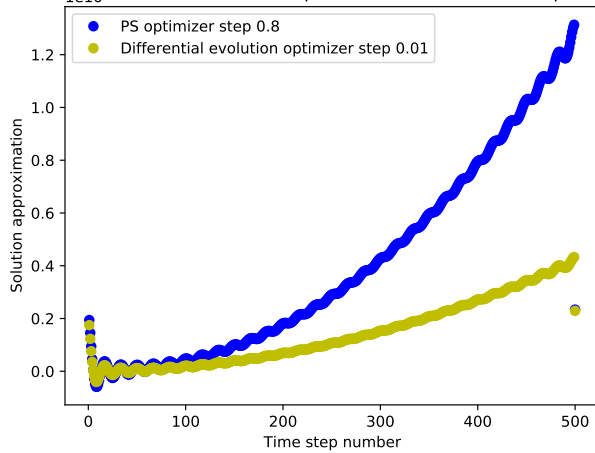
where the first multiplicative factor is the reciprocal of the permeability, and  $\alpha, \beta, \gamma \in \{0, 1, 2, 3\}$ . The corresponding cost function with the electromagnetic tensor is,

$$\boxed{\mathcal{C}_{\mathcal{E}}^E(\lambda, \lambda_0^E)} \equiv \left( \lambda_0^E \right)^2 + \operatorname{Re} \left\{ \langle g_{jm} | A_i^\dagger A_i | \widetilde{g_{jm}} \rangle \mp \left( \frac{2}{\mu_0} \right) \frac{8\pi G \Delta_i \Delta_n}{c^4} F_{\mu\alpha} | g_{\alpha\beta} \rangle F_{\nu\beta} \times \dots \right. \\ \left. A_i | g_{jm} \rangle - \left( \frac{F^{\delta\gamma} F_{\delta\gamma}}{4 \mu_0} \right) \langle g_{jm} | A_i^\dagger | g_{\mu\nu} \rangle \pm \left( \frac{2}{\mu_0} \right) \frac{8\pi G \Delta_i \Delta_n}{c^4} \langle \widetilde{g_{jm}} | A_x^\dagger F_{\mu\alpha} | g_{\alpha\beta} \rangle F_{\nu\beta} - \dots \right. \\ \left. \frac{4\pi G \Delta_i \Delta_n}{c^4} F^{\delta\gamma} F_{\delta\gamma} | g_{\mu\nu} \rangle - \left( \frac{8\pi G \Delta_i \Delta_n}{c^4} \right)^2 \right\} .$$

Differential Evolution & Nevergran Optimizers for the Einstein equation



PS & Differential Evolution optimizers for the Einstein equation



Differential Evolution & Nevergran Optimizers for the Einstein equation

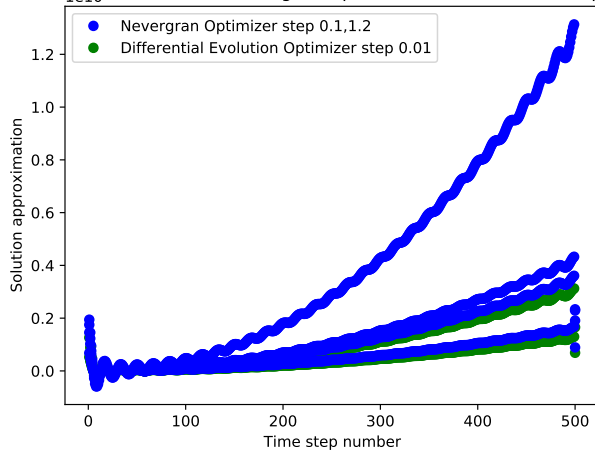


Figure 16: Plots of one component of the Einstein field equation solutions for the point particle stress-energy tensor. In the first plot, under the Nevergran optimizer, solutions to the Einstein field equations obtained with both the Nevergran and Imfil optimizers fluctuate before increasing monotonically until the last 500th time step of the evolution. In the second plot, comparing the performance of the Particle Swarm and Differential Evolution optimizers, numerical simulation of the quantum circuits for the Einstein point particle mass stress-energy tensor reveals that the Particle Swarm optimizer is more capable of exhausting a broader subset of Hilbert space. In the third plot, a more thorough comparison of the Differential Evolution and Nevergran optimizers can be determined by the time evolution step of the optimizer, in addition to the initial condition of the evolution determined by the ansatz

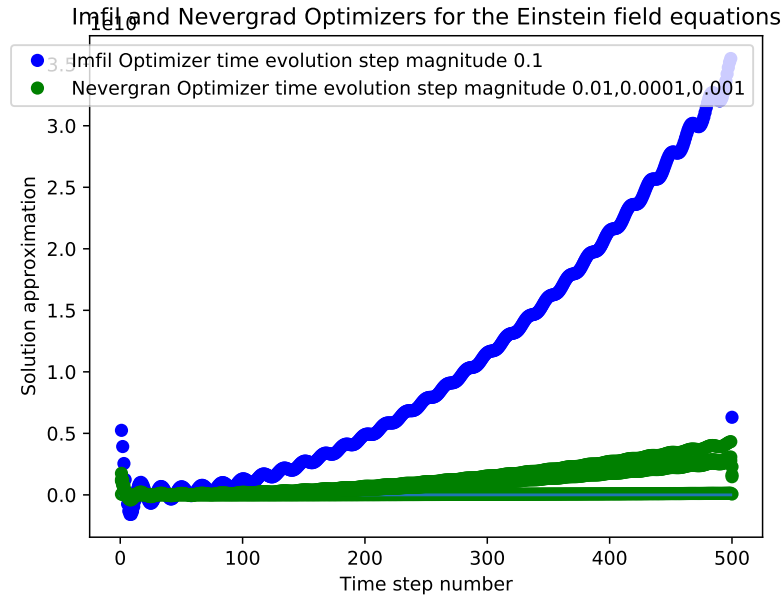
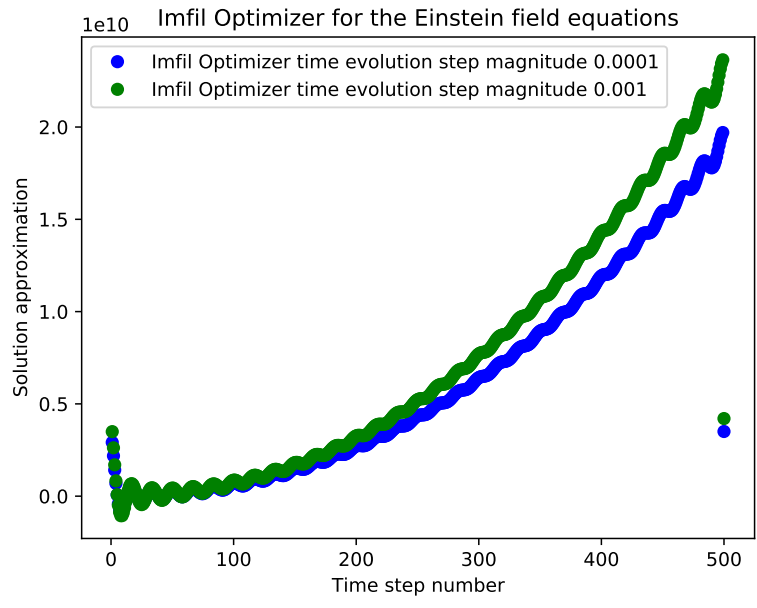
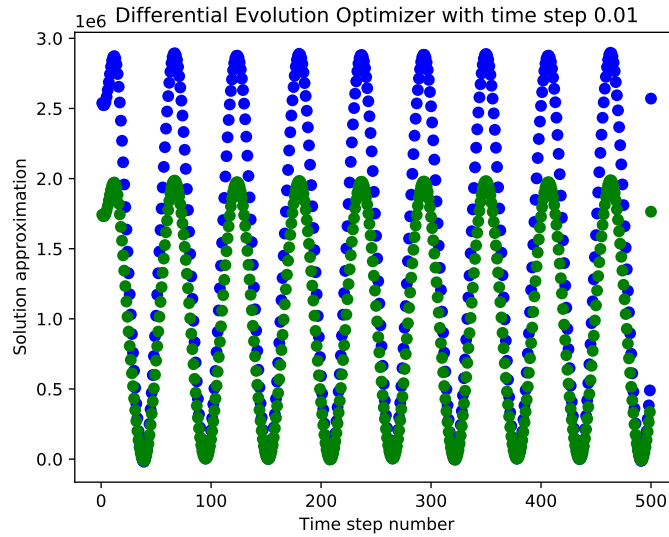
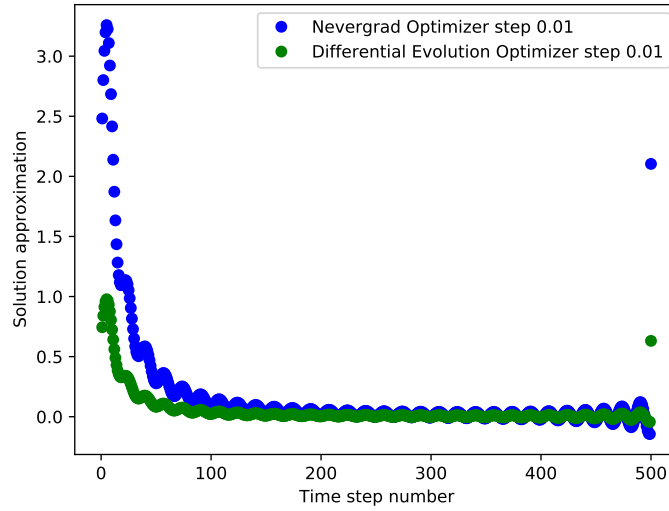


Figure 17: Additional plots of Einstein field equations solutions for the point particle stress-energy tensor. To further investigate optimizers that were used in the VQA for solving other nonlinear problems of interest, the Nevergrad and Imfil optimizers provide nearly identical performance for approximating solutions when 500 time steps of evolution are taken.

Differential Evolution and Nevergrad Optimizers for the Einstein equation



Differential Evolution and Nevergrad Optimizers for the Einstein equation

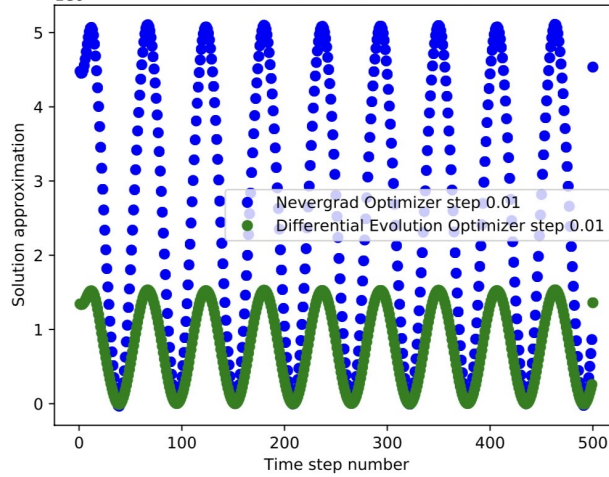


Figure 18: *Extracting measurements from other components of the the Einstein Field Equations.* To investigate the dependence of the initial choice of the ansatz for approximating other components of the Lorentzian manifold, 500 time steps of evolution are simulated under the Differential Evolution, Nevergrad, and Particle Swarm optimizers.

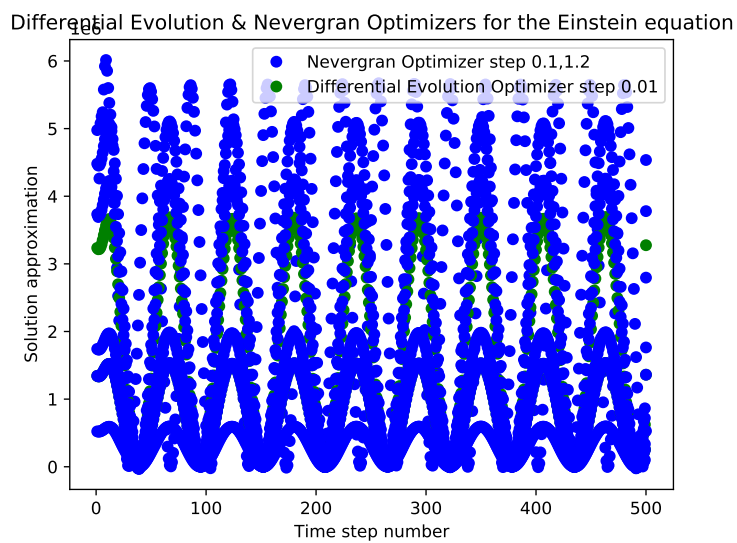
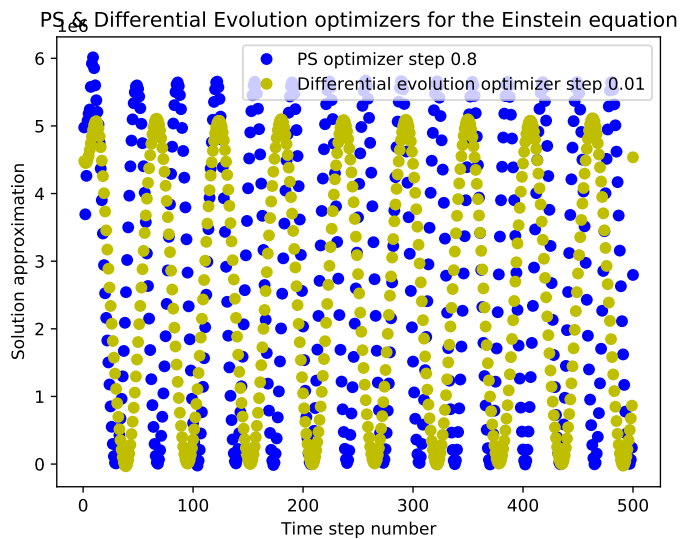


Figure 19: *Extracting measurements from other components of the the Einstein Field Equations.* Qualitatively similar sinusoidal solutions can also be approximated by the variational quantum algorithm.

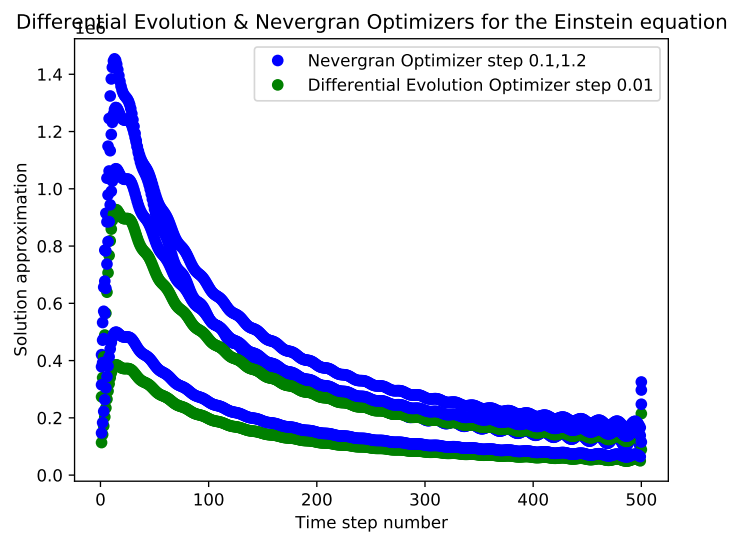
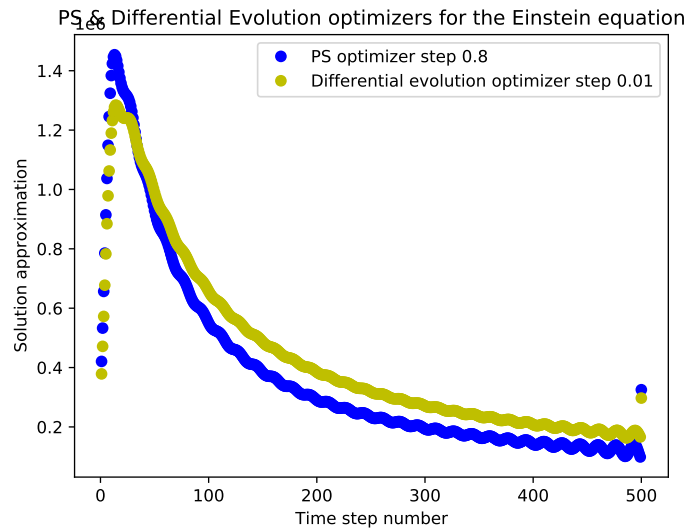
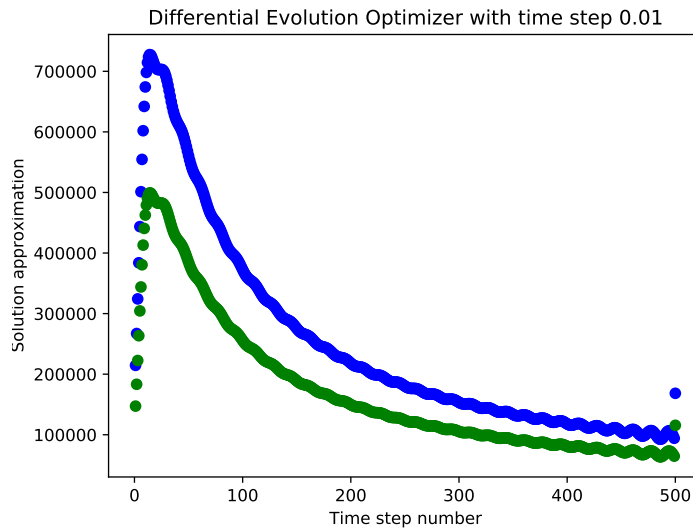


Figure 20: *Additional numerical experiments from those presented in Figure 8.* To further investigate the dependence of the initial choice of the ansatz for approximating other components of the Lorentzian manifold, dependencies between the space-time trajectory of the point pass particle and the corresponding gravitational attraction are obtained.

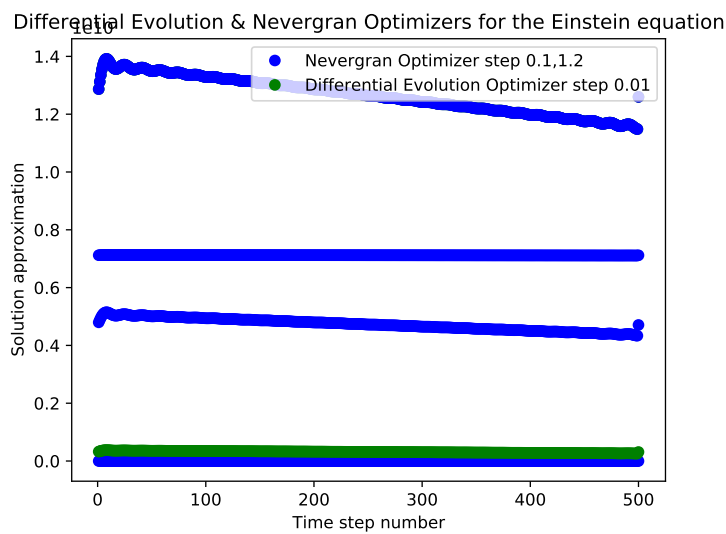
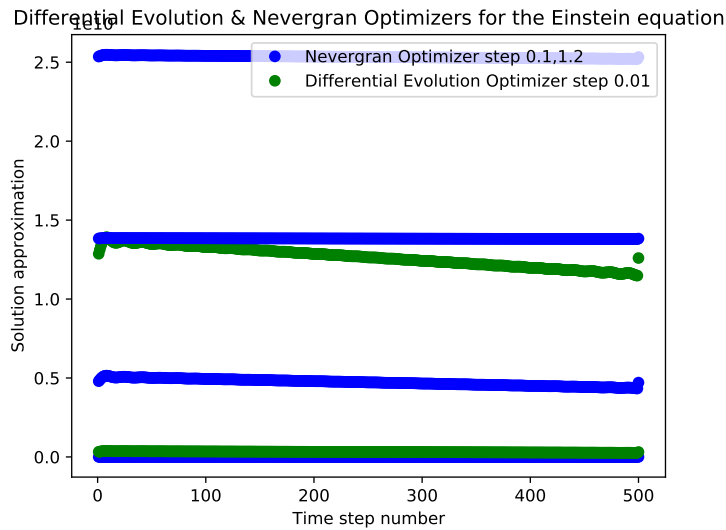
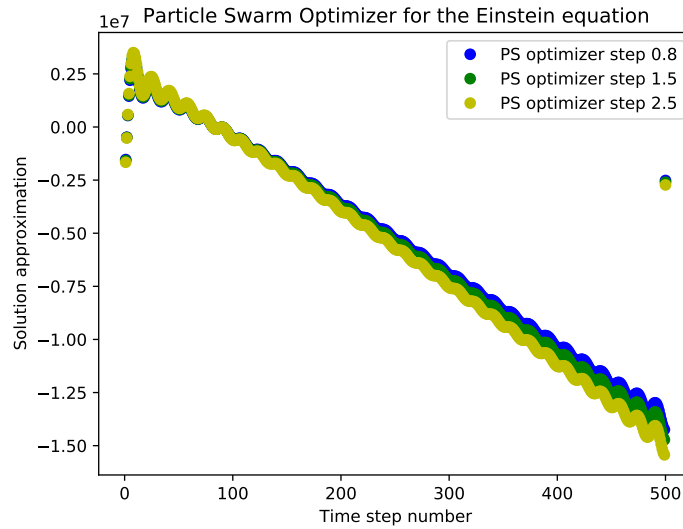


Figure 21: *Extracting measurements from the Einstein field equations with the equilibrium fluid stress-energy tensor.* From comparison with exact solutions to the Einstein equation with the fluid stress-energy tensor, previous investigations in the literature of exact solutions to the field equations are lines with negative slope.

Figure 22: Differential Evolution & Nevergrad Optimizers for the Einstein equation

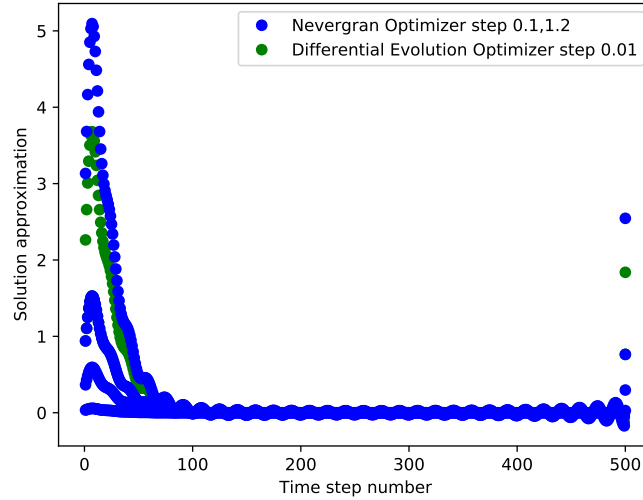


Figure 23: Differential Evolution and Nevergrad Optimizers for the Einstein equation

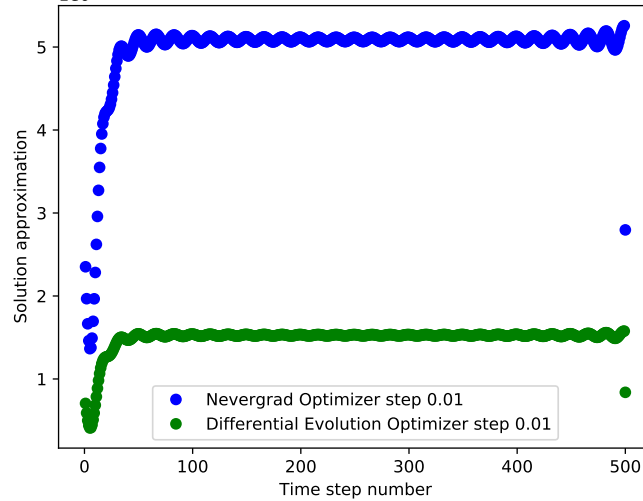


Figure 24: Differential Evolution Optimizer with time step 0.01

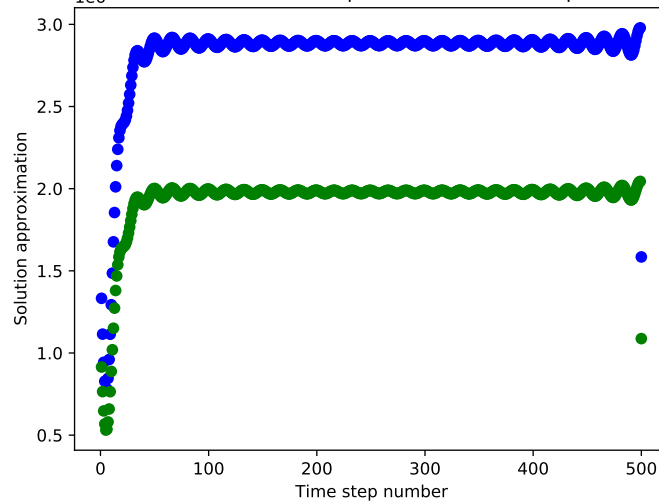


Figure 22: *Extracting measurements from the Einstein field equations with the electromagnetic stress-energy tensor.* Under different assumptions on the stress-energy tensor, we obtain additional quantum simulation results for the electromagnetic stress-energy tensor, in which exact solutions to the field equations are the hyperbolic secant and tangent functions.

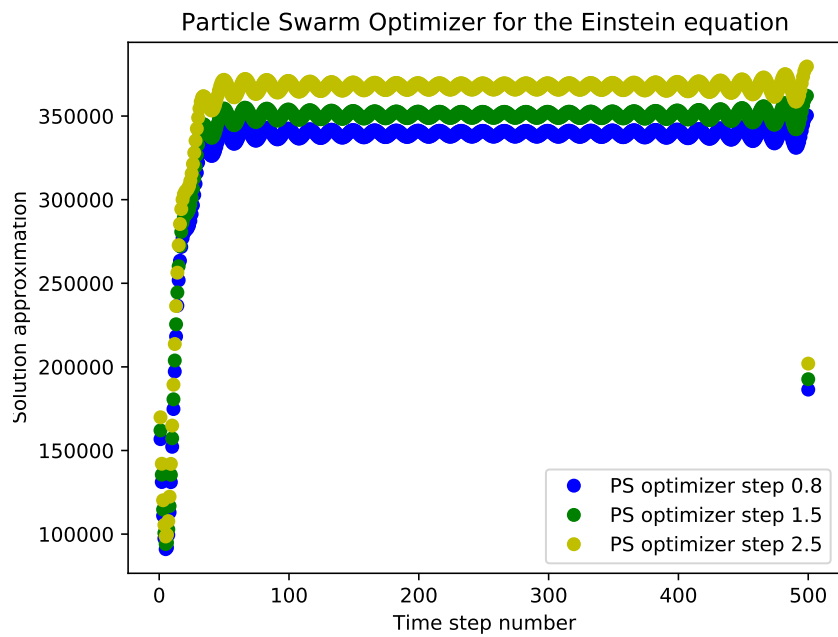
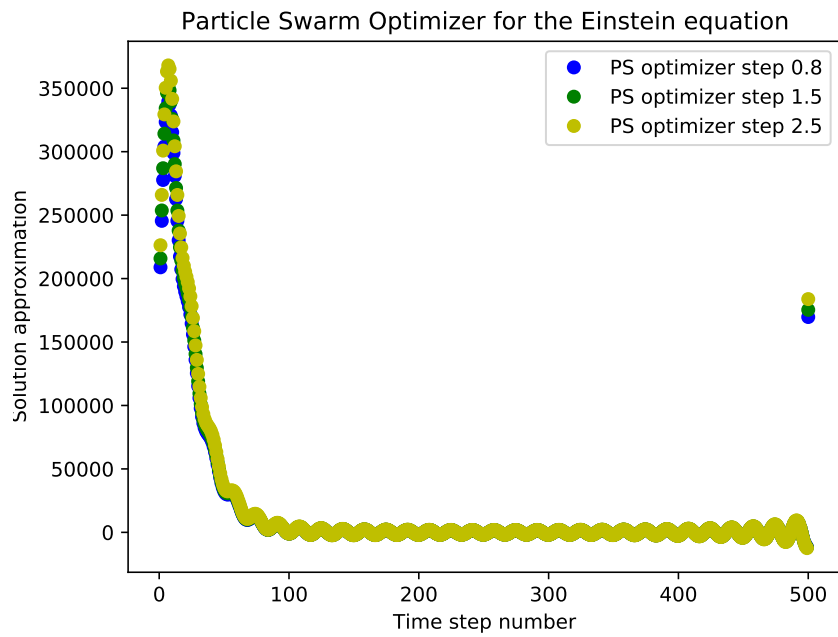


Figure 23: *Extracting measurements from the Einstein field equations with the electromagnetic stress-energy tensor with the Particle Swarm optimizer.* Besides optimizers that were numerically investigated in plots from the previous figure, implementing the variational quantum algorithm for different time steps and initial conditions with the Particle Swarm optimizer yield qualitatively similar results.

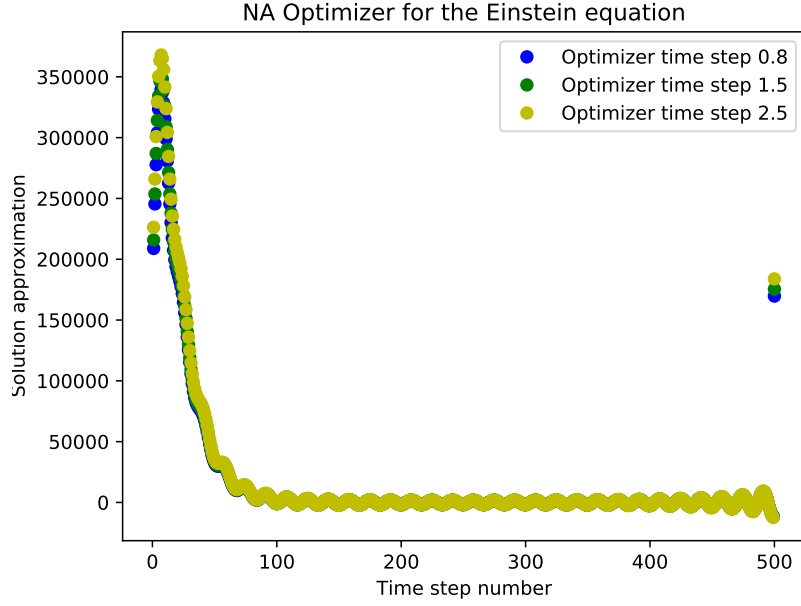


Figure 24: *Extracting measurements from the Einstein field equations with the electromagnetic stress-energy tensor with the NA stochastic optimizer.* The NA optimizer exhibits identical performance with other stochastic optimizers described in the previous figure.

## 4.5 Maxwell equations

### Cost function derivation

The time evolved variational state for components of the electric and magnetic fields whose oscillations and trajectories throughout space are governed by the Maxwell equations can be similarly obtained, in which for three degrees of freedom in standard Euclidean space, the equations take the form,

$$\left(\frac{\partial}{\partial x}, \frac{\partial}{\partial y}, \frac{\partial}{\partial z}\right) \times (E_x, E_y, E_z) = -\frac{\partial(B_x, B_y, B_z)}{\partial t}$$

↕

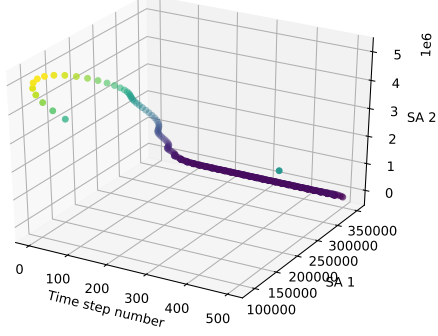
$$\mathbf{x}\left(\frac{\partial}{\partial y}E_z - \frac{\partial}{\partial z}E_y\right) - \mathbf{y}\left(\frac{\partial}{\partial x}E_z - \frac{\partial}{\partial z}E_x\right) + \mathbf{z}\left(\frac{\partial}{\partial x}E_y - \frac{\partial}{\partial y}E_x\right) = -\frac{\partial(B_x, B_y, B_z)}{\partial t}$$

Resolving the electric and magnetic fields by each component, and subsequently substituting in for the variationally prepared states for the electric field, implies,

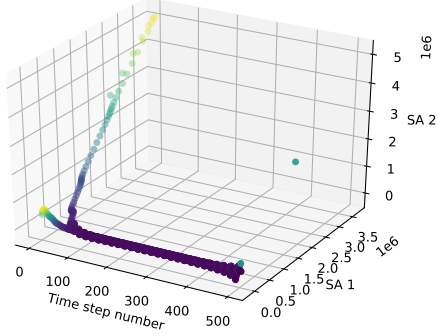
$$\begin{cases} \mathbf{x}\left(\frac{\partial}{\partial y}E_z - \frac{\partial}{\partial z}E_y\right) = -\frac{\partial B_x}{\partial t} \\ -\mathbf{y}\left(\frac{\partial}{\partial x}E_z - \frac{\partial}{\partial z}E_x\right) = -\frac{\partial B_y}{\partial t} \\ \mathbf{z}\left(\frac{\partial}{\partial x}E_y - \frac{\partial}{\partial y}E_x\right) = -\frac{\partial B_z}{\partial t} \end{cases}$$

↕

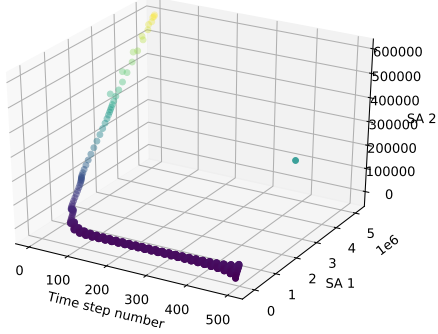
PS & Differential Evolution optimizers for the Einstein equation



Differential Evolution & Nevergran Optimizers for the Einstein equation



Differential Evolution and Nevergrad Optimizers for the Einstein equation



Differential Evolution & Nevergran Optimizers for the Einstein equation

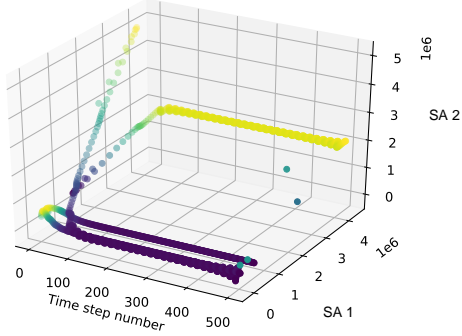
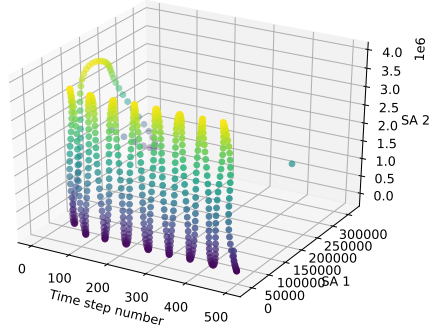
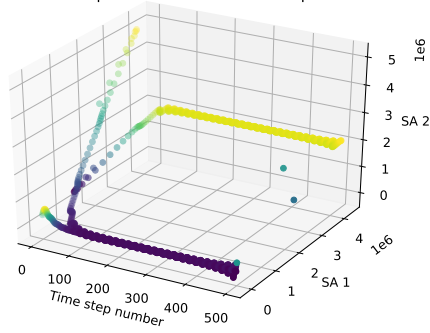


Figure 25: *Extracting measurements from the Einstein field equations with the electromagnetic stress-energy tensor.* Three-dimensional solution curves plots reveal similar characteristics of solutions described in previous figures.

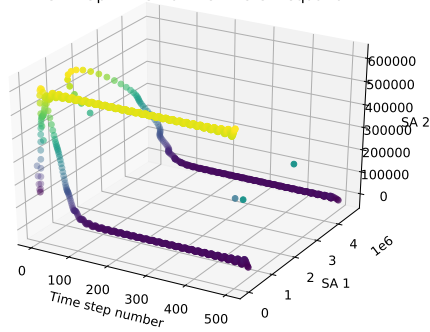
Differential Evolution Optimizer for the Einstein Equations



VD-CMA Optimizer for the Einstein equation



VD-CMA Optimizer for the Einstein equation



VD-CMA optimizer for the Einstein equation

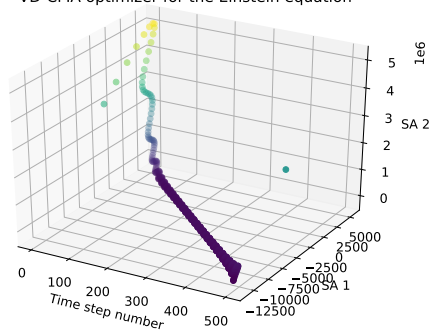
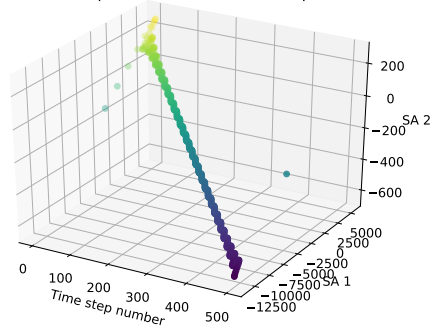
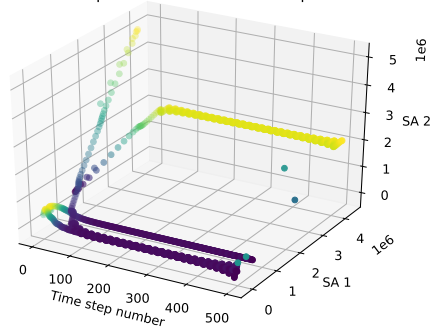


Figure 26: *Extracting measurements from the Einstein field equations with the electromagnetic stress-energy tensor.* Three-dimensional solution curves plots reveal similar characteristics of solutions described in previous figures.

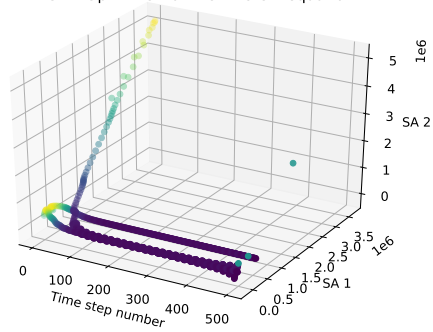
VD-CMA Optimizer for the Einstein equation



VD-CMA optimizer for the Einstein equation



VD-CMA Optimizer for the Einstein equation



VD-CMA optimizer for the Einstein equation

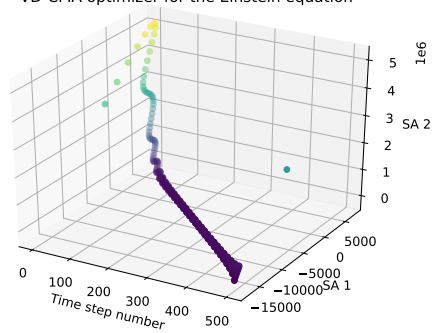
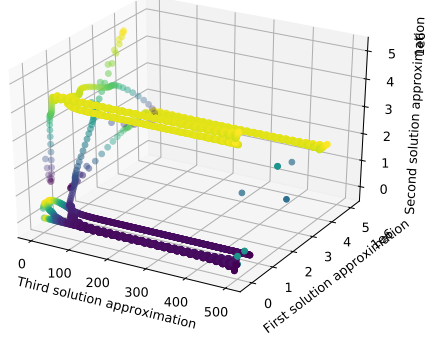
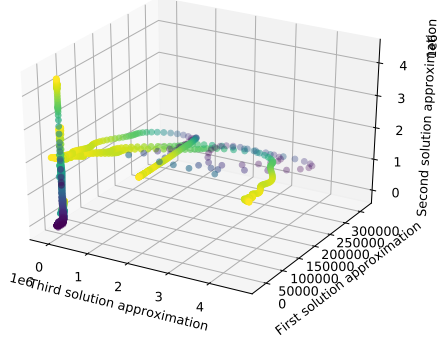


Figure 27: *Extracting measurements from the Einstein field equations with the electromagnetic stress-energy tensor.* Three-dimensional solution curves plots reveal similar characteristics of solutions described in previous figures.

VD-CMA optimizer for the Einstein equation



VD-CMA optimizer for the Einstein equation



VD-CMA Optimizer for the Einstein equation

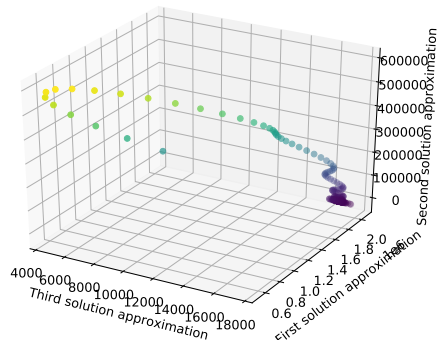
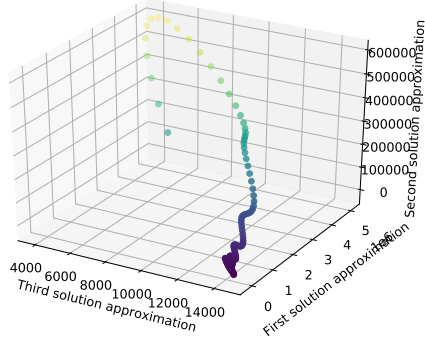
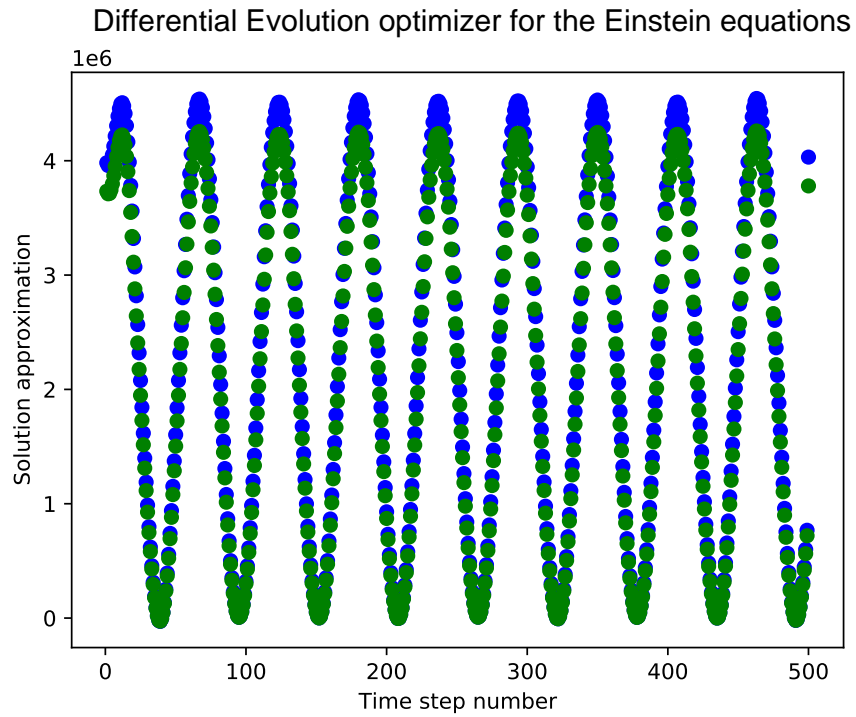


Figure 28: *Extracting measurements from the Einstein field equations for three-dimensions of motion.* Three-dimensional spatial solution curves plots reveal similar characteristics of solutions described in previous figures.



Differential Evolution Optimizer for the Einstein equation

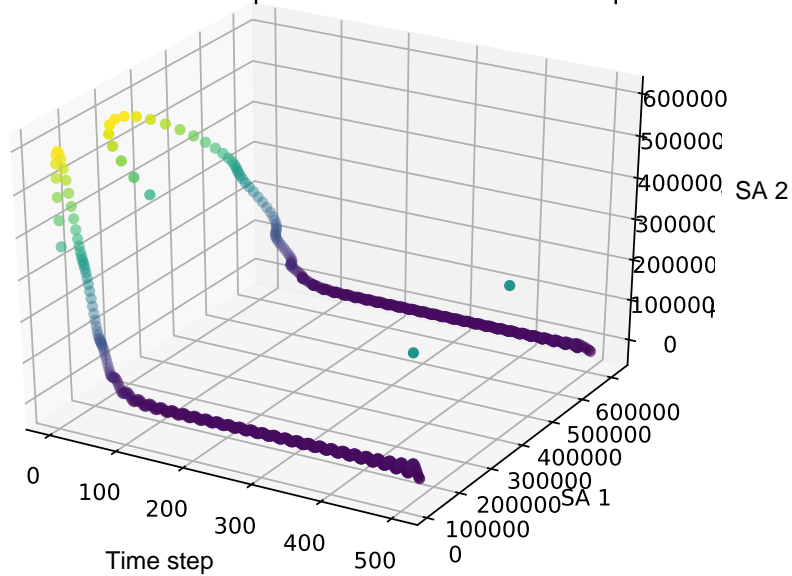


Figure 29: *Extracting measurements for sinusoidal components of solutions to the Einstein equations.* As provided in the previous figure, running additional iterations of the quantum algorithm for two ansatzes, whose ZGR parameters are deliberately chosen to be close to each other, yields two solutions curves with coinciding periods of motion.

VD-CMA Optimizer for the Einstein equation

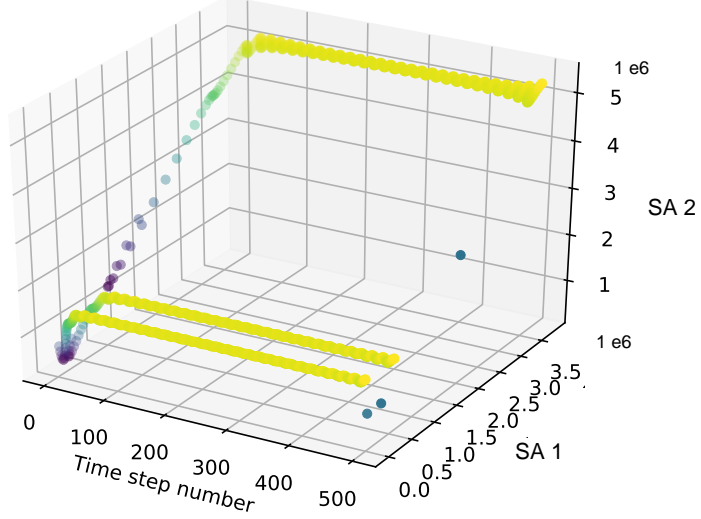


Figure 30: *Final Einstein solution approximation.*

$$\begin{cases} \mathbf{x} \left( \frac{A_y - 1}{\Delta y} |E_z\rangle - \frac{A_z - 1}{\Delta z} |E_y\rangle \right) = -\frac{1}{\tau} (|\widetilde{B}_x\rangle - |B_x\rangle) \\ -\mathbf{y} \left( \frac{A_x - 1}{\Delta x} |E_z\rangle - \frac{A_z - 1}{\Delta z} |E_x\rangle \right) = -\frac{1}{\tau} (|\widetilde{B}_y\rangle - |B_y\rangle) \\ \mathbf{z} \left( \frac{A_x - 1}{\Delta x} |E_y\rangle - \frac{A_y - 1}{\Delta y} |E_x\rangle \right) = -\frac{1}{\tau} (|\widetilde{B}_z\rangle - |B_z\rangle) \end{cases}$$

$\Updownarrow$

$$\begin{cases} -\tau \left( \frac{A_y - 1}{\Delta y} |E_z\rangle - \frac{A_z - 1}{\Delta z} |E_y\rangle \right) + |B_x\rangle = |\widetilde{B}_x\rangle \\ \tau \left( \frac{A_x - 1}{\Delta x} |E_z\rangle - \frac{A_z - 1}{\Delta z} |E_x\rangle \right) + |B_y\rangle = |\widetilde{B}_y\rangle \\ -\tau \left( \frac{A_x - 1}{\Delta x} |E_y\rangle - \frac{A_y - 1}{\Delta y} |E_x\rangle \right) + |B_z\rangle = |\widetilde{B}_z\rangle . \end{cases}$$

From variational states corresponding to the magnetic field obtained from states prepared for the electric field, substitution for components of the electric field yields the following cost function dependent on spatial derivatives of the magnetic field, whose entries read off as,

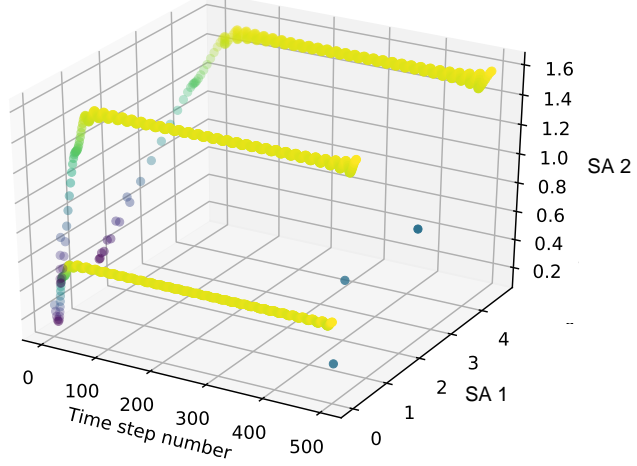
$$\underbrace{\text{Sgn}}_{=+1 \text{ for } i \text{ odd}, =-1 \text{ for } i \text{ even}} \tau \left( \frac{A_y - 1}{\Delta y} |B_y\rangle - \frac{A_z - 1}{\Delta z} |B_z\rangle \right) = \frac{\mu_0 \epsilon_0}{\tau} (|\widetilde{E}_x\rangle - |E_x\rangle) . \quad (\text{Sgn equation})$$

From the corresponding variational state for the electric field, the index  $i$  for the electric field has corresponding indices  $j$  for the magnetic field which can be read off from the table below,

$i$ (RHS of Sgn equation)	$y$	$z$	$A_y$	$A_z$	$\Delta y$	$\Delta z$
1	3	2	$A_y$	$A_z$	$\Delta y$	$\Delta z$
2	3	1	$A_x$	$A_z$	$\Delta x$	$\Delta z$
3	2	1	$A_x$	$A_y$	$\Delta x$	$\Delta y$

which provides indices for the components of the magnetic field given a component of the electric field. The resulting variational state for time evolution of the electric field forwards by  $\tau$  is,

VD-CMA Optimizer for the Einstein equation



VD-CMA Optimizer with time step 0.01

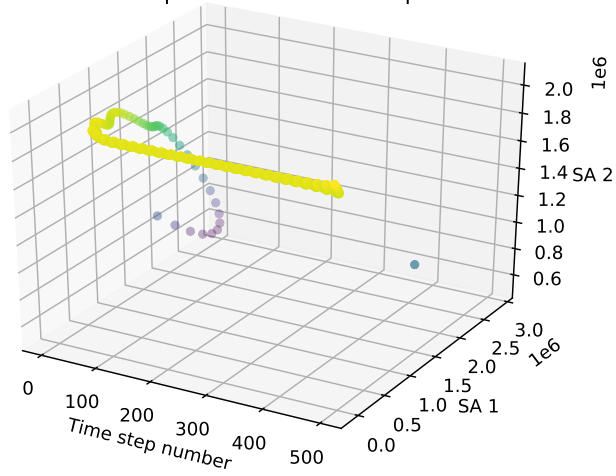


Figure 31: *Extracting measurements from the Einstein field equations with the electromagnetic stress-energy tensor.* Three-dimensional solution curves plots reveal similar characteristics of solutions described in previous figures.

$$\text{Sgn} \frac{\tau^2}{\mu_0 \epsilon_0} \left( \frac{A_y - \mathbf{1}}{\Delta y} |B_y\rangle - \frac{A_y - \mathbf{1}}{\Delta z} |B_z\rangle \right) + |E_x\rangle = |\widetilde{E_x}\rangle .$$

We obtain the cost function by expanding the following norm,

$$\begin{aligned} C_{B_x}^M(\lambda, \lambda_0^{E_y}, \lambda_1^{E_z}, \lambda_0^{M_{B_x}}) &= \left\| |\widetilde{B_x}\rangle - |B_x\rangle \right\|^2 \\ &\Downarrow \\ &\left\| -\tau \left( \frac{A_y - \mathbf{1}}{\Delta y} |E_z\rangle - \frac{A_z - \mathbf{1}}{\Delta z} |E_y\rangle \right) \right\|^2 \\ &\Downarrow \\ &(\lambda_0^{M_{B_x}})^2 + \tau^2 \left( \frac{1}{\Delta y} \langle E_z | (A_y - \mathbf{1})^\dagger - \frac{1}{\Delta z} \langle E_y | (A_z - \mathbf{1})^\dagger \right) \times \dots \\ &\quad \left( \frac{1}{\Delta y} (A_y - \mathbf{1}) |E_z\rangle - \frac{1}{\Delta z} (A_z - \mathbf{1}) |E_y\rangle \right) \\ &\Downarrow \\ &\frac{\tau^2}{(\Delta y)^2} - \frac{2\tau^2}{\Delta y \Delta z} \left( (A_y |E_z\rangle - |E_z\rangle) (A_z |E_y\rangle - |E_y\rangle) \right) + \frac{\tau^2}{(\Delta z)^2} . \end{aligned}$$

Rearrangements of the superposition scaled in the second order difference  $\Delta y \Delta z$  corresponding to the first component of the magnetic field, is of the form,

$$\langle E_y | A_z^\dagger A_y |E_z\rangle - \langle E_y | A_y |E_z\rangle - \langle E_y | A_z^\dagger |E_z\rangle + \langle E_z | |E_z\rangle .$$

From the state above, terms are rearranged further by introducing accompanying variational states for each participating component of the magnetic field. In particular, for variational parameters corresponding to the second and third components of the electric field, the superposition for the cost function is equivalent to,

$$\begin{aligned} &(\lambda_0^{M_{B_x}})^2 + \frac{\tau^2}{(\Delta y)^2} + \frac{\tau^2}{(\Delta z)^2} - \frac{2\tau^2}{\Delta y \Delta z} \text{Re} \left\{ \langle \widetilde{E_z} | | \widetilde{E_y} \rangle - \dots \right. \\ &\frac{\tau^2}{\Delta y \Delta z \mu_0 \epsilon_0} |\widetilde{E_z}\rangle \left\{ \Delta x (A_z |B_y\rangle - |B_y\rangle) - \Delta y (A_y |B_x\rangle - |B_x\rangle) \right\} + \dots \\ &\frac{\tau^2}{\Delta x \Delta y \mu_0 \epsilon_0} |\widetilde{E_y}\rangle \left\{ \Delta y (A_z |B_z\rangle - |B_z\rangle) - \Delta z (A_y |B_y\rangle - |B_y\rangle) \right\} - \dots \\ &\frac{\tau^2}{\Delta x \Delta y \mu_0 \epsilon_0} \left\{ \Delta x (A_z |B_y\rangle - |B_y\rangle) - \Delta y (A_y |B_x\rangle - |B_x\rangle) \right\} + \dots \end{aligned}$$

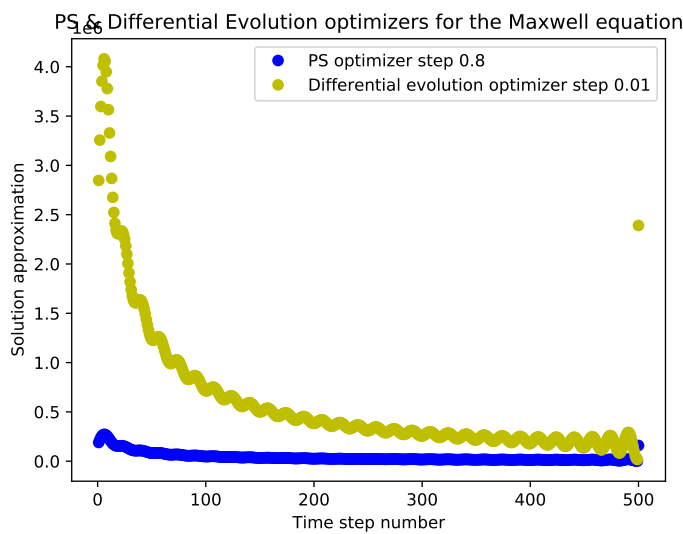
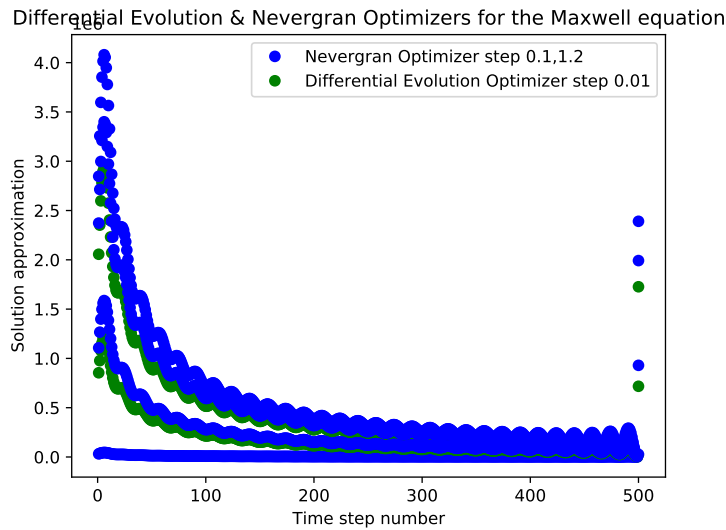
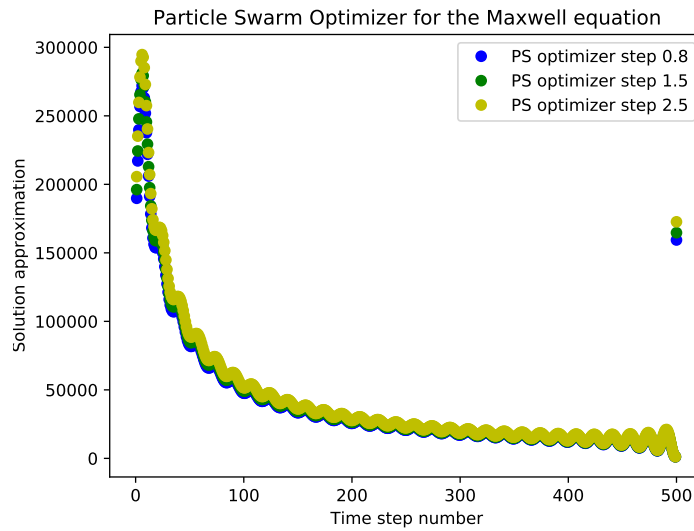


Figure 32: *Extracting measurements from the Maxwell equations.* Approximating solutions to the Maxwell equations yields solutions that appear similar to those of the Einstein equation with the electromagnetic stress-energy tensor provided in *Figure 10*, in which the solution approximation relaxes to a steady-state value as the solution state is evolved forwards in time.

Differential Evolution and Nevergrad Optimizers for the Maxwell equation

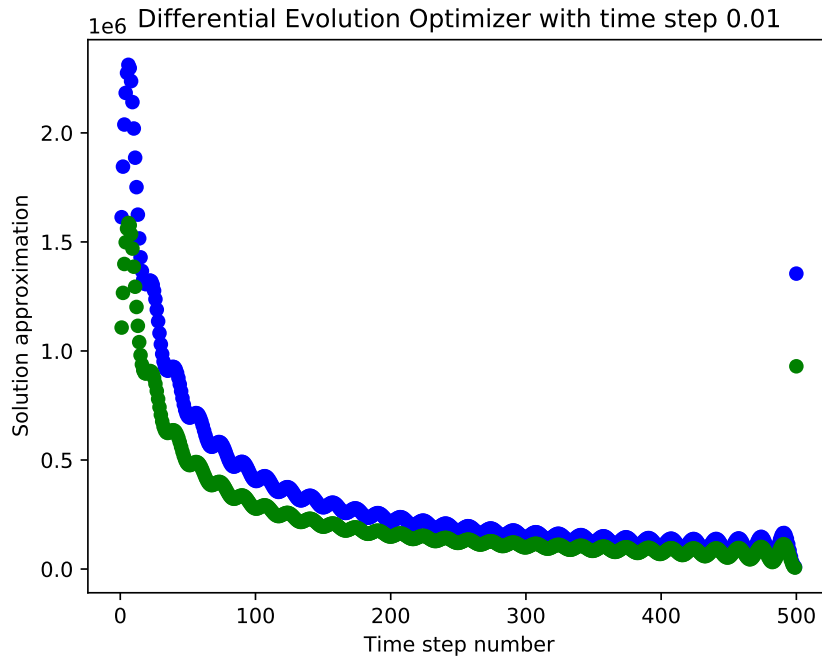
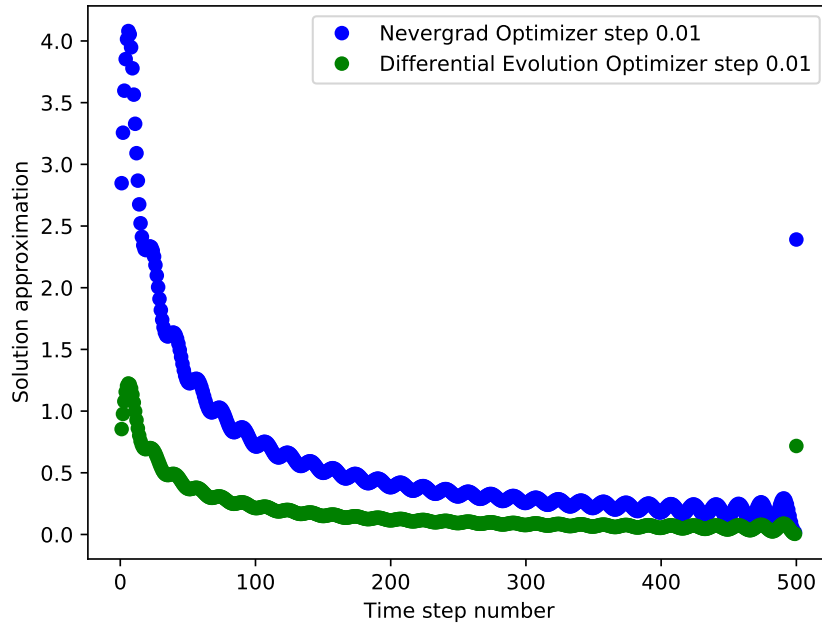
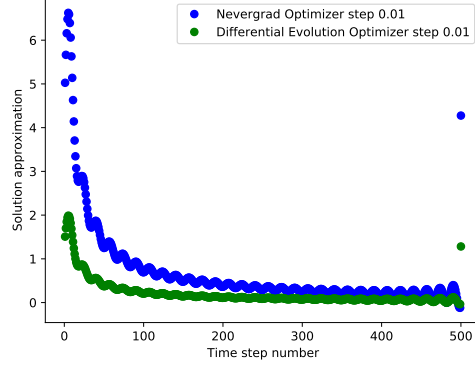
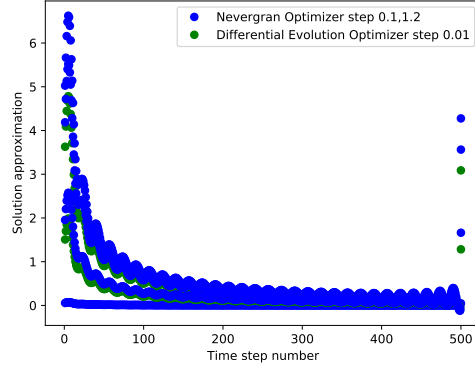


Figure 33: *Extracting measurements from the Maxwell equations.* Repeating the numerical experiments from the previous figure with the Differential Evolution and Nevergrad optimizers yields similar results.

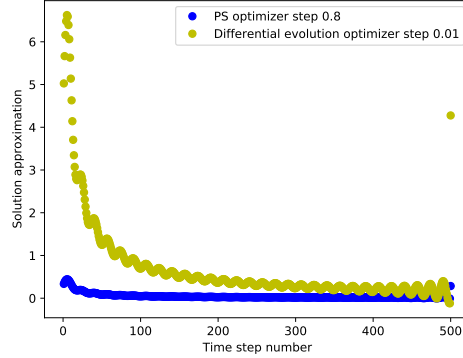
Differential Evolution and Nevergrad Optimizers for the Maxwell equation



Differential Evolution & Nevergrad Optimizers for the Maxwell equation



PS & Differential Evolution optimizers for the Maxwell equation



Particle Swarm Optimizer for the Maxwell equation

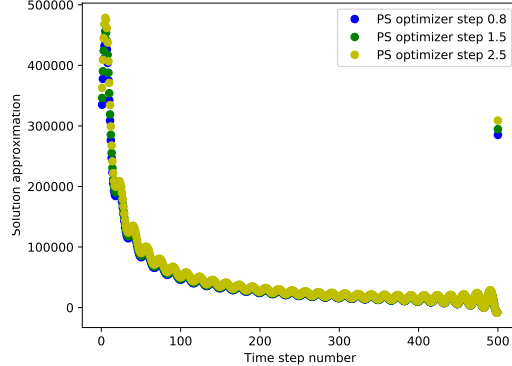


Figure 34: *Extracting measurements from the Maxwell equations with a second ZGR-QFT ansatz candidate dependent upon the potential of the electric field.* Under the Differential Evolution, Nevergrad, and Particle Swarm optimizers, the variational procedure approximates solutions which approach the steady state velocity at different exponential rates than the approximating solution curves provided in *Figure 12* and *Figure 13*.

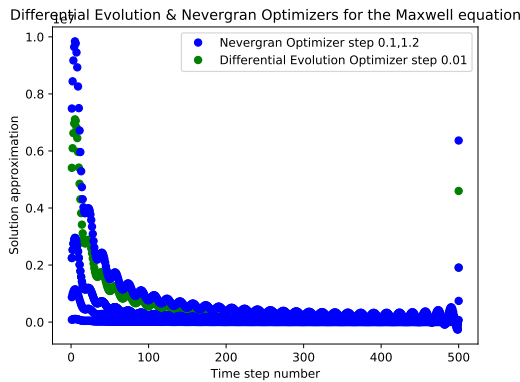
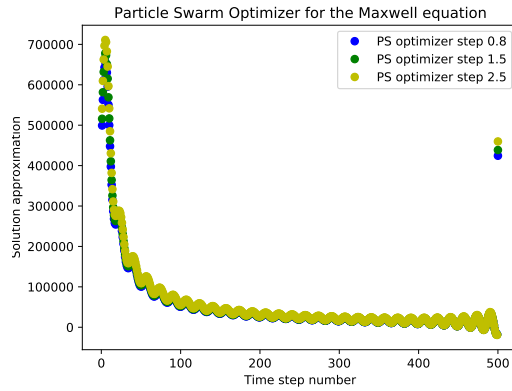
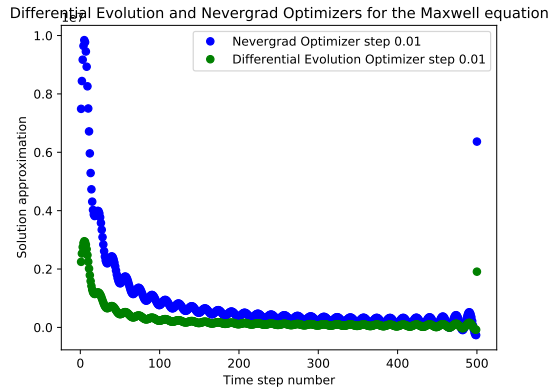
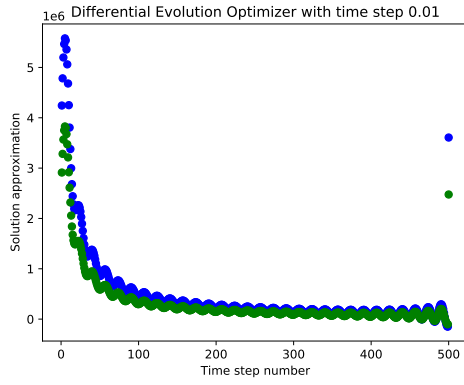


Figure 35: *Extracting measurements from the Maxwell equations with a third ZGR-QFT ansatz candidate dependent upon the potential, and upon the first derivative of the electric field.* Under the Differential Evolution, Nevergrad, and Particle Swarm optimizers, the variational procedure approximates solutions which approach the steady state velocity at different exponential rates than the approximating solution curves provided in *Figure 12* and *Figure 13*.



$$\begin{aligned} & \frac{2\tau^4}{\Delta x(\Delta y)^2 \mu_0 \epsilon_0} \langle E_{\mathbf{y}} | \widetilde{B}_{\mathbf{y}} \rangle - \frac{2\tau^4}{(\Delta y)^2 \Delta z \mu_0 \epsilon_0} A_z |E_{\mathbf{y}}\rangle + \frac{2\tau^4}{(\Delta y)^2 \Delta z \mu_0 \epsilon_0} |E_{\mathbf{y}}\rangle + \dots \\ & \frac{2\tau^4}{\Delta x \Delta y \Delta z \mu_0 \epsilon_0} A_y |E_{\mathbf{x}}\rangle - \frac{2\tau^4}{\Delta x \Delta y \Delta z \mu_0 \epsilon_0} |E_{\mathbf{z}}\rangle + \frac{2\tau^4}{\Delta y (\Delta z)^2 \mu_0 \epsilon_0} A_z |E_{\mathbf{z}}\rangle - \dots \\ & \left. \frac{2\tau^4}{\Delta y (\Delta z)^2 \mu_0 \epsilon_0} |E_{\mathbf{z}}\rangle + \frac{2\tau^4}{(\Delta y)^2 \Delta z \mu_0 \epsilon_0} A_y |E_{\mathbf{y}}\rangle - \frac{2\tau^4}{(\Delta y)^2 \Delta z \mu_0 \epsilon_0} |E_{\mathbf{y}}\rangle \right\}, \end{aligned}$$

providing the second cost function.

## 4.6 Boussinesq type equation

### Cost function derivation

The equation with smooth solutions  $u$  is,

$$\begin{aligned} & u_{tt} - u_{xx} - 2\alpha(uu_x)_x - \beta u_{xxt} = 0 \\ & \Downarrow \\ & \frac{1}{\tau^2} |u(t+2\tau)\rangle - \frac{1}{\tau^2} |u(t+\tau)\rangle - \{A_x^\dagger - 2\mathbf{1} + A_x\} |u\rangle - 2\alpha \left\{ |u\rangle \times \left\{ \frac{A_x - \mathbf{1}}{\Delta x} \right\} |u\rangle \right\}_x - \dots \\ & \frac{\beta}{(\Delta x)^2} \left\{ \{A_x^\dagger - 2\mathbf{1} + A_x\} |u\rangle \right\}_{tt} = 0. \end{aligned}$$

Differentiating the final term with respect to time yields,

$$\begin{aligned} & \frac{\beta}{(\Delta x)^2} \left\{ \frac{1}{\tau} (\{A_x^\dagger - 2\mathbf{1} + A_x\} |u(t+\tau)\rangle - \{A_x^\dagger - 2\mathbf{1} + A_x\} |u(t)\rangle) \right\}_t \\ & \Downarrow \\ & \frac{\beta}{(\Delta x)^2 \tau} \left\{ \frac{1}{\tau} (\{A_x^\dagger - 2\mathbf{1} + A_x\} |u(t+2\tau)\rangle - \{A_x^\dagger - 2\mathbf{1} + A_x\} |u(t+\tau)\rangle) - \dots \right. \\ & \left. \left\{ \{A_x^\dagger - 2\mathbf{1} + A_x\} |u(t+\tau)\rangle - \dots \{A_x^\dagger - 2\mathbf{1} + A_x\} |u(t)\rangle \right\} \right\} \end{aligned}$$

Rearranging the state before differentiation with respect to space yields,

$$\begin{aligned} & 2\alpha \left\{ |u\rangle \times \left\{ \frac{A_x - \mathbf{1}}{\Delta x} \right\} |u\rangle \right\}_x \\ & \Downarrow \\ & 2\alpha \left\{ \frac{A_x - \mathbf{1}}{\Delta x} \right\} \left\{ |u\rangle \times \left\{ \frac{A_x - \mathbf{1}}{\Delta x} \right\} |u\rangle \right\} \\ & \Downarrow \\ & 2\alpha \left\{ \frac{A_x |u\rangle - |u\rangle}{\Delta x} \times \frac{A_x |u\rangle - |u\rangle}{\Delta x} \right\} \end{aligned}$$

$$\begin{aligned}
& \Downarrow \\
& \frac{2\alpha}{(\Delta x)^2} \left\{ A_x |u\rangle \langle u| A_x^\dagger - 2A_x |u\rangle \langle u| + |u\rangle \langle u| \right\} \\
& \Downarrow \\
& \frac{4\alpha}{(\Delta x)^2} \left\{ \lambda^2 - A_x |u\rangle \langle u| \right\}
\end{aligned}$$

The time evolved variational state quadratically scaled in the time step is,

$$\begin{aligned}
\frac{1}{\tau^2} |u(t+\tau)\rangle &= \frac{1}{\tau^2} |u(t+2\tau)\rangle - A_x^\dagger |u\rangle + 2|u\rangle + A_x |u\rangle - \frac{4\alpha}{(\Delta x)^2} \left\{ \lambda^2 - A_x |u\rangle \langle u| \right\} - \dots \\
&\frac{\beta}{\tau^2(\Delta x)^2} \left\{ A_x^\dagger |u(t+2\tau)\rangle - 2|u(t+2\tau)\rangle + A_x |u(t+2\tau)\rangle - A_x^\dagger |u(t+\tau)\rangle + 2|u(t+\tau)\rangle + \dots \right. \\
&A_x |u(t+\tau)\rangle - A_x^\dagger |u(t+\tau)\rangle + 2|u(t+\tau)\rangle - A_x |u(t+\tau)\rangle - A_x^\dagger |u(t)\rangle + 2|u(t)\rangle - A_x |u(t)\rangle \left. \right\}.
\end{aligned}$$

Rescaling by  $\tau^2$  from the time evolved variational state from a previous second application of the time derivative gives,

$$\begin{aligned}
|u(t+\tau)\rangle &= |u(t+2\tau)\rangle - \left\{ \left( \frac{\beta}{(\Delta x)^2} - \tau^2 \right) A_x^\dagger + \left( 2 \frac{\beta}{(\Delta x)^2} - \frac{4\langle u|\alpha}{(\Delta x)^2} - \tau^2 \right) A_x + \dots \right. \\
&\quad \left. 2 \left( \frac{\beta}{(\Delta x)^2} - \tau^2 \right) \right\} |u\rangle - \dots \\
&\frac{4\alpha}{(\Delta x)^2} \lambda^2 - \frac{\beta}{(\Delta x)^2} \left\{ (A_x^\dagger - 2 + A_x) |u(t+2\tau)\rangle - \dots \right. \\
&\quad \left. (2A_x^\dagger - 4) |u(t+\tau)\rangle \right\}
\end{aligned}$$

Expanding the cost function yields,

$$\begin{aligned}
\mathcal{C}^B(\lambda, \lambda_0) &= \left\| |u(t+\tau)\rangle - |u(t)\rangle \right\|^2 \\
&\Downarrow \\
&\left\| |u(t+2\tau)\rangle - \dots \right. \\
&\quad \left. \left\{ \left( \frac{\beta}{(\Delta x)^2} - \tau^2 \right) A_x^\dagger + \left( 2 \frac{\beta}{(\Delta x)^2} - \frac{4\langle u|\alpha}{(\Delta x)^2} - \tau^2 \right) A_x + 2 \left( \frac{\beta}{(\Delta x)^2} - \tau^2 \right) \right\} |u\rangle - \dots \right. \\
&\quad \left. \frac{4\alpha}{(\Delta x)^2} |\lambda|^2 - \frac{\beta}{(\Delta x)^2} \left\{ (A_x^\dagger - 2 + A_x) |u(t+2\tau)\rangle - (2A_x^\dagger - 4) |u(t+\tau)\rangle \right\} - |u(t)\rangle \right\|^2.
\end{aligned}$$

Proceeding with the expansion, we collect terms from squaring the norm,

$$\left\| - \left\{ \left( \frac{\beta}{(\Delta x)^2} - \tau^2 \right) A_x^\dagger + \left( 2 \frac{\beta}{(\Delta x)^2} - 4 \frac{\langle u | \alpha}{(\Delta x)^2} - \tau^2 \right) A_x + \dots \right. \right. \\ \left. \left. 2 \left( \frac{\beta}{(\Delta x)^2} - \tau^2 - \frac{1}{2} \right) \right\} |u\rangle - \dots \right. \\ \left. \frac{\beta}{(\Delta x)^2} \left\{ \left( A_x^\dagger - 2 - \frac{(\Delta x)^2}{\beta} + A_x \right) |u(t+2\tau)\rangle - \dots \right. \right. \\ \left. \left. (2A_x^\dagger - 4) |u(t+\tau)\rangle \right\} \right\| ^2,$$

with,

$$\left\{ \left( \frac{\beta}{(\Delta x)^2} - \tau^2 \right) A_x^\dagger + \left( 2 \frac{\beta}{(\Delta x)^2} - 4 \frac{\langle u | \alpha}{(\Delta x)^2} - \tau^2 \right) A_x + \dots \right. \\ \left. 2 \left( \frac{\beta}{(\Delta x)^2} - \tau^2 - \frac{1}{2} \right) \right\} |u\rangle \left\{ \left( \frac{\beta}{(\Delta x)^2} - \tau^2 \right) A_x^\dagger \right. \\ \left. \left( 2 \frac{\beta}{(\Delta x)^2} - 4 \frac{\langle u | \alpha}{(\Delta x)^2} - \tau^2 \right) A_x + 2 \left( \frac{\beta}{(\Delta x)^2} - \tau^2 - \frac{1}{2} \right) \right\} |u\rangle ,$$

corresponding to the first term of the expansion,

$$2 \left\{ \left( \frac{\beta}{(\Delta x)^2} - \tau^2 \right) A_x^\dagger + \left( 2 \frac{\beta}{(\Delta x)^2} - 4 \frac{\langle u | \alpha}{(\Delta x)^2} - \tau^2 \right) A_x + \dots \right. \\ \left. 2 \left( \frac{\beta}{(\Delta x)^2} - \tau^2 - \frac{1}{2} \right) \right\} |u\rangle \times \dots \\ \frac{\beta}{(\Delta x)^2} \left\{ \left( A_x^\dagger - 2 - \frac{(\Delta x)^2}{\beta} + A_x \right) |u(t+2\tau)\rangle - \dots \right. \\ \left. (2A_x^\dagger - 4) |u(t+\tau)\rangle \right\} + ,$$

corresponding to the second term of the expansion, and the superposition,

$$\frac{\beta}{(\Delta x)^2} \left\{ \left( A_x^\dagger - 2 - \frac{(\Delta x)^2}{\beta} + A_x \right) |u(t+2\tau)\rangle - (2A_x^\dagger - 4) |u(t+\tau)\rangle \right\} \times \dots \\ \left\{ \left( A_x^\dagger - 2 - \frac{(\Delta x)^2}{\beta} + A_x \right) |u(t+2\tau)\rangle - (2A_x^\dagger - 4) |u(t+\tau)\rangle \right\} \\ \left\{ \left( \frac{\beta}{(\Delta x)^2} - \tau^2 \right) A_x^\dagger |u\rangle + \left( 2 \frac{\beta}{(\Delta x)^2} - 4 \frac{\langle u | \alpha}{(\Delta x)^2} - \tau^2 \right) A_x |u\rangle + \dots \right. \\ \left. 2 \left( \frac{\beta}{(\Delta x)^2} - \tau^2 - \frac{1}{2} \right) |u\rangle \right\} \left\{ \left( \frac{\beta}{(\Delta x)^2} - \tau^2 \right) A_x^\dagger |u\rangle + \dots \right. \\ \left. \left( 2 \frac{\beta}{(\Delta x)^2} - 4 \frac{\langle u | \alpha}{(\Delta x)^2} - \tau^2 \right) A_x |u\rangle + 2 \left( \frac{\beta}{(\Delta x)^2} - \tau^2 - \frac{1}{2} \right) |u\rangle \right\} ,$$

corresponding to the last term. Term by term, we continue by consolidating each prefactor for all quantum states in the superposition, in which,

$$\begin{aligned}
& \left( \frac{\beta}{(\Delta x)^2} - \tau^2 \right) A_x^\dagger |u\rangle \times \left( \frac{\beta}{(\Delta x)^2} - \tau^2 \right) A_x^\dagger |u\rangle + \dots \\
& \left( \left( \frac{\beta}{(\Delta x)^2} - \tau^2 \right) A_x^\dagger |u\rangle \right) \left( 2 \frac{\beta}{(\Delta x)^2} - 4 \dots \right. \\
& \quad \left. \frac{\langle u | \alpha}{(\Delta x)^2} - \tau^2 \right) A_x |u\rangle + \dots \\
& \left( \frac{\beta}{(\Delta x)^2} - \tau^2 \right) A_x^\dagger |u\rangle \times 2 \left( \frac{\beta}{(\Delta x)^2} - \frac{1}{2} \right) |u\rangle + \left( 2 \frac{\beta}{(\Delta x)^2} - 4 \frac{\langle u | \alpha}{(\Delta x)^2} - \tau^2 \right) A_x |u\rangle \dots \\
& \quad \left( \frac{\beta}{(\Delta x)^2} - \tau^2 \right) A_x^\dagger |u\rangle + \dots \\
& \left( 2 \frac{\beta}{(\Delta x)^2} - 4 \frac{\langle u | \alpha}{(\Delta x)^2} - \tau^2 \right) A_x |u\rangle \times \left( 2 \frac{\beta}{(\Delta x)^2} - \dots \right. \\
& \left. 4 \frac{\langle u | \alpha}{(\Delta x)^2} - \tau^2 \right) A_x |u\rangle + \left( 2 \frac{\beta}{(\Delta x)^2} - 4 \frac{\langle u | \alpha}{(\Delta x)^2} - \tau^2 \right) A_x |u\rangle \times 2 \left( \frac{\beta}{(\Delta x)^2} - \tau^2 - \frac{1}{2} \right) |u\rangle + \dots \\
& 2 \left( \frac{\beta}{(\Delta x)^2} - \tau^2 - \frac{1}{2} \right) |u\rangle \left( \frac{\beta}{(\Delta x)^2} - \tau^2 \right) A_x^\dagger |u\rangle + 2 \left( \frac{\beta}{(\Delta x)^2} - \tau^2 - \frac{1}{2} \right) |u\rangle \times \dots \\
& \quad \left( 2 \frac{\beta}{(\Delta x)^2} - 4 \frac{\langle u | \alpha}{(\Delta x)^2} - \tau^2 \right) A_x |u\rangle + \dots \\
& 2 \left( \frac{\beta}{(\Delta x)^2} - \tau^2 - \frac{1}{2} \right) |u\rangle 2 \left( \frac{\beta}{(\Delta x)^2} - \tau^2 - \frac{1}{2} \right) |u\rangle
\end{aligned}$$

for the four terms previously obtained. Next, we pursue further rearrangements by grouping together terms depending on whether a scalar prefactor is projected onto a quantum state for the solution  $u$ ,

$$\begin{aligned}
& \left( \frac{\beta}{(\Delta x)^2} - \tau^2 \right)^2 \lambda^2 + \dots \\
& \left( \frac{\beta}{(\Delta x)^2} A_x^\dagger |u\rangle - \tau^2 A_x^\dagger |u\rangle \right) \left( \frac{2\beta}{(\Delta x)^2} A_x |u\rangle - \dots \right. \\
& \quad \left. \frac{4 \langle u | \alpha}{(\Delta x)^2} A_x |u\rangle - \tau^2 A_x |u\rangle \right) + \dots \\
& \left( \frac{\beta}{(\Delta x)^2} A_x^\dagger |u\rangle - \tau^2 A_x^\dagger |u\rangle \right) \left( \frac{2\beta}{(\Delta x)^2} |u\rangle - |u\rangle \right) + \dots \\
& \left( 2 \frac{\beta}{(\Delta x)^2} A_x |u\rangle - 4 \frac{\langle u | \alpha}{(\Delta x)^2} A_x |u\rangle - \tau^2 A_x |u\rangle \right) \left( \frac{\beta}{(\Delta x)^2} A_x |u\rangle - \tau^2 A_x |u\rangle \right) + \dots \\
& \lambda^2 \left( 2 \frac{\beta}{(\Delta x)^2} - 4 \frac{\langle u | \alpha}{(\Delta x)^2} - \tau^2 \right) \left( 2 \frac{\beta}{(\Delta x)^2} - 4 \frac{\langle u | \alpha}{(\Delta x)^2} - \tau^2 \right) \\
& \quad \Downarrow \\
& \left( \frac{\beta}{(\Delta x)^2} - \tau^2 \right)^2 \lambda^2 + \frac{\beta}{(\Delta x)^2} A_x^\dagger |u\rangle \frac{2\beta}{(\Delta x)^2} A_x |u\rangle - \frac{\beta}{(\Delta x)^2} A_x^\dagger |u\rangle \frac{4 \langle u | \alpha}{(\Delta x)^2} A_x |u\rangle \dots \\
& - \frac{\beta}{(\Delta x)^2} A_x^\dagger |u\rangle \tau^2 A_x |u\rangle - \tau^2 A_x^\dagger |u\rangle \frac{2\beta}{(\Delta x)^2} A_x |u\rangle + \tau^2 A_x^\dagger |u\rangle \frac{4 \langle u | \alpha}{(\Delta x)^2} A_x |u\rangle + 2 \tau^4 \langle u | A_x^\dagger A_x^\dagger |u\rangle \\
& 2 \left\{ \left( \frac{\beta}{(\Delta x)^2} - \tau^2 \right) A_x^\dagger + \left( 2 \frac{\beta}{(\Delta x)^2} - 4 \frac{\langle u | \alpha}{(\Delta x)^2} - \tau^2 \right) A_x + 2 \left( \frac{\beta}{(\Delta x)^2} - \tau^2 - \frac{1}{2} \right) \right\} |u\rangle \times \dots \\
& \quad \frac{\beta}{(\Delta x)^2} \left\{ \left( A_x^\dagger - 2 - \frac{(\Delta x)^2}{\beta} + A_x \right) |u(t+2\tau)\rangle - \left( 2A_x^\dagger - 4 \right) |u(t+\tau)\rangle \right\}.
\end{aligned}$$

Grouping together expectation terms into several quantum superposition takes the form,

$$\begin{aligned}
& 2 \left\{ \frac{\beta}{(\Delta x)^2} A_x^\dagger |u\rangle - \tau^2 A_x^\dagger |u\rangle + 2 \frac{\beta}{(\Delta x)^2} A_x |u\rangle - 4 \frac{\langle u | \alpha}{(\Delta x)^2} A_x |u\rangle - \tau^2 A_x |u\rangle + \dots \right. \\
& \qquad \qquad \qquad \left. 2 \frac{\beta}{(\Delta x)^2} |u\rangle - \tau^2 |u\rangle - |u\rangle \right\} \times \dots \\
& \qquad \qquad \qquad \left\{ \frac{\beta}{(\Delta x)^2} A_x^\dagger |u(t+2\tau)\rangle - \frac{2\beta}{(\Delta x)^2} |u(t+2\tau)\rangle - \dots \right. \\
& \qquad \qquad \qquad |u(t+2\tau)\rangle + \frac{\beta}{(\Delta x)^2} A_x |u(t+2\tau)\rangle - \frac{2\beta}{(\Delta x)^2} |u(t+\tau)\rangle + \dots \\
& \qquad \qquad \qquad \left. \frac{4\beta}{(\Delta x)^2} |u(t+\tau)\rangle \right\} \dots \\
& \frac{\beta}{(\Delta x)^2} \left\{ (A_x^\dagger - 2 - \frac{(\Delta x)^2}{\beta} + A_x) |u(t+2\tau)\rangle - (2A_x^\dagger - 4) |u(t+\tau)\rangle \right\} \times \dots \\
& \qquad \qquad \qquad \frac{\beta}{(\Delta x)^2} \left\{ A_x^\dagger |u(t+2\tau)\rangle - 2 |u(t+2\tau)\rangle + \dots \right. \\
& \qquad \qquad \qquad \left. A_x |u(t+2\tau)\rangle - |u(t+2\tau)\rangle - 2A_x^\dagger |u(t+\tau)\rangle + 4 |u(t+\tau)\rangle \right\}.
\end{aligned}$$

For fixed  $\beta$ , given the spatial increment associated with the second partial derivative with respect to space, the superposition takes the form,

$$\begin{aligned}
& \left( \frac{\beta}{(\Delta x)^2} \right)^2 \left\{ (A_x^\dagger - 2 - \frac{(\Delta x)^2}{\beta} + A_x) |u(t+2\tau)\rangle \times (A_x^\dagger - 2 - \frac{(\Delta x)^2}{\beta} + A_x) |u(t+2\tau)\rangle - 2 \dots \right. \\
& \qquad \qquad \qquad (A_x^\dagger - 2 - \frac{(\Delta x)^2}{\beta} + A_x) |u(t+2\tau)\rangle \times (2A_x^\dagger - 4) |u(t+\tau)\rangle + \dots \\
& \qquad \qquad \qquad \left. (2A_x^\dagger - 4) |u(t+\tau)\rangle \times (2A_x^\dagger - 4) |u(t+\tau)\rangle \right\},
\end{aligned}$$

which is equivalent to,

$$\begin{aligned}
& \left( \frac{\beta}{(\Delta x)^2} \right)^2 \left\{ (A_x^\dagger - 2 - \frac{(\Delta x)^2}{\beta}) |u(t+2\tau)\rangle \times (A_x^\dagger - 2 - \frac{\beta}{(\Delta x)^2} + A_x) |u(t+2\tau)\rangle + A_x |u(t+2\tau)\rangle \times \dots \right. \\
& \qquad \qquad \qquad (A_x^\dagger - 2 - \frac{(\Delta x)^2}{\beta} + A_x) |u(t+2\tau)\rangle - \dots \\
& \qquad \qquad \qquad A_x^\dagger |u(t+\tau)\rangle (2A_x^\dagger - 4) |u(t+\tau)\rangle - (2 + \frac{\beta}{(\Delta x)^2}) |u(t+2\tau)\rangle (2A_x^\dagger - 4) |u(t+\tau)\rangle + \dots \\
& \qquad \qquad \qquad A_x |u(t+2\tau)\rangle (2A_x^\dagger - 4) |u(t+\tau)\rangle + \dots \\
& \qquad \qquad \qquad \left. (2A_x^\dagger |u(t+\tau)\rangle - 4 |u(t+\tau)\rangle) (2A_x^\dagger |u(t+\tau)\rangle - 4 |u(t+\tau)\rangle) \right\}.
\end{aligned}$$

From the superposition state, expectation terms of time evolved variational states can be multiplied onto other time evolved variational states, as,

$$\begin{aligned}
& \left( \frac{\beta}{(\Delta x)^2} \right)^2 \left\{ \left( A_x^\dagger |u(t+2\tau)\rangle - 2|u(t+2\tau)\rangle - \frac{(\Delta x)^2}{\beta} |u(t+2\tau)\rangle \right) \times \dots \right. \\
& \left( A_x^\dagger |u(t+2\tau)\rangle - 2|u(t+2\tau)\rangle - \frac{\beta}{(\Delta x)^2} |u(t+2\tau)\rangle + A_x |u(t+2\tau)\rangle \right) + \dots \\
& \left( A_x |u(t+2\tau)\rangle A_x^\dagger |u(t+2\tau)\rangle - 2A_x |u(t+2\tau)\rangle - A_x |u(t+2\tau)\rangle \frac{(\Delta x)^2}{\beta} |u(t+2\tau)\rangle \right) - \dots \\
& \quad A_x^\dagger |u(t+\tau)\rangle (2A_x^\dagger |u(t+\tau)\rangle - 4|u(t+\tau)\rangle) - \dots \\
& \quad \left( 2 + \frac{\beta}{(\Delta x)^2} \right) |u(t+2\tau)\rangle (2A_x^\dagger |u(t+\tau)\rangle - 4|u(t+\tau)\rangle) + \dots \\
& \quad A_x |u(t+2\tau)\rangle 2A_x^\dagger |u(t+\tau)\rangle - A_x |u(t+2\tau)\rangle 4|u(t+\tau)\rangle + \dots \\
& \left. 4|\lambda|^2 - 2A_x^\dagger |u(t+\tau)\rangle 4|u(t+\tau)\rangle - 4|u(t+\tau)\rangle 2A_x^\dagger |u(t+\tau)\rangle - 16\lambda^2 \right\}.
\end{aligned}$$

The resultant superposition is,

$$\begin{aligned}
& \left( \frac{\beta}{(\Delta x)^2} \right)^2 \left\{ \left( A_x^\dagger |u(t+2\tau)\rangle - 2|u(t+2\tau)\rangle - \frac{(\Delta x)^2}{\beta} |u(t+2\tau)\rangle \right) \left( A_x^\dagger |u(t+2\tau)\rangle - 2|u(t+2\tau)\rangle - \dots \right. \right. \\
& \quad \left. \left. \frac{\beta}{(\Delta x)^2} |u(t+2\tau)\rangle \right) + \dots \right. \\
& \quad \left( A_x^\dagger |u(t+2\tau)\rangle - 2|u(t+2\tau)\rangle - \frac{(\Delta x)^2}{\beta} |u(t+2\tau)\rangle \right) A_x |u(t+2\tau)\rangle + \dots \\
& \quad \left( A_x |u(t+2\tau)\rangle A_x^\dagger - 2A_x - A_x |u(t+2\tau)\rangle \frac{(\Delta x)^2}{\beta} \right) |u(t+2\tau)\rangle - \dots \\
& \quad \left( A_x^\dagger |u(t+\tau)\rangle 2A_x^\dagger - 4 - \left( 2 + \frac{\beta}{(\Delta x)^2} + \dots \right. \right. \\
& \quad \left. \left. 4A_x \right) |u(t+2\tau)\rangle 2A_x^\dagger + \left( 2 + \frac{\beta}{(\Delta x)^2} \right) 4|u(t+2\tau)\rangle - \dots \right. \\
& \quad \left. A_x |u(t+2\tau)\rangle 2A_x^\dagger - 8A_x^\dagger |u(t+\tau)\rangle \right) |u(t+\tau)\rangle - 12\lambda^2 \left. \right\}
\end{aligned}$$

The desired superposition now takes the form,

$$\begin{aligned}
& \left( \frac{\beta}{(\Delta x)^2} \right)^2 \left\{ \left( A_x^\dagger |u(t+2\tau)\rangle - 2|u(t+2\tau)\rangle \right) \dots \right. \\
& \quad \left( A_x^\dagger |u(t+2\tau)\rangle - 2|u(t+2\tau)\rangle - \dots \right. \\
& \quad \left. \frac{\beta}{(\Delta x)^2} |u(t+2\tau)\rangle \right) - \dots \\
& \quad \frac{(\Delta x)^2}{\beta} |u(t+2\tau)\rangle \left( A_x^\dagger |u(t+2\tau)\rangle - 2|u(t+2\tau)\rangle - \dots \right. \\
& \quad \left. \frac{\beta}{(\Delta x)^2} |u(t+2\tau)\rangle \right) + \dots \\
& \quad \left( A_x^\dagger |u(t+2\tau)\rangle A_x - \dots \right. \\
& \quad \left. 2|u(t+2\tau)\rangle A_x - \frac{(\Delta x)^2}{\beta} |u(t+2\tau)\rangle A_x + A_x |u(t+2\tau)\rangle A_x^\dagger - 2A_x - \dots \right. \\
& \quad \left. A_x |u(t+2\tau)\rangle \frac{(\Delta x)^2}{\beta} |u(t+2\tau)\rangle - 12\lambda^2 \right\},
\end{aligned}$$

leading to the following state,

$$\begin{aligned} & \left( \frac{\beta}{(\Delta x)^2} \right)^2 \left\{ \lambda^2 - A_x^\dagger |u(t+2\tau)\rangle 2 |u(t+2\tau)\rangle - \dots \right. \\ & A_x^\dagger |u(t+2\tau)\rangle \frac{\beta}{(\Delta x)^2} |u(t+2\tau)\rangle - 2 |u(t+2\tau)\rangle A_x^\dagger |u(t+2\tau)\rangle + \dots \\ & \quad \left. 4\lambda^2 + 2 |u(t+2\tau)\rangle \frac{\beta}{(\Delta x)^2} |u(t+2\tau)\rangle - \dots \right. \\ & \left. \frac{(\Delta x)^2}{\beta} |u(t+2\tau)\rangle A_x^\dagger |u(t+2\tau)\rangle - 2 \frac{(\Delta x)^2}{\beta} \lambda^2 + \lambda^2 - 12\lambda^2 \right\} \end{aligned}$$

The superposition above is equivalent to,

$$\begin{aligned} & \left( \frac{\beta}{(\Delta x)^2} \right)^2 \left\{ - \left( 6 + 2 \frac{(\Delta x)^2}{\beta} \right) \lambda^2 + (A_x^\dagger |u(t+2\tau)\rangle A_x - 2 |u(t+2\tau)\rangle A_x - \frac{(\Delta x)^2}{\beta} |u(t+2\tau)\rangle A_x + \dots \right. \\ & \quad \left. A_x |u(t+2\tau)\rangle A_x^\dagger - \dots \right. \\ & \quad \left. 2A_x - A_x |u(t+2\tau)\rangle \frac{(\Delta x)^2}{\beta} - 2A_x^\dagger |u(t+2\tau)\rangle - A_x^\dagger \frac{\beta}{(\Delta x)^2} |u(t+2\tau)\rangle - \dots \right. \\ & \quad \left. 2 |u(t+2\tau)\rangle A_x^\dagger + 2 \frac{\beta}{(\Delta x)^2} |u(t+2\tau)\rangle - \frac{(\Delta x)^2}{\beta} |u(t+2\tau)\rangle A_x^\dagger \right) |u(t+2\tau)\rangle - \dots \\ & \quad \left. (A_x^\dagger |u(t+\tau)\rangle 2A_x^\dagger - 4 - \left( 2 + \frac{\beta}{(\Delta x)^2} + 4A_x \right) |u(t+2\tau)\rangle 2A_x^\dagger + \dots \right. \\ & \quad \left. \left( 2 + \frac{\beta}{(\Delta x)^2} \right) 4 |u(t+2\tau)\rangle - A_x |u(t+2\tau)\rangle 2A_x^\dagger - \dots \right. \\ & \quad \left. 8A_x^\dagger |u(t+\tau)\rangle \right) |u(t+\tau)\rangle \left. \right\} \end{aligned}$$

Rearrangements of the last term of the expansion yield,

$$\begin{aligned} & \frac{\beta}{(\Delta x)^2} \left\{ (A_x^\dagger - 2 - \frac{(\Delta x)^2}{\beta} + A_x) |u(t+2\tau)\rangle - \right. \\ & \left. (2A_x^\dagger - 4) |u(t+\tau)\rangle \right\} \left\{ (A_x^\dagger - 2 - \frac{(\Delta x)^2}{\beta} + A_x) |u(t+2\tau)\rangle - (2A_x^\dagger - 4) |u(t+\tau)\rangle \right\} \\ & \quad \Downarrow \\ & \frac{\beta}{(\Delta x)^2} \left\{ A_x^\dagger |u(t+2\tau)\rangle - 2 |u(t+2\tau)\rangle - \dots \right. \\ & \quad \left. \frac{(\Delta x)^2}{\beta} |u(t+2\tau)\rangle + \dots A_x |u(t+2\tau)\rangle \right\} \times \dots \\ & \left\{ A_x^\dagger |u(t+2\tau)\rangle - 2 |u(t+2\tau)\rangle - \frac{(\Delta x)^2}{\beta} |u(t+2\tau)\rangle + A_x |u(t+2\tau)\rangle - \dots \right. \\ & \quad \left. 2A_x^\dagger |u(t+\tau)\rangle + 4 |u(t+\tau)\rangle \right\} \\ & \quad \Downarrow \\ & \frac{\beta}{(\Delta x)^2} \left\{ (A_x^\dagger |u(t+2\tau)\rangle - \dots \right. \\ & \quad \left. 2 |u(t+2\tau)\rangle - \frac{(\Delta x)^2}{\beta} |u(t+2\tau)\rangle \right) \left\{ A_x^\dagger |u(t+2\tau)\rangle - 2 |u(t+\tau)\rangle \dots \right. \\ & \quad \left. - \frac{(\Delta x)^2}{\beta} |u(t+2\tau)\rangle + A_x |u(t+2\tau)\rangle - 2A_x^\dagger |u(t+2\tau)\rangle + 4 |u(t+\tau)\rangle \right\} + \dots \end{aligned}$$

$$A_x |u(t+2\tau)\rangle \left\{ A_x^\dagger |u(t+2\tau)\rangle - 2 |u(t+2\tau)\rangle - \frac{(\Delta x)^2}{\beta} |u(t+2\tau)\rangle + \dots \right. \\ \left. A_x |u(t+2\tau)\rangle - 2A_x^\dagger |u(t+\tau)\rangle + 4 |u(t+\tau)\rangle \right\}$$

Further distributing terms,

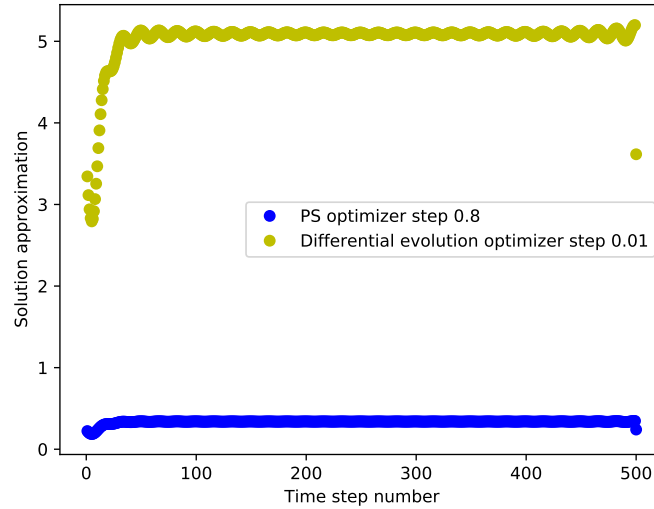
$$\frac{\beta}{(\Delta x)^2} \left\{ (A_x^\dagger |u(t+2\tau)\rangle - 2 |u(t+2\tau)\rangle) \times \dots \right. \\ \left\{ A_x^\dagger |u(t+2\tau)\rangle - 2 |u(t+\tau)\rangle - \frac{(\Delta x)^2}{\beta} |u(t+2\tau)\rangle + A_x |u(t+2\tau)\rangle - 2A_x^\dagger |u(t+2\tau)\rangle + \dots \right. \\ \left. 4 |u(t+\tau)\rangle \right\} - \dots \\ \frac{(\Delta x)^2}{\beta} |u(t+2\tau)\rangle \left\{ A_x^\dagger |u(t+2\tau)\rangle - 2 |u(t+\tau)\rangle - \frac{(\Delta x)^2}{\beta} |u(t+2\tau)\rangle + \dots \right. \\ \left. + A_x |u(t+2\tau)\rangle - 2A_x^\dagger |u(t+2\tau)\rangle + 4 |u(t+\tau)\rangle \right\} + \dots \\ A_x |u(t+2\tau)\rangle A_x^\dagger |u(t+2\tau)\rangle - A_x |u(t+2\tau)\rangle 2 |u(t+2\tau)\rangle - \dots \\ A_x |u(t+2\tau)\rangle \frac{(\Delta x)^2}{\beta} |u(t+2\tau)\rangle + \lambda^2 - A_x |u(t+2\tau)\rangle 2A_x^\dagger |u(t+\tau)\rangle + \dots \\ A_x |u(t+2\tau)\rangle 4 |u(t+\tau)\rangle \left. \right\}$$

Continuing, we group together several product states of variational states for the solution time evolved forwards one or two time steps,

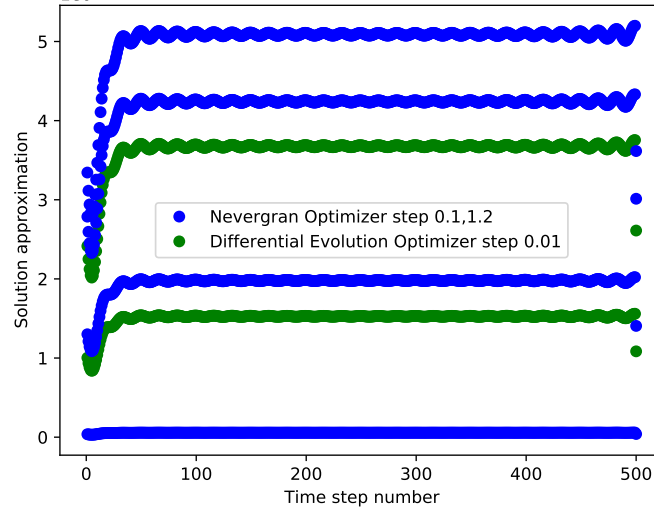
$$\frac{\beta}{(\Delta x)^2} \left\{ \lambda^2 - A_x^\dagger |u(t+2\tau)\rangle 2 |u(t+\tau)\rangle - A_x^\dagger |u(t+2\tau)\rangle \frac{(\Delta x)^2}{\beta} |u(t+2\tau)\rangle + \dots \right. \\ A_x^\dagger |u(t+2\tau)\rangle A_x |u(t+2\tau)\rangle - A_x^\dagger |u(t+2\tau)\rangle 2A_x^\dagger |u(t+2\tau)\rangle + A_x^\dagger |u(t+2\tau)\rangle 4 |u(t+\tau)\rangle - \dots \\ \left. 2 |u(t+2\tau)\rangle_x^\dagger |u(t+2\tau)\rangle + 4\lambda^2 + \dots \right. \\ 2 |u(t+\tau)\rangle \frac{(\Delta x)^2}{\beta} |u(t+2\tau)\rangle - 2 |u(t+2\tau)\rangle A_x |u(t+2\tau)\rangle + 2 |u(t+2\tau)\rangle 2A_x^\dagger |u(t+2\tau)\rangle - 8\lambda^2 - \dots \\ \frac{(\Delta x)^2}{\beta} |u(t+2\tau)\rangle A_x^\dagger |u(t+2\tau)\rangle - \frac{(\Delta x)^2}{\beta} |u(t+2\tau)\rangle 2 |u(t+\tau)\rangle - \left( \frac{(\Delta x)^2}{\beta} \right)^2 \lambda^2 + \dots \\ \left. \frac{(\Delta x)^2}{\beta} |u(t+2\tau)\rangle A_x |u(t+2\tau)\rangle - \frac{(\Delta x)^2}{\beta} |u(t+2\tau)\rangle 2A_x^\dagger |u(t+2\tau)\rangle - \frac{(\Delta x)^2}{\beta} |u(t+2\tau)\rangle 4 |u(t+\tau)\rangle \right\} \\ \Downarrow \\ \frac{\beta}{(\Delta x)^2} \left\{ \lambda^2 - (A_x^\dagger |u(t+2\tau)\rangle 2 - A_x^\dagger |u(t+2\tau)\rangle 4 + \frac{(\Delta x)^2}{\beta} |u(t+2\tau)\rangle 2) |u(t+\tau)\rangle - \dots \right. \\ (A_x^\dagger |u(t+2\tau)\rangle) \frac{(\Delta x)^2}{\beta} - A_x^\dagger |u(t+2\tau)\rangle - A_x^\dagger |u(t+2\tau)\rangle 2A_x^\dagger 2 |u(t+2\tau)\rangle A_x^\dagger + \dots \\ \left. 2 |u(t+\tau)\rangle \frac{(\Delta x)^2}{\beta} - 2 |u(t+2\tau)\rangle A_x - 2 |u(t+2\tau)\rangle 2A_x^\dagger + \frac{(\Delta x)^2}{\beta} |u(t+2\tau)\rangle A_x^\dagger - \dots \right. \\ \left. \frac{(\Delta x)^2}{\beta} |u(t+2\tau)\rangle A_x + \frac{(\Delta x)^2}{\beta} |u(t+2\tau)\rangle 2A_x^\dagger \right) |u(t+2\tau)\rangle \left. \right\}$$

The resulting cost function is factorized according to the time step that the variational state for the solution of the nonlinear problem is evolved forwards by,

PS & Differential Evolution optimizers for the Boussinesq-type equation



Differential Evolution & Nevergran Optimizers for the Boussinesq-type equation



Particle Swarm Optimizer for the Boussinesq-type equation

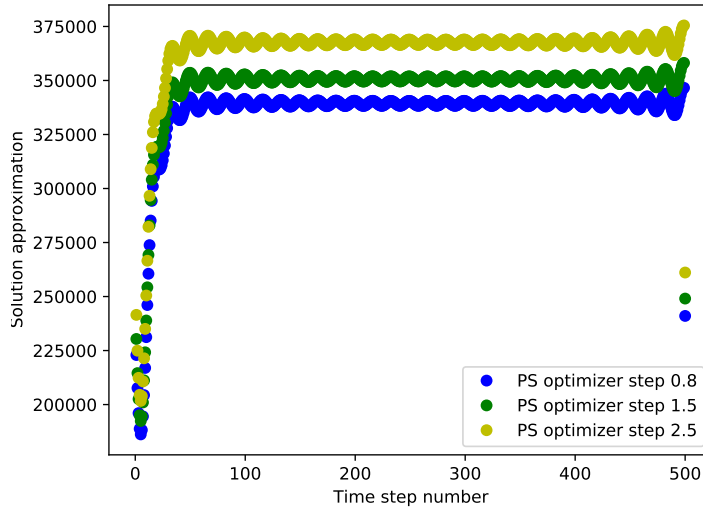


Figure 36: *Extracting measurements from the Boussinesq-type equation.* Approximating solutions to the Boussinesq equation yields solutions that are qualitatively similar to those obtained from the Einstein equations with the electromagnetic stress-energy tensor provided in *Figure 11*.

$$\begin{aligned}
\boxed{\mathcal{C}^B(\lambda, \lambda_0^B)} &= \left(\lambda_0^B\right)^2 + \text{Re} \left\{ 2 \left(\frac{\beta}{(\Delta x)^2}\right)^2 \langle \tilde{u} | A_x^\dagger | \tilde{u} \rangle - 2 \left(\frac{\beta}{(\Delta x)^2}\right)^2 \frac{(\Delta x)^2}{\beta} \langle \tilde{u} | \tilde{u} \rangle - 2 \left(\frac{\beta}{(\Delta x)^2}\right)^2 \times \dots \right. \\
&\quad \langle \tilde{u} | A_x A_x^\dagger | \tilde{u} \rangle + 2 \left(\frac{\beta}{(\Delta x)^2}\right)^2 \left(2 + \frac{\beta}{(\Delta x)^2}\right) \langle \tilde{u} | A_x | \tilde{u} \rangle + 4 \left(\frac{\beta}{(\Delta x)^2}\right)^2 \langle \tilde{u} | A_x A_x | \tilde{u} \rangle - \dots \\
&\quad 4 \left(\frac{\beta}{(\Delta x)^2}\right)^2 \left(2 + \frac{\beta}{(\Delta x)^2}\right) \langle \tilde{u} | \tilde{u} \rangle + 2 \left(\frac{\beta}{(\Delta x)^2}\right)^2 \langle \tilde{u} | A_x A_x | \tilde{u} \rangle + 8 \left(\frac{\beta}{(\Delta x)^2}\right)^2 \langle \tilde{u} | A_x^\dagger | \tilde{u} \rangle - \dots \\
&\quad \left(\frac{\beta}{(\Delta x)^2}\right)^2 \langle \tilde{u} | A_x^\dagger A_x^\dagger | \tilde{u} \rangle + 2 \left(\frac{\beta}{(\Delta x)^2}\right)^2 \langle \tilde{u} | A_x^\dagger | \tilde{u} \rangle + \left(\frac{\beta}{(\Delta x)^2}\right)^2 \frac{(\Delta x)^2}{\beta} \langle \tilde{u} | A_x^\dagger | \tilde{u} \rangle - \dots \\
&\quad \left(\frac{\beta}{(\Delta x)^2}\right)^2 \langle \tilde{u} | A_x^\dagger A_x | \tilde{u} \rangle - \left(\frac{\beta}{(\Delta x)^2}\right)^2 \langle \tilde{u} | A_x A_x | \tilde{u} \rangle + 2 \left(\frac{\beta}{(\Delta x)^2}\right)^2 A_x | \tilde{u} \rangle + \dots \\
&\quad \left(\frac{\beta}{(\Delta x)^2}\right)^2 \frac{(\Delta x)^2}{\beta} \langle \tilde{u} | A_x | \tilde{u} \rangle - 2 \left(\frac{\beta}{(\Delta x)^2}\right)^2 \langle \tilde{u} | A_x^\dagger | \tilde{u} \rangle - \left(\frac{\beta}{(\Delta x)^2}\right)^3 \langle \tilde{u} | A_x^\dagger | \tilde{u} \rangle + \dots \\
&\quad 2 \left(\frac{\beta}{(\Delta x)^2}\right)^2 \langle \tilde{u} | A_x | \tilde{u} \rangle - 2 \left(\frac{\beta}{(\Delta x)^2}\right)^3 \langle \tilde{u} | \tilde{u} \rangle + \left(\frac{\beta}{(\Delta x)^2}\right) \langle \tilde{u} | A_x | \tilde{u} \rangle + \dots \\
&\quad \left(\frac{\beta}{(\Delta x)^2}\right) \langle \tilde{u} | A_x^\dagger | \tilde{u} \rangle + \left(\frac{\beta}{(\Delta x)^2}\right)^2 \langle \tilde{u} | A_x^\dagger | \tilde{u} \rangle + 4 \left(\frac{\beta}{(\Delta x)^2}\right)^2 \left( \langle \tilde{u} | A_x A_x^\dagger | \tilde{u} \rangle \right) A_x^\dagger | \tilde{u} \rangle - \dots \\
&\quad 2 \left(\frac{\beta}{(\Delta x)^2}\right) \langle \tilde{u} | \tilde{u} \rangle + 2 \left(\frac{\beta}{(\Delta x)^2}\right)^2 \langle \tilde{u} | A_x^\dagger | \tilde{u} \rangle + 4 \left(\frac{\beta}{(\Delta x)^2}\right)^2 \langle \tilde{u} | A_x | \tilde{u} \rangle - \dots \\
&\quad \left(\frac{\beta}{(\Delta x)^2}\right) \langle \tilde{u} | A_x | \tilde{u} \rangle + \left(\frac{\beta}{(\Delta x)^2}\right) \langle \tilde{u} | A_x^\dagger | \tilde{u} \rangle - 2 \left(\frac{\beta}{(\Delta x)^2}\right) \langle \tilde{u} | A_x | \tilde{u} \rangle + \left(\frac{2\beta^3}{(\Delta x)^6}\right) \langle u | A_x^\dagger A_x^\dagger | u \rangle - \dots \\
&\quad \alpha \left(\frac{\beta^2}{(\Delta x)^6}\right) A_x^\dagger | u \rangle \left( \langle u | A_x | u \rangle \right) - \tau^2 \left(\frac{\beta^2}{(\Delta x)^4}\right) \langle u | A_x^\dagger A_x^\dagger | u \rangle - 2 \tau^2 \left(\frac{\beta^2}{(\Delta x)^4}\right) \langle u | A_x^\dagger A_x^\dagger | u \rangle + \dots \\
&\quad \left. 4 \tau^2 \alpha \left(\frac{\beta}{(\Delta x)^2}\right)^2 A_x^\dagger | u \rangle \left( \langle u | A_x | u \rangle \right) + \tau^4 \left(\frac{\beta}{(\Delta x)^2}\right)^2 \langle u | A_x^\dagger A_x^\dagger | u \rangle \right\} .
\end{aligned}$$

## 4.7 Lin-Tsien equation

### Cost function derivation

The equation is,

$$\begin{aligned}
&2u_{tx} + u_x u_{xx} - u_{yy} = 0 \\
&\quad \Downarrow \\
&\frac{2}{\tau \Delta x} (A_x - \mathbf{1}) |u(x, y, t + \tau)\rangle + \left(\frac{A_x - \mathbf{1}}{\Delta x}\right) |u(x, y, t)\rangle \left(\frac{A_x^\dagger - 2\mathbf{1} + A_x}{(\Delta x)^2}\right) |u(x, y, t)\rangle - \dots \\
&\quad \left\{ \left(\frac{A_y^\dagger - 2\mathbf{1} + A_y}{(\Delta y)^2}\right) |u(x, y, t)\rangle \right\} = 0
\end{aligned}$$

After representing all spatial and time derivatives with the corresponding quantum operators, the PDE takes the form,



$$\begin{aligned}
& \left( \frac{\tau}{(\Delta x)^2} \right)^2 \left( A_x |u(x, y, t)\rangle \left( A_x^\dagger - 2 \right) \right) \cdots \\
& |u(x, y, t)\rangle + \mathbf{1} - |u(x, y, t)\rangle A_x^\dagger |u(x, y, t)\rangle - \cdots \\
& |u(x, y, t)\rangle A_x |u(x, y, t)\rangle + 2 - \cdots \\
& \left. \frac{1}{(\Delta y)^2} \left( A_y^\dagger |u(x, y, t)\rangle - 2 |u(x, y, t)\rangle + A_y |u(x, y, t)\rangle \right) \right\}^2 \times \cdots \\
& \left( \frac{\tau}{(\Delta x)^2} \right)^2 \left\{ \left( A_x |u(x, y, t)\rangle \left( A_x^\dagger - 2 \right) |u(x, y, t)\rangle \right)^2 + \cdots \right. \\
& \left. 2 \left\{ A_x |u(x, y, t)\rangle \left( A_x^\dagger - 2 \right) |u(x, y, t)\rangle \right\} \times \cdots \right. \\
& \left. \left( \mathbf{1} - |u(x, y, t)\rangle A_x^\dagger |u(x, y, t)\rangle - |u(x, y, t)\rangle A_x |u(x, y, t)\rangle + 2 \right) \right\} + \cdots \\
& \left( \mathbf{1} - |u(x, y, t)\rangle A_x^\dagger |u(x, y, t)\rangle - |u(x, y, t)\rangle A_x |u(x, y, t)\rangle + \cdots \right. \\
& \left. 2 - \frac{1}{(\Delta y)^2} \left( A_y^\dagger |u(x, y, t)\rangle - 2 |u(x, y, t)\rangle + A_y |u(x, y, t)\rangle \right) \right)^2 .
\end{aligned}$$

To obtain the desired cost function, we determine all terms in the quantum superposition resulting from the expansion of terms above. Rearrangements imply,

$$\begin{aligned}
& 3 - |u(x, y, t)\rangle A_x^\dagger |u(x, y, t)\rangle - |u(x, y, t)\rangle A_x |u(x, y, t)\rangle - \frac{A_y^\dagger}{(\Delta y)^2} |u(x, y, t)\rangle + \cdots \\
& \frac{2}{(\Delta y)^2} |u(x, y, t)\rangle - \frac{A_y}{(\Delta y)^2} |u(x, y, t)\rangle \\
& \Downarrow \\
& 3 - \left( |u(x, y, t)\rangle A_x^\dagger - |u(x, y, t)\rangle A_x - \frac{1}{(\Delta y)^2} (A_y^\dagger - 2\mathbf{1} + A_y) \right) |u(x, y, t)\rangle .
\end{aligned}$$

Squaring the last term of the expansion for the cost function above gives,

$$\begin{aligned}
& \left( 3 - ( |u(x, y, t)\rangle A_x^\dagger - |u(x, y, t)\rangle A_x - \frac{1}{(\Delta y)^2} (A_y^\dagger - 2\mathbf{1} + A_y) ) |u(x, y, t)\rangle \right)^2 \\
& \Downarrow \\
& \left( 3 - ( |u(x, y, t)\rangle A_x^\dagger - |u(x, y, t)\rangle A_x - \frac{1}{(\Delta y)^2} (A_y^\dagger - 2\mathbf{1} + A_y) ) |u(x, y, t)\rangle \right) \times \cdots \\
& \left( 3 - \langle u(x, y, t) | ( |u(x, y, t)\rangle A_x^\dagger - |u(x, y, t)\rangle A_x - \frac{1}{(\Delta y)^2} (A_y^\dagger - 2\mathbf{1} + A_y) )^\dagger \right) ,
\end{aligned}$$

which is further rearranged as,

$$\begin{aligned}
9 - & \left( 3 \left( \langle u(x, y, t) | \left( |u(x, y, t)\rangle A_x^\dagger - |u(x, y, t)\rangle A_x - \frac{1}{(\Delta y)^2} (A_y^\dagger - 2\mathbf{1} + A_y) \right)^\dagger \right) \right) - \dots \\
& 3 \left( |u(x, y, t)\rangle A_x^\dagger - |u(x, y, t)\rangle A_x - \frac{1}{(\Delta y)^2} (A_y^\dagger - 2\mathbf{1} + A_y) \right) |u(x, y, t)\rangle + \dots \\
& \left( |u(x, y, t)\rangle A_x^\dagger - |u(x, y, t)\rangle A_x - \frac{1}{(\Delta y)^2} (A_y^\dagger - 2\mathbf{1} + A_y) \right) |u(x, y, t)\rangle \times \dots \\
& \langle u(x, y, t) | \left( |u(x, y, t)\rangle A_x^\dagger - |u(x, y, t)\rangle A_x - \frac{1}{(\Delta y)^2} (A_y^\dagger - 2\mathbf{1} + A_y) \right)^\dagger .
\end{aligned}$$

In order from the superposition above, we distribute terms amongst the superposition, and take the Hermitian conjugate of the last term,

$$\begin{aligned}
9 - & \left( 3 \left( \langle u(x, y, t) | A_x^\dagger |u(x, y, t)\rangle - \langle u(x, y, t) | A_x |u(x, y, t)\rangle - \frac{A_y^\dagger}{(\Delta y)^2} |u(x, y, t)\rangle - \dots \right. \right. \\
& \left. \left. 2 |u(x, y, t)\rangle + A_y |u(x, y, t)\rangle \right) - \dots \right. \\
& 3 \left( \langle u(x, y, t) | A_x |u(x, y, t)\rangle - \langle u(x, y, t) | A_x^\dagger |u(x, y, t)\rangle - \dots \right. \\
& \left. \frac{A_y^\dagger}{(\Delta y)^2} |u(x, y, t)\rangle - \dots \right. \\
& \left. \frac{2}{(\Delta y)^2} |u(x, y, t)\rangle - \dots \right. \\
& \left. \frac{A_y}{(\Delta y)^2} |u(x, y, t)\rangle \right) + \left( \langle u(x, y, t) | A_x |u(x, y, t)\rangle - \dots \right. \\
& \left. \langle u(x, y, t) | A_x^\dagger |u(x, y, t)\rangle - \frac{A_y^\dagger}{(\Delta y)^2} |u(x, y, t)\rangle \right) \times \dots \\
& \left( |u(x, y, t)\rangle A_x^\dagger - |u(x, y, t)\rangle A_x - \frac{1}{(\Delta y)^2} (A_y^\dagger - 2\mathbf{1} + A_y) \right) |u(x, y, t)\rangle \times \dots \\
& \langle u(x, y, t) | A_x |u(x, y, t)\rangle \langle u(x, y, t) | A_x |u(x, y, t)\rangle - \dots \\
& \langle u(x, y, t) | A_x |u(x, y, t)\rangle \langle u(x, y, t) | A_x^\dagger |u(x, y, t)\rangle - \dots \\
& \langle u(x, y, t) | A_x |u(x, y, t)\rangle \frac{A_y^\dagger}{(\Delta y)^2} |u(x, y, t)\rangle + \dots \\
& \langle u(x, y, t) | A_x |u(x, y, t)\rangle \frac{2}{(\Delta y)^2} |u(x, y, t)\rangle - \langle u(x, y, t) | A_x |u(x, y, t)\rangle \dots \\
& \frac{A_y}{(\Delta y)^2} |u(x, y, t)\rangle - \langle u(x, y, t) | A_x^\dagger |u(x, y, t)\rangle \langle u(x, y, t) | A_x |u(x, y, t)\rangle - \dots \\
& \langle u(x, y, t) | A_x^\dagger |u(x, y, t)\rangle \times \dots \\
& \langle u(x, y, t) | A_x^\dagger |u(x, y, t)\rangle .
\end{aligned}$$

Besides these rearrangements, additional expectation terms in the superposition are of the following form,

$$\begin{aligned}
& \langle u(x, y, t) | A_x^\dagger | u(x, y, t) \rangle \frac{A_y^\dagger}{(\Delta y)^2} | u(x, y, t) \rangle - \langle u(x, y, t) | A_x^\dagger | u(x, y, t) \rangle \frac{2}{(\Delta y)^2} \cdots \\
& | u(x, y, t) \rangle \langle u(x, y, t) | A_x^\dagger | u(x, y, t) \rangle \frac{A_y}{(\Delta y)^2} | u(x, y, t) \rangle - \frac{A_y^\dagger}{(\Delta y)^2} | u(x, y, t) \rangle \langle u(x, y, t) | A_x | u(x, y, t) \rangle - \cdots \\
& \frac{A_y^\dagger}{(\Delta y)^2} | u(x, y, t) \rangle \langle u(x, y, t) | A_x^\dagger | u(x, y, t) \rangle + \frac{A_y^\dagger}{(\Delta y)^2} | u(x, y, t) \rangle \frac{A_y^\dagger}{(\Delta y)^2} | u(x, y, t) \rangle - \cdots \\
& \frac{A_y^\dagger}{(\Delta y)^2} | u(x, y, t) \rangle \frac{2}{(\Delta y)^2} | u(x, y, t) \rangle + \frac{A_y^\dagger}{(\Delta y)^2} | u(x, y, t) \rangle \frac{A_y}{(\Delta y)^2} | u(x, y, t) \rangle \times \cdots \\
& \langle u(x, y, t) | A_x A_x | u(x, y, t) \rangle - \langle u(x, y, t) | A_x A_x^\dagger | u(x, y, t) \rangle - \cdots \\
& \langle u(x, y, t) | A_x \frac{A_y}{(\Delta y)^2} + \langle u(x, y, t) | A_x \frac{2}{(\Delta y)^2} - \langle u(x, y, t) | A_x \cdots \\
& \frac{A_y^\dagger}{(\Delta y)^2} - \langle u(x, y, t) | A_x^\dagger A_x | u(x, y, t) \rangle - \langle u(x, y, t) | A_x^\dagger \cdots \\
& A_x^\dagger | u(x, y, t) \rangle + \langle u(x, y, t) | A_x^\dagger \frac{A_y}{(\Delta y)^2} - \langle u(x, y, t) | A_x^\dagger \frac{2}{(\Delta y)^2} - \cdots \\
& A_x^\dagger | u(x, y, t) \rangle - \frac{A_y^\dagger}{(\Delta y)^2} A_x | u(x, y, t) \rangle - \cdots \\
& \frac{A_y^\dagger}{(\Delta y)^2} A_x^\dagger | u(x, y, t) \rangle + \langle u(x, y, t) | \frac{1}{(\Delta y)^2} \times \frac{1}{(\Delta y)^2} | u(x, y, t) \rangle - \langle u(x, y, t) | \frac{2}{(\Delta y)^2} \times \cdots \\
& \frac{A_y^\dagger}{(\Delta y)^2} | u(x, y, t) \rangle + \frac{1}{(\Delta y)^2} \frac{1}{(\Delta y)^2} \cdot
\end{aligned}$$

Continuing, we further expand terms after distributing states from the expansion of the norm to determine the cost function whose ground state we investigate,

$$\begin{aligned}
& (\langle u(x, y, t) | A_x A_x - \langle u(x, y, t) | A_x A_x^\dagger - \langle u(x, y, t) | A_x^\dagger A_x - \langle u(x, y, t) | A_x^\dagger A_x^\dagger - A_x^\dagger - \cdots \\
& \frac{A_y^\dagger}{(\Delta x)^2} A_x - \frac{A_y^\dagger}{(\Delta y)^2} A_x^\dagger + \cdots \\
& \langle u(x, y, t) | \frac{1}{(\Delta y)^4} - \langle u(x, y, t) | \frac{2}{(\Delta y)^2} \times \frac{A_x^\dagger}{(\Delta y)^2} - 3 \langle u(x, y, t) | A_x - \cdots \\
& 3 \langle u(x, y, t) | A_x^\dagger - \frac{A_y^\dagger}{(\Delta y)^2} - \frac{2}{(\Delta y)^2} - \cdots \\
& \frac{A_y}{(\Delta y)^2} + A_x^\dagger \frac{A_y^\dagger}{(\Delta y)^2} + 2 \frac{A_x^\dagger}{(\Delta y)^2} - A_x^\dagger \frac{A_y}{(\Delta y)^2} + \cdots \\
& A_x \frac{A_y^\dagger}{(\Delta y)^2} - A_x \frac{2}{(\Delta y)^2} | u(x, y, t) \rangle \\
& 9 - (3 \langle u(x, y, t) | A_x^\dagger - 3 \langle u(x, y, t) | A_x - 3 \frac{A_y^\dagger}{(\Delta y)^2} - 2 + A_y + \cdots \\
& \langle u(x, y, t) | A_x A_x - \langle u(x, y, t) | A_x A_x^\dagger - \langle u(x, y, t) | A_x^\dagger A_x - \langle u(x, y, t) | A_x^\dagger A_x^\dagger - A_x^\dagger - \cdots \\
& \frac{A_y^\dagger}{(\Delta x)^2} A_x - \frac{A_y^\dagger}{(\Delta y)^2} A_x^\dagger + \cdots \\
& \langle u(x, y, t) | \frac{1}{(\Delta y)^4} - \langle u(x, y, t) | \frac{2}{(\Delta y)^2} \times \frac{A_x^\dagger}{(\Delta y)^2} - 3 \langle u(x, y, t) | A_x - \cdots
\end{aligned}$$

$$\begin{aligned}
& 3 \langle u(x, y, t) | A_x^\dagger - \frac{A_y^\dagger}{(\Delta y)^2} - \frac{2}{(\Delta y)^2} - \dots \\
& \frac{A_y}{(\Delta y)^2} + A_x^\dagger \frac{A_y^\dagger}{(\Delta y)^2} + 2 \frac{A_x^\dagger}{(\Delta y)^2} - A_x^\dagger \frac{A_y}{(\Delta y)^2} + \dots \\
& A_x \frac{A_y^\dagger}{(\Delta y)^2} - A_x \frac{2}{(\Delta y)^2} |u(x, y, t)\rangle \Big) \\
& \Updownarrow
\end{aligned}$$

$$\left( A_x |u(x, y, t)\rangle \left( A_x^\dagger - 2 \right) |u(x, y, t)\rangle \right) \left( \langle u(x, y, t) | A_x^\dagger ( A_x^\dagger - 2 )^\dagger |u(x, y, t)\rangle \right) .$$

We continue rearranging terms from the superposition obtained in previous steps above,

$$\begin{aligned}
& \left( A_x |u(x, y, t)\rangle \left( A_x^\dagger - 2 \right) |u(x, y, t)\rangle \langle u(x, y, t) | A_x^\dagger ( A_x - 2 ) \langle u(x, y, t) | \right) \\
& \Updownarrow \\
& \left( A_x |u(x, y, t)\rangle \left( A_x^\dagger A_x^\dagger - 2A_x^\dagger \right) \left( A_x - 2 \right) \langle u(x, y, t) | \right) \\
& \Updownarrow \\
& \left( A_x |u(x, y, t)\rangle \left( A_x^\dagger - 2A_x^\dagger A_x^\dagger - 2\mathbf{1} + 4A_x^\dagger \right) \langle u(x, y, t) | \right) \\
& \Updownarrow \\
& \left( A_x |u(x, y, t)\rangle A_x^\dagger \langle u(x, y, t) | - 2A_x |u(x, y, t)\rangle A_x^\dagger A_x^\dagger \langle u(x, y, t) | - 2A_x \right. \\
& \qquad \qquad \qquad \left. |u(t)\rangle |u(t + \tau)\rangle + \dots \right) \\
& 4 A_x |u(x, y, t)\rangle A_x^\dagger |u(x, y, t)\rangle \Big) \\
& 2 \left( \langle u(x, y, t) | A_x A_x |u(x, y, t)\rangle - \langle u(x, y, t) | 2A_x |u(x, y, t)\rangle \right) \times \dots \\
& \left( 3 - \langle u(x, y, t) | A_x |u(x, y, t)\rangle - \langle u(x, y, t) | A_x^\dagger |u(x, y, t)\rangle \right) .
\end{aligned}$$

Collecting expectation values from the multiplication of quantum states yields,

$$\begin{aligned}
& 6 \langle u(x, y, t) | A_x A_x |u(x, y, t)\rangle \langle u(x, y, t) | A_x |u(x, y, t)\rangle - \dots \\
& 2 \langle u(x, y, t) | A_x A_x |u(x, y, t)\rangle \langle u(x, y, t) | \dots \\
& \qquad \qquad \qquad A_x^\dagger |u(x, y, t)\rangle - \dots \\
& 6 \langle u(x, y, t) | 2A_x |u(x, y, t)\rangle \langle u(x, y, t) | A_x |u(x, y, t)\rangle - \dots \\
& 2 \langle u(x, y, t) | A_x A_x |u(x, y, t)\rangle \dots \\
& \langle u(x, y, t) | A_x^\dagger |u(x, y, t)\rangle + \dots \\
& 2 \langle u(x, y, t) | 2A_x |u(x, y, t)\rangle \dots \\
& \langle u(x, y, t) | A_x^\dagger |u(x, y, t)\rangle \\
& \Updownarrow \\
& 6 \langle u(x, y, t) | A_x A_x \lambda^2 A_x |u(x, y, t)\rangle - 2 \langle u(x, y, t) | A_x A_x \lambda^2 A_x^\dagger |u(x, y, t)\rangle - \dots \\
& 6 \langle u(x, y, t) | 2A_x \lambda^2 |u(x, y, t)\rangle - 2 \langle u(x, y, t) | A_x A_x \lambda^2 A_x^\dagger |u(x, y, t)\rangle + \dots \\
& 2 \langle u(x, y, t) | 2A_x \lambda^2 A_x^\dagger |u(x, y, t)\rangle .
\end{aligned}$$

Previous rearrangements imply,

$$\begin{aligned}
& (6 \langle u(x, y, t) | A_x A_x \lambda^2 A_x - 2 \langle u(x, y, t) | A_x A_x \lambda^2 A_x^\dagger - \dots \\
& 6 \langle u(x, y, t) | 2 A_x \lambda^2 - 2 \langle u(x, y, t) | A_x A_x \lambda^2 A_x^\dagger + 2 \langle u(x, y, t) | 2 A_x \lambda^2 A_x^\dagger + \dots \\
& \langle u(x, y, t) | A_x A_x - \langle u(x, y, t) | A_x A_x^\dagger - \langle u(x, y, t) | A_x^\dagger A_x - \langle u(x, y, t) | A_x^\dagger A_x^\dagger - A_x^\dagger - \dots \\
& \frac{A_y^\dagger}{(\Delta x)^2} A_x - \frac{A_y^\dagger}{(\Delta y)^2} A_x^\dagger + \langle u(x, y, t) | \frac{1}{(\Delta y)^4} - \langle u(x, y, t) | \frac{2}{(\Delta y)^2} \frac{A_x^\dagger}{(\Delta y)^2} - \dots \\
& 3 \langle u(x, y, t) | A_x - 3 \langle u(x, y, t) | A_x^\dagger - \frac{A_y^\dagger}{(\Delta y)^2} - \frac{2}{(\Delta y)^2} - \dots \\
& \frac{A_y}{(\Delta y)^2} + A_x^\dagger \frac{A_y^\dagger}{(\Delta y)^2} + 2 \frac{A_x^\dagger}{(\Delta y)^2} - A_x^\dagger \frac{A_y}{(\Delta y)^2} + \dots \\
& A_x \frac{A_y^\dagger}{(\Delta y)^2} - A_x \frac{2}{(\Delta y)^2} ) |u(x, y, t)\rangle ,
\end{aligned}$$

from which rearrangements of the final collection of terms yields,

$$\begin{aligned}
& \frac{\tau}{(\Delta x)^2} \left\{ A_x |u(x, y, t + \tau)\rangle A_x |u(x, y, t)\rangle (A_x^\dagger - 2) |u(x, y, t)\rangle + \dots \right. \\
& \left. A_x |u(x, y, t + \tau)\rangle - A_x |u(x, y, t + \tau)\rangle |u(x, y, t)\rangle (A_x^\dagger |u(x, y, t)\rangle - A_x |u(x, y, t)\rangle) + 2 \right\} - \dots \\
& \frac{\tau}{(\Delta x)^2} \frac{A_x |u(x, y, t + \tau)\rangle}{(\Delta y)^2} (A_y^\dagger |u(x, y, t)\rangle - 2 |u(x, y, t)\rangle + A_y |u(x, y, t)\rangle) \\
& \Downarrow \\
& \frac{\tau}{(\Delta x)^2} \left\{ A_x |u(x, y, t + \tau)\rangle A_x |u(x, y, \tau)\rangle A_x^\dagger |u(x, y, t)\rangle - \dots \right. \\
& \quad A_x |u(x, y, t + \tau)\rangle A_x |u(x, y, t)\rangle 2 |u(x, y, t)\rangle + \dots \\
& A_x |u(x, y, t + \tau)\rangle - A_x |u(x, y, t + \tau)\rangle |u(x, y, t)\rangle A_x^\dagger |u(x, y, t)\rangle - \dots \\
& \quad \left. A_x |u(x, y, t + \tau)\rangle A_x |u(x, y, t)\rangle |u(x, y, t)\rangle \langle u(x, y, t) | A_x^\dagger + 2 \right\} - \dots \\
& \frac{\tau}{(\Delta x)^2 (\Delta y)^2} (A_x |u(x, y, t)\rangle A_x^\dagger |u(x, y, t)\rangle - \dots \\
& \quad A_x |u(x, y, t + \tau)\rangle 2 |u(x, y, t)\rangle) .
\end{aligned}$$

In conclusion, the cost function takes the form,

$$\begin{aligned}
\boxed{\mathcal{C}^{L-T}(\lambda, \lambda_0^{L-T})} &= (\lambda_0^{L-T})^2 + \text{Re} \left\{ \left( \frac{\tau}{(\Delta x)^2} \right)^2 \langle u | A_x^\dagger A_x^\dagger | \tilde{u} \rangle - 2 \left( \frac{\tau}{(\Delta x)^2} \right)^2 \langle u | A_x^\dagger A_x^\dagger A_x^\dagger | u \rangle - \dots \right. \\
& 2 \left( \frac{\tau}{(\Delta x)^2} \right)^2 \langle \tilde{u} | A_x | u \rangle + 6 \lambda^2 \langle u | A_x A_x A_x | u \rangle - 2 \lambda^2 \langle u | A_x A_x A_x^\dagger | u \rangle - \dots \\
& \quad 4 \lambda^2 \langle u | A_x A_x^\dagger | u \rangle + \langle u | A_x A_x | u \rangle + \langle u | A_x A_x^\dagger | u \rangle + \langle u | A_x^\dagger A_x | u \rangle + \dots \\
& \langle u | A_x^\dagger A_x^\dagger | u \rangle - A_x^\dagger | u \rangle + \frac{1}{(\Delta x)^2} A_y^\dagger A_x | u \rangle + \frac{1}{(\Delta y)^2} A_y^\dagger A_x^\dagger | u \rangle + \frac{1}{(\Delta y)^4} \langle u | u \rangle + \dots \\
& \frac{2}{(\Delta y)^4} A_x^\dagger | u \rangle + 3 \langle u | A_x | u \rangle + 3 \langle u | A_x^\dagger | u \rangle + \frac{1}{(\Delta y)^2} A_y^\dagger | u \rangle + 2 | u \rangle + \frac{1}{(\Delta y)^2} A_x^\dagger | u \rangle + \dots \\
& \quad \left. 3 \langle u | A_x^\dagger | u \rangle + \frac{1}{(\Delta y)^2} A_y^\dagger | u \rangle - \frac{2}{(\Delta y)^2} | u \rangle + \frac{1}{(\Delta y)^2} A_y | u \rangle + \frac{1}{(\Delta y)^2} A_x^\dagger A_y^\dagger | u \rangle + \dots \right\}
\end{aligned}$$

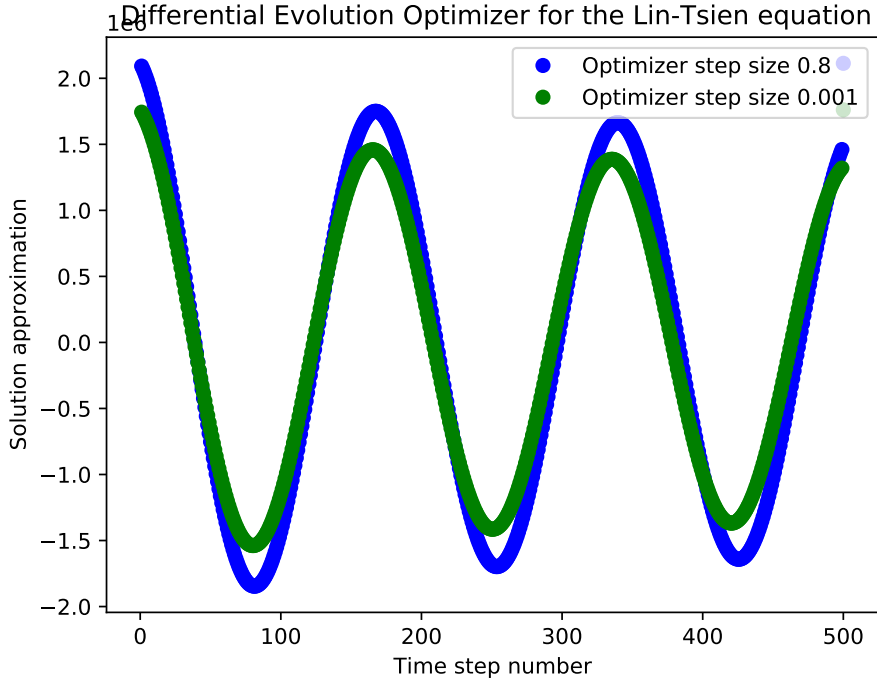


Figure 37: *Extracting measurements from the Lin-Tsien equation.* Solution approximations to the Lin-Tsien equation approximate exact, analytically known sinusoidal solutions. In comparison to the Differential Evolution optimizer, varying the time step of evolution for other optimizers produces far less reliable approximations.

$$\left. \begin{aligned}
 & 2 \frac{1}{(\Delta y)^2} A_x^\dagger |u\rangle + \frac{1}{(\Delta y)^2} A_x^\dagger A_y |u\rangle + \frac{1}{(\Delta y)^2} A_x A_y^\dagger |u\rangle + 2 \frac{1}{(\Delta y)^2} A_x |u\rangle + \dots \\
 & \frac{1}{(\Delta x)^2} \langle u | A_x^\dagger A_x |u\rangle A_x^\dagger |u\rangle - \frac{2\tau}{(\Delta x)^2} \langle u | A_x^\dagger A_x |u\rangle + \frac{\tau}{(\Delta x)^2 (\Delta y)^2} \langle u | A_x A_x |u\rangle + \dots \\
 & \left. \langle u | A_x |u\rangle + 2 \frac{\tau}{(\Delta x)^2} + \frac{\tau}{(\Delta x)^2} \langle \tilde{u} | A_x^\dagger A_x | \tilde{u} \rangle \right\} .
 \end{aligned}$$

## 4.8 Camassa-Holm equation

### Cost function derivation

For  $\kappa \equiv 1$ , the equation after introducing the standard quantum state transformation for evolution of the variational state for the solution is equivalent to,

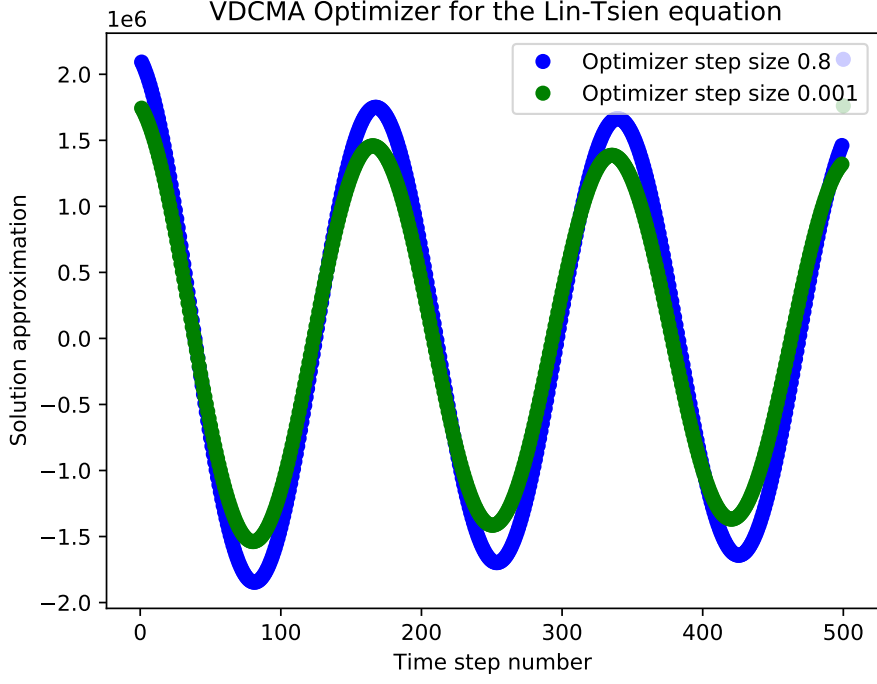
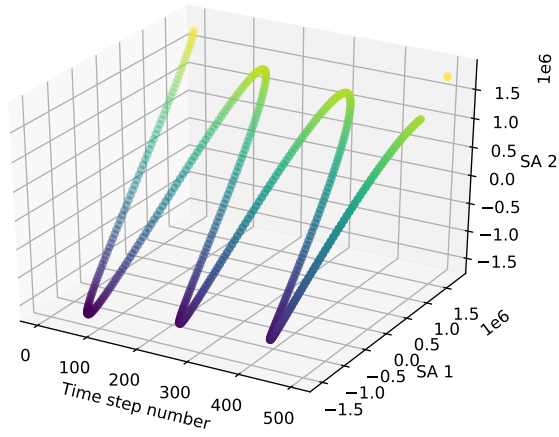


Figure 38: *Extracting measurements from the Lin-Tsien equation with the VD-CMA stochastic optimizer.* Performing time-evolution of solution states for the Lin-Tsien equation with stochastic optimizers yields identical results as with the solution approximations with deterministic optimizers.

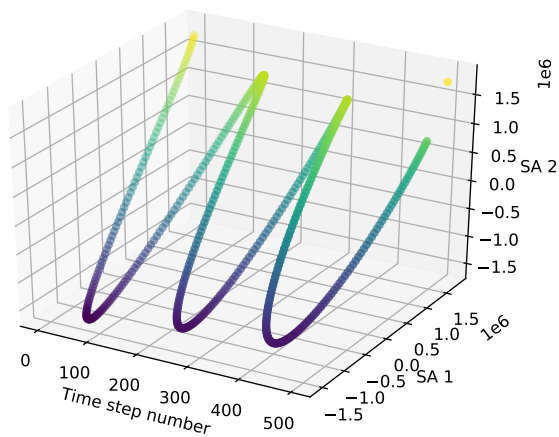
$$\begin{aligned}
 u_t &= 2u_x u_{xx} + uu_{xxx} - (3u + 2\kappa)u_x + u_{xxt} \\
 &\quad \Downarrow \\
 \frac{|u(x, t + \tau)\rangle - |u(x, t)\rangle}{\tau} &= 2\left(\frac{A_x - \mathbf{1}}{\Delta x}\right) |u(x, t)\rangle \left(\frac{A_x^\dagger - \mathbf{21} + A_x}{(\Delta x)^2}\right) \times \dots \\
 &\quad |u(x, t)\rangle + \frac{|u(x, t)\rangle}{\Delta x} \times \dots \\
 &\quad \left[ \left(\frac{A_x^\dagger - \mathbf{21} + A_x}{(\Delta x)^2}\right) |u(x, t + \tau)\rangle - \dots \right. \\
 &\quad \left. \left(\frac{A_x^\dagger - \mathbf{21} + A_x}{(\Delta x)^2}\right) |u(x, t)\rangle \right] - (3|u(x, t)\rangle + 2) \left(\frac{A_x - \mathbf{1}}{\Delta x}\right) |u(x, t)\rangle + \left(\frac{A_x^\dagger - \mathbf{21} + A_x}{(\Delta x)^2}\right) |u(x, t)\rangle)_t .
 \end{aligned}$$

We evaluate the first order time derivative and additional terms of the superposition,

Differential Evolution Optimizer for the Lin-Tsien Equation



Differential Evolution Optimizer for the Lin-Tsien Equation



Differential Evolution Optimizer for the Lin-Tsien Equation

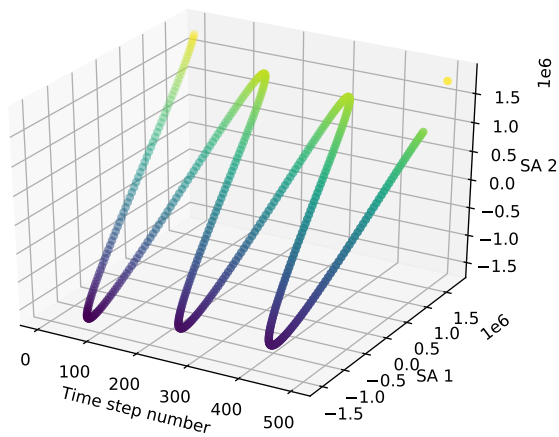
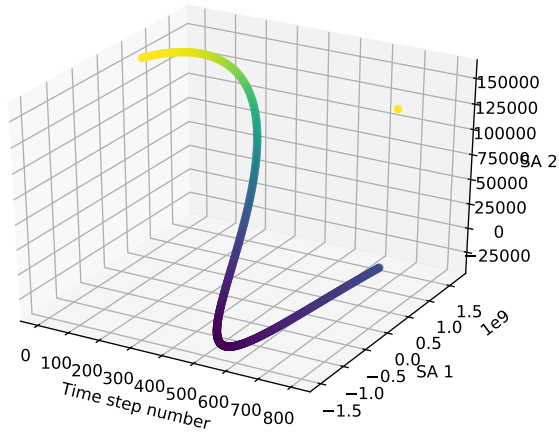
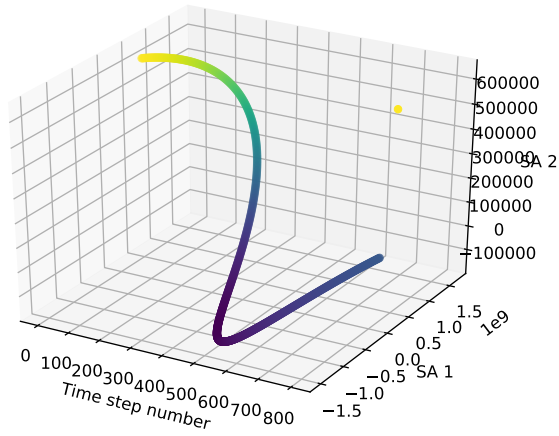


Figure 39: *Extracting measurements from the Lin-Tsien equation with the VD-CMA stochastic optimizer.* Performing time-evolution of solution states for the Lin-Tsien equation with stochastic optimizers yields identical results as with the solution approximations with deterministic optimizers.

Nevergrad Optimizer for two ansatze of the Lin-Tsien equation



Nevergrad optimizer for two ansatze of the Lin-Tsien equation



Nevergrad optimizer for two ansatze of the Lin-Tsien equation

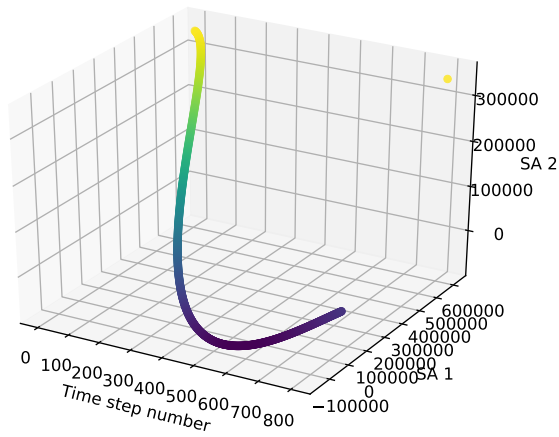


Figure 40: *Extracting measurements from the Lin-Tsien equation with deterministic optimizers.* Performing time-evolution of solution states for the Lin-Tsien equation with deterministic optimizers yields similar as with the solution approximations with deterministic optimizers.

## Nevergrad optimizer for two ansatze of the Lin-Tsien equation

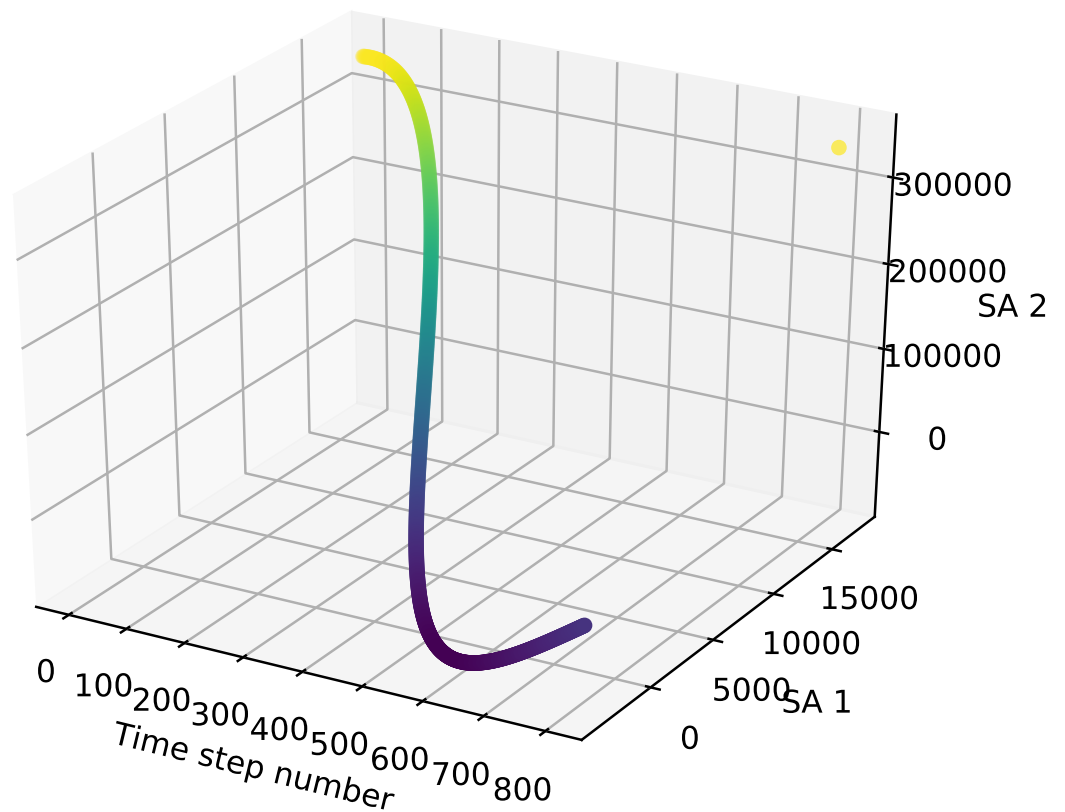
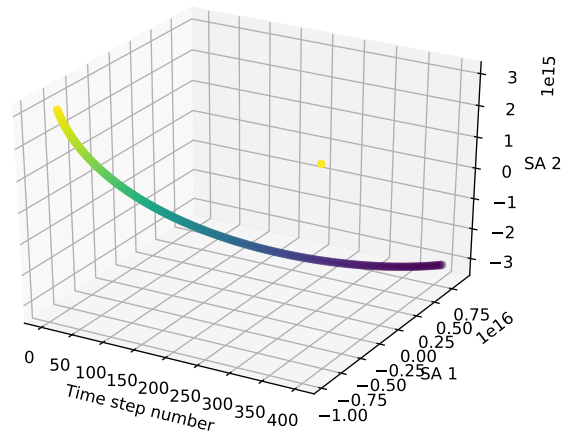
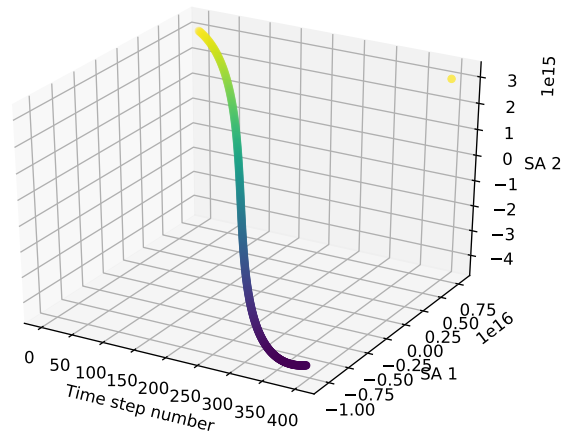


Figure 41: *Extracting measurements from the Lin-Tsien equation with deterministic optimizers.* Performing time-evolution of solution states for the Lin-Tsien equation with deterministic optimizers yields similar as with the solution approximations with deterministic optimizers.

Differential Evolution Optimizers for the Lin-Tsien equation



Differential Evolution Optimizers for the Lin-Tsien equation



Differential Evolution Optimizers for the Lin-Tsien equation

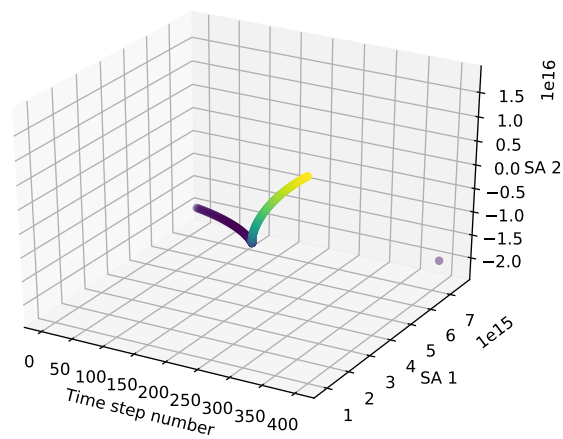
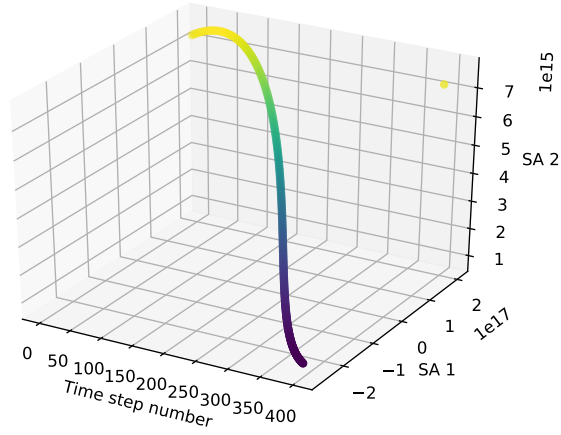
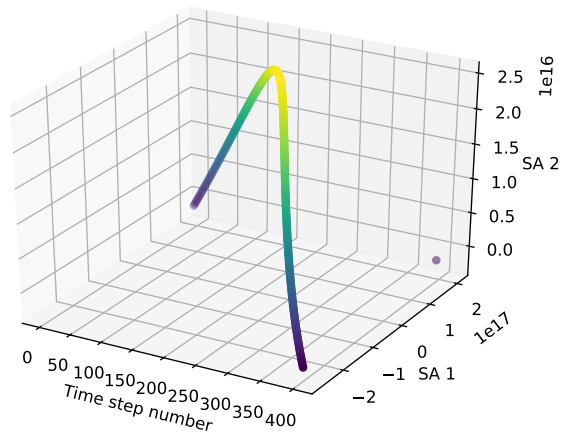


Figure 42: *Extracting measurements from the Lin-Tsien equation with 400 time steps of evolution.* Performing time-evolution of solution states for the Lin-Tsien equation yields qualitatively different results from previous approximation results. The Hilbert space coverage of two ansatzes is compared.

Differential Evolution Optimizers for the Lin-Tsien equation



Differential Evolution Optimizers for the Lin-Tsien equation



Differential Evolution Optimizers for the Lin-Tsien equation

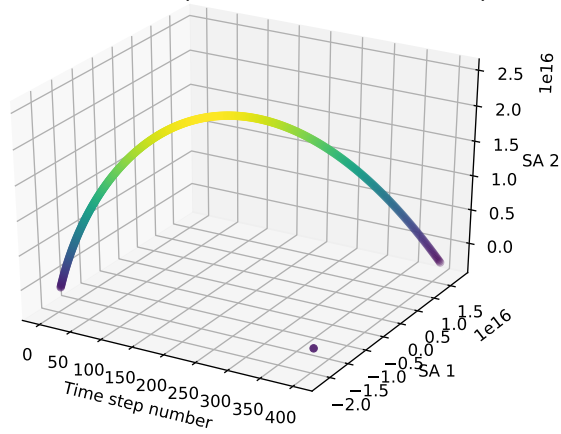
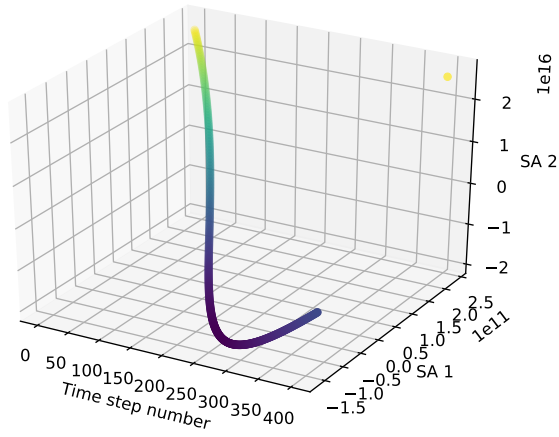
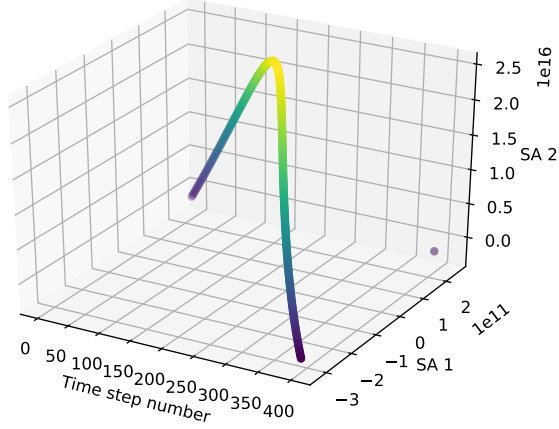


Figure 43: *Extracting measurements from the Lin-Tsien equation with 400 time steps of evolution. Performing time-evolution of solution states for the Lin-Tsien equation yields qualitatively different results from previous approximation results. The Hilbert space coverage of two ansatzes is compared.*

Differential Evolution Optimizer for the Lin-Tsien equation



Differential Evolution Optimizer for the Lin-Tsien equation



Differential Evolution Optimizer for the Lin-Tsien equation

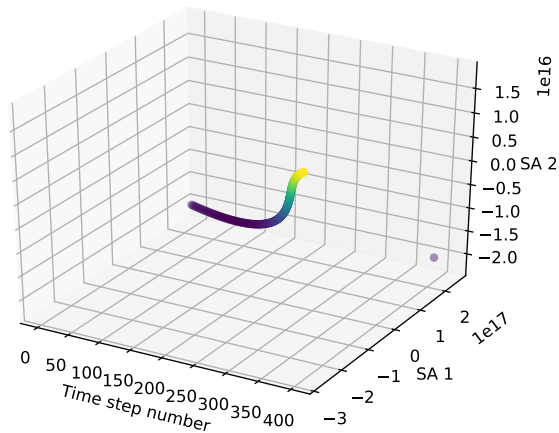
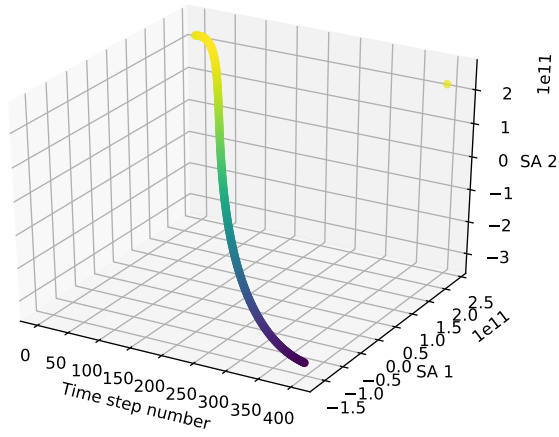
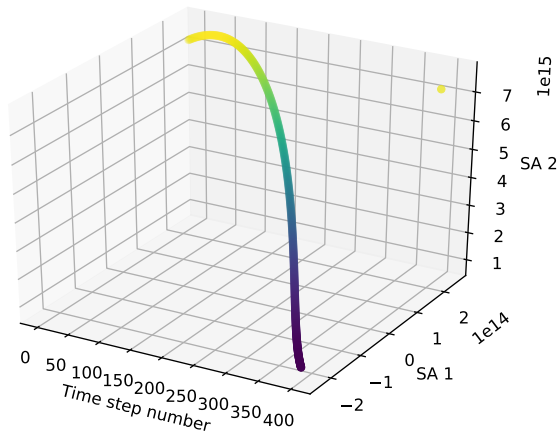


Figure 44: *Extracting measurements from the Lin-Tsien equation with 400 time steps of evolution. Performing time-evolution of solution states for the Lin-Tsien equation yields qualitatively different results from previous approximation results. The Hilbert space coverage of two ansatzes is compared.*

Differential Evolution Optimizer for the Lin-Tsien equation



Differential Evolution Optimizer for the Lin-Tsien equation



Differential Evolution Optimizer for the Lin-Tsien equation

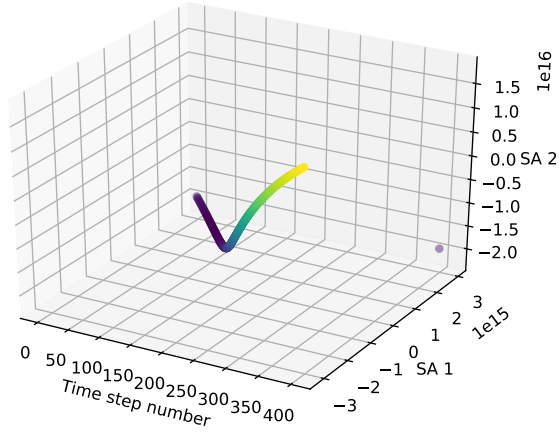


Figure 45: *Extracting measurements from the Lin-Tsien equation with 400 time steps of evolution. Performing time-evolution of solution states for the Lin-Tsien equation yields qualitatively different results from previous approximation results. The Hilbert space coverage of two ansatzes is compared.*

## Differential Evolution Optimizer for the Lin-Tsien equation

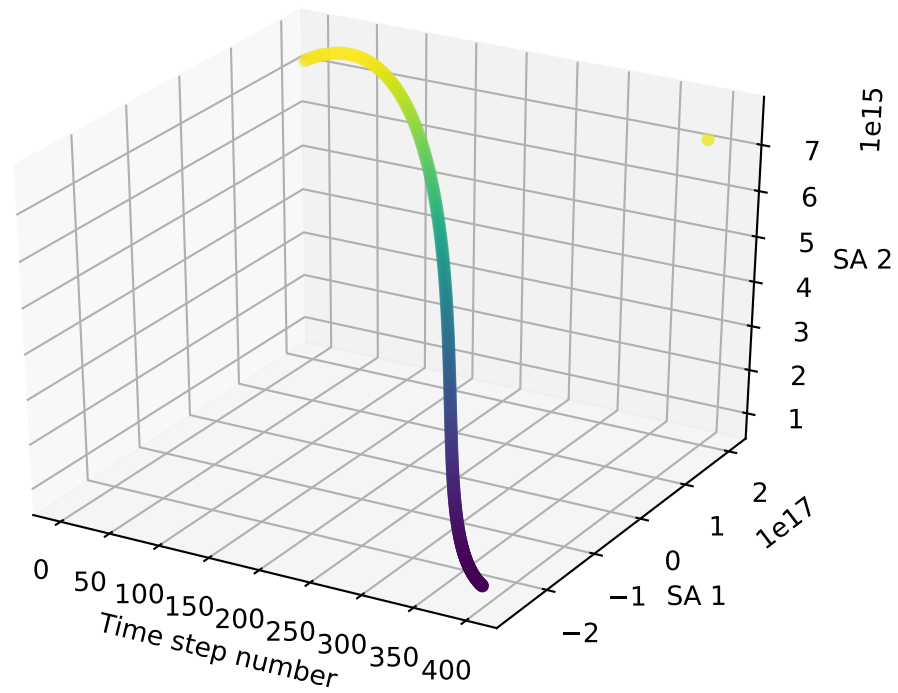
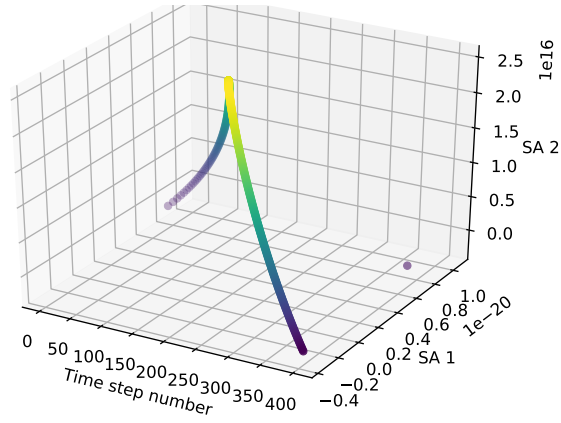
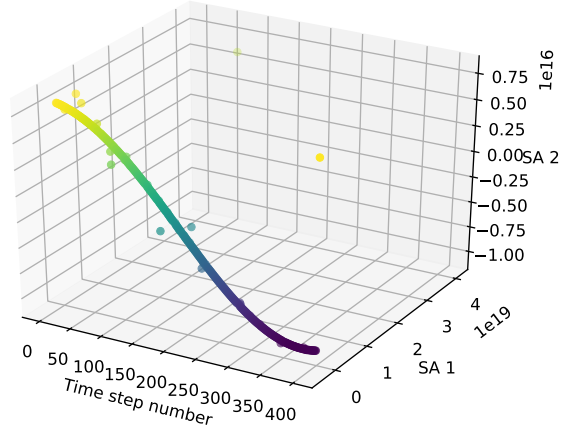


Figure 46: *Extracting measurements from the Lin-Tsien equation with 400 time steps of evolution.* Performing time-evolution of solution states for the Lin-Tsien equation yields qualitatively different results from previous approximation results. The Hilbert space coverage of two ansatze is compared.

Nevergrad Optimizer for the Lin-Tsien equation



Particle Swarm Optimizer for the Lin-Tsien equation



Differential Evolution Optimizer for the Lin-Tsien equation

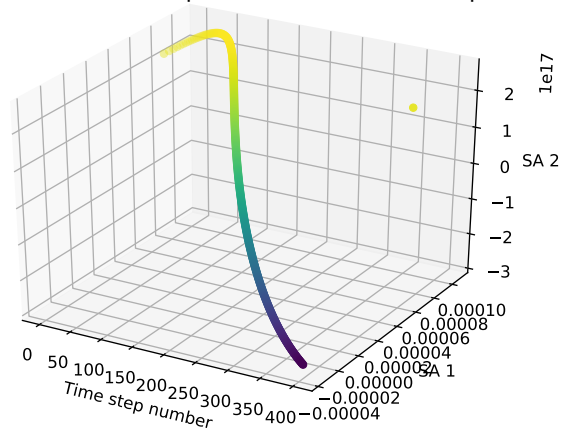
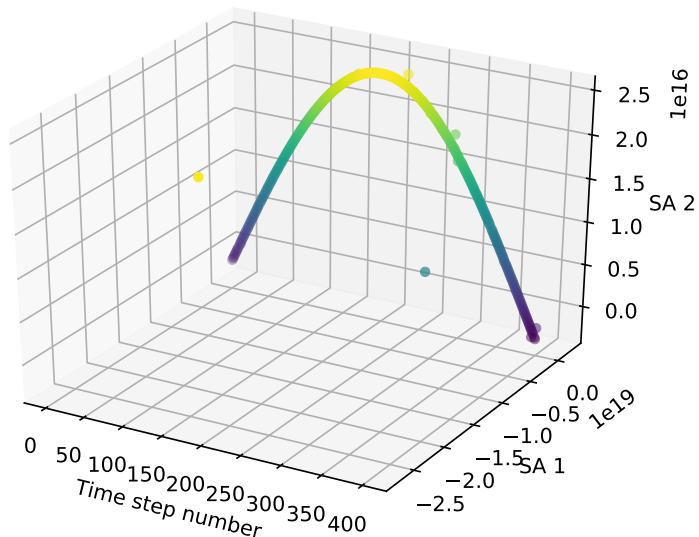


Figure 47: *Extracting measurements from the Lin-Tsien equation with 400 time steps of evolution. Performing time-evolution of solution states for the Lin-Tsien equation yields qualitatively different results from previous approximation results.*

Particle Swarm Optimizer for the Lin-Tsien equation



Particle Swarm Optimizer for the Lin-Tsien equation

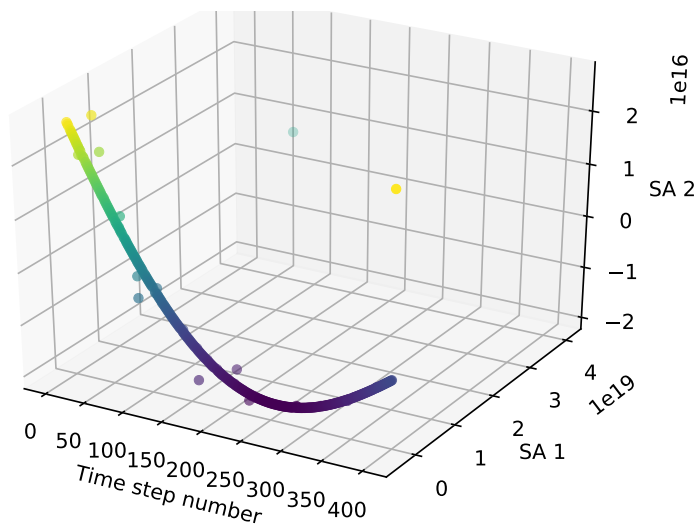
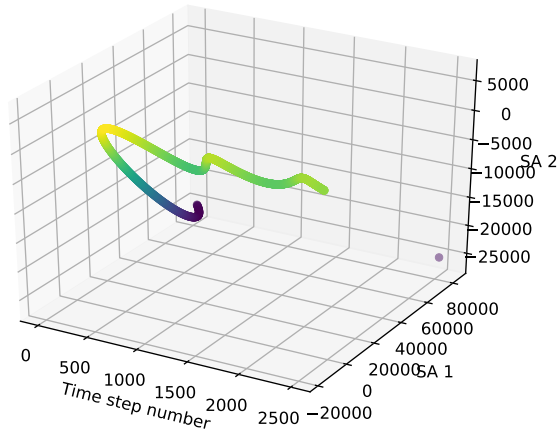
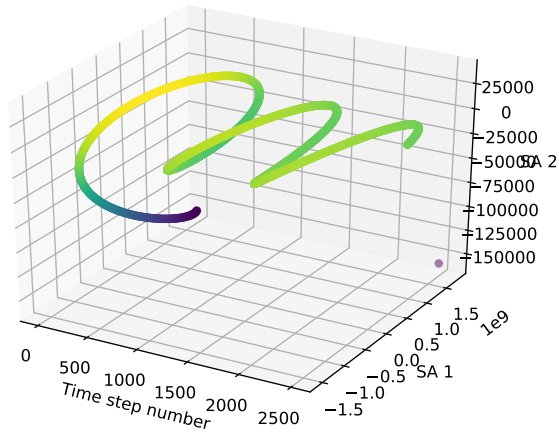


Figure 48: *Extracting measurements from the Lin-Tsien equation with 400 time steps of evolution. Performing time-evolution of solution states for the Lin-Tsien equation yields qualitatively different results from previous approximation results.*

Differential Evolution Optimizer for the Lin-Tsien PDE



Differential Evolution Optimizer for the Lin-Tsien PDE



Nevergrad Optimizer for the Lin-Tsien PDE

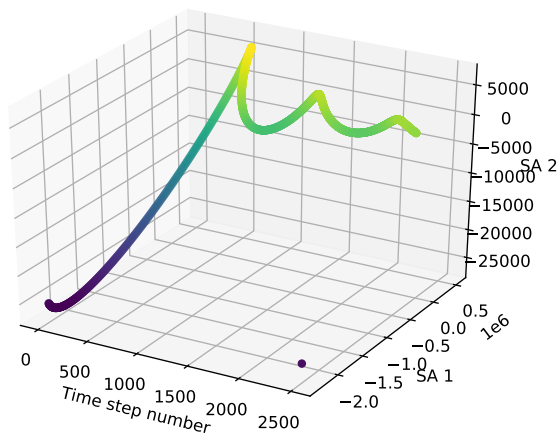
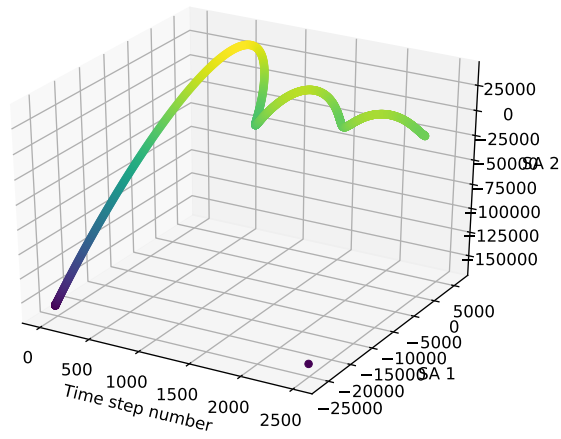
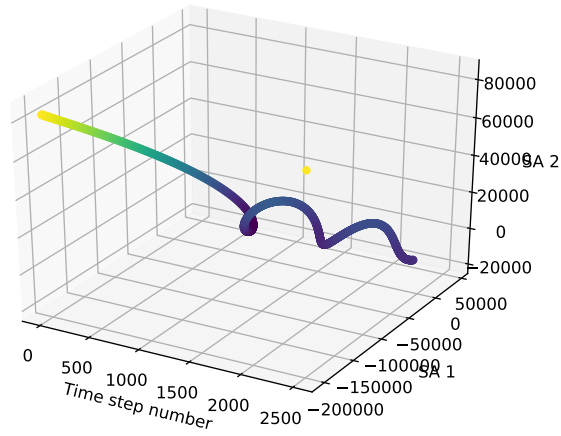


Figure 49: *Extracting measurements from the Lin-Tsien equation with 2500 time steps of evolution. Performing time-evolution of solution states for the Lin-Tsien equation yields qualitatively different results from previous approximation results.*

Differential Evolution Optimizer for the Lin-Tsien PDE



Differential Evolution Optimizer for the Lin-Tsien PDE



Differential Evolution Optimizer for the Lin-Tsien PDE

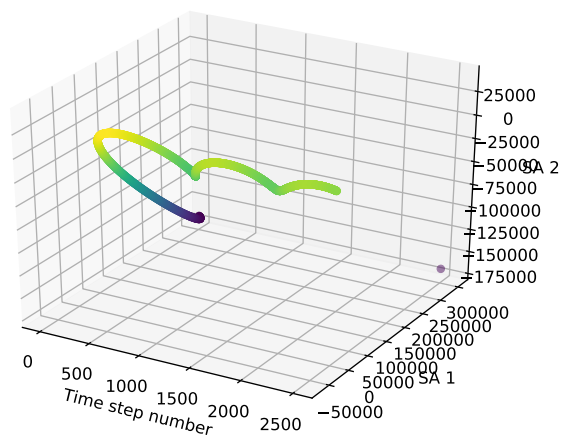


Figure 50: *Extracting measurements from the Lin-Tsien equation with 2500 time steps of evolution. Performing time-evolution of solution states for the Lin-Tsien equation yields qualitatively different results from previous approximation results.*

## Differential Evolution and Nevergrad Optimizers for the Lin-Tsien PDE

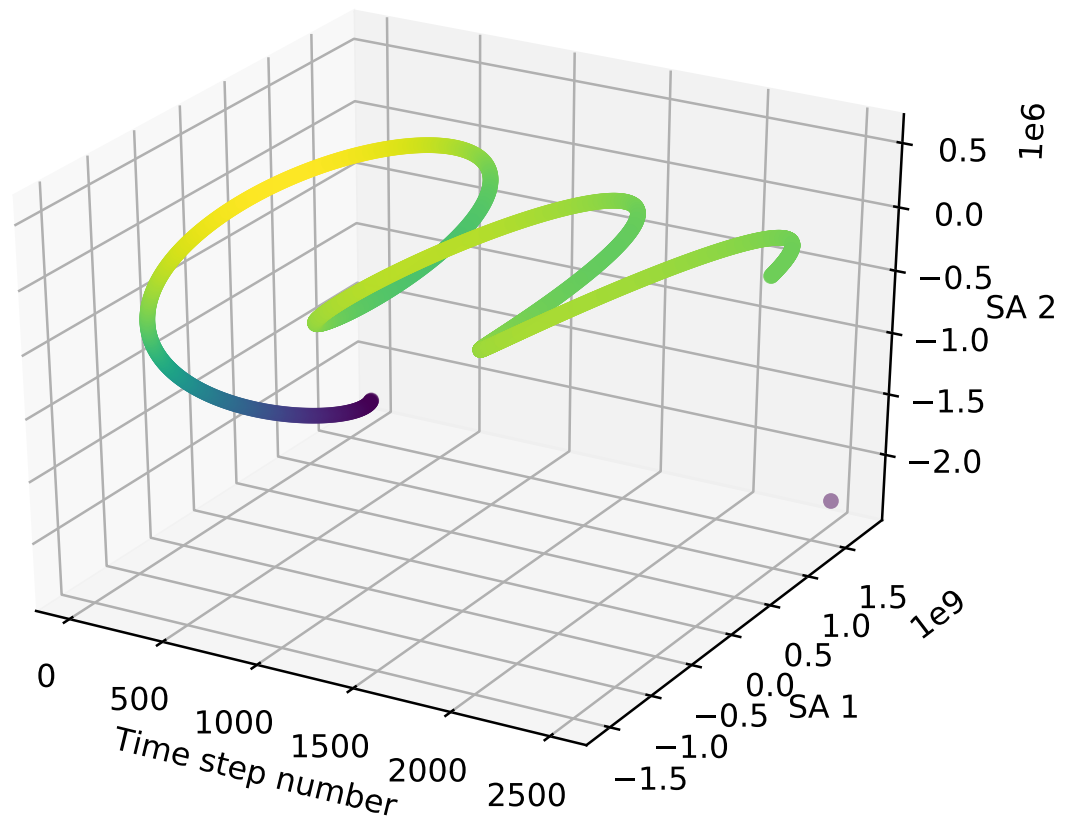


Figure 51: *Extracting measurements from the Lin-Tsien equation with 2500 time steps of evolution.* Performing time-evolution of solution states for the Lin-Tsien equation yields qualitatively different results from previous approximation results.

$$\begin{aligned}
& \frac{\left(\frac{A_x^\dagger - 2\mathbf{1} + A_x}{(\Delta x)^2}\right) |u(x, t + \tau)\rangle - \left(\frac{A_x^\dagger - 2\mathbf{1} + A_x}{(\Delta x)^2}\right) |u(x, t)\rangle}{(\Delta x)\tau} \\
& \quad \Downarrow \\
& (3|u(x, t)\rangle + 2)\left(\frac{A_x - \mathbf{1}}{\Delta x}\right) |u(x, t)\rangle = \frac{1}{\Delta x} (3|u(x, t)\rangle + 2) \times \dots \\
& \quad (A_x |u(x, t)\rangle - |u(x, t)\rangle) = \frac{1}{\Delta x} (\{3|u(x, t)\rangle\} \dots \\
& \quad \{A_x |u(x, t)\rangle\} - \{3|u(x, t)\rangle\}\{|u(x, t)\rangle\} + 2A_x |u(x, t)\rangle - 2|u(x, t)\rangle) \\
& \quad \Downarrow \\
& \left(\frac{A_x^\dagger - 2\mathbf{1} + A_x}{(\Delta x)^2}\right) |u(x, t)\rangle = \frac{1}{(\Delta x)^2} (A_x^\dagger |u(x, t)\rangle - 2|u(x, t)\rangle + A_x |u(x, t)\rangle) \\
& \quad \Downarrow \\
& \left(\frac{A_x^\dagger - 2\mathbf{1} + A_x}{(\Delta x)^2}\right) |u(x, t + \tau)\rangle = \frac{1}{(\Delta x)^2} (A_x^\dagger |u(x, t + \tau)\rangle - \dots \\
& \quad 2|u(x, t + \tau)\rangle + A_x |u(x, t + \tau)\rangle) \\
& \quad \Downarrow \\
& \left(\frac{A_x - \mathbf{1}}{\Delta x}\right) |u(x, t)\rangle \left(\frac{A_x^\dagger - 2\mathbf{1} + A_x}{(\Delta x)^2}\right) |u(x, t)\rangle \\
& \quad \Downarrow \\
& \frac{1}{(\Delta x)^3} \left[ \{A_x - \mathbf{1}\} |u(x, t)\rangle A_x^\dagger - 2\{A_x - \mathbf{1}\} |u(x, t)\rangle + \{A_x - \mathbf{1}\} |u(x, t)\rangle A_x \right] |u(x, t)\rangle
\end{aligned}$$

for terms on the right hand side of the equation, and,

$$\begin{aligned}
& \frac{1}{(\Delta x)^3} \left[ A_x |u(x, t)\rangle A_x^\dagger - |u(x, t)\rangle A_x^\dagger - 2A_x |u(x, t)\rangle - |u(x, t)\rangle + A_x |u(x, t)\rangle A_x - |u(x, t)\rangle A_x \right] |u(x, t)\rangle \\
& \quad \Downarrow \\
& \frac{1}{(\Delta x)^3} \left[ A_x |u(x, t)\rangle A_x^\dagger |u(x, t)\rangle - |u(x, t)\rangle A_x^\dagger |u(x, t)\rangle - 2A_x \right],
\end{aligned}$$

for terms on the left hand side of the equation. As a consequence of previous manipulations, the time evolved variational state corresponding to the solution takes the form,

$$\begin{aligned}
|u(x, t + \tau)\rangle = \tau \left\{ \frac{2}{(\Delta x)^3} (A_x |u(x, t)\rangle A_x^\dagger |u(x, t)\rangle - |u(x, t)\rangle A_x^\dagger |u(x, t)\rangle - 2A_x) + \dots \right. \\
\frac{|u(x, t)\rangle}{(\Delta x)^3} (A_x^\dagger |u(x, t + \tau)\rangle - 2|u(x, t + \tau)\rangle + A_x |u(x, t)\rangle) - \dots \\
\left. \frac{|u(x, t)\rangle}{(\Delta x)^3} \left( A_x^\dagger |u(x, t)\rangle - 2|u(x, t)\rangle + A_x |u(x, t)\rangle \right) - \dots \right. \\
\frac{1}{\Delta x} (3|u(x, t)\rangle A_x |u(x, t)\rangle - 3|u(x, t)\rangle |u(x, t)\rangle + 2A_x |u(x, t)\rangle - 2|u(x, t)\rangle) + \dots \\
\left. \frac{\left(\frac{A_x^\dagger - 2\mathbf{1} + A_x}{(\Delta x)^2}\right) |u(x, t + \tau)\rangle - \left(\frac{A_x^\dagger - 2\mathbf{1} + A_x}{(\Delta x)^2}\right) |u(x, t)\rangle}{(\Delta x)\tau} \right\}
\end{aligned}$$

In turn, the superposition above yields the cost function that can be identified with the expansion of the norm below, after consolidating terms with the time evolved variational state of the solution,

$$\begin{aligned}
\left(1 + \frac{2}{(\Delta x)^3 \tau}\right) |u(x, t + \tau)\rangle &= \tau \left\{ \frac{2}{(\Delta x)^3} (A_x |u(x, t)\rangle A_x^\dagger |u(x, t)\rangle - |u(x, t)\rangle A_x^\dagger |u(x, t)\rangle - 2A_x) + \dots \right. \\
&\quad \left. \frac{|u(x, t)\rangle}{(\Delta x)^3} \left( A_x^\dagger |u(x, t + \tau)\rangle - 2|u(x, t + \tau)\rangle + A_x |u(x, t)\rangle \right) - \dots \right. \\
&\quad \left. \frac{|u(x, t)\rangle}{(\Delta x)^3} \left( A_x^\dagger |u(x, t)\rangle - 2|u(x, t)\rangle + A_x |u(x, t)\rangle \right) - \dots \right. \\
&\quad \left. \frac{1}{\Delta x} \left( 3|u(x, t)\rangle A_x |u(x, t)\rangle - 3|u(x, t)\rangle |u(x, t)\rangle + 2A_x |u(x, t)\rangle - 2|u(x, t)\rangle \right) + \dots \right. \\
&\quad \left. \frac{\left( \frac{A_x^\dagger - 2\mathbf{1} + A_x}{(\Delta x)^2} |u(x, t + \tau)\rangle - \left( \frac{A_x^\dagger - 2\mathbf{1} + A_x}{(\Delta x)^2} |u(x, t)\rangle \right) \right)}{(\Delta x)\tau} \right\} \\
&\quad \Downarrow \\
|u(x, t + \tau)\rangle &= \frac{\tau}{\left(1 + \frac{2}{(\Delta x)^3 \tau}\right)} \left\{ \frac{2}{(\Delta x)^3} (A_x |u(x, t)\rangle A_x^\dagger |u(x, t)\rangle - |u(x, t)\rangle A_x^\dagger |u(x, t)\rangle - 2A_x) + \dots \right. \\
&\quad \left. \frac{|u(x, t)\rangle}{(\Delta x)^3} \left( A_x^\dagger |u(x, t + \tau)\rangle - 2|u(x, t + \tau)\rangle + A_x |u(x, t)\rangle \right) - \dots \right. \\
&\quad \left. \frac{|u(x, t)\rangle}{(\Delta x)^3} \left( A_x^\dagger |u(x, t)\rangle - 2|u(x, t)\rangle + A_x |u(x, t)\rangle \right) - \dots \right. \\
&\quad \left. \frac{1}{\Delta x} \left( 3|u(x, t)\rangle A_x |u(x, t)\rangle - 3|u(x, t)\rangle |u(x, t)\rangle + 2A_x |u(x, t)\rangle - 2|u(x, t)\rangle \right) + \dots \right. \\
&\quad \left. \frac{\left( \frac{A_x^\dagger - 2\mathbf{1} + A_x}{(\Delta x)^2} |u(x, t + \tau)\rangle - \left( \frac{A_x^\dagger - 2\mathbf{1} + A_x}{(\Delta x)^2} |u(x, t)\rangle \right) \right)}{(\Delta x)\tau} \right\}.
\end{aligned}$$

Expanding the square of the following norm yields,

$$\begin{aligned}
\mathcal{C}^{\text{C-H}} &= \left\| |u(x, t + \tau)\rangle - |u(x, t)\rangle \right\|^2 \\
&\quad \Downarrow \\
&= \left\| \frac{\tau}{\left(1 + \frac{2}{(\Delta x)^3 \tau}\right)} \left\{ \frac{2}{(\Delta x)^3} (A_x |u(x, t)\rangle A_x^\dagger |u(x, t)\rangle - |u(x, t)\rangle A_x^\dagger |u(x, t)\rangle - 2A_x) + \dots \right. \right. \\
&\quad \left. \frac{|u(x, t)\rangle}{(\Delta x)^3} \left( A_x^\dagger |u(x, t + \tau)\rangle - 2|u(x, t + \tau)\rangle + A_x |u(x, t)\rangle \right) - \dots \right. \\
&\quad \left. \frac{|u(x, t)\rangle}{(\Delta x)^3} \left( A_x^\dagger |u(x, t)\rangle - 2|u(x, t)\rangle + A_x |u(x, t)\rangle \right) - \dots \right. \\
&\quad \left. \frac{1}{\Delta x} \left( 3|u(x, t)\rangle A_x |u(x, t)\rangle - 3|u(x, t)\rangle |u(x, t)\rangle + 2A_x |u(x, t)\rangle - 2|u(x, t)\rangle \right) + \dots \right. \\
&\quad \left. \frac{\left( \frac{A_x^\dagger - 2\mathbf{1} + A_x}{(\Delta x)^2} |u(x, t + \tau)\rangle - \left( \frac{A_x^\dagger - 2\mathbf{1} + A_x}{(\Delta x)^2} |u(x, t)\rangle \right) \right)}{(\Delta x)\tau} \right\} - |u(x, t)\rangle \right\|^2.
\end{aligned}$$

As with derivations of previous cost functions, the first component of the superposition is solely dependent upon the initial choice of variational parameter  $\lambda$ , while remaining terms are inversely proportional with respect to either the time step  $\tau$  with which the solution state is evolved, or the grid resolution  $\Delta x$ . The superposition is of the form,

$$\begin{aligned}
& \lambda^2 + \left\{ \frac{\tau}{\left(1 + \frac{2}{(\Delta x)^{3\tau}}\right)} \left\{ \frac{2}{(\Delta x)^3} (A_x |u(x, t)\rangle A_x^\dagger |u(x, t)\rangle - |u(x, t)\rangle A_x^\dagger |u(x, t)\rangle - 2A_x) + \dots \right. \right. \\
& \quad \left. \frac{|u(x, t)\rangle}{(\Delta x)^3} (A_x^\dagger |u(x, t + \tau)\rangle - 2|u(x, t + \tau)\rangle + A_x |u(x, t)\rangle) - \dots \right. \\
& \quad \left. \frac{|u(x, t)\rangle}{(\Delta x)^3} (A_x^\dagger |u(x, t)\rangle - 2|u(x, t)\rangle + A_x |u(x, t)\rangle) - \dots \right. \\
& \quad \left. \frac{1}{\Delta x} (3|u(x, t)\rangle A_x |u(x, t)\rangle - 3|u(x, t)\rangle |u(x, t)\rangle + 2A_x |u(x, t)\rangle - 2|u(x, t)\rangle) + \dots \right. \\
& \quad \left. \frac{\left( \frac{A_x^\dagger - 2\mathbf{1} + A_x}{(\Delta x)^2} |u(x, t + \tau)\rangle - \left( \frac{A_x^\dagger - 2\mathbf{1} + A_x}{(\Delta x)^2} |u(x, t)\rangle \right) \right)}{(\Delta x)\tau} \right\}^2 + \dots \\
& 2\lambda^2 \frac{\tau}{\left(1 + \frac{2}{(\Delta x)^{3\tau}}\right)} \left\{ \frac{2}{(\Delta x)^3} (A_x |u(x, t)\rangle A_x^\dagger |u(x, t)\rangle - |u(x, t)\rangle A_x^\dagger |u(x, t)\rangle - 2A_x) + \dots \right. \\
& \quad \left. \frac{|u(x, t)\rangle}{(\Delta x)^3} (A_x^\dagger |u(x, t + \tau)\rangle - 2|u(x, t + \tau)\rangle + A_x |u(x, t)\rangle) - \dots \right. \\
& \quad \left. \frac{|u(x, t)\rangle}{(\Delta x)^3} (A_x^\dagger |u(x, t)\rangle - 2|u(x, t)\rangle + A_x |u(x, t)\rangle) - \dots \right. \\
& \quad \left. \frac{1}{\Delta x} (3|u(x, t)\rangle A_x |u(x, t)\rangle - 3|u(x, t)\rangle |u(x, t)\rangle + 2A_x |u(x, t)\rangle - 2|u(x, t)\rangle) + \dots \right. \\
& \quad \left. \frac{\left( \frac{A_x^\dagger - 2\mathbf{1} + A_x}{(\Delta x)^2} |u(x, t + \tau)\rangle - \left( \frac{A_x^\dagger - 2\mathbf{1} + A_x}{(\Delta x)^2} |u(x, t)\rangle \right) \right)}{(\Delta x)\tau} \right\}
\end{aligned}$$

Expanding all terms in the order that they appear in the superposition following  $\lambda^2$  yields,

$$\begin{aligned}
& \left\{ \frac{\tau}{\left(1 + \frac{2}{(\Delta x)^{3\tau}}\right)} \left\{ \frac{2}{(\Delta x)^3} (A_x |u(x, t)\rangle A_x^\dagger |u(x, t)\rangle - |u(x, t)\rangle A_x^\dagger |u(x, t)\rangle - 2A_x) + \dots \right. \right. \\
& \quad \left. \frac{|u(x, t)\rangle}{(\Delta x)^3} (A_x^\dagger |u(x, t + \tau)\rangle - 2|u(x, t + \tau)\rangle + A_x |u(x, t)\rangle) - \dots \right. \\
& \quad \left. \frac{|u(x, t)\rangle}{(\Delta x)^3} (A_x^\dagger |u(x, t)\rangle - 2|u(x, t)\rangle + A_x |u(x, t)\rangle) - \dots \right. \\
& \quad \left. \frac{1}{\Delta x} (3|u(x, t)\rangle A_x |u(x, t)\rangle - 3|u(x, t)\rangle |u(x, t)\rangle + 2A_x |u(x, t)\rangle - 2|u(x, t)\rangle) + \dots \right. \\
& \quad \left. \frac{\left( \frac{A_x^\dagger - 2\mathbf{1} + A_x}{(\Delta x)^2} |u(x, t + \tau)\rangle - \left( \frac{A_x^\dagger - 2\mathbf{1} + A_x}{(\Delta x)^2} |u(x, t)\rangle \right) \right)}{(\Delta x)\tau} \right\}^2 \right\}.
\end{aligned}$$

We square the terms included in the superposition above to obtain,

$$\begin{aligned}
& \left\{ \frac{\tau}{\left(1 + \frac{2}{(\Delta x)^{3\tau}}\right)} \left\{ \frac{2}{(\Delta x)^3} (A_x |u(x, t)\rangle A_x^\dagger |u(x, t)\rangle - |u(x, t)\rangle A_x^\dagger |u(x, t)\rangle - 2A_x) + \dots \right. \right. \\
& \quad \left. \frac{|u(x, t)\rangle}{(\Delta x)^3} (A_x^\dagger |u(x, t + \tau)\rangle - 2|u(x, t + \tau)\rangle + A_x |u(x, t)\rangle) - \dots \right. \\
& \quad \left. \frac{|u(x, t)\rangle}{(\Delta x)^3} (A_x^\dagger |u(x, t)\rangle - 2|u(x, t)\rangle + A_x |u(x, t)\rangle) - \dots \right. \\
& \quad \left. \frac{1}{\Delta x} (3|u(x, t)\rangle A_x |u(x, t)\rangle - 3|u(x, t)\rangle |u(x, t)\rangle + 2A_x |u(x, t)\rangle - 2|u(x, t)\rangle) \right\}^2 + \dots
\end{aligned}$$

$$\begin{aligned}
& \left\{ \frac{\left( \frac{A_x^\dagger - 2\mathbf{1} + A_x}{(\Delta x)^2} |u(x, t + \tau)\rangle - \left( \frac{A_x^\dagger - 2\mathbf{1} + A_x}{(\Delta x)^2} |u(x, t)\rangle \right) \right\}^2 + \dots \\
& \quad 2 \frac{\left( \frac{A_x^\dagger - 2\mathbf{1} + A_x}{(\Delta x)^2} |u(x, t + \tau)\rangle - \left( \frac{A_x^\dagger - 2\mathbf{1} + A_x}{(\Delta x)^2} |u(x, t)\rangle \right) \right. \\
& \quad \left. (\Delta x)\tau \right\} \times \dots \\
& \left\{ \frac{\tau}{\left( 1 + \frac{2}{(\Delta x)^{3\tau}} \right)} \frac{2}{(\Delta x)^3} (A_x |u(x, t)\rangle A_x^\dagger |u(x, t)\rangle - |u(x, t)\rangle A_x^\dagger |u(x, t)\rangle - 2A_x) + \dots \right. \\
& \quad \frac{|u(x, t)\rangle}{(\Delta x)^3} (A_x^\dagger |u(x, t + \tau)\rangle - 2|u(x, t + \tau)\rangle + A_x |u(x, t)\rangle) - \dots \\
& \quad \left. \frac{|u(x, t)\rangle}{(\Delta x)^3} (A_x^\dagger |u(x, t)\rangle - 2|u(x, t)\rangle + A_x |u(x, t)\rangle) \right\} - \dots \\
& \quad \frac{1}{\Delta x} \left( 3|u(x, t)\rangle A_x |u(x, t)\rangle - 3|u(x, t)\rangle |u(x, t)\rangle + 2A_x |u(x, t)\rangle - 2|u(x, t)\rangle \right) \Big\}^2
\end{aligned}$$

Furthermore, following necessary rearrangements of the expansion provides,

$$\begin{aligned}
& \left\{ \frac{\tau}{\left( 1 + \frac{2}{(\Delta x)^{3\tau}} \right)} \left\{ \frac{2}{(\Delta x)^3} \left( A_x |u(x, t)\rangle A_x^\dagger |u(x, t)\rangle - |u(x, t)\rangle A_x^\dagger |u(x, t)\rangle - 2A_x \right) + \dots \right. \right. \\
& \quad \frac{|u(x, t)\rangle}{(\Delta x)^3} \left( A_x^\dagger |u(x, t + \tau)\rangle - 2|u(x, t + \tau)\rangle + A_x |u(x, t)\rangle \right) - \dots \\
& \quad \left. \frac{|u(x, t)\rangle}{(\Delta x)^3} \left( A_x^\dagger |u(x, t)\rangle - 2|u(x, t)\rangle + A_x |u(x, t)\rangle \right) \right\} - \dots \\
& \quad \left. \frac{1}{\Delta x} \left( 3|u(x, t)\rangle A_x |u(x, t)\rangle - 3|u(x, t)\rangle |u(x, t)\rangle + 2A_x |u(x, t)\rangle - 2|u(x, t)\rangle \right) \right\}^2 .
\end{aligned}$$

Distributing further,

$$\begin{aligned}
& \frac{\tau^2}{\left( 1 + \frac{2}{(\Delta x)^{3\tau}} \right)^2} \left\{ \frac{2}{(\Delta x)^3} \left( A_x |u(x, t)\rangle A_x^\dagger |u(x, t)\rangle - |u(x, t)\rangle A_x^\dagger |u(x, t)\rangle - 2A_x \right) + \dots \right. \\
& \quad \frac{|u(x, t)\rangle}{(\Delta x)^3} \left( A_x^\dagger |u(x, t + \tau)\rangle - 2|u(x, t + \tau)\rangle + A_x |u(x, t)\rangle \right) - \dots \\
& \quad \left. \frac{|u(x, t)\rangle}{(\Delta x)^3} \left( A_x^\dagger |u(x, t)\rangle - 2|u(x, t)\rangle + A_x |u(x, t)\rangle \right) \right\}^2 - \dots \\
& \quad \frac{\tau^2}{\Delta x \left( 1 + \frac{2}{(\Delta x)^{3\tau}} \right)^2} \left( 3|u(x, t)\rangle A_x |u(x, t)\rangle - \dots \right. \\
& \quad \left. 3|u(x, t)\rangle |u(x, t)\rangle + 2A_x |u(x, t)\rangle - 2|u(x, t)\rangle \right) \Big\}^2 .
\end{aligned}$$

From the resulting terms above, the terms of the superposition following the prefactor dependent upon  $\tau^2$  is,



$$\begin{aligned}
& \left. \begin{aligned} & 9 \langle u(x, t) | A_x^\dagger \langle u(x, t) | |u(x, t)\rangle A_x |u(x, t)\rangle \end{aligned} \right) - \dots \\
& 2 \left( \begin{aligned} & 3 |u(x, t)\rangle A_x |u(x, t)\rangle - 3 \langle u(x, t) | A_x |u(x, t)\rangle \end{aligned} \right) \times \dots \\
& \left( \begin{aligned} & 2 A_x |u(x, t)\rangle - 2 \langle u(x, t) | \end{aligned} \right) + \dots \\
& \left( \begin{aligned} & \langle u(x, t) | 4 A_x |u(x, t)\rangle - \langle u(x, t) | 8 A_x |u(x, t)\rangle + \langle u(x, t) | 8 \langle u(x, t) | \end{aligned} \right) \left. \right)
\end{aligned}$$

Expanding the squares of expectation values in the above superposition,

$$\begin{aligned}
& \frac{\tau^2}{\left(1 + \frac{2}{(\Delta x)^{3\tau}}\right)^2} \left\{ \begin{aligned} & \frac{4}{(\Delta x)^6} \left( \langle u(x, t) | A_x \langle u(x, t) | A_x^\dagger - \dots \right. \\ & A_x |u(x, t)\rangle A_x^\dagger |u(x, t)\rangle - 2 \langle u(x, t) | A_x \langle u(x, t) | A_x |u(x, t)\rangle A_x^\dagger |u(x, t)\rangle + \dots \\ & \left. \langle u(x, t) | A_x \langle u(x, t) | |u(x, t)\rangle A_x^\dagger |u(x, t)\rangle \right) + \dots \\ & \frac{1}{(\Delta x)^6} \left( \langle u(x, t) | A_x^\dagger |u(x, t + \tau)\rangle \langle u(x, t + \tau) | A_x |u(x, t)\rangle - \dots \right. \\ & 2 \langle u(x, t) | |u(x, t + \tau)\rangle \langle u(x, t + \tau) | A_x |u(x, t)\rangle + \dots \\ & \left. \langle u(x, t) | A_x |u(x, t)\rangle \langle u(x, t + \tau) | A_x |u(x, t)\rangle \right) + \dots \\ & \frac{8}{(\Delta x)^9} \left( \begin{aligned} & \langle u(x, t) | A_x^\dagger \langle u(x, t + \tau) | A_x |u(x, t)\rangle A_x^\dagger |u(x, t)\rangle - \dots \\ & 2 \langle u(x, t) | |u(x, t + \tau)\rangle A_x |u(x, t)\rangle A_x^\dagger |u(x, t)\rangle + \langle u(x, t) | A_x |u(x, t)\rangle - \dots \\ & \langle u(x, t) | A_x^\dagger |u(x, t + \tau)\rangle |u(x, t)\rangle A_x^\dagger |u(x, t)\rangle - \dots \\ & 2 \langle u(x, t) | |u(x, t + \tau)\rangle |u(x, t)\rangle A_x^\dagger |u(x, t)\rangle - \dots \end{aligned} \right) \\ & \left. \langle u(x, t) | A_x |u(x, t)\rangle A_x |u(x, t)\rangle A_x^\dagger |u(x, t)\rangle \right) + \dots \\ & 2 \left( \frac{2}{(\Delta x)^3} \left( A_x |u(x, t)\rangle A_x^\dagger |u(x, t)\rangle - |u(x, t)\rangle A_x^\dagger |u(x, t)\rangle - 2 A_x \right) + \dots \right. \\ & \left. \frac{|u(x, t)\rangle}{(\Delta x)^3} \left( A_x^\dagger |u(x, t + \tau)\rangle - 2 |u(x, t + \tau)\rangle + A_x |u(x, t)\rangle \right) \right) + \dots \\ & \left. \frac{|u(x, t)\rangle}{(\Delta x)^3} \left( A_x^\dagger |u(x, t)\rangle - 2 |u(x, t)\rangle + A_x |u(x, t)\rangle \right) \right\}
\end{aligned}$$

while the cross term resulting in the superposition with prefactor  $\frac{\tau^2}{\Delta x \left(1 + \frac{2}{(\Delta x)^{2\tau}}\right)^2}$  takes the form,

$$\begin{aligned}
& \frac{2\tau^2}{\Delta x \left(1 + \frac{2}{(\Delta x)^{3\tau}}\right)^2} \left( \begin{aligned} & 6 |u(x, t)\rangle A_x |u(x, t)\rangle A_x |u(x, t)\rangle - \dots \\ & 6 \langle u(x, t) | |u(x, t)\rangle A_x |u(x, t)\rangle - \dots \\ & 6 |u(x, t)\rangle A_x |u(x, t)\rangle A_x |u(x, t)\rangle + \dots \\ & 6 \langle u(x, t) | |u(x, t)\rangle A_x |u(x, t)\rangle \end{aligned} \right).
\end{aligned}$$

Overall, the superposition with prefactor  $\frac{\tau^2}{\Delta x \left(1 + \frac{2}{(\Delta x)^{3\tau}}\right)^2}$  becomes,

$$\begin{aligned} & \frac{\tau^2}{\Delta x \left(1 + \frac{2}{(\Delta x)^{3\tau}}\right)^2} \left( \left( \langle u(x, t) | A_x^\dagger \langle u(x, t) | 9 | u(x, t) \rangle A_x | u(x, t) \rangle - \dots \right. \right. \\ & \quad \left. \left. 6 \langle u(x, t) | A_x^\dagger \langle u(x, t) | | u(x, t) \rangle A_x | u(x, t) \rangle + \dots \right. \right. \\ & \quad \left. \left. 9 \langle u(x, t) | A_x^\dagger \langle u(x, t) | | u(x, t) \rangle A_x | u(x, t) \rangle \right) - \dots \right. \\ & \quad \left. 2 \left( 6 | u(x, t) \rangle A_x | u(x, t) \rangle A_x | u(x, t) \rangle - 6 \langle u(x, t) | | u(x, t) \rangle A_x | u(x, t) \rangle - \dots \right. \right. \\ & \quad \left. \left. 6 | u(x, t) \rangle A_x | u(x, t) \rangle A_x | u(x, t) \rangle + \dots \right. \right. \\ & \quad \left. \left. 6 \langle u(x, t) | | u(x, t) \rangle A_x | u(x, t) \rangle \right) + \dots \right. \\ & \quad \left. \left( \langle u(x, t) | 4 A_x | u(x, t) \rangle - \langle u(x, t) | 8 A_x | u(x, t) \rangle + \langle u(x, t) | 8 | u(x, t) \rangle \right) \right), \end{aligned}$$

implying that the finalized cost function the quantum state whose ground state we approximate is,

$$\begin{aligned} \boxed{\mathcal{C}^{\text{C-H}}(\lambda, \lambda_0^{\text{C-H}})} &= (\lambda_0^{\text{C-H}})^2 + \text{Re} \left\{ \frac{4\lambda^2}{(\Delta x)^3} \frac{\tau}{\left(1 + \frac{2}{(\Delta x)^{3\tau}}\right)} \langle u | A_x A_x | u \rangle - \dots \right. \\ & \quad \left. \frac{2\lambda^2}{(\Delta x)^3} \frac{\tau}{\left(1 + \frac{2}{(\Delta x)^{3\tau}}\right)} \langle u | A_x | u \rangle - \dots \right. \\ & \quad \frac{8\lambda^2}{(\Delta x)^3} \frac{\tau}{\left(1 + \frac{2}{(\Delta x)^{3\tau}}\right)} A_x | u \rangle + \frac{4\lambda^2}{(\Delta x)^4} \frac{\tau}{\left(1 + \frac{2}{(\Delta x)^{3\tau}}\right)} A_x^\dagger | \tilde{u} \rangle + \frac{8\lambda^2}{(\Delta x)^6} \frac{\tau}{\left(1 + \frac{2}{(\Delta x)^{3\tau}}\right)} | \tilde{u} \rangle + \dots \\ & \quad \frac{8\lambda^2}{(\Delta x)^6} \frac{\tau}{\left(1 + \frac{2}{(\Delta x)^{3\tau}}\right)} A_x | u \rangle + \frac{8\lambda^2}{(\Delta x)^6} \frac{\tau}{\left(1 + \frac{2}{(\Delta x)^{3\tau}}\right)} A_x^\dagger | u \rangle - \dots \\ & \quad \frac{4\lambda^2}{(\Delta x)^6} \frac{\tau}{\left(1 + \frac{2}{(\Delta x)^{3\tau}}\right)} A_x^\dagger | u \rangle - \frac{8\lambda^2}{(\Delta x)^6} \frac{\tau}{\left(1 + \frac{2}{(\Delta x)^{3\tau}}\right)} | \tilde{u} \rangle - \frac{4\lambda^2}{(\Delta x)^6} \frac{\tau}{\left(1 + \frac{2}{(\Delta x)^{3\tau}}\right)} A_x | u \rangle - \dots \\ & \quad \frac{4\lambda^2}{(\Delta x)^6} \frac{\tau}{\left(1 + \frac{2}{(\Delta x)^{3\tau}}\right)} - \left( \frac{3}{\Delta x} \right) \frac{4\lambda^2}{(\Delta x)^3} \frac{\tau}{\left(1 + \frac{2}{(\Delta x)^{3\tau}}\right)} \langle u | A_x^\dagger | u \rangle + \frac{12\lambda^2}{(\Delta x)^4} \frac{\tau}{\left(1 + \frac{2}{(\Delta x)^{3\tau}}\right)} \langle u | | u \rangle + \dots \\ & \quad \frac{8\lambda^2}{(\Delta x)^4} \frac{\tau}{\left(1 + \frac{2}{(\Delta x)^{3\tau}}\right)} A_x | u \rangle + \frac{4\lambda^2}{(\Delta x)^4} \frac{\tau}{\left(1 + \frac{2}{(\Delta x)^{3\tau}}\right)} | u \rangle + \left( \frac{4\lambda^2}{(\Delta x)^4} \right) \left( \frac{2}{(\Delta x)^3} \right) \frac{\tau}{\left(1 + \frac{2}{(\Delta x)^{3\tau}}\right)} A_x^\dagger | \tilde{u} \rangle - \dots \\ & \quad \left( \frac{4\lambda^2}{(\Delta x)^5} \right) \left( \frac{2}{(\Delta x)^3} \right) \frac{\tau}{\left(1 + \frac{2}{(\Delta x)^{3\tau}}\right)} | \tilde{u} \rangle + 2 \left( \frac{4\lambda^2}{(\Delta x)^4} \right) \left( \frac{2}{(\Delta x)^3} \right) \frac{\tau}{\left(1 + \frac{2}{(\Delta x)^{3\tau}}\right)} A_x | \tilde{u} \rangle - \dots \end{aligned}$$

$$\begin{aligned}
& \left( \frac{4\lambda^2}{(\Delta x)^4} \right) \left( \frac{2}{(\Delta x)^3} \right) \frac{\tau}{\left(1 + \frac{2}{(\Delta x)^{3\tau}}\right)} A_x^\dagger |u\rangle + \left( \frac{4\lambda^2}{(\Delta x)^4} \right) \left( \frac{2}{(\Delta x)^3} \right) \frac{\tau}{\left(1 + \frac{2}{(\Delta x)^{3\tau}}\right)} |u\rangle - \dots \\
& \left( \frac{4\lambda^2}{(\Delta x)^4} \right) \left( \frac{2}{(\Delta x)^3} \right) \frac{\tau}{\left(1 + \frac{2}{(\Delta x)^{3\tau}}\right)} A_x |u\rangle + \frac{8\tau^2}{\left(1 + \frac{2}{(\Delta x)^{3\tau}}\right)^2} \left( \frac{1}{(\Delta x)^6} \right) \langle u | A_x A_x |u\rangle - \dots \\
& \frac{8\tau^2}{\left(1 + \frac{2}{(\Delta x)^{3\tau}}\right)^2} \left( \frac{1}{(\Delta x)^6} \right) \left( \langle u | A_x A_x^\dagger |u\rangle \right) \left( \langle u | A_x |u\rangle \right) + \frac{4\tau^2}{\left(1 + \frac{2}{(\Delta x)^{3\tau}}\right)^2} \left( \frac{1}{(\Delta x)^6} \right) \times \dots \\
& \left( \langle u | |u\rangle \right) \left( \langle u | A_x A_x^\dagger |u\rangle \right) + \frac{4\tau^2}{\left(1 + \frac{2}{(\Delta x)^{3\tau}}\right)^2} \left( \frac{1}{(\Delta x)^6} \right) \left( \langle u | A_x^\dagger | \tilde{u} \rangle \right) \left( \langle \tilde{u} | A_x |u\rangle \right) - \dots \\
& \frac{4\tau^2}{\left(1 + \frac{2}{(\Delta x)^{3\tau}}\right)^2} \left( \frac{2}{(\Delta x)^6} \right) \left( \langle u | | \tilde{u} \rangle \right) \left( \langle \tilde{u} | A_x |u\rangle \right) + \frac{4\tau^2}{\left(1 + \frac{1}{(\Delta x)^{3\tau}}\right)^2} \left( \frac{2}{(\Delta x)^6} \right) \left( \langle u | A_x |u\rangle \right) \times \dots \\
& \left( \langle \tilde{u} | A_x |u\rangle \right) + \frac{4\tau^2}{\left(1 + \frac{1}{(\Delta x)^{3\tau}}\right)^2} \left( \frac{8}{(\Delta x)^9} \right) \left( \langle u | A_x^\dagger A_x^\dagger | \tilde{u} \rangle \right) \left( \langle u | A_x |u\rangle \right) - \dots \\
& \frac{4\tau^2}{\left(1 + \frac{1}{(\Delta x)^{3\tau}}\right)^2} \left( \frac{16}{(\Delta x)^9} \right) \left( \langle u | | \tilde{u} \rangle \right) \left( \langle u | A_x A_x |u\rangle \right) + \frac{4\tau^2}{\left(1 + \frac{1}{(\Delta x)^{3\tau}}\right)^2} \left( \frac{8}{(\Delta x)^9} \right) \langle u | A_x |u\rangle - \dots \\
& \frac{4\tau^2}{\left(1 + \frac{1}{(\Delta x)^{3\tau}}\right)^2} \left( \frac{8}{(\Delta x)^9} \right) \left( \langle u | A_x^\dagger | \tilde{u} \rangle \right) \left( \langle u | A_x |u\rangle \right) - \frac{4\tau^2}{\left(1 + \frac{1}{(\Delta x)^{3\tau}}\right)^2} \left( \frac{16}{(\Delta x)^9} \right) \left( \langle u | | \tilde{u} \rangle \right) \times \dots \\
& \left( \langle u | A_x |u\rangle \right) - \frac{4\tau^2}{\left(1 + \frac{1}{(\Delta x)^{3\tau}}\right)^2} \left( \frac{8}{(\Delta x)^9} \right) \left( \langle u | A_x |u\rangle \right) \left( \langle u | A_x A_x |u\rangle \right) + \frac{\tau^2}{\left(1 + \frac{1}{(\Delta x)^{3\tau}}\right)^2} \times \dots \\
& \left( \frac{4}{(\Delta x)^3} \right) \langle u | A_x A_x |u\rangle - \frac{\tau^2}{\left(1 + \frac{1}{(\Delta x)^{3\tau}}\right)^2} \left( \frac{4}{(\Delta x)^3} \right) \langle u | A_x |u\rangle - \frac{\tau^2}{\left(1 + \frac{1}{(\Delta x)^{3\tau}}\right)^2} \left( \frac{8}{(\Delta x)^3} \right) A_x |u\rangle + \dots \\
& \frac{2\tau^2}{(\Delta x)^3 \left(1 + \frac{1}{(\Delta x)^{3\tau}}\right)^2} \langle \tilde{u} | A_x |u\rangle + \frac{4\tau^2}{(\Delta x)^3 \left(1 + \frac{1}{(\Delta x)^{3\tau}}\right)^2} \langle \tilde{u} | |u\rangle + \dots \\
& \frac{2\tau^2}{(\Delta x)^3 \left(1 + \frac{1}{(\Delta x)^{3\tau}}\right)^2} \langle u | A_x^\dagger |u\rangle + \frac{2\tau^2}{(\Delta x)^3 \left(1 + \frac{1}{(\Delta x)^{3\tau}}\right)^2} \langle u | A_x^\dagger |u\rangle + \frac{9\tau^2}{\Delta x \left(1 + \frac{2}{(\Delta x)^{2\tau}}\right)^2} \left( \langle u | |u\rangle \right) \times \dots \\
& \left( \langle u | A_x^\dagger A_x |u\rangle \right) - \frac{6\tau^2}{\Delta x \left(1 + \frac{1}{(\Delta x)^{3\tau}}\right)^2} \left( \langle u | |u\rangle \right) \left( \langle u | A_x^\dagger A_x |u\rangle \right) - \dots \\
& \frac{9\tau^2}{\Delta x \left(1 + \frac{1}{(\Delta x)^{3\tau}}\right)^2} \left( \langle u | |u\rangle \right) \left( \langle u | A_x^\dagger A_x |u\rangle \right) - 12 \left( \langle u | A_x^\dagger |u\rangle \right) A_x |u\rangle - 12 \left( \langle u | |u\rangle \right) A_x |u\rangle + \dots \\
& \left. 12 \left( \langle u | |u\rangle \right) A_x |u\rangle + 4 \langle u | A_x |u\rangle - 8 \langle u | A_x |u\rangle + 8 \langle u | |u\rangle \right\} .
\end{aligned}$$

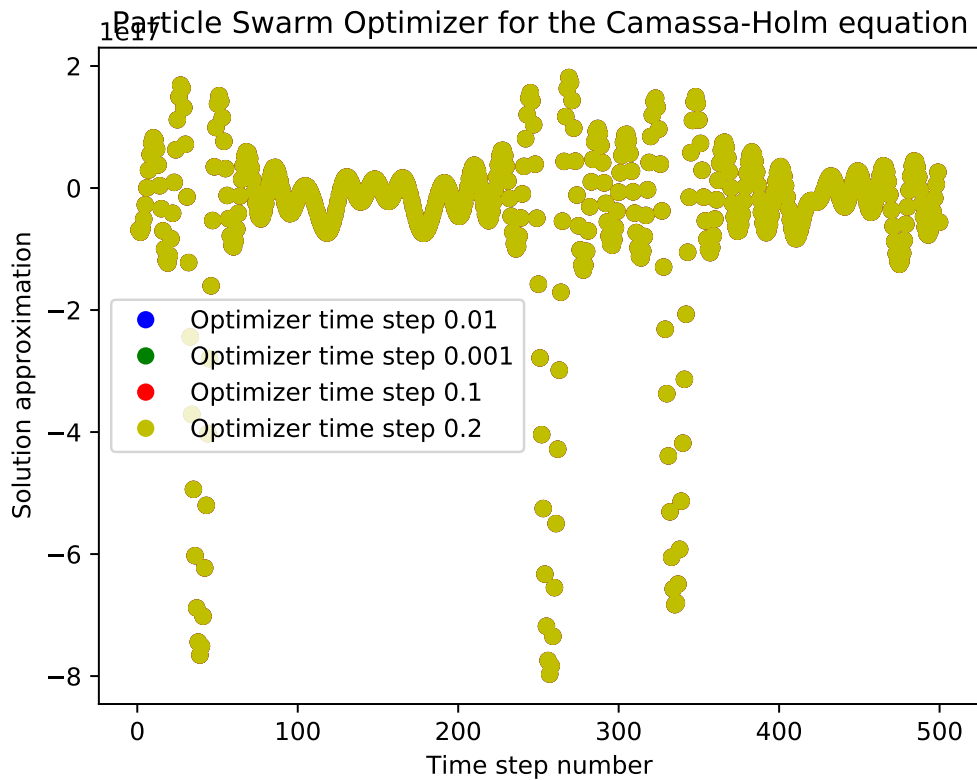
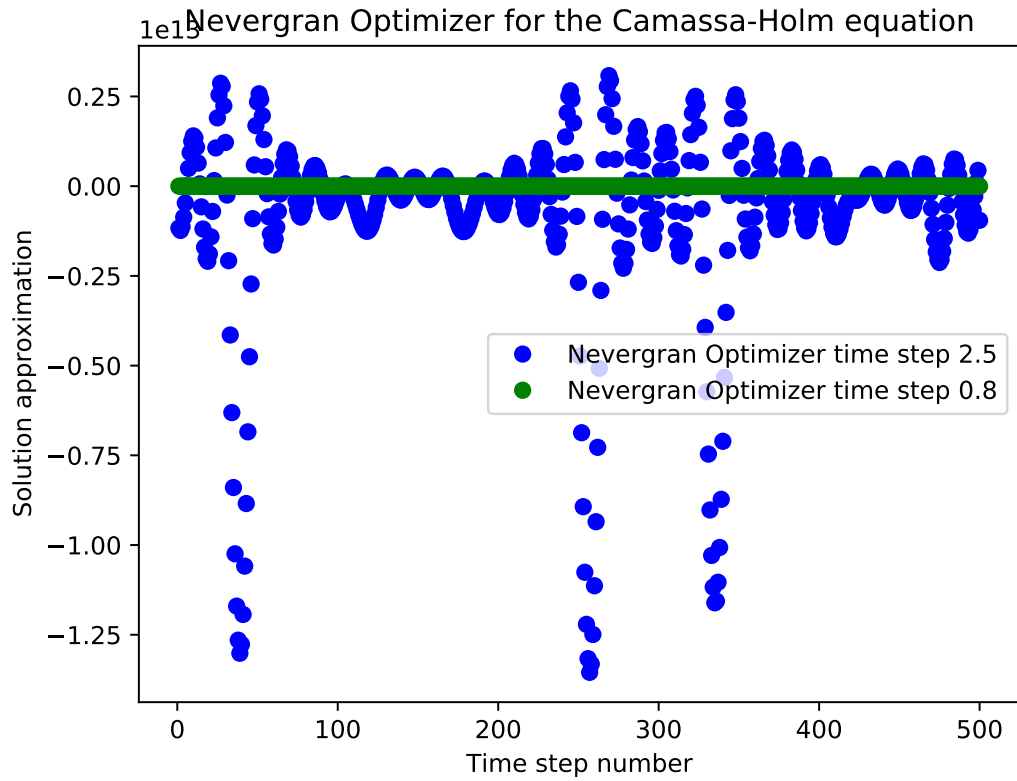


Figure 52: *Extracting measurements from the Camassa-Holm equation corresponding to the periodic peakon and cuspon solutions.* Implementing the variational quantum algorithm for different time steps and initial conditions with the Particle Swarm optimizer yield qualitatively similar results. Varying the time step magnitude on the Particle Swarm optimizer presents no difference in the solution approximation.

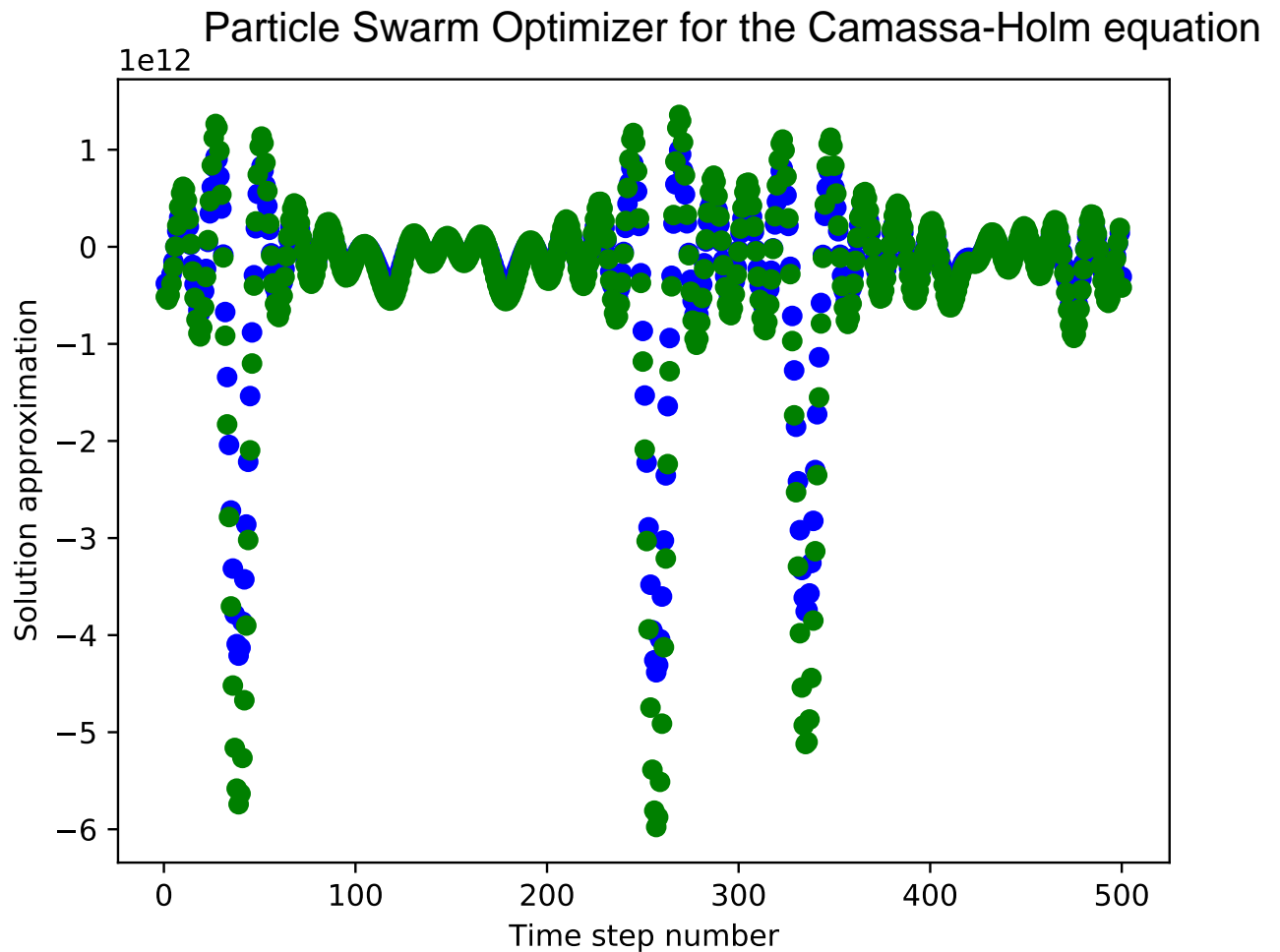
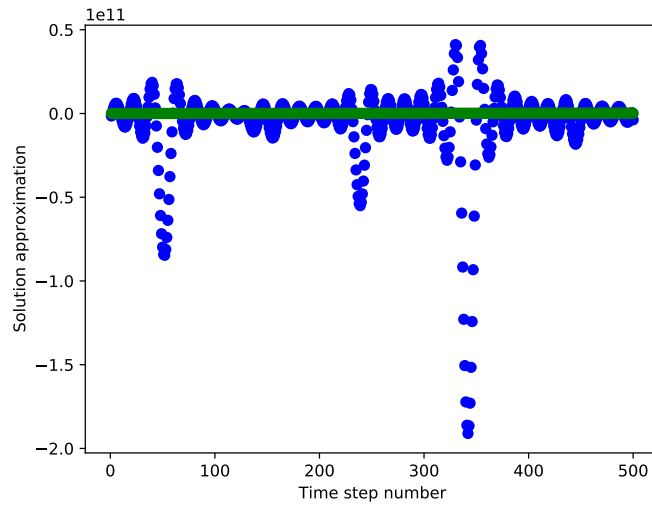
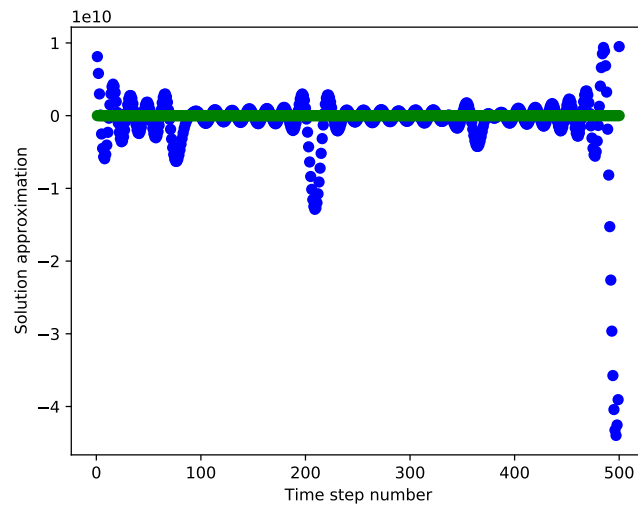


Figure 53: *Extracting measurements from the Camassa-Holm equation.* Implementing the variational quantum algorithm for different time steps and initial conditions with the Particle Swarm optimizer yield qualitatively similar results. Comparing the solution approximations for the PDE from each of the two ansatzes reveals that the ansatz with the higher amplitude encoded through the initial condition fluctuates more significantly about the beginning and ending phases of motion over each period.

Nevergrad and Imfil Optimizers for the Camassa-Holm equation



Nevergrad and Imfil Optimizers for the Camassa-Holm equation



Nevergrad and Imfil Optimizers for the Camassa-Holm equation

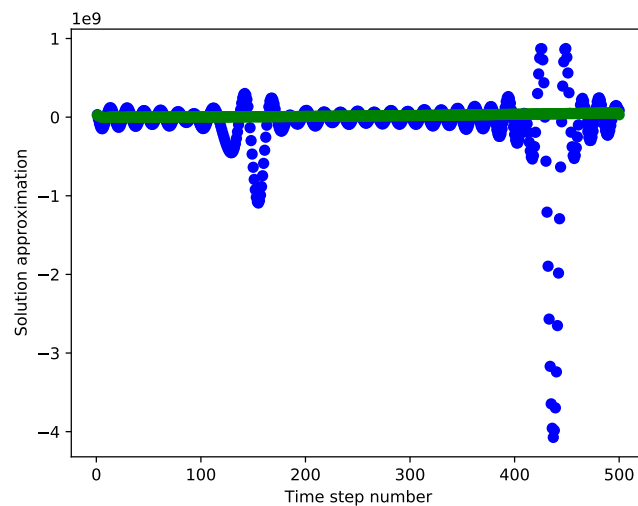


Figure 54: *Extracting measurements from the Camassa-Holm equation corresponding to additional periodic peakon and cuspon solutions.* Implementing the variational quantum algorithm for different time steps and initial conditions, predominantly with the Nevergrad and Imfil optimizers, provides qualitatively similar results for solution approximations.

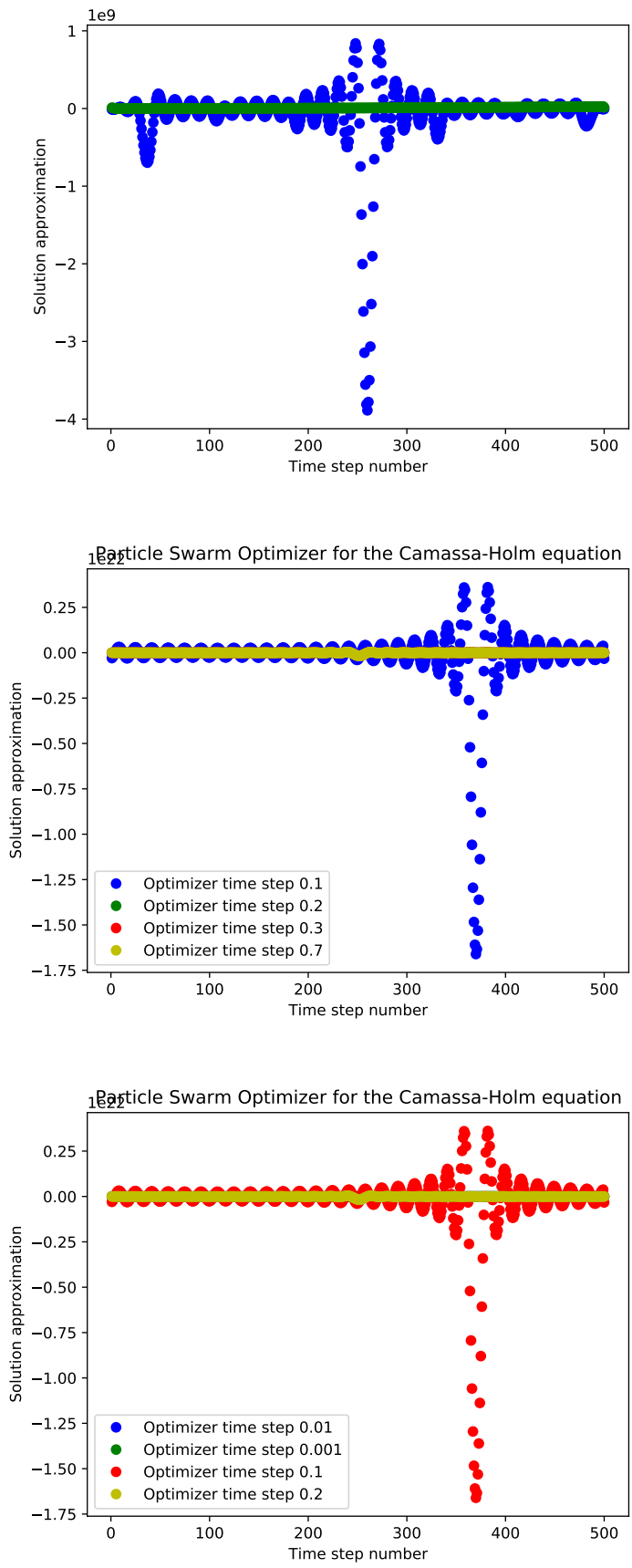


Figure 55: *Extracting measurements from the Camassa-Holm equation corresponding to additional solutions.* Implementing the variational quantum algorithm for different time steps and initial conditions, predominantly with the Nevergrad and Imfil optimizers, provides qualitatively similar results for solution approximations.

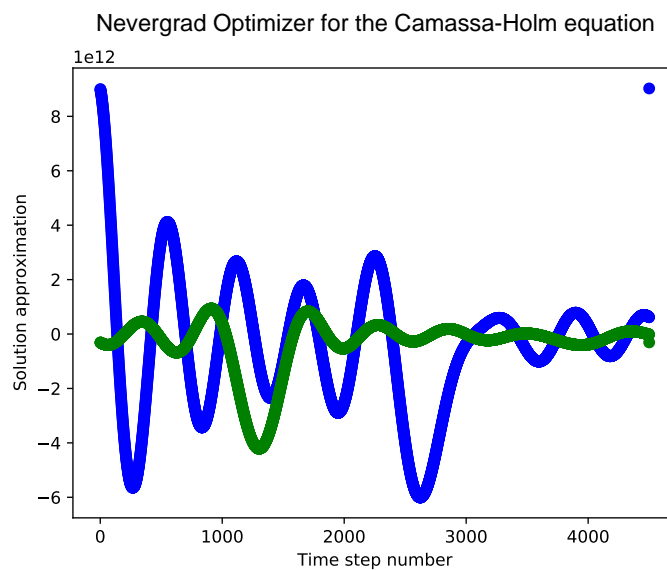
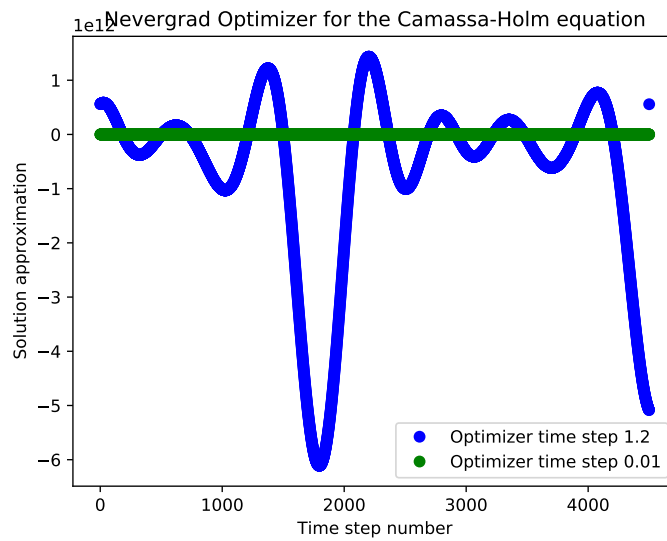
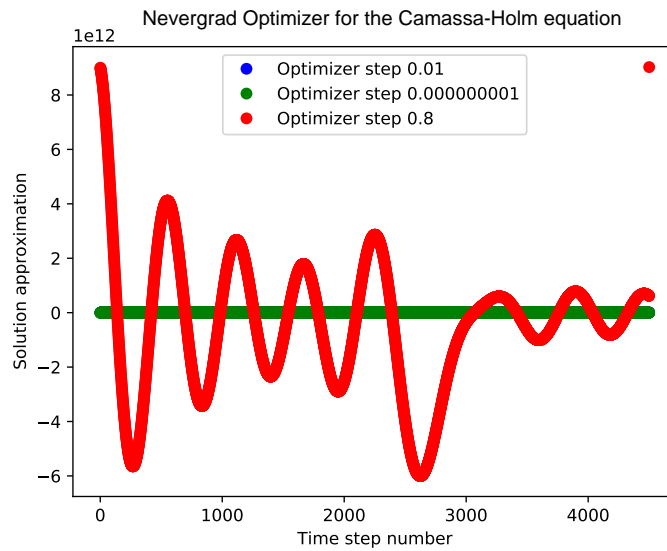


Figure 56: *Extracting measurements from the Camassa-Holm equation.* Implementing the variational quantum algorithm for 4500 time steps yields sinusoidal profiles of motion.

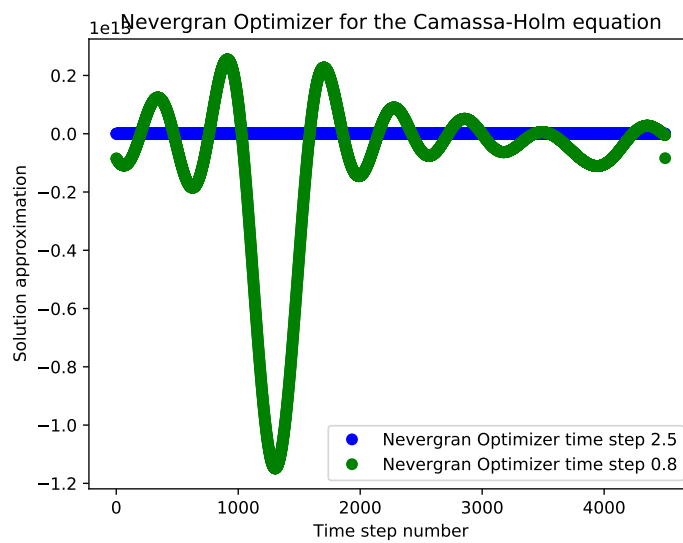
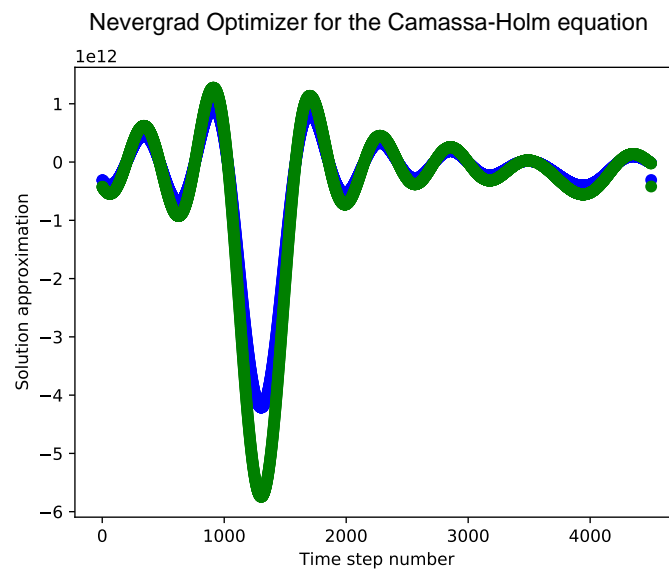
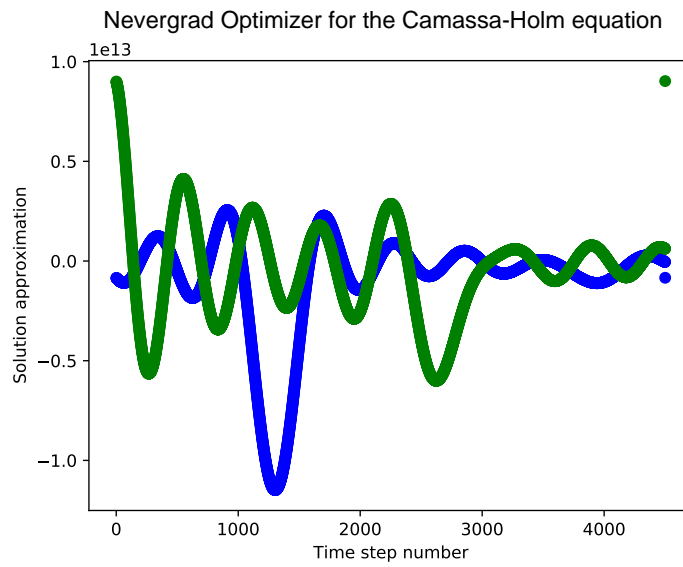
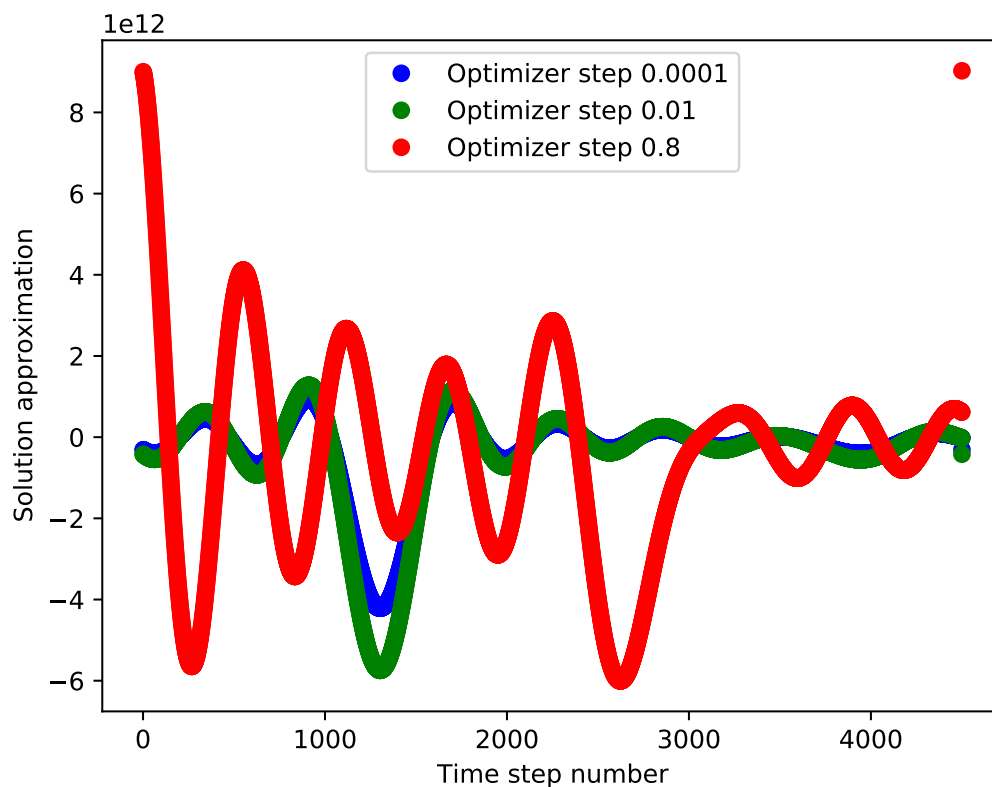


Figure 57: *Extracting measurements from the Camassa-Holm equation.* Implementing the variational quantum algorithm for 4500 time steps yields sinusoidal profiles of motion.

Nevergrad Optimizer for the Camassa-Holm equation



Nevergrad Optimizer for the Camassa-Holm equation

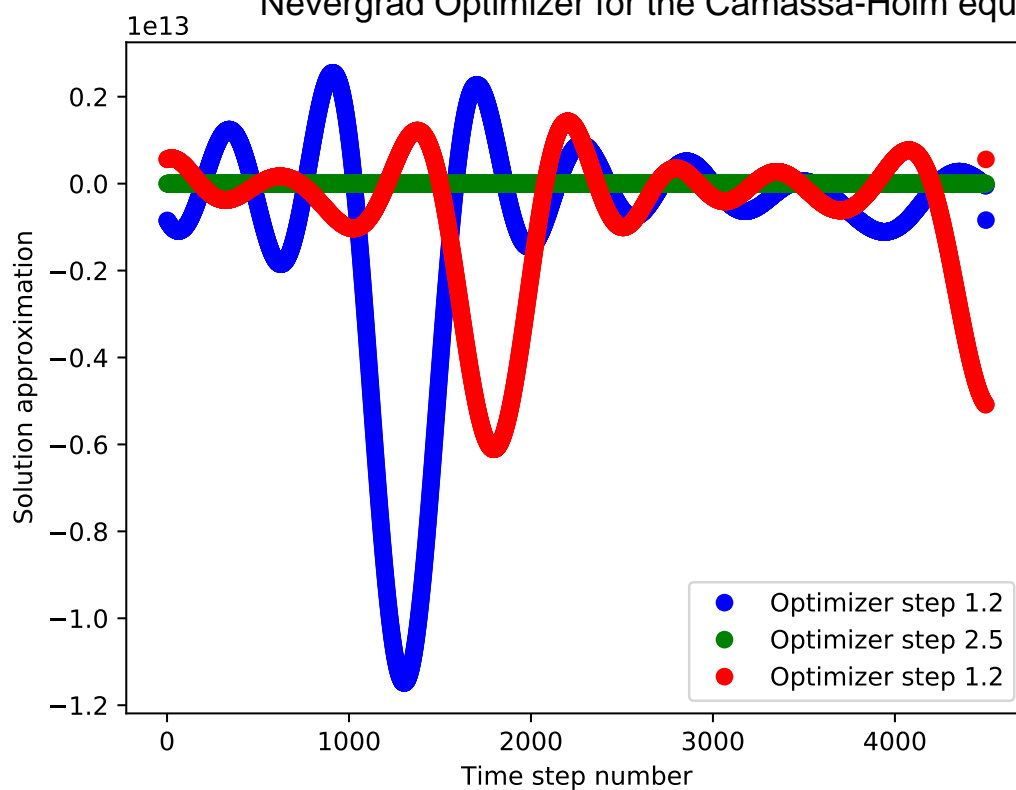


Figure 58: *Extracting measurements from the Camassa-Holm equation.* Implementing the variational quantum algorithm for 4500 time steps yields sinusoidal profiles of motion.

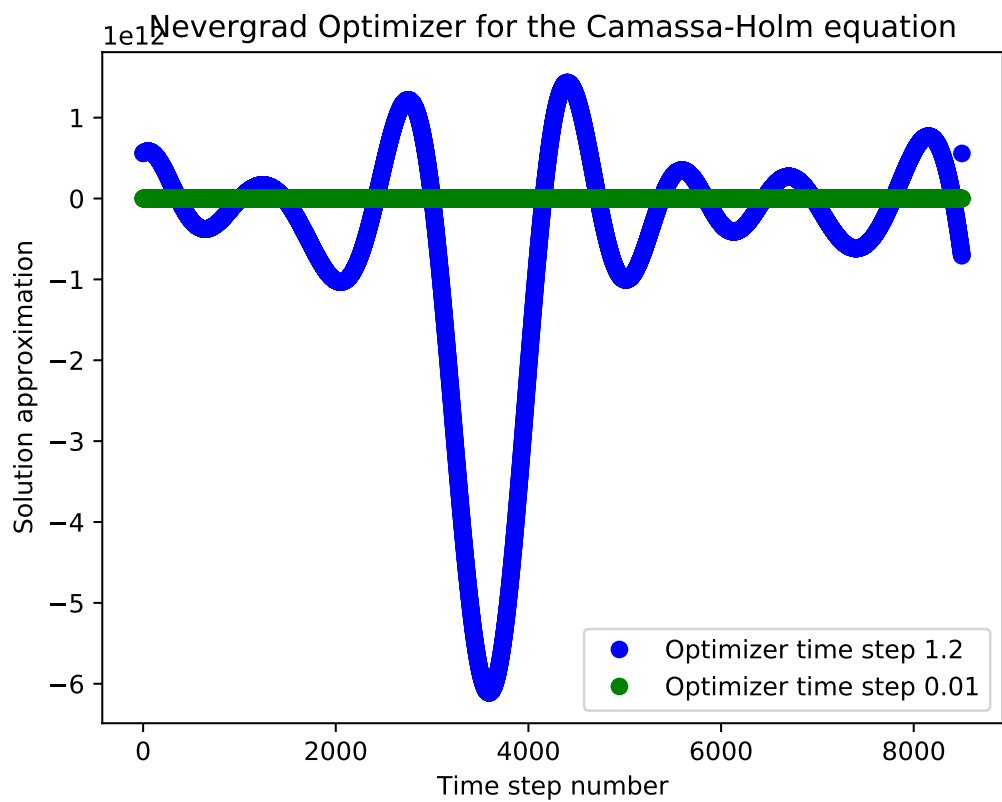
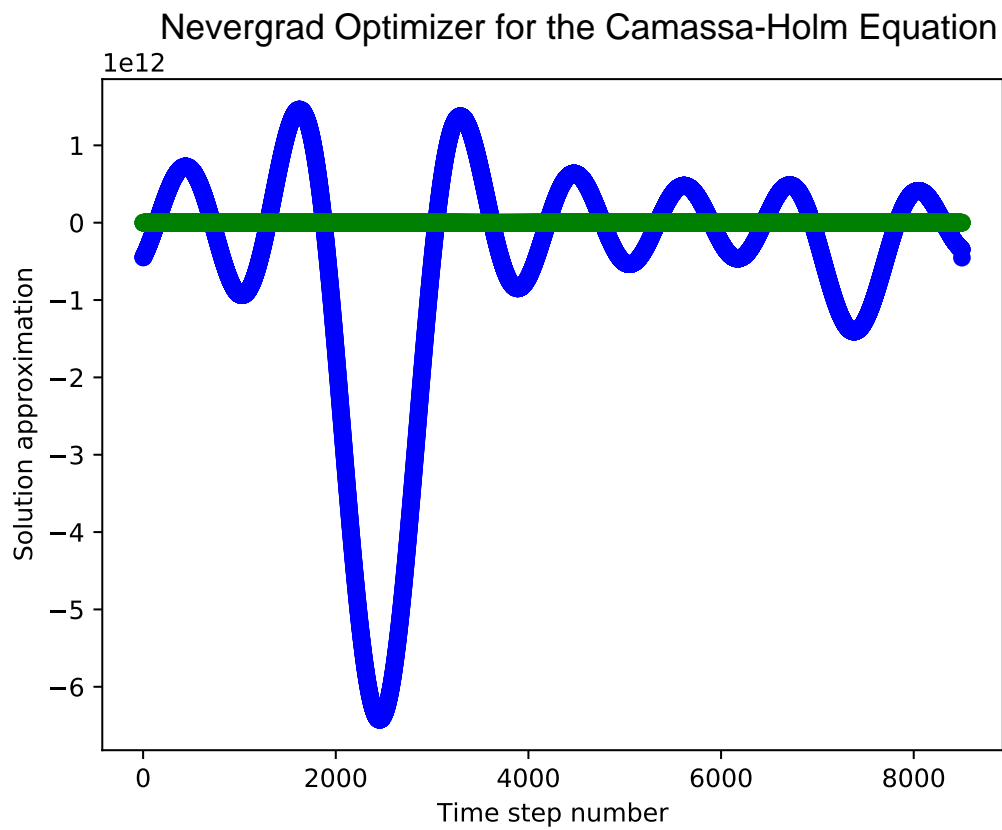


Figure 59: *Extracting measurements from the Camassa-Holm equation with 8500 time steps.* Implementing the variational quantum algorithm for 8500 time steps yields sinusoidal profiles of motion, with varying fluctuations near the beginning and end of the time evolution that are dependent upon the initial conditions.

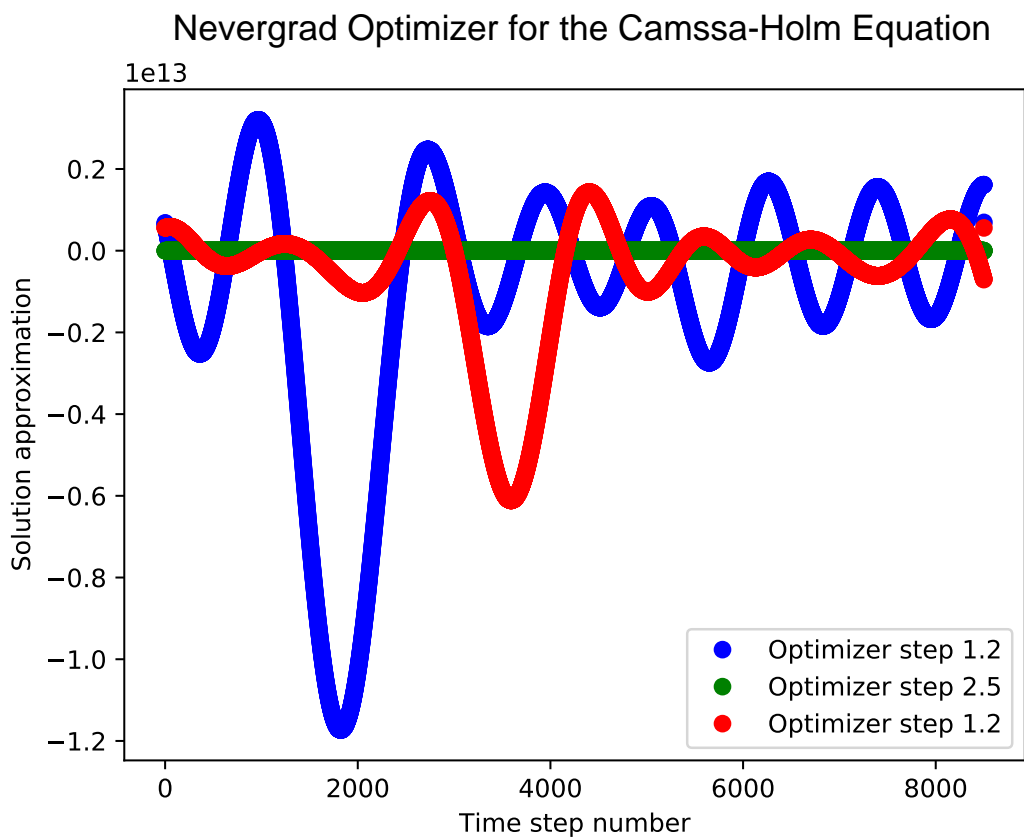
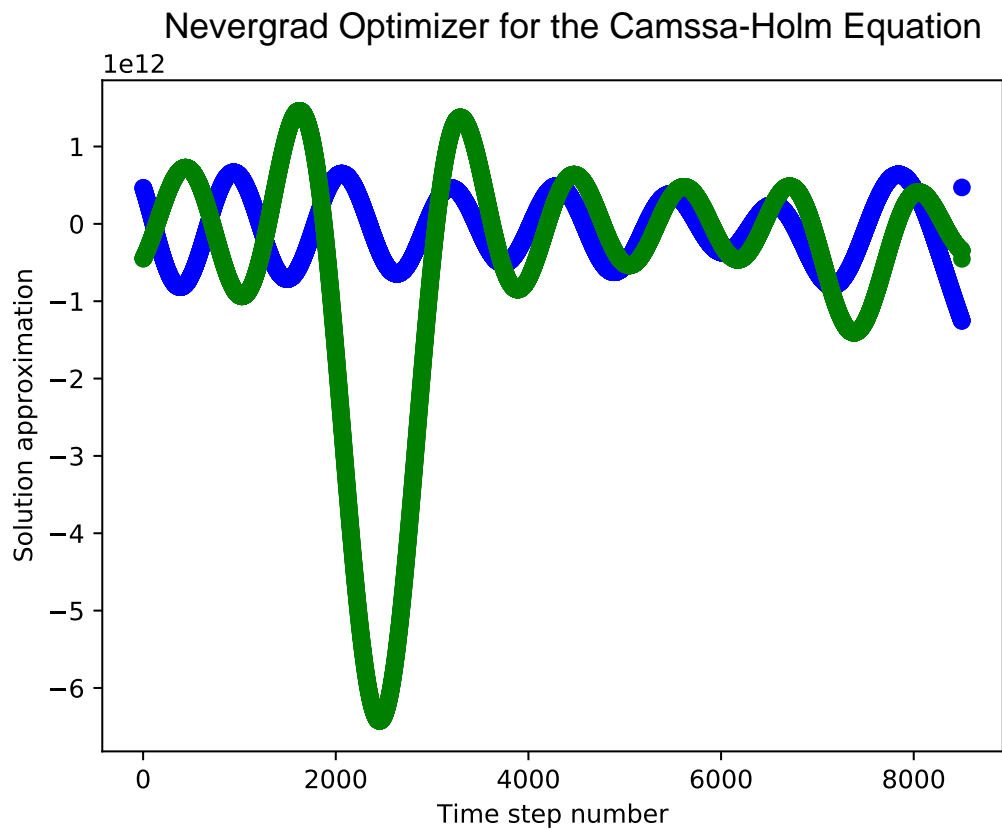


Figure 60: *Extracting measurements from the Camassa-Holm equation with 8500 time steps. Implementing the variational quantum algorithm for 8500 time steps yields sinusoidal profiles of motion.*

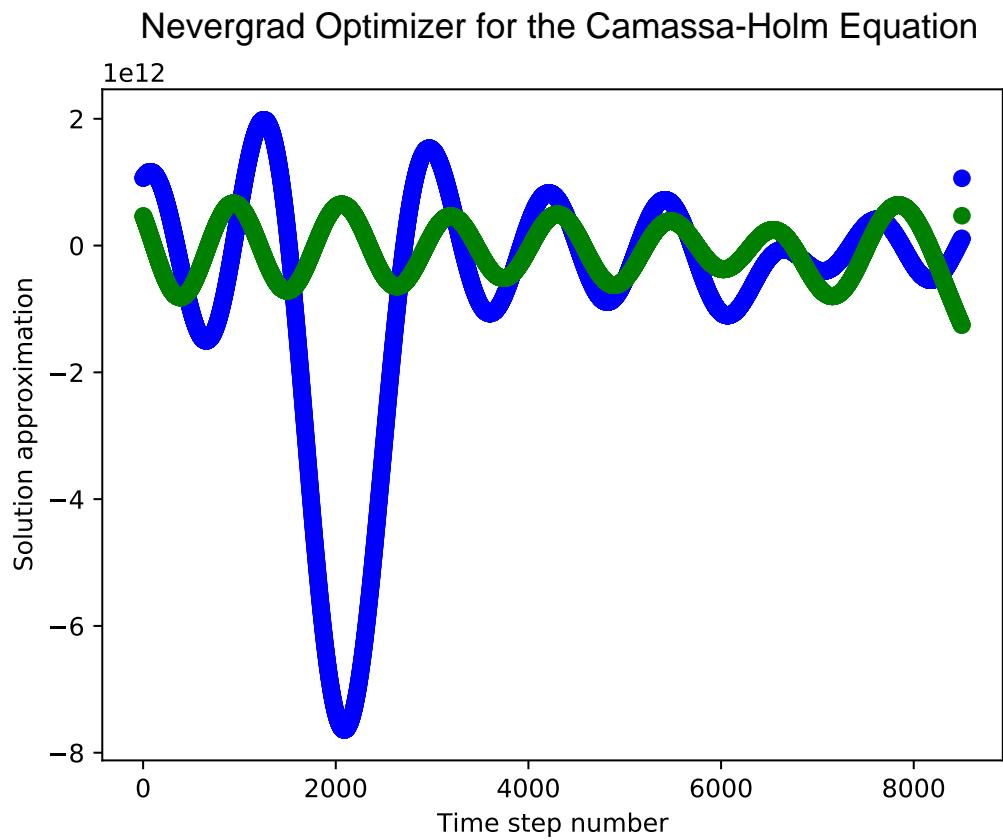
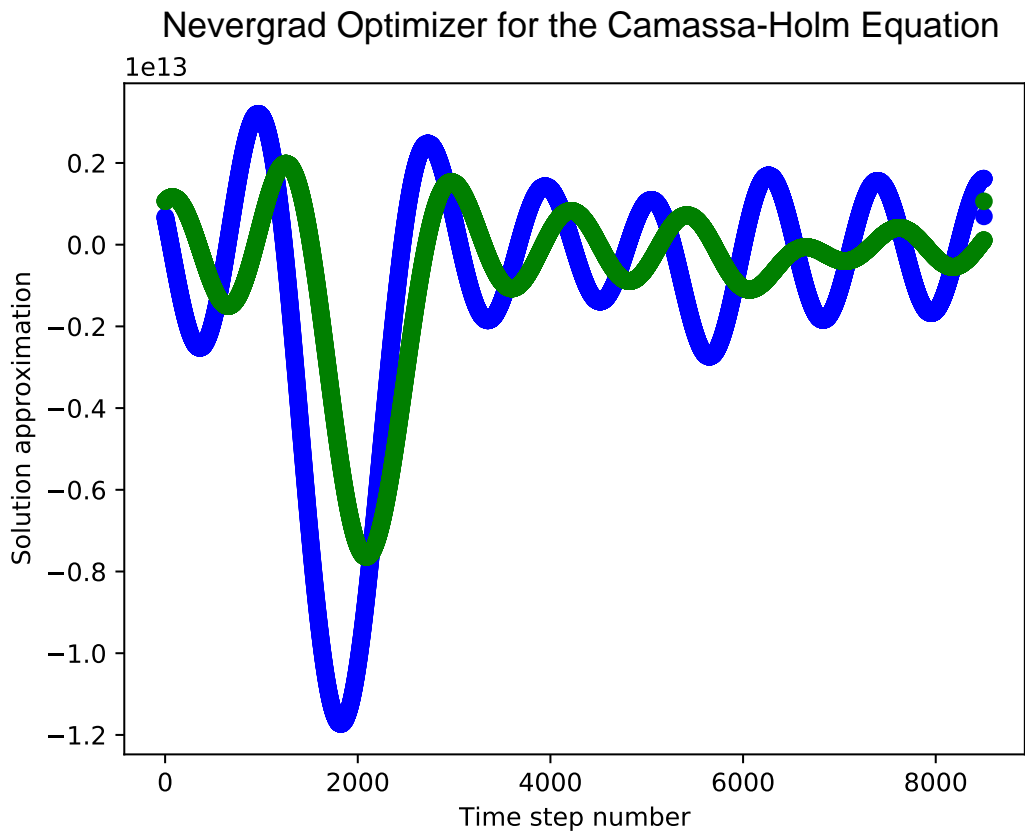


Figure 61: *Extracting measurements from the Camassa-Holm equation with 8500 time steps. Implementing the variational quantum algorithm for 8500 time steps yields sinusoidal profiles of motion.*

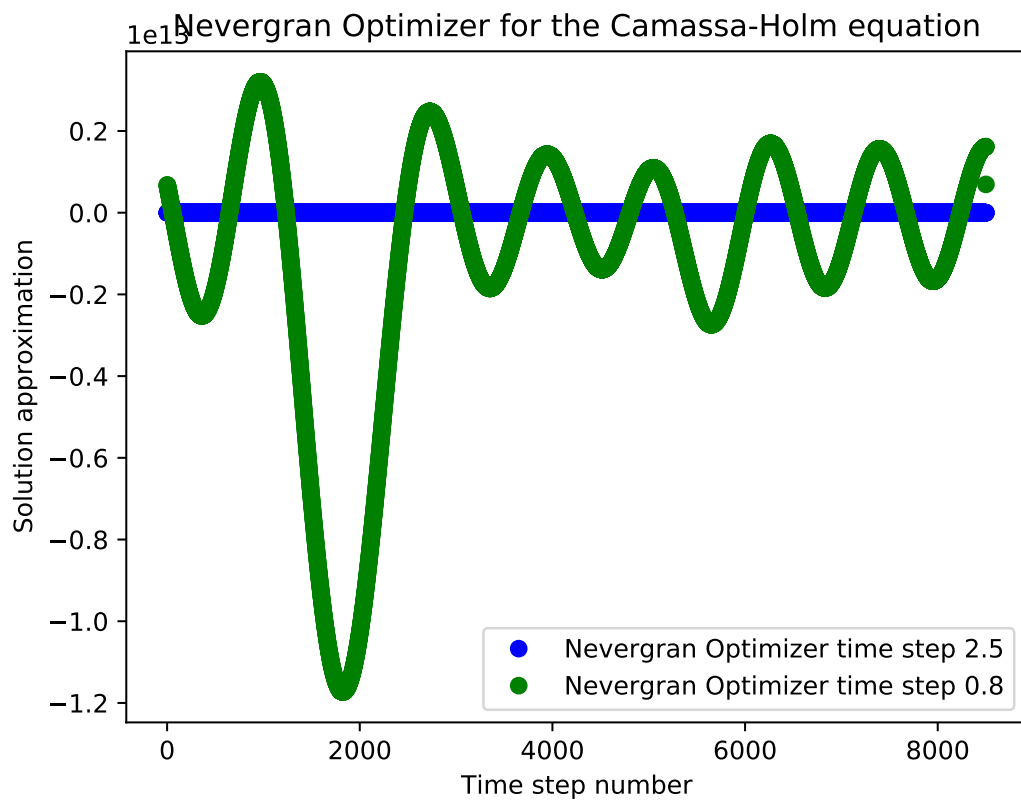
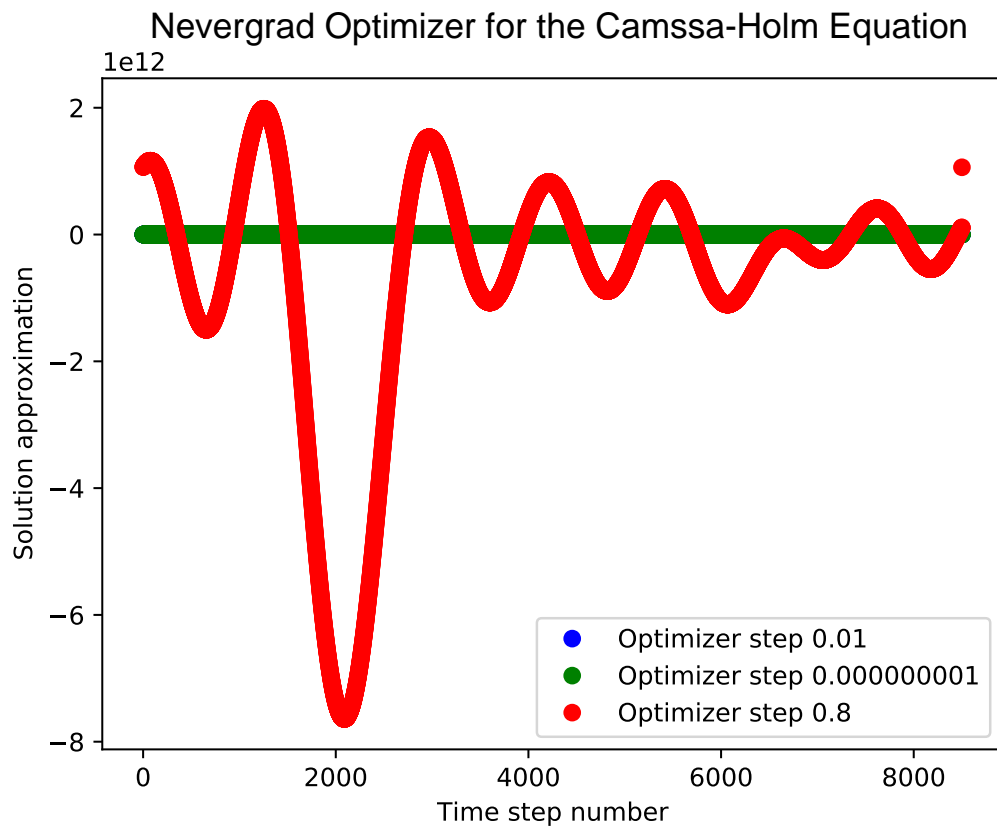


Figure 62: *Extracting measurements from the Camassa-Holm equation with 8500 time steps. Implementing the variational quantum algorithm for 8500 time steps yields sinusoidal profiles of motion.*

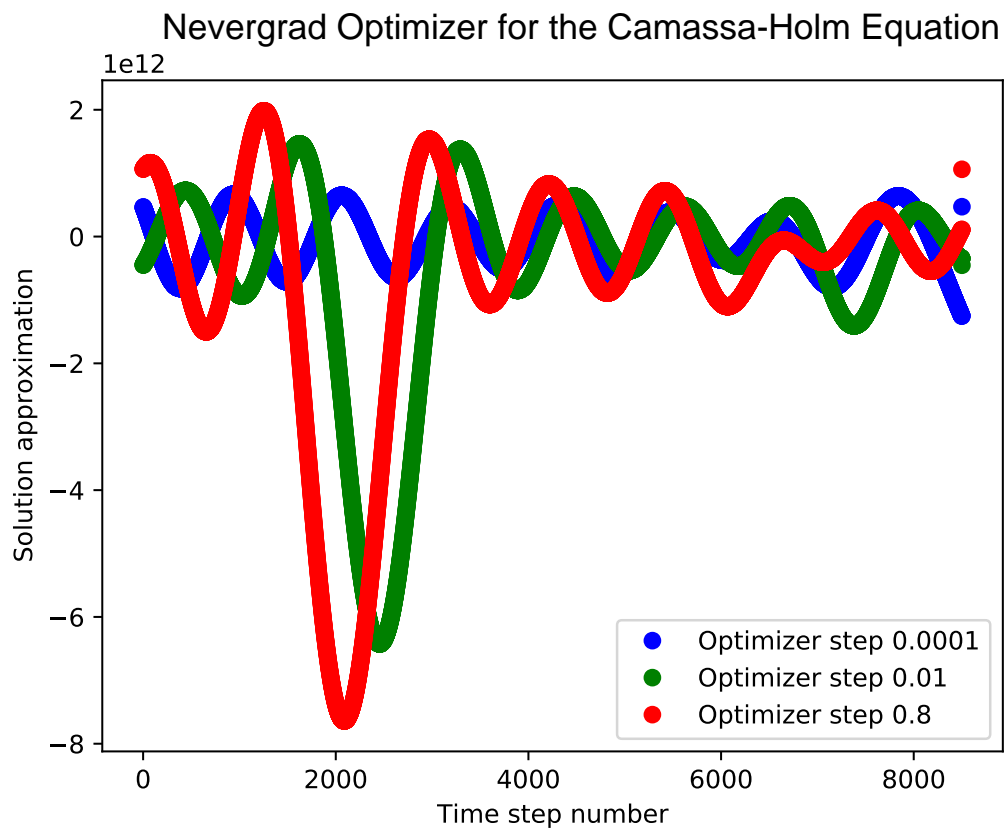
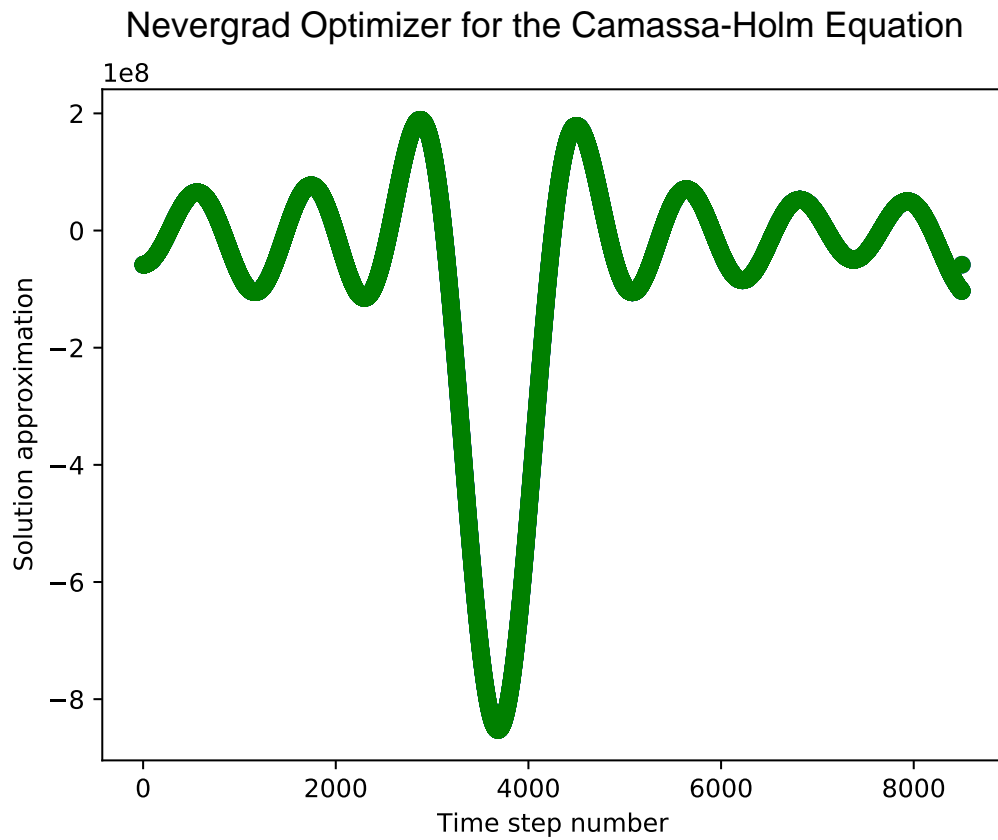


Figure 63: *Extracting measurements from the Camassa-Holm equation with 8500 time steps. Implementing the variational quantum algorithm for 8500 time steps yields sinusoidal profiles of motion.*

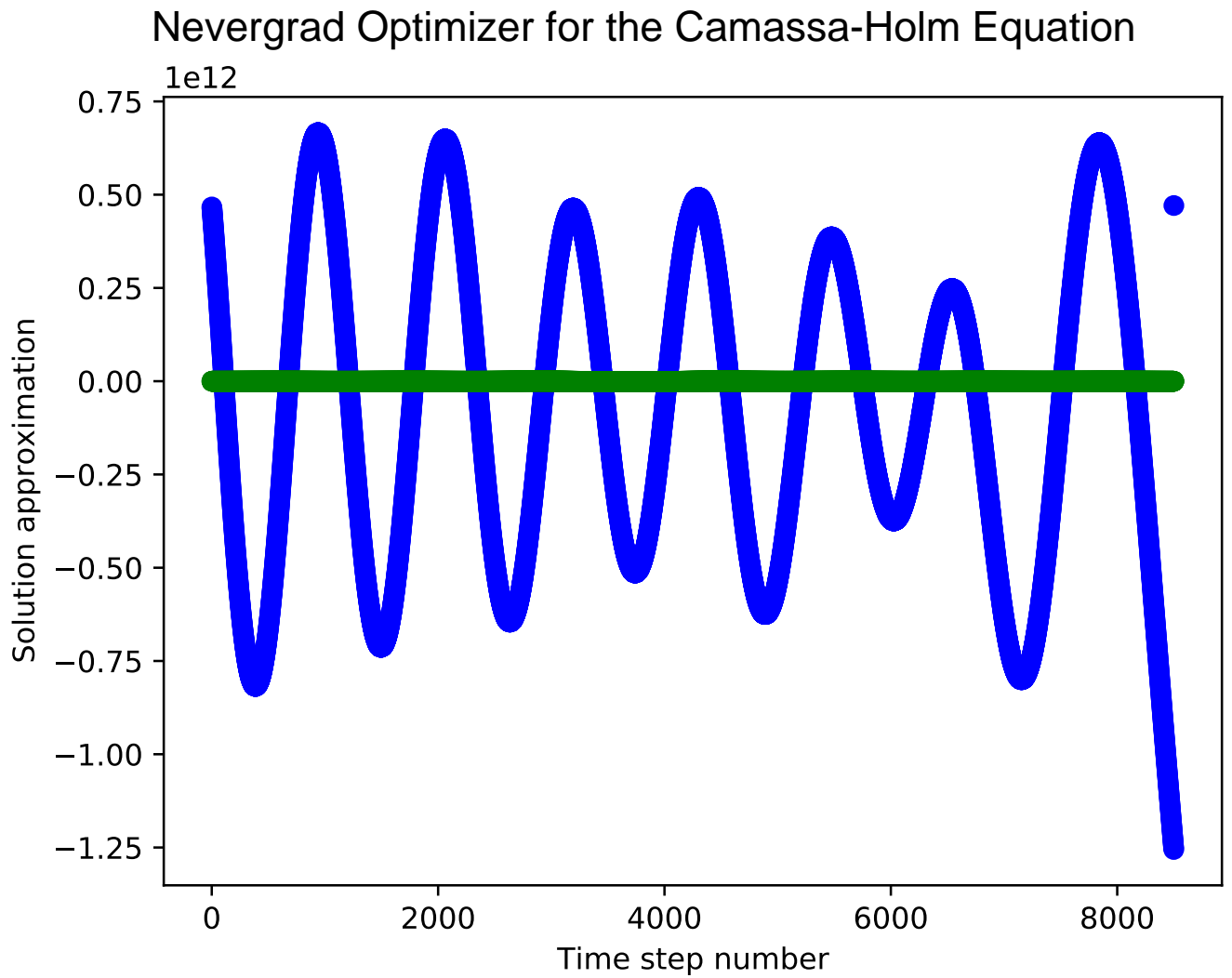


Figure 64: *Extracting measurements from the Camassa-Holm equation corresponding to additional soliton solutions with a different ZGR-QFT ansatz.* Implementing the variational quantum algorithm for different time steps and initial conditions yields solutions approximations with amplitudes that approximately remain constant throughout the entire duration of the time-evolution. The solution attains a global minimum near the end of the time evolution, as indicated from the blue curve.

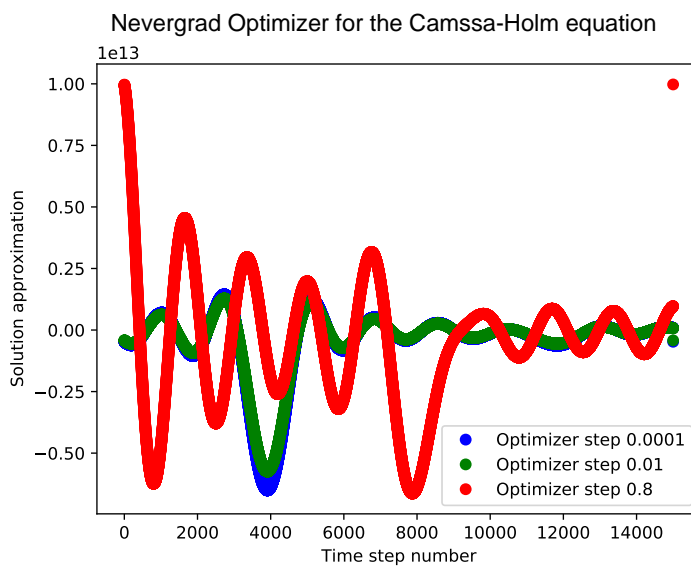
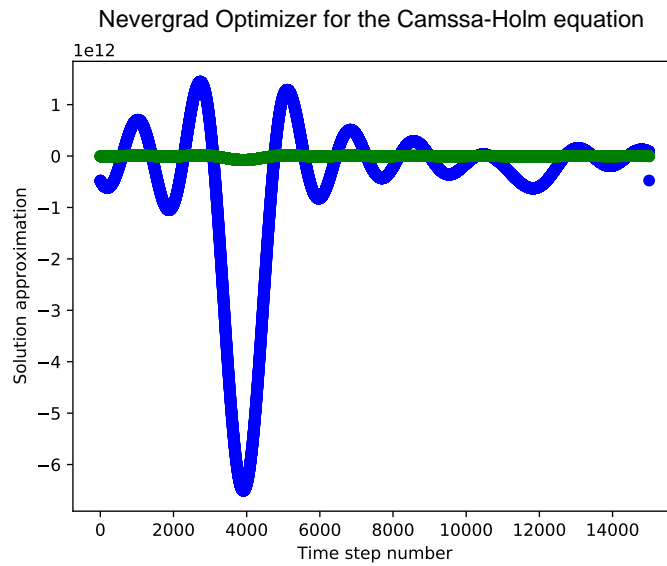
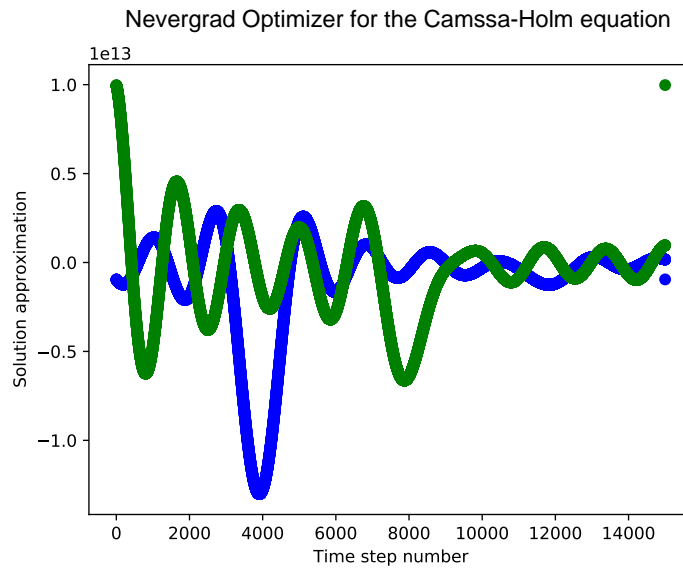


Figure 65: *Extracting measurements from the Camassa-Holm equation with 15000 time steps.* Implementing the variational quantum algorithm for 15000 time steps yields sinusoidal profiles of motion, with more fluctuations throughout the evolution than the profiles provided in previous numerical experiments.

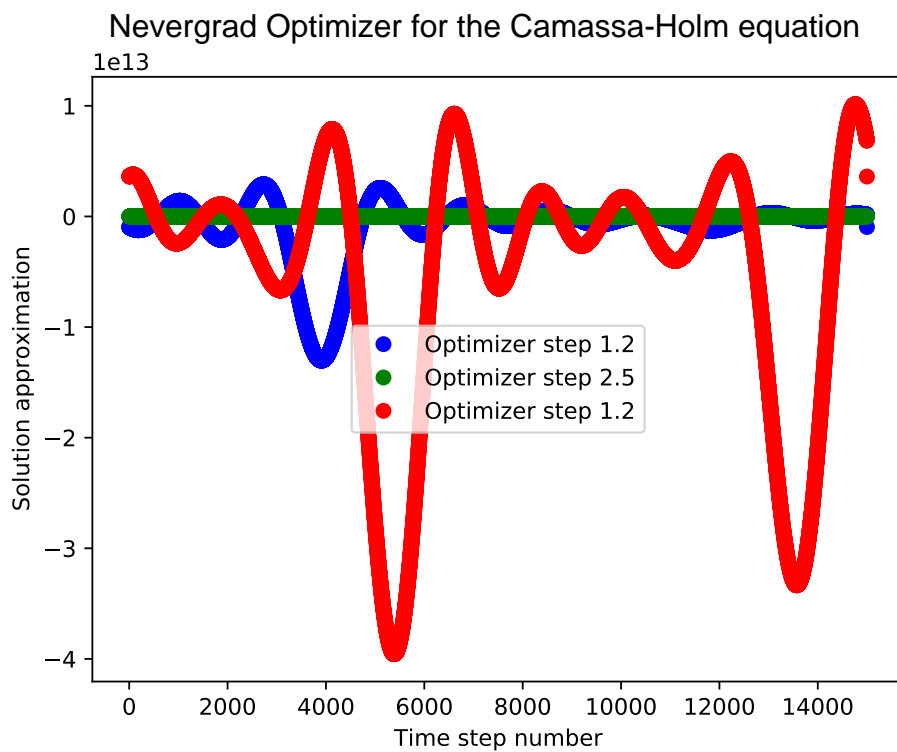
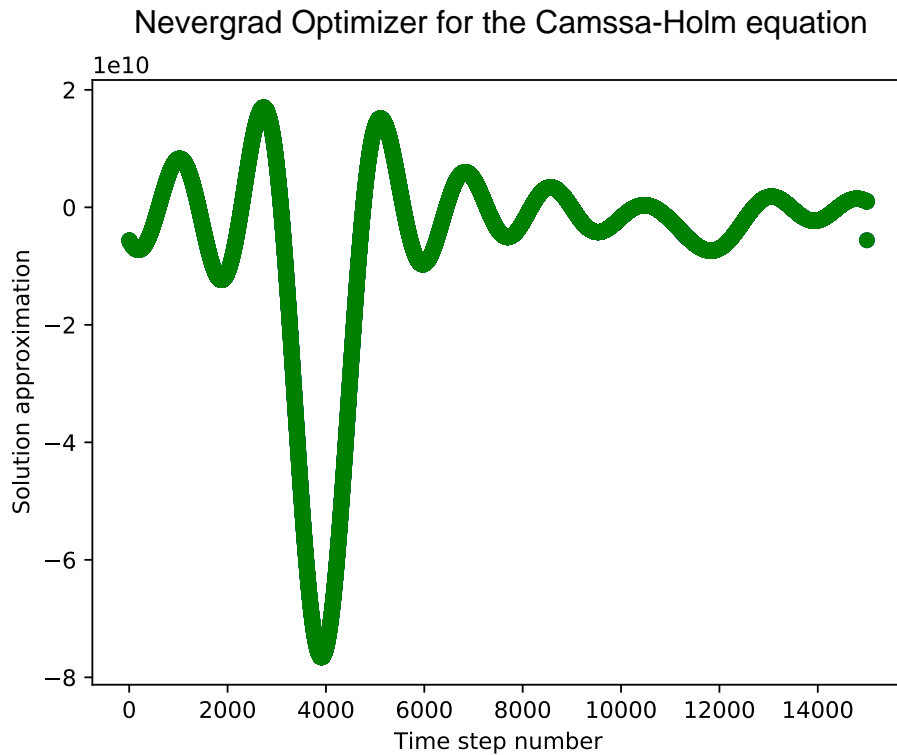


Figure 66: *Extracting measurements from the Camassa-Holm equation with 15000 time steps.* Implementing the variational quantum algorithm for 15000 time steps yields sinusoidal profiles of motion, with more fluctuations throughout the evolution than the profiles provided in previous numerical experiments.

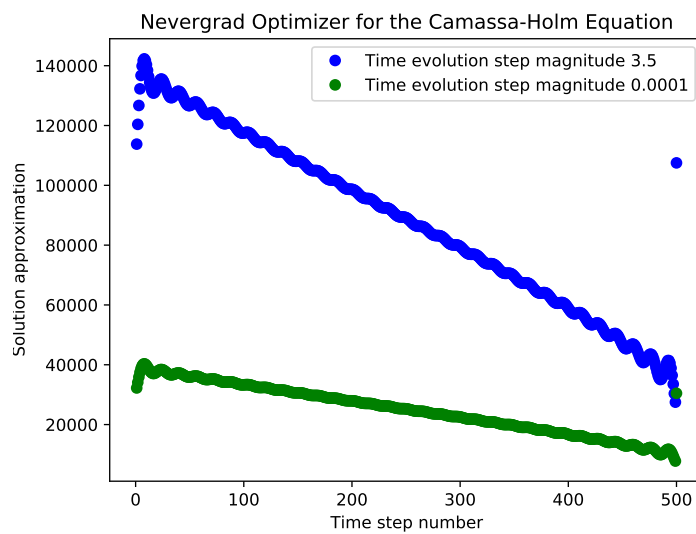
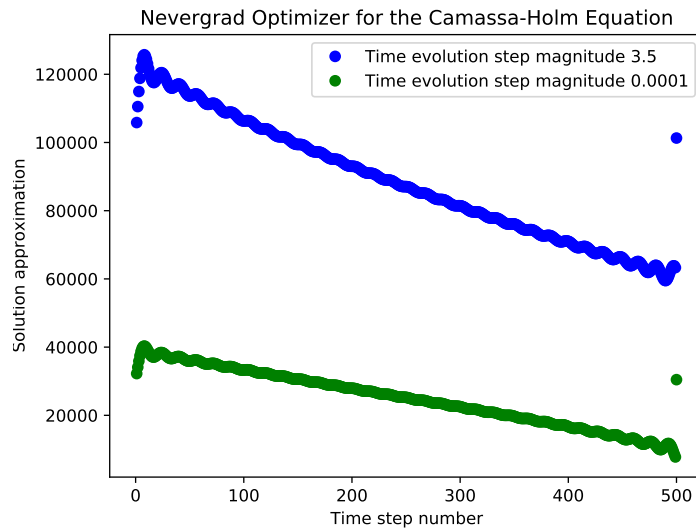
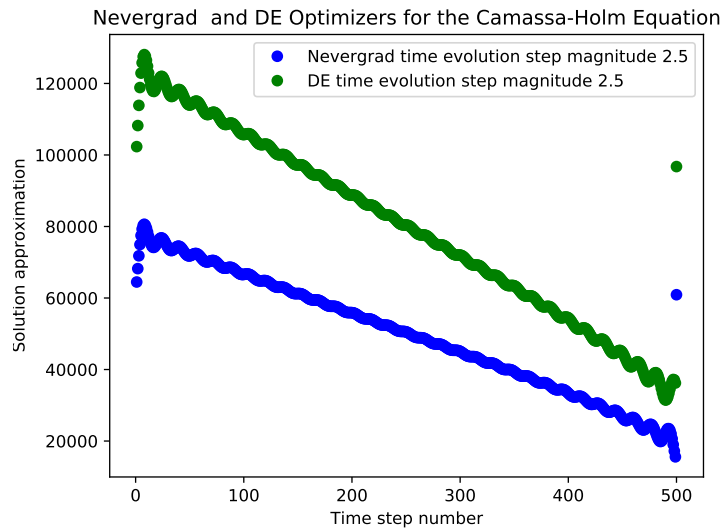


Figure 67: *Extracting measurements from the Camassa-Holm equation corresponding to additional soliton solutions with a different ZGR-QFT ansatz. Implementing the variational quantum algorithm for different time steps and initial conditions yields solutions approximations to the arcsine soliton solution to the Camassa-Holm equation.*

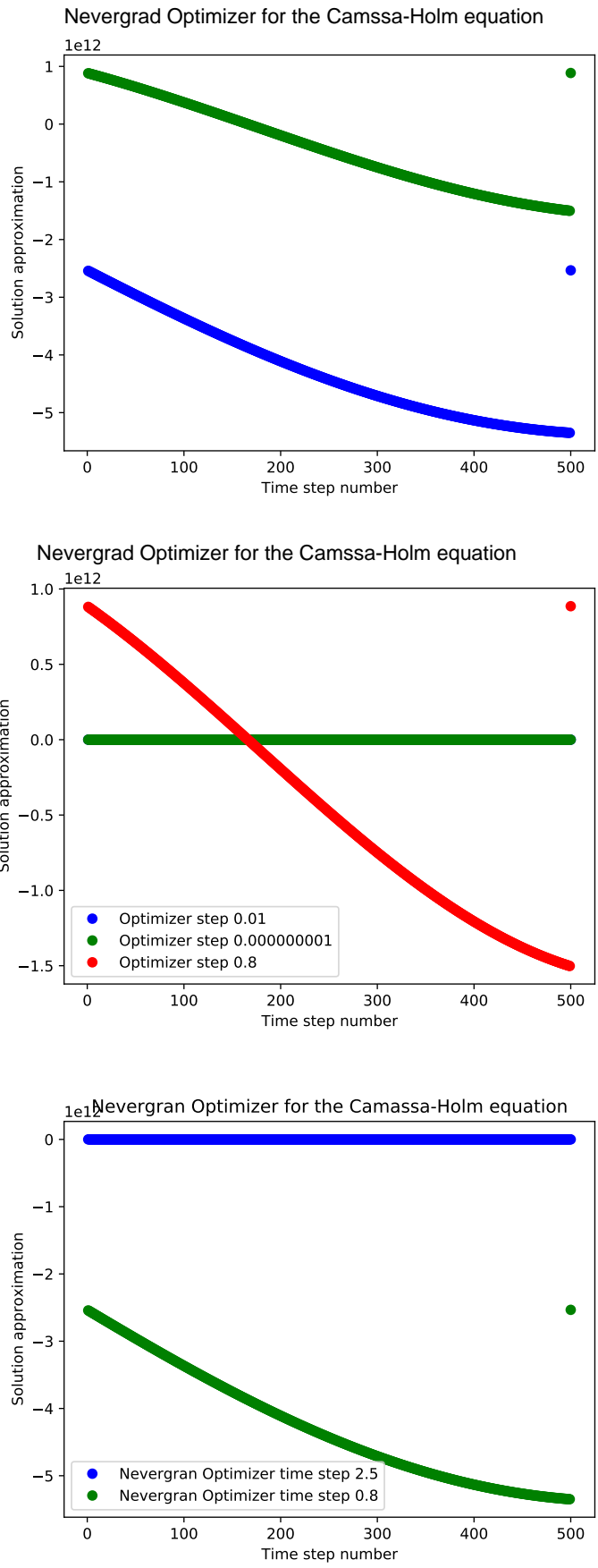


Figure 68: *Extracting measurements from the Camassa-Holm equation corresponding to additional soliton solutions with a different ZGR-QFT ansatz. Implementing the variational quantum algorithm for different time steps and initial conditions yields solutions approximations to other solutions to the Camassa-Holm equation, in which there is a significantly longer period of motion.*

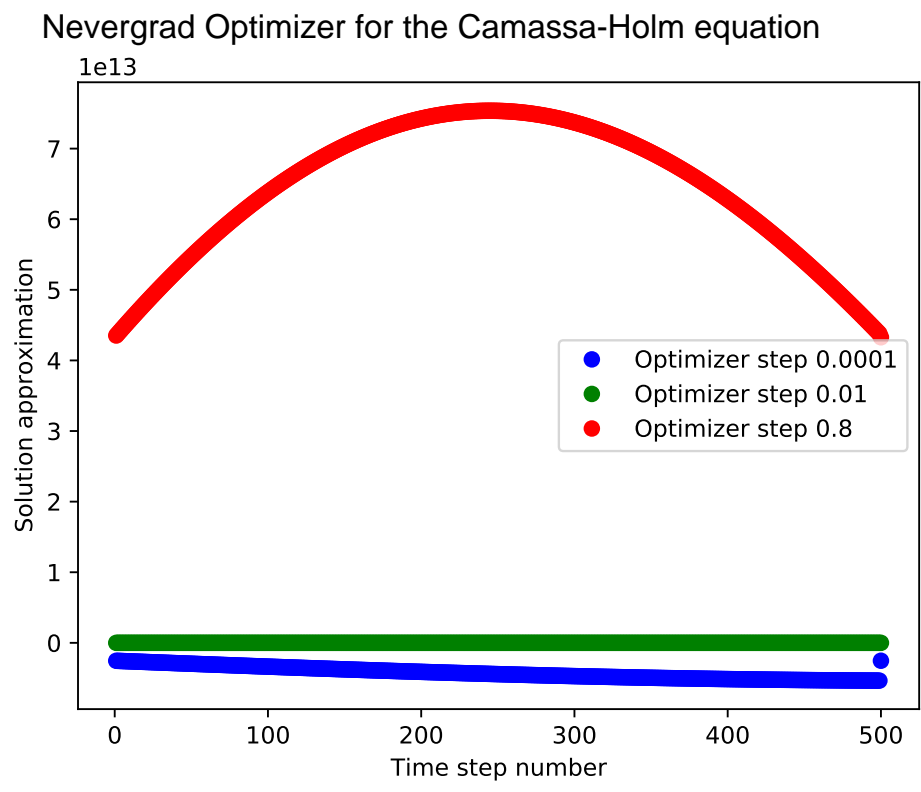
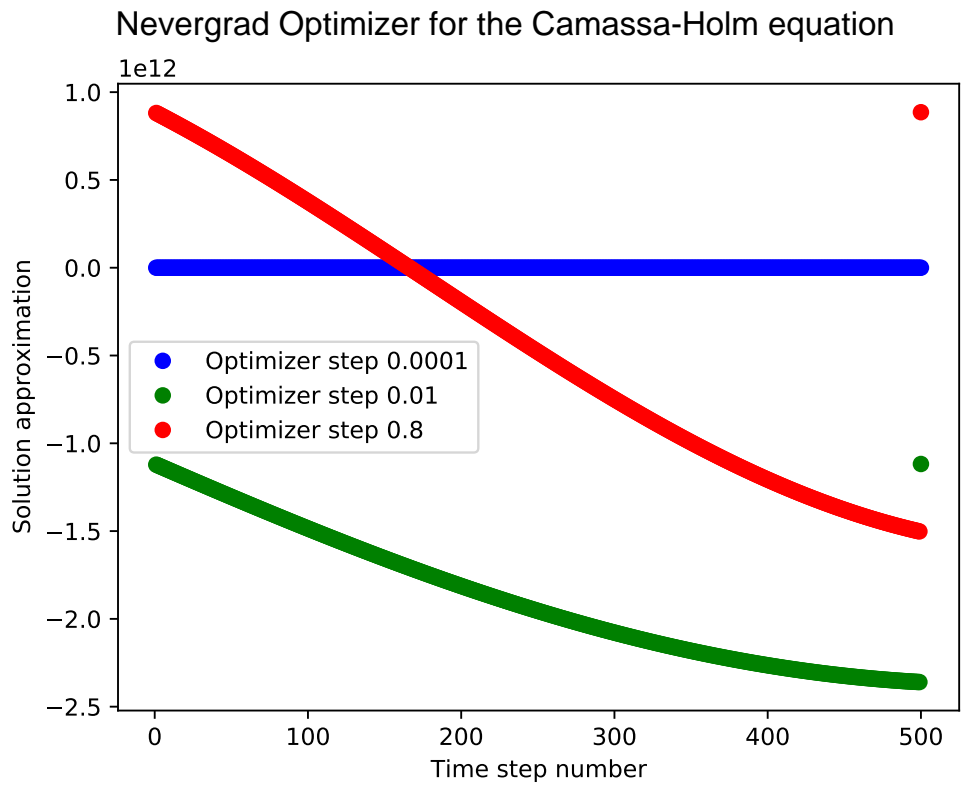


Figure 69: *Extracting measurements from the Camassa-Holm equation corresponding to additional soliton solutions with a different ZGR-QFT ansatz. Implementing the variational quantum algorithm for different time steps and initial conditions yields solutions approximations to other solutions to the Camassa-Holm equation, in which there is a significantly longer period of motion.*

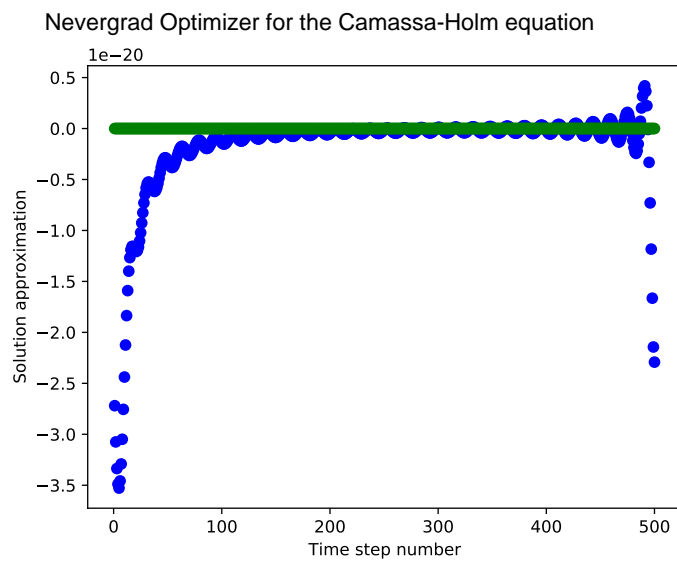
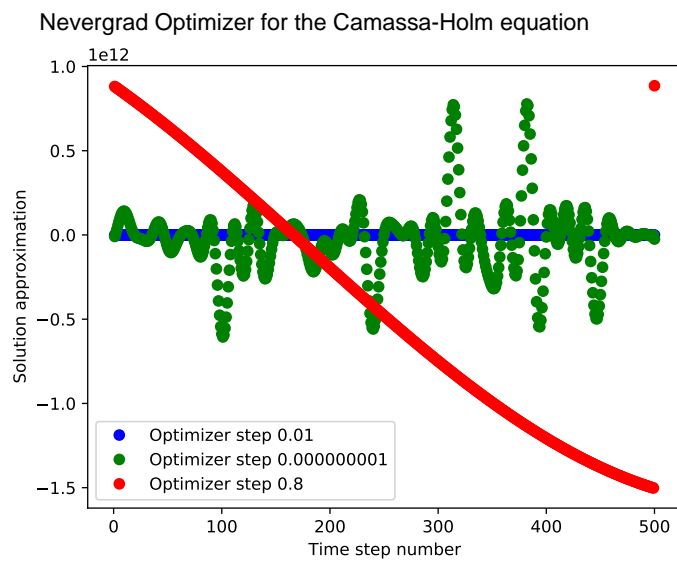
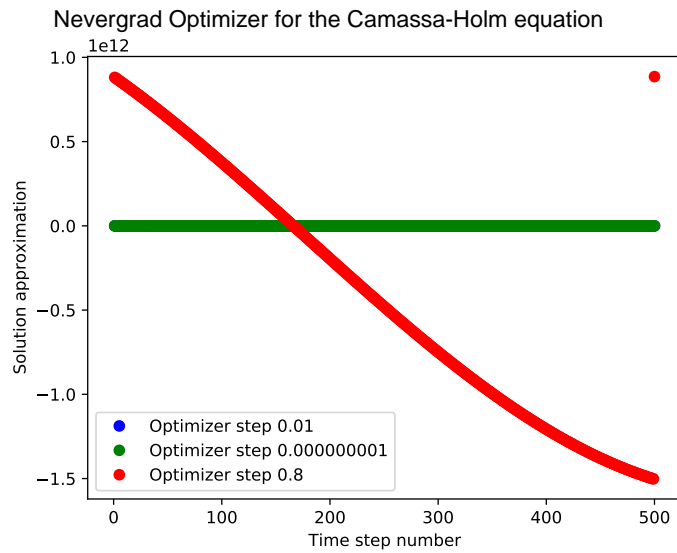


Figure 70: *Extracting measurements from the Camassa-Holm equation corresponding to additional soliton solutions with a different ZGR-QFT ansatz. Implementing the variational quantum algorithm for different time steps and initial conditions yields solutions approximations to other solutions to the Camassa-Holm equation, in which there can be a mixture of accelerated, and of retarded, periods of motion.*

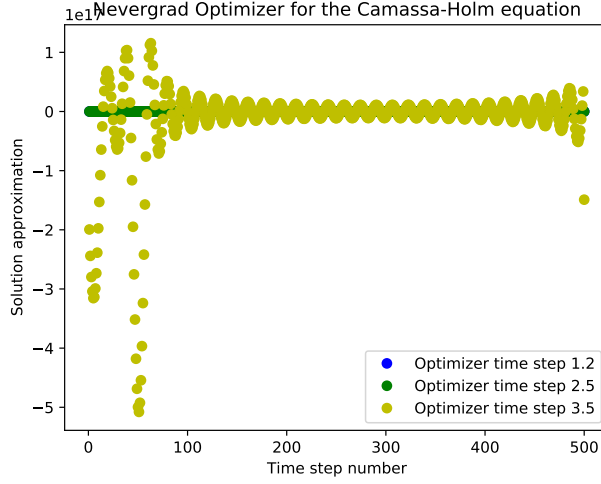


Figure 71: *Extracting measurements from the Camassa-Holm equation corresponding to additional soliton solutions with a different ZGR-QFT ansatz.* Implementing the variational quantum algorithm for different time steps and initial conditions yields solutions approximations to other solutions to the Camassa-Holm equation, in which there can be a mixture of accelerated, and of retarded, periods of motion.

## 4.9 Drinfeld-Sokolov-Wilson equations

### Cost function derivation

In comparison to previous cost functions, one can also provide multiple cost functions for solving PDE systems. One such system includes,

$$\begin{aligned}\frac{\partial u}{\partial t} + 3v \frac{\partial v}{\partial x} &= 0, \\ \frac{\partial v}{\partial t} &= 2 \frac{\partial^3 v}{\partial x^3} + \frac{\partial u}{\partial x} + 2u \frac{\partial v}{\partial x}.\end{aligned}$$

Along the lines of previous arrangements, we obtain expressions for the time evolved variational states of the solutions  $u, v$  to the system, each of which are individually of the form,

$$\begin{aligned}\frac{|u(t + \tau)\rangle - |u\rangle}{t} + 3|v\rangle \left(\frac{A_x^\dagger - \mathbf{1}}{\Delta x}\right) |v\rangle &= 0 \\ \Downarrow \\ |u(t + \tau)\rangle &= -3tv \left(\frac{A_x^\dagger - \mathbf{1}}{\Delta x}\right) |v\rangle + |v\rangle \\ \Downarrow \\ \mathcal{C}_u^{\text{DSW}}(\lambda, \lambda_0) &= \left\| |u(t + \tau)\rangle - |u(t)\rangle \right\|^2 = \left\| \left(-3t|v\rangle \left(\frac{A_x^\dagger - \mathbf{1}}{\Delta x}\right) |v\rangle + |v\rangle\right) - |u(t)\rangle \right\|^2 \\ \Downarrow \\ &= \left(-3t|v\rangle \left(\frac{A_x^\dagger - \mathbf{1}}{\Delta x}\right) |v\rangle + |v\rangle\right)^2 - 2\left(-3t|v\rangle \left(\frac{A_x^\dagger - \mathbf{1}}{\Delta x}\right) |v\rangle + |v\rangle\right) |u(t)\rangle + \lambda^2\end{aligned}$$

$$\begin{aligned}
& \Downarrow \\
& \left( \left\{ -3t |v\rangle \left( \frac{A_x^\dagger - \mathbf{1}}{\Delta x} \right) |v\rangle \right\}^2 - 6t |v\rangle \left( \frac{A_x^\dagger - \mathbf{1}}{\Delta x} \right) |v\rangle + \lambda^2 \right) |u(t)\rangle + \lambda^2 \\
& \Downarrow \\
& \left( 9t^2 |v\rangle \frac{(A_x - \mathbf{1})}{(\Delta x)^2} \lambda^2 - 6t |v\rangle \left( \frac{A_x^\dagger - \mathbf{1}}{\Delta x} \right) |v\rangle + \lambda^2 \right) |u(t)\rangle + \lambda^2 \\
& \Downarrow \\
\boxed{C_u^{DSW}(\lambda, \lambda_0^u)} &= \frac{9t^2}{(\Delta x)^2} (\lambda_0^u)^2 \langle u | A_x^\dagger |v\rangle - \frac{9t^2}{(\Delta x)^2} (\lambda_0^u)^2 |u\rangle - \frac{6t |v\rangle}{\Delta x} \langle v | A_x |u\rangle + (\lambda_0^u)^2 |u\rangle + (\lambda_0^u)^2 ,
\end{aligned}$$

for the first equation of the system, and,

$$\begin{aligned}
\frac{|v(t+\tau)\rangle - |v\rangle}{t} &= 2 \left\{ \frac{\frac{A_x^\dagger - 2\mathbf{1} + A_x}{(\Delta x)^2} |v(t+\tau)\rangle - \frac{A_x^\dagger - 2\mathbf{1} + A_x}{(\Delta x)^2} |v\rangle}{\Delta x} \right\} + \left( \frac{A_x^\dagger - \mathbf{1}}{\Delta x} \right) |u\rangle + 2 |u\rangle \left( \frac{A_x^\dagger - \mathbf{1}}{\Delta x} \right) |v\rangle \\
& \Downarrow \\
|v(t+\tau)\rangle &= \tau \left( 2 \left\{ \frac{\frac{A_x^\dagger - 2\mathbf{1} + A_x}{(\Delta x)^2} |v(t+\tau)\rangle - \frac{A_x^\dagger - 2\mathbf{1} + A_x}{(\Delta x)^2} |v\rangle}{\Delta x} \right\} + \left( \frac{A_x^\dagger - \mathbf{1}}{\Delta x} \right) |u\rangle + 2 |u\rangle \left( \frac{A_x^\dagger - \mathbf{1}}{\Delta x} \right) |v\rangle \right) + |v\rangle \\
& \Downarrow \\
C_v^{DSW}(\lambda, \lambda_0) &= \left\| |v(t+\tau)\rangle - |v\rangle \right\|^2 \\
& \Downarrow \\
& \left\| \tau \left( 2 \left\{ \frac{\frac{A_x^\dagger - 2\mathbf{1} + A_x}{(\Delta x)^2} |v(t+\tau)\rangle - \frac{A_x^\dagger - 2\mathbf{1} + A_x}{(\Delta x)^2} |v\rangle}{\Delta x} \right\} + \left( \frac{A_x^\dagger - \mathbf{1}}{\Delta x} \right) |u\rangle + 2 |u\rangle \left( \frac{A_x^\dagger - \mathbf{1}}{\Delta x} \right) |v\rangle \right) + |v\rangle - |v\rangle \right\|^2 \\
& \Downarrow \\
& \left\| 2 \frac{\tau}{(\Delta x)^3} \left\{ \left( A_x^\dagger - 2\mathbf{1} + A_x \right) |v(t+\tau)\rangle - \left( A_x^\dagger - 2\mathbf{1} + A_x \right) |v\rangle \right\} + A_x^\dagger |u\rangle - |u\rangle + \dots \right. \\
& \qquad \qquad \qquad \left. \left. 2 |v\rangle \left( A_x^\dagger |v\rangle - |v\rangle \right) \right\|^2 \right. \\
& \Downarrow \\
& \left( 2 \frac{\tau}{(\Delta x)^3} \left\{ \left( A_x^\dagger - 2\mathbf{1} + A_x \right) |v(t+\tau)\rangle - \left( A_x^\dagger - 2\mathbf{1} + A_x \right) |v\rangle \right\} + A_x^\dagger |u\rangle - |u\rangle \right)^2 + \dots \\
& \left( 4 \frac{\tau}{(\Delta x)^3} \left\{ \left( A_x^\dagger - 2\mathbf{1} + A_x \right) |v(t+\tau)\rangle - \left( A_x^\dagger - 2\mathbf{1} + A_x \right) |v\rangle \right\} + A_x^\dagger |u\rangle - |u\rangle \right) \times \dots \\
& \qquad \qquad \qquad \left( \langle v | A_x |v\rangle + \lambda^2 \right) + \left( 2 |v\rangle \left( A_x^\dagger |v\rangle - |v\rangle \right) \right)^2 ,
\end{aligned}$$

for the second equation of the system, from which expanding the first term in the wavefunction yields,

$$\begin{aligned}
& \left( 2 \frac{\tau}{(\Delta x)^3} \left\{ (A_x^\dagger - 2\mathbf{1} + A_x) |v(t+\tau)\rangle - (A_x^\dagger - 2\mathbf{1} + A_x) |v\rangle \right\} + A_x^\dagger |u\rangle - |u\rangle \right)^2 \\
& \quad \Downarrow \\
& \left( 2 \frac{\tau}{(\Delta x)^3} \left\{ (A_x^\dagger - 2\mathbf{1} + A_x) |v(t+\tau)\rangle - (A_x^\dagger - 2\mathbf{1} + A_x) |v\rangle \right\} \right)^2 + \dots \\
& 4 \frac{\tau}{(\Delta x)^3} \left\{ (A_x^\dagger - 2\mathbf{1} + A_x) |v(t+\tau)\rangle - (A_x^\dagger - 2\mathbf{1} + A_x) |v\rangle \right\} (A_x^\dagger |u\rangle - |u\rangle) + \dots \\
& \quad \quad \quad (A_x^\dagger |u\rangle - |u\rangle)^2 \\
& \quad \quad \quad \Downarrow \\
& \left( 2 \frac{\tau}{(\Delta x)^3} \right)^2 \left\{ \left( (A_x^\dagger - 2\mathbf{1} + A_x) |v(t+\tau)\rangle \right)^2 - 2 (A_x^\dagger - 2\mathbf{1} + A_x) |v(t+\tau)\rangle \times \dots \right. \\
& \quad \quad \quad \left. (A_x^\dagger - 2\mathbf{1} + A_x) |v\rangle + \left( (A_x^\dagger - 2\mathbf{1} + A_x) |v\rangle \right)^2 \right\} + \dots \\
& 4 \frac{\tau}{(\Delta x)^3} \left\{ (A_x^\dagger - 2\mathbf{1} + A_x) |v(t+\tau)\rangle - (A_x^\dagger - 2\mathbf{1} + A_x) |v\rangle \right\} (A_x^\dagger |u\rangle - |u\rangle) + \dots \\
& \quad \quad \quad (A_x^\dagger |u\rangle - |u\rangle)^2 \\
& \quad \quad \quad \Downarrow \\
& \left( 2 \frac{\tau}{(\Delta x)^3} \right)^2 \left\{ \left( (A_x^\dagger - 2\mathbf{1} + A_x) |v(t+\tau)\rangle \right) \left( (A_x^\dagger - 2\mathbf{1} + A_x) |v(t+\tau)\rangle \right) - \dots \right. \\
& \quad \quad \quad \left. 2 \left( A_x^\dagger |v(t+\tau)\rangle - 2|v(t+\tau)\rangle + A_x |v(t+\tau)\rangle \right) \left( A_x^\dagger |v\rangle - 2|v\rangle + A_x |v\rangle \right) + \dots \right. \\
& \quad \quad \quad \left. \left( (A_x^\dagger - 2\mathbf{1} + A_x) |v\rangle \right) \left( (A_x^\dagger - 2\mathbf{1} + A_x) |v\rangle \right) \right\},
\end{aligned}$$

corresponding to the second equation of the system. We proceed,

$$\begin{aligned}
& \left( 2 \frac{\tau}{(\Delta x)^3} \right)^2 \left\{ \left( \left( A_x^\dagger |v(t+\tau)\rangle - 2|v(t+\tau)\rangle + A_x |v(t+\tau)\rangle \right) \right) \times \dots \right. \\
& \quad \quad \quad \left. \left( \left( A_x^\dagger |v(t+\tau)\rangle - 2|v(t+\tau)\rangle + A_x |v(t+\tau)\rangle \right) \right) - \dots \right. \\
& \quad \quad \quad \left. 2 \left( A_x^\dagger |v(t+\tau)\rangle - 2|v(t+\tau)\rangle + A_x |v(t+\tau)\rangle \right) \left( A_x^\dagger |v\rangle - 2|v\rangle + A_x |v\rangle \right) + \dots \right. \\
& \quad \quad \quad \left. (A_x^\dagger |v\rangle - 2|v\rangle + A_x |v\rangle) (A_x^\dagger |v\rangle - 2|v\rangle + A_x |v\rangle) \right\} \\
& \quad \quad \quad \Downarrow \\
& \left( 2 \frac{\tau}{(\Delta x)^3} \right)^2 \left\{ \left( \langle v(t+\tau) | A_x A_x^\dagger |v(t+\tau)\rangle - \langle v(t+\tau) | 2A_x^\dagger |v(t+\tau)\rangle + \dots \right. \right. \\
& \quad \quad \quad \langle v(t+\tau) | A_x^\dagger A_x^\dagger |v(t+\tau)\rangle - \langle v(t+\tau) | 2A_x^\dagger |v(t+\tau)\rangle - \langle v(t+\tau) | 4|v(t+\tau)\rangle - \dots \\
& \quad \quad \quad \langle v(t+\tau) | 2A_x^\dagger |v(t+\tau)\rangle + \langle v(t+\tau) | A_x^\dagger A_x^\dagger |v(t+\tau)\rangle - \langle v(t+\tau) | 2A_x |v(t+\tau)\rangle + \dots \\
& \quad \quad \quad \left. \left. \langle v(t+\tau) | A_x^\dagger A_x |v(t+\tau)\rangle \right) - \dots \right. \\
& \quad \quad \quad \left. 2 \left( \langle v | A_x A_x^\dagger |v(t+\tau)\rangle - \langle v | 2A_x^\dagger |v(t+\tau)\rangle - \langle v | A_x^\dagger A_x^\dagger |v(t+\tau)\rangle - \dots \right. \right.
\end{aligned}$$



$$\begin{aligned}
\boxed{\mathcal{C}_v^{\text{DSW}}(\lambda, \lambda_0^v)} &= (\lambda_0^v)^2 + \text{Re} \left\{ \left( \frac{2\tau}{(\Delta x)^3} \right)^2 \langle \tilde{v} | A_x A_x^\dagger | \tilde{v} \rangle + 2 \left( \frac{2\tau}{(\Delta x)^3} \right)^2 \langle \tilde{v} | A_x^\dagger | \tilde{v} \rangle + \dots \right. \\
&\left( \frac{2\tau}{(\Delta x)^3} \right)^2 \langle \tilde{v} | A_x^\dagger A_x^\dagger | \tilde{v} \rangle + 2 \left( \frac{2\tau}{(\Delta x)^3} \right)^2 \langle \tilde{v} | A_x^\dagger | \tilde{v} \rangle - 4 \left( \frac{2\tau}{(\Delta x)^3} \right)^2 \langle \tilde{v} | \tilde{v} \rangle + 2 \left( \frac{2\tau}{(\Delta x)^3} \right)^2 \langle \tilde{v} | A_x^\dagger | \tilde{v} \rangle + \dots \\
&4 \left( \frac{2\tau}{(\Delta x)^3} \right)^2 \langle \tilde{v} | A_x | \tilde{v} \rangle + \left( \frac{2\tau}{(\Delta x)^3} \right)^2 \langle \tilde{v} | A_x^\dagger A_x | \tilde{v} \rangle + 2 \left( \frac{2\tau}{(\Delta x)^3} \right)^2 \langle v | A_x A_x^\dagger | \tilde{v} \rangle - \dots \\
&4 \left( \frac{2\tau}{(\Delta x)^3} \right)^2 \langle v | A_x^\dagger | \tilde{v} \rangle + 4 \left( \frac{2\tau}{(\Delta x)^3} \right)^2 \langle v | A_x^\dagger | \tilde{v} \rangle + 2 \left( \frac{2\tau}{(\Delta x)^3} \right)^2 \langle v | A_x^\dagger A_x^\dagger | \tilde{v} \rangle + \dots \\
&4 \left( \frac{2\tau}{(\Delta x)^3} \right)^2 \langle v | A_x | \tilde{v} \rangle + 8 \left( \frac{2\tau}{(\Delta x)^3} \right)^2 \langle v | \tilde{v} \rangle - 4 \left( \frac{2\tau}{(\Delta x)^3} \right)^2 \langle v | A_x^\dagger | \tilde{v} \rangle - \dots \\
&4 \left( \frac{2\tau}{(\Delta x)^3} \right)^2 \langle v | A_x A_x | \tilde{u} \rangle + 4 \left( \frac{2\tau}{(\Delta x)^3} \right)^2 \langle v | A_x | \tilde{u} \rangle - 2 \left( \frac{2\tau}{(\Delta x)^3} \right)^2 \langle v | A_x^\dagger A_x | \tilde{v} \rangle + \dots \\
&\left( \frac{2\tau}{(\Delta x)^3} \right)^2 \langle v | A_x^\dagger A_x^\dagger | v \rangle - 2 \left( \frac{2\tau}{(\Delta x)^3} \right)^2 \langle v | A_x^\dagger | v \rangle - \dots \\
&4 \left( \frac{2\tau}{(\Delta x)^3} \right)^2 \langle v | v \rangle - 4 \left( \frac{2\tau}{(\Delta x)^3} \right)^2 \langle v | A_x | v \rangle + \frac{4\tau}{(\Delta x)^3} A_x^\dagger | \tilde{v} \rangle \left( \langle v | A_x | v \rangle \right) - \dots \\
&\frac{8\tau}{(\Delta x)^3} | \tilde{v} \rangle \left( \langle v | A_x | v \rangle \right) + \frac{4\tau}{(\Delta x)^3} A_x | \tilde{v} \rangle \left( \langle v | A_x | v \rangle \right) - \dots \\
&\frac{4\tau}{(\Delta x)^3} A_x^\dagger | v \rangle \left( \langle v | A_x | v \rangle \right) + \frac{4\tau}{(\Delta x)^3} | v \rangle \left( \langle v | A_x | v \rangle \right) - \frac{2\tau}{(\Delta x)^3} A_x | v \rangle \left( \langle v | A_x | v \rangle \right) + \dots \\
&A_x^\dagger | u \rangle \left( \langle v | A_x | v \rangle \right) - | u \rangle \left( \langle v | A_x | v \rangle \right) + \lambda^2 \frac{4\tau}{(\Delta x)^3} A_x^\dagger | \tilde{v} \rangle - \dots \\
&\lambda^2 \frac{8\tau}{(\Delta x)^3} | \tilde{v} \rangle + \lambda^2 \frac{4\tau}{(\Delta x)^3} A_x | \tilde{v} \rangle + \lambda^2 \frac{4\tau}{(\Delta x)^3} A_x^\dagger | v \rangle + \lambda^2 \frac{8\tau}{(\Delta x)^3} | v \rangle + \dots \\
&\lambda^2 \frac{4\tau}{(\Delta x)^3} A_x | v \rangle A_x^\dagger | v \rangle + | v \rangle + \langle u | A_x A_x^\dagger | u \rangle + \dots \\
&2 \langle u | A_x^\dagger | u \rangle + \left( 4 | v \rangle \right) \left( \langle v | A_x^\dagger | v \rangle \right) A_x^\dagger | u \rangle - \left( 4 | v \rangle \right) \left( \langle v | A_x^\dagger | v \rangle \right) | u \rangle - \dots \\
&\left. 2 \langle v | v \rangle \left( A_x^\dagger | v \rangle \right) + 2 \langle v | v \rangle \left( | v \rangle \right) \right\} .
\end{aligned}$$

for the second equation of the system. As a result, we obtain time evolved variational states for solutions  $u, v$ , which yield the following two cost functions, respectively denoted  $\mathcal{C}_u$  and  $\mathcal{C}_v$ . In comparison to other PDEs and the initial conditions under which they are solved in the library, we perform optimization for each cost function simultaneously to determine the ground state corresponding to solutions achieved classically.

## 4.10 Hunter-Saxton equation

### Cost function derivation

The partial differential equation reads,

$$\begin{aligned}
(u_t + uu_x)_x &= \frac{1}{2} u_x^2 \\
&\Downarrow \\
(|\tilde{u}\rangle + |u\rangle |u\rangle_x)_x &= \langle u | \frac{1}{2} |u\rangle_x \\
&\Downarrow \\
\left( \frac{A_x - \mathbf{1}}{\Delta x} \right) (|\tilde{u}\rangle + |u\rangle) \left( \left( \frac{A_x - \mathbf{1}}{\Delta x} \right) |u\rangle \right) &= \left( \frac{A_x - \mathbf{1}}{\Delta x} \right) \langle u | \frac{1}{2} \left( \frac{A_x - \mathbf{1}}{\Delta x} \right) |u\rangle
\end{aligned}$$

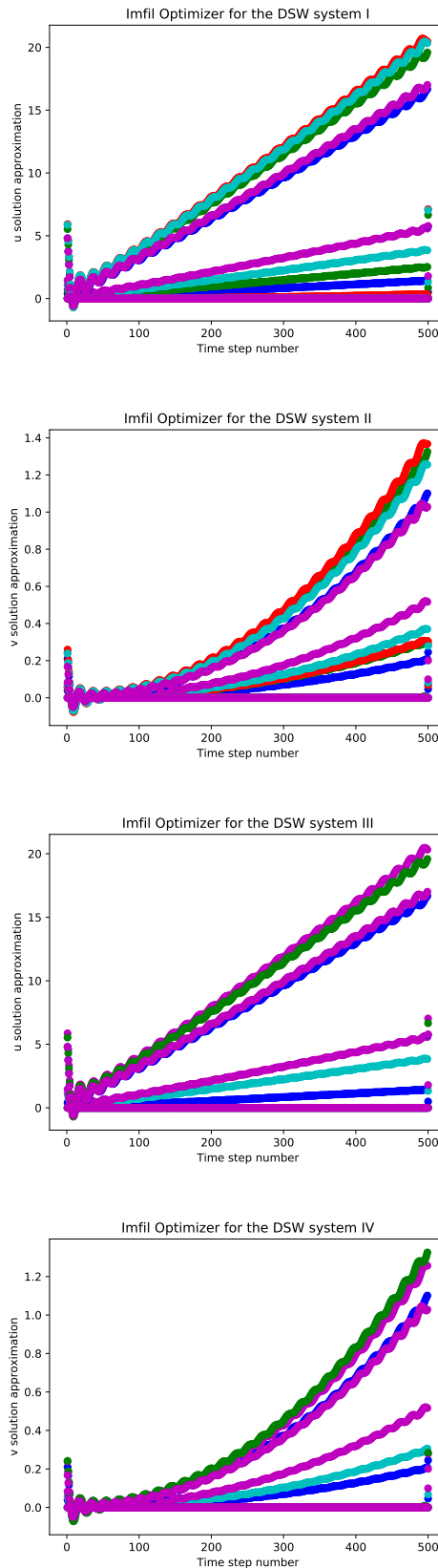


Figure 72: *Extracting measurements from the DSW partial differential equation system for approximating traveling wave solutions.* Collecting extracted measurements corresponding to approximations of solutions to the DSW system with the Scipy Imfil optimizer yields approximations to one type of standing wave solution. For this particular solution, the traveling wave attains periodic maxima surrounding discontinuities of a few analytically known exact solutions from the tangent function. Solutions to each component of the PDE system are provided sequentially.

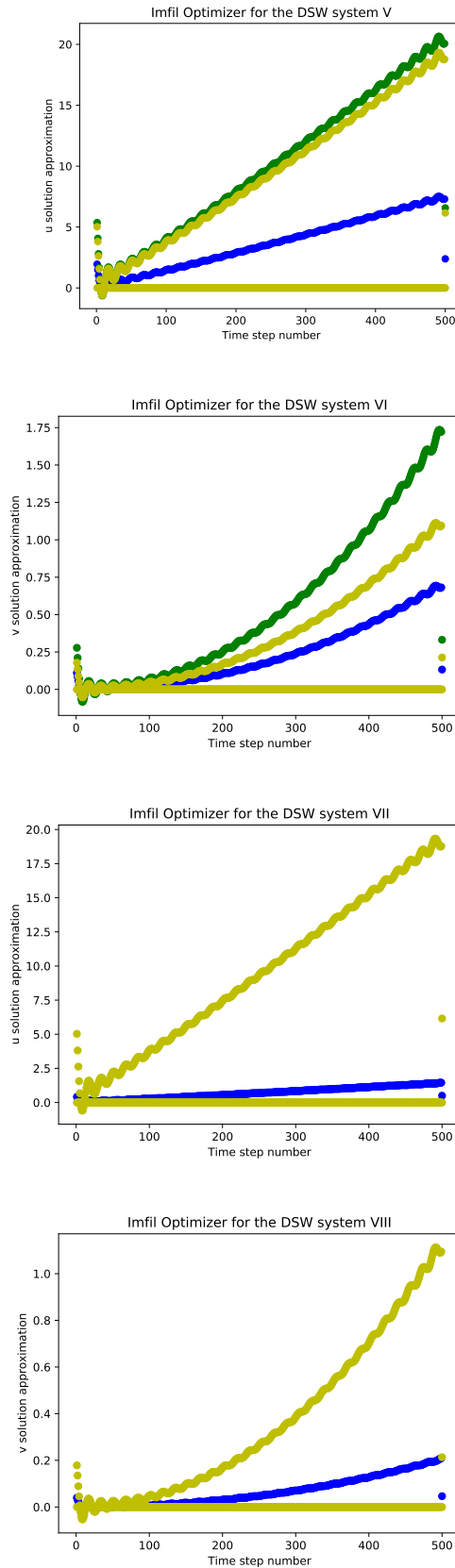
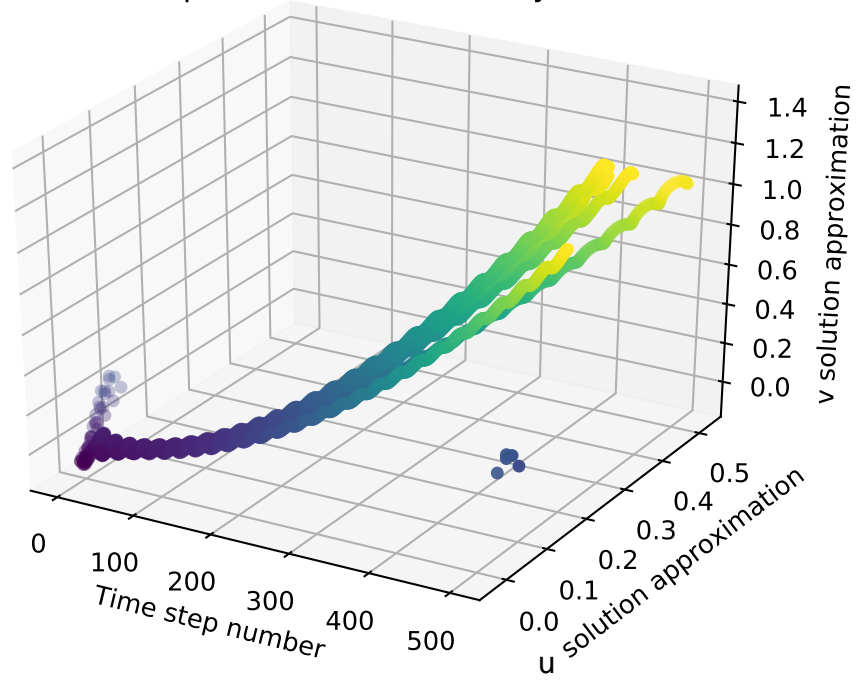


Figure 73: *Extracting measurements from the DSW partial differential equation system for approximating traveling wave solutions.* A continuation of solution approximations in continued from the previous figure, in which  $v$  solution approximations of the DSW system are approximated with a constrained optimization scheme from approximations of a  $u$  solution.

Imfil Optimizer for the DSW system



Imfil Optimizer for the DSW system

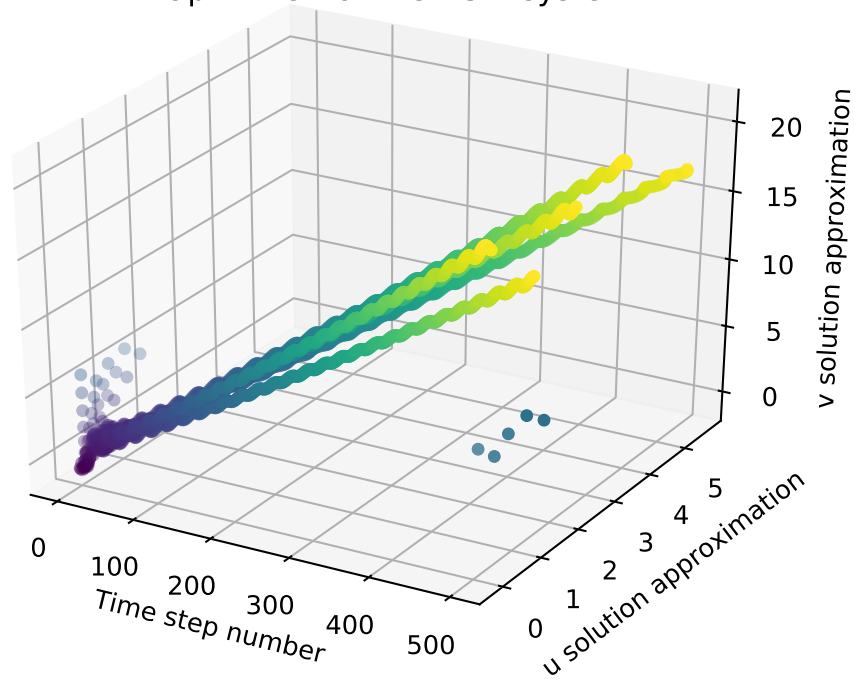


Figure 74: Three-dimensional plots of solution curves from both components of the DSW system. Components of solutions obtained in the previous two figures are presented in three-dimensional Euclidean space.

$$\begin{aligned}
& \left( \frac{A_x - \mathbf{1}}{\Delta x} \right) |\tilde{u}\rangle + \left( \frac{A_x - \mathbf{1}}{\Delta x} \right) |u\rangle \left( \frac{A_x - \mathbf{1}}{\Delta x} \right) |u\rangle = \frac{1}{2} \left( \frac{A_x^\dagger |u\rangle - |u\rangle}{\Delta x} \right) \left( \frac{A_x |u\rangle - |u\rangle}{\Delta x} \right) \\
& \frac{A_x |u\rangle - |\tilde{u}\rangle}{\Delta x} + \left( \frac{A_x |u\rangle - |u\rangle}{\Delta x} \right) \left( \frac{A_x |u\rangle - |u\rangle}{\Delta x} \right) = \frac{1}{2(\Delta x)^2} \left( \langle u | A_x^\dagger A_x^\dagger |u\rangle - \langle u | A_x^\dagger |u\rangle - \dots \right. \\
& \left. \langle u | A_x^\dagger |u\rangle + \langle u | u\rangle \right).
\end{aligned}$$

We obtain the time evolved variational state by expanding one more superposition, followed by isolating for  $|\tilde{u}\rangle$ ,

$$\begin{aligned}
\frac{A_x |\tilde{u}\rangle - |\tilde{u}\rangle}{\Delta x} + \frac{1}{(\Delta x)^2} \left( \langle u | A_x^\dagger A_x |u\rangle - \langle u | A_x |u\rangle - \langle u | A_x^\dagger |u\rangle + \langle u | u\rangle \right) &= \frac{1}{2(\Delta x)^2} \left( \langle u | A_x^\dagger A_x^\dagger |u\rangle - \dots \right. \\
& \left. \langle u | A_x^\dagger |u\rangle - \langle u | A_x |u\rangle + \langle u | u\rangle \right) \\
|\tilde{u}\rangle = -\Delta x \left\{ \frac{1}{2(\Delta x)^2} \left( \langle u | A_x^\dagger A_x^\dagger |u\rangle - \langle u | A_x^\dagger |u\rangle - \langle u | A_x |u\rangle + \langle u | u\rangle \right) - \frac{1}{(\Delta x)^2} \left( \langle u | A_x^\dagger A_x |u\rangle - \dots \right. \right. \\
& \left. \left. \langle u | A_x |u\rangle - \langle u | A_x^\dagger |u\rangle + \langle u | u\rangle \right) - A_x |u\rangle_t \right\}.
\end{aligned}$$

We compute the cost function below,

$$\begin{aligned}
\mathcal{C}^{\text{H-S}}(\lambda, \lambda_0) = \left\| |\tilde{u}\rangle - |u\rangle \right\|^2 = \left\| -\Delta x \left\{ \frac{1}{2(\Delta x)^2} \left( \langle u | A_x^\dagger A_x^\dagger |u\rangle - \dots \right. \right. \right. \\
\left. \left. \langle u | A_x^\dagger |u\rangle - \langle u | A_x |u\rangle + \langle u | u\rangle \right) - \dots \right. \\
\left. \frac{1}{(\Delta x)^2} \left( \langle u | A_x^\dagger A_x |u\rangle - \dots \right. \right. \\
\left. \left. \langle u | A_x |u\rangle - \langle u | A_x^\dagger |u\rangle + \langle u | u\rangle \right) - A_x |\tilde{u}\rangle \right\} - |u\rangle \left\|^2.
\end{aligned}$$

Expanding the norm is equivalent to,

$$\begin{aligned}
& \left\| -\frac{1}{2\Delta x} \langle u | A_x^\dagger A_x^\dagger |u\rangle - \left( \frac{1}{2(\Delta x)} + \frac{1}{(\Delta x)} \right) \langle u | A_x^\dagger |u\rangle - \dots \right. \\
& \left. \left( \frac{1}{2\Delta x} + \frac{1}{(\Delta x)^2} \right) \langle u | u\rangle - \Delta x A_x |u\rangle_t - |u\rangle \right\|^2 \\
& \frac{1}{\Delta x} \left( \frac{1}{2} \langle u | A_x^\dagger A_x^\dagger |u\rangle - \left( \frac{1}{2(\Delta x)} + \frac{1}{(\Delta x)} \right) \langle u | A_x^\dagger |u\rangle \right)^2 - \dots \\
& \frac{1}{2\Delta x} \left( \langle u | A_x^\dagger A_x^\dagger |u\rangle - \dots \right. \\
& \left. \left( \frac{1}{2(\Delta x)} + \frac{1}{(\Delta x)} \right) \langle u | A_x^\dagger |u\rangle \right) \left( \left( \frac{1}{2\Delta x} + \frac{1}{(\Delta x)^2} \right) \langle u | u\rangle - \dots \right. \\
& \left. \Delta x A_x |\tilde{u}\rangle - |u\rangle \right) + \dots \\
& \left( \left( \frac{1}{2\Delta x} + \frac{1}{(\Delta x)^2} \right) \langle u | u\rangle - \Delta x A_x |\tilde{u}\rangle - |u\rangle \right)^2
\end{aligned}$$

We obtain,

$$\begin{aligned}
\boxed{\mathcal{C}^{\text{H-S}}(\lambda, \lambda_0^{\text{H-S}})} &= (\lambda_0^{\text{H-S}})^2 + \text{Re} \left\{ \frac{1}{4\Delta x} \left( \langle u | A_x A_x | u \rangle \right) \left( \langle u | A_x^\dagger A_x^\dagger | u \rangle \right) - \dots \right. \\
&\quad \frac{1}{2\Delta x} \left( \frac{1}{2\Delta x} + \frac{1}{\Delta x} \right) \left( \langle u | A_x^\dagger | u \rangle \right) \left( \langle u | A_x^\dagger A_x^\dagger | u \rangle \right) - \dots \\
&\quad \frac{1}{2\Delta x} \left( \langle u | A_x^\dagger A_x^\dagger | u \rangle \right) \left( \left( \frac{1}{2\Delta x} + \frac{1}{\Delta x} \right) \langle u | A_x^\dagger | u \rangle \right) + \dots \\
&\quad \frac{1}{\Delta x} \left( \frac{1}{2\Delta x} + \frac{1}{\Delta x} \right)^2 \left( \langle v | A_x^\dagger | v \rangle \right) \left( \langle v | A_x | v \rangle \right) + \frac{1}{2} \frac{1}{(\Delta x)^2} \left( \langle u | | u \rangle \times \dots \right. \\
&\quad \left. \left( \frac{1}{2\Delta x} + \frac{1}{\Delta x} \right) \langle u | A_x^\dagger | u \rangle \right) - \left( \frac{1}{2\Delta x} + \frac{1}{\Delta x} \right) \langle u | A_x^\dagger | u \rangle \left( A_x | \tilde{u} \rangle \right) - \dots \\
&\quad \frac{\langle u |}{\Delta x} \left( \frac{1}{2\Delta x} - \frac{1}{\Delta x} \right) \langle u | A_x^\dagger | u \rangle + \frac{1}{\Delta x} \left( \frac{1}{2\Delta x} + \frac{1}{(\Delta x)^2} \right) \left( \langle u | A_x^\dagger A_x^\dagger | u \rangle \right) \left( \langle u | | u \rangle \right) - \dots \\
&\quad \left( \frac{1}{2\Delta x} + \frac{1}{\Delta x} \right) \langle u | A_x^\dagger | u \rangle \left( A_x | \tilde{u} \rangle \right) + \frac{1}{\Delta x} \left( \frac{1}{2\Delta x} + \frac{1}{\Delta x} \right) \langle u | \left( \langle u | A_x^\dagger | u \rangle \right) + \dots \\
&\quad \frac{1}{\Delta x} \left( \frac{1}{2\Delta x} + \frac{1}{(\Delta x)^2} \right)^2 \left( \langle u | | u \rangle \right) \left( \langle u | | u \rangle \right) - \dots \\
&\quad \left( \frac{1}{2\Delta x} + \frac{1}{(\Delta x)^2} \right) \left( \langle u | | u \rangle \right) \left( A_x | \tilde{u} \rangle \right) + \langle u | \frac{1}{\Delta x} \left( \frac{1}{2\Delta x} + \frac{1}{(\Delta x)^2} \right) \langle u | | u \rangle + \dots \\
&\quad \langle u | | u \rangle \frac{1}{\Delta x} \left( \frac{1}{2\Delta x} + \frac{1}{(\Delta x)^2} \right)^2 \langle u | | u \rangle + \left( \frac{1}{2\Delta x} + \frac{1}{(\Delta x)^2} \right) \langle u | | u \rangle \left( A_x | \tilde{u} \rangle \right) - \dots \\
&\quad - \langle u | \left( \frac{1}{2\Delta x} + \frac{1}{(\Delta x)^2} \right) \langle u | | u \rangle - \left( A_x | \tilde{u} \rangle \right) \left( \left( \frac{1}{2\Delta x} + \frac{1}{(\Delta x)^2} \right) \langle u | | u \rangle \right) + \dots \\
&\quad \quad \quad (\Delta x)^2 \langle \tilde{u} | A_x^\dagger A_x | u \rangle + \langle u | \Delta x A_x | \tilde{u} \rangle - \dots \\
&\quad \left. \langle u | \left( \frac{1}{2\Delta x} + \frac{1}{(\Delta x)^2} \right) + 2 \langle u | | u \rangle + \langle u | \Delta x A_x | \tilde{u} \rangle \right\} .
\end{aligned}$$

The desired cost function is given by the ultimate linear combination of expectation values above.

## 5 Supplementary materials references

- [1] Aktosun, T. Exact Solutions to the Sine-Gordon Equation. arXiv: 1003.2453v1.
- [2] Apte, A., Auroux, D. & Ramaswamy, M. Observers for Compressible Navier-Stokes Equation. arXiv: 1503.05259 (2015).
- [3] Arnaudon, M. & Cruzeiro, A.B. Lagrangian Navier-Stokes Diffusions of Manifolds: Variational Principle and Stability. arXiv: 1004.2176 (2010).
- [4] Charnyi, S., Heister, T., Olshanskii, M.A. & Rebholz, L.G. On conservation laws of Navier-Stokes Galerkin discretizations. *Journal of Computational Physics* **337** 289-308 (2016).
- [5] Demange, S. Qadri, U. Juniper, M., and Pina, F. Global modes of viscous heated jets with real gas effects. *Journal of Fluid Mechanics*, 937, A7 (2022).
- [6] Fan, K. and Zhou, C. Exact Solutions of Damped Improved Boussinesq Equations by Extended ( $G'/G$ )-Expansion Method. *Complexity*, 4128249 (2020).

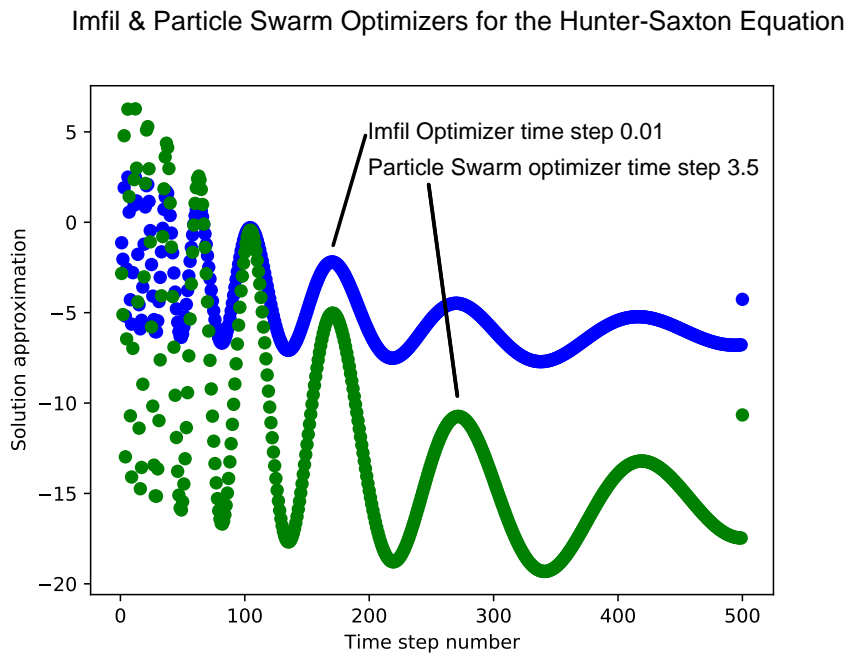
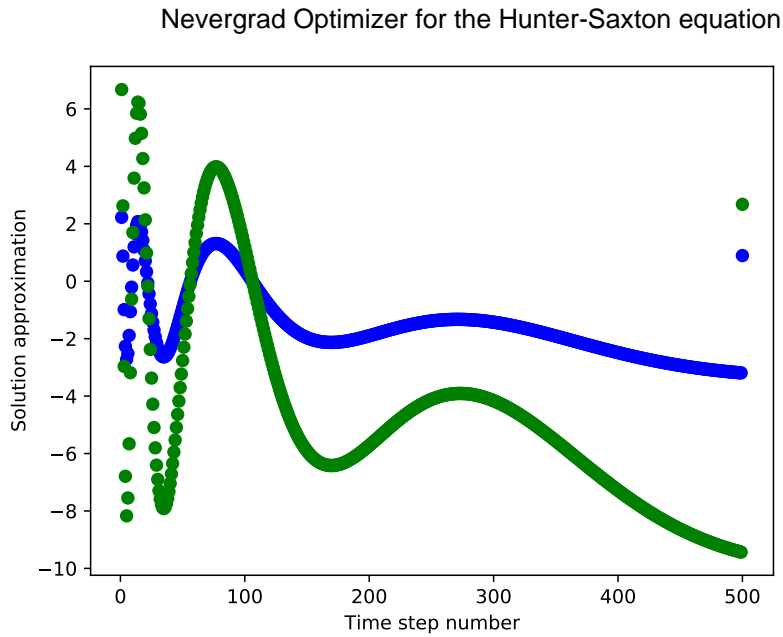
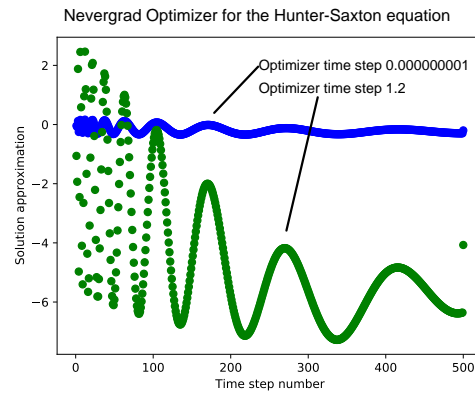
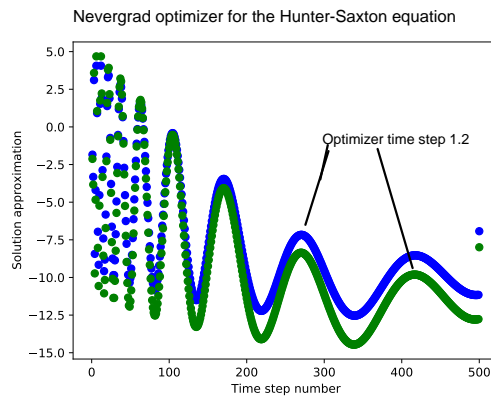


Figure 75: *Extracting measurements from the Hunter-Saxton equation.* Implementing the variational quantum algorithm for different time steps and initial conditions yields solutions approximations to Hunter-Saxton equation, in which the VQA exhibits difficulty in efficiently approximating the nonlinearities of the PDE; in approximately the first 100 time steps of the evolution, solution approximations across all deterministic optimizers largely fluctuate, after which a sinusoidal-like curve for solution approximations emerges.



Imfil & Particle Swarm Optimizers for the Hunter-Saxton Equation

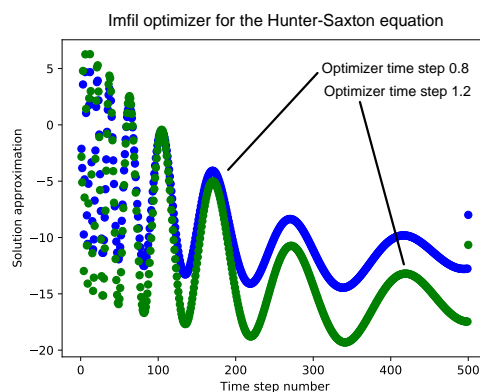
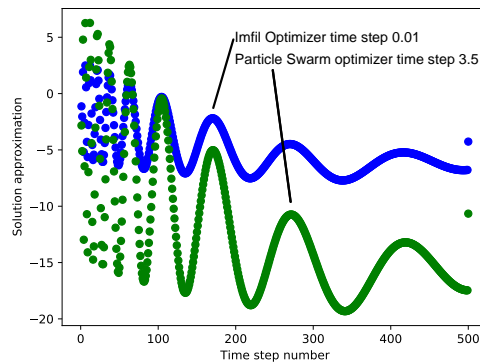


Figure 76: *Extracting measurements from the Hunter-Saxton equation.* Implementing the variational quantum algorithm for different time steps and initial conditions yields solutions approximations to Hunter-Saxton equation, in which the VQA exhibits difficulty in efficiently approximating the nonlinearities of the PDE; in approximately the first 100 time steps of the evolution, solution approximations across all deterministic optimizers largely fluctuate, after which a sinusoidal-like curve for solution approximations emerges.

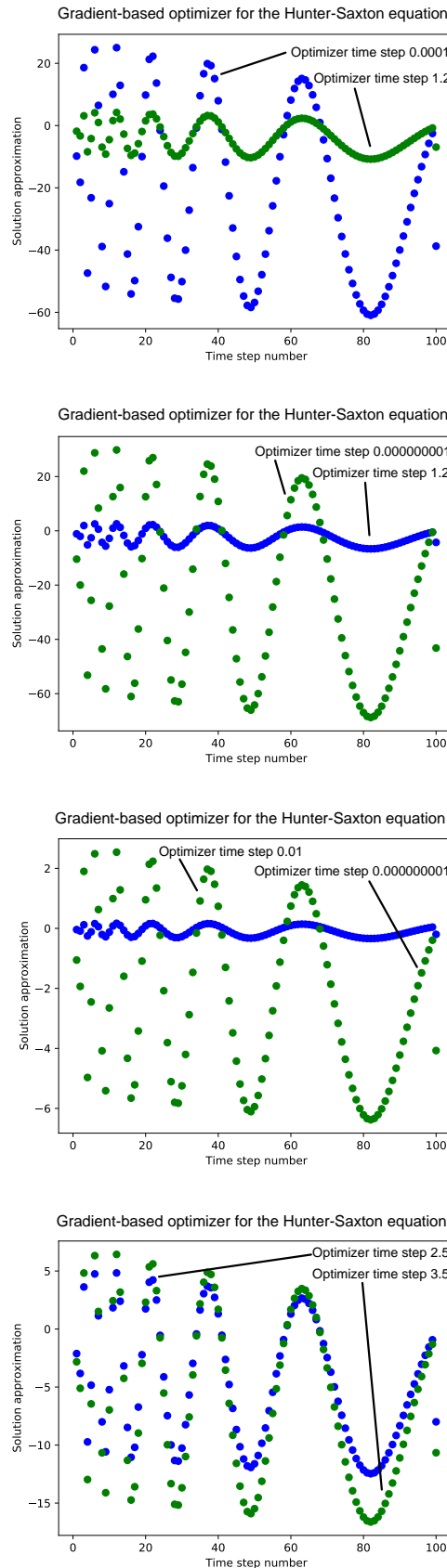
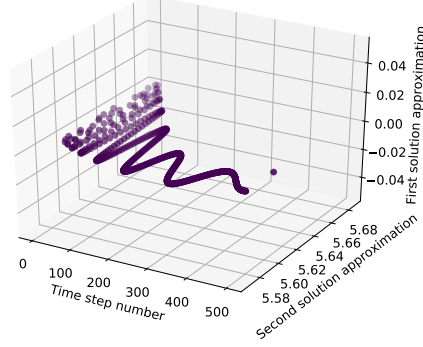
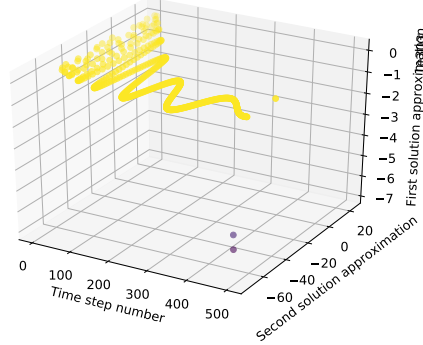


Figure 77: *Extracting measurements from the Hunter-Saxton equation with the gradient-based optimizer for the first 100 time steps of the evolution.* Collecting extracted measurements corresponding to approximations of solutions to the Hunter-Saxton equation with the gradient-based optimizer yields better performance than in the solution approximations produced by the deterministic optimizer that were provided in the previous figure, which in contrast significantly fluctuate before approaching a damped sinusoidal motion.

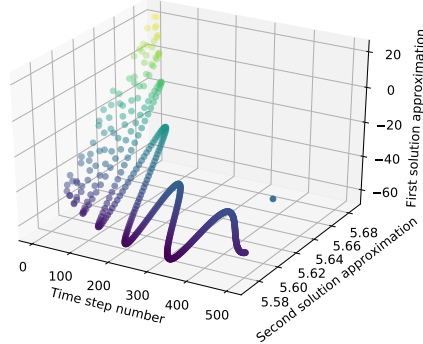
Nevergrad and Imfil Optimizers for the Hunter-Saxton equation



Nevergrad Optimizer for the Hunter-Saxton equation



Particle Swarm Optimizer for the Hunter-Saxton equation



Nevergrad for the Hunter-Saxton equation

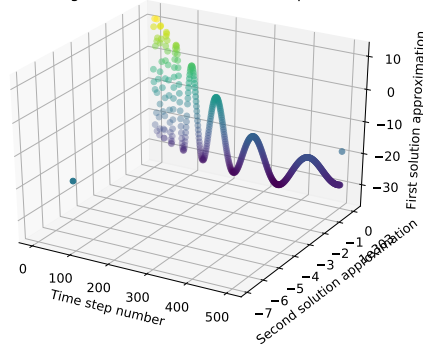


Figure 78: *Extracting measurements from the Hunter-Saxton equation.* Three-dimensional solution curves plots reveal similar characteristics of solutions described in the previous figure.

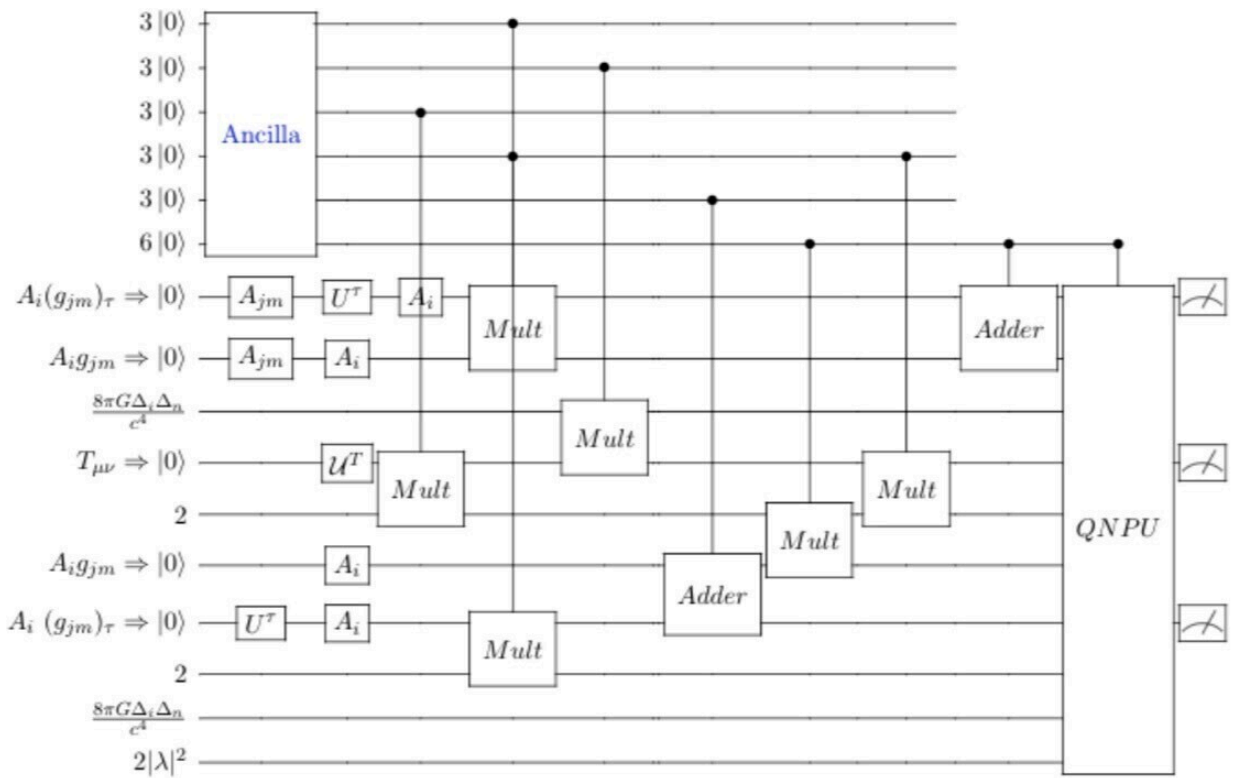


Figure 79: *Quantum circuit for the Einstein equation.* Quantum registers of the above form are time evolved for approximating solutions to the Einstein equations. From a generalized version of the cost function including the contributions from the stress-energy tensor,

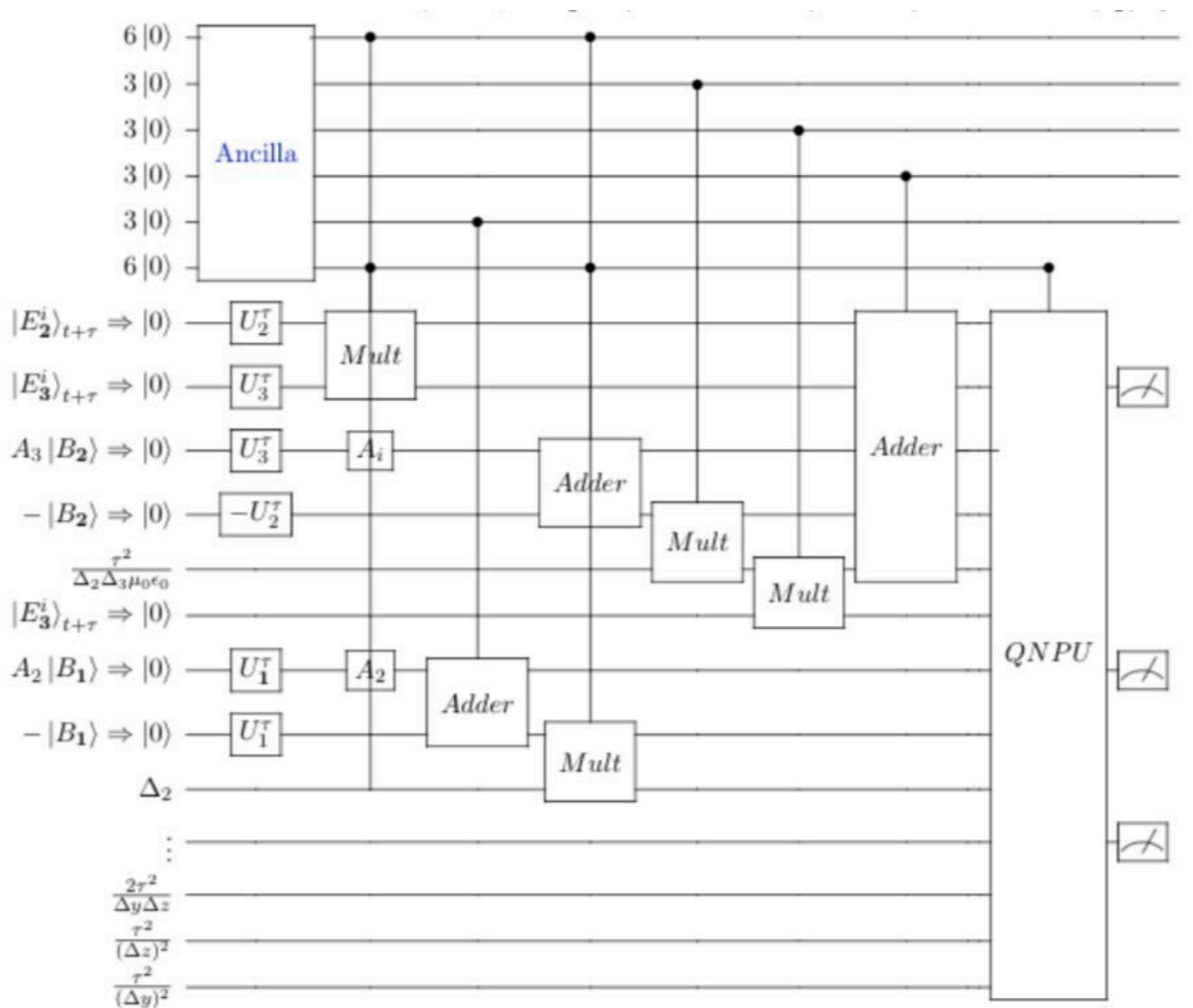


Figure 80: Quantum circuit for one component of the magnetic field from the Maxwell equations. Quantum registers are initialized in the manner as depicted above.

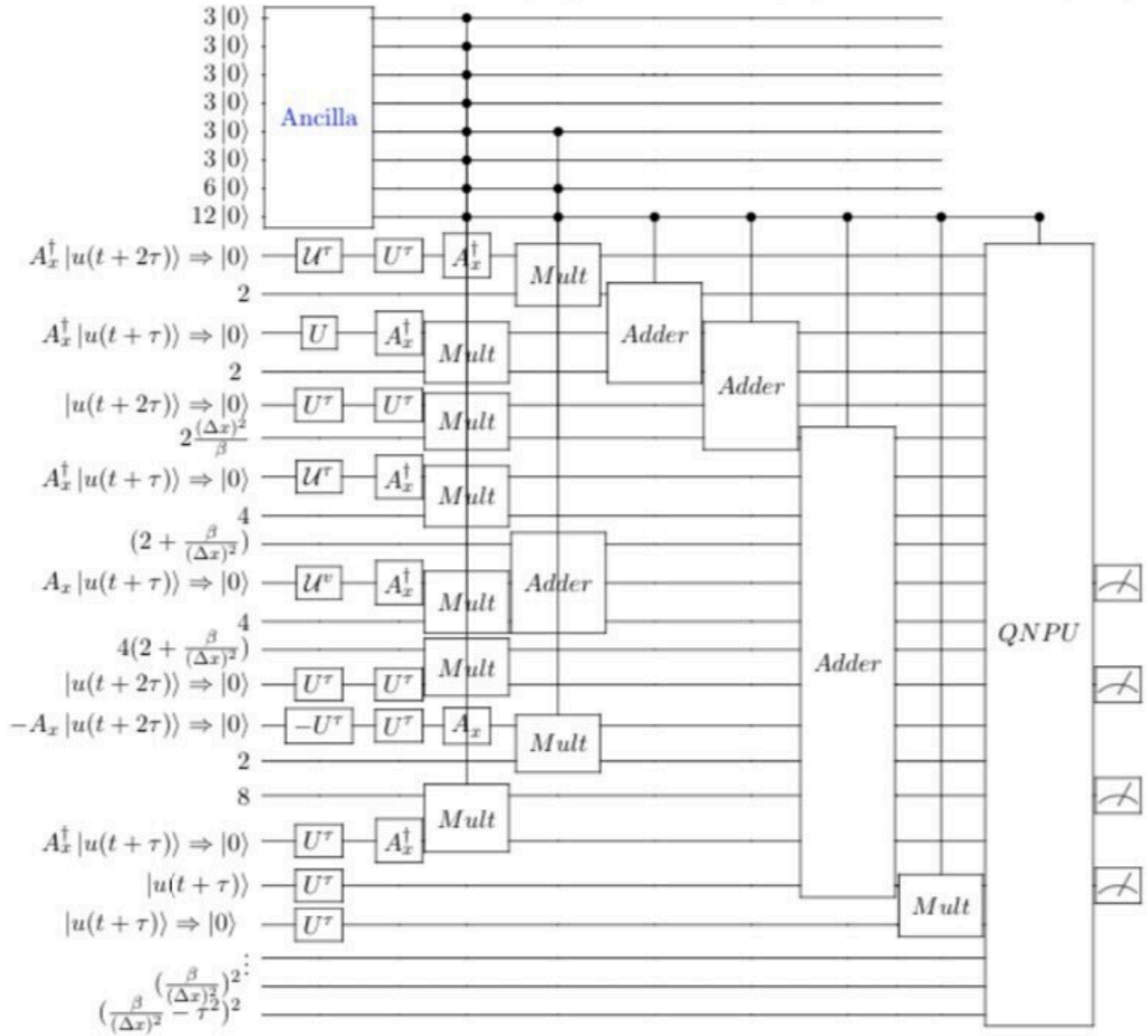


Figure 81: *Quantum circuit for the Boussinesq-type equation.* Quantum circuit registers for the time-evolution of the B-type equation are provided above.

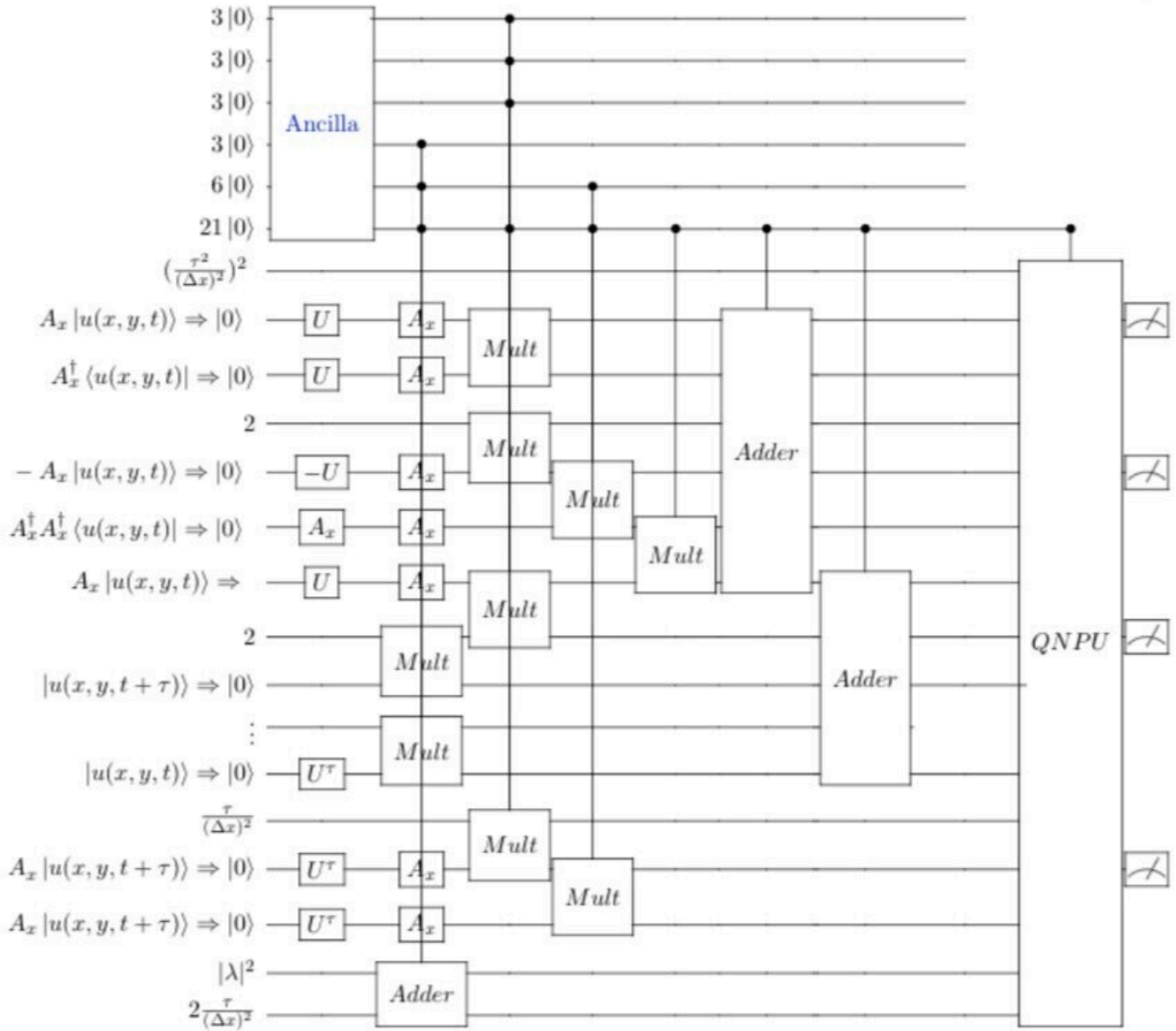


Figure 82: Quantum circuit for the Lin-Tsien equation. Quantum registers are of the form displayed above.

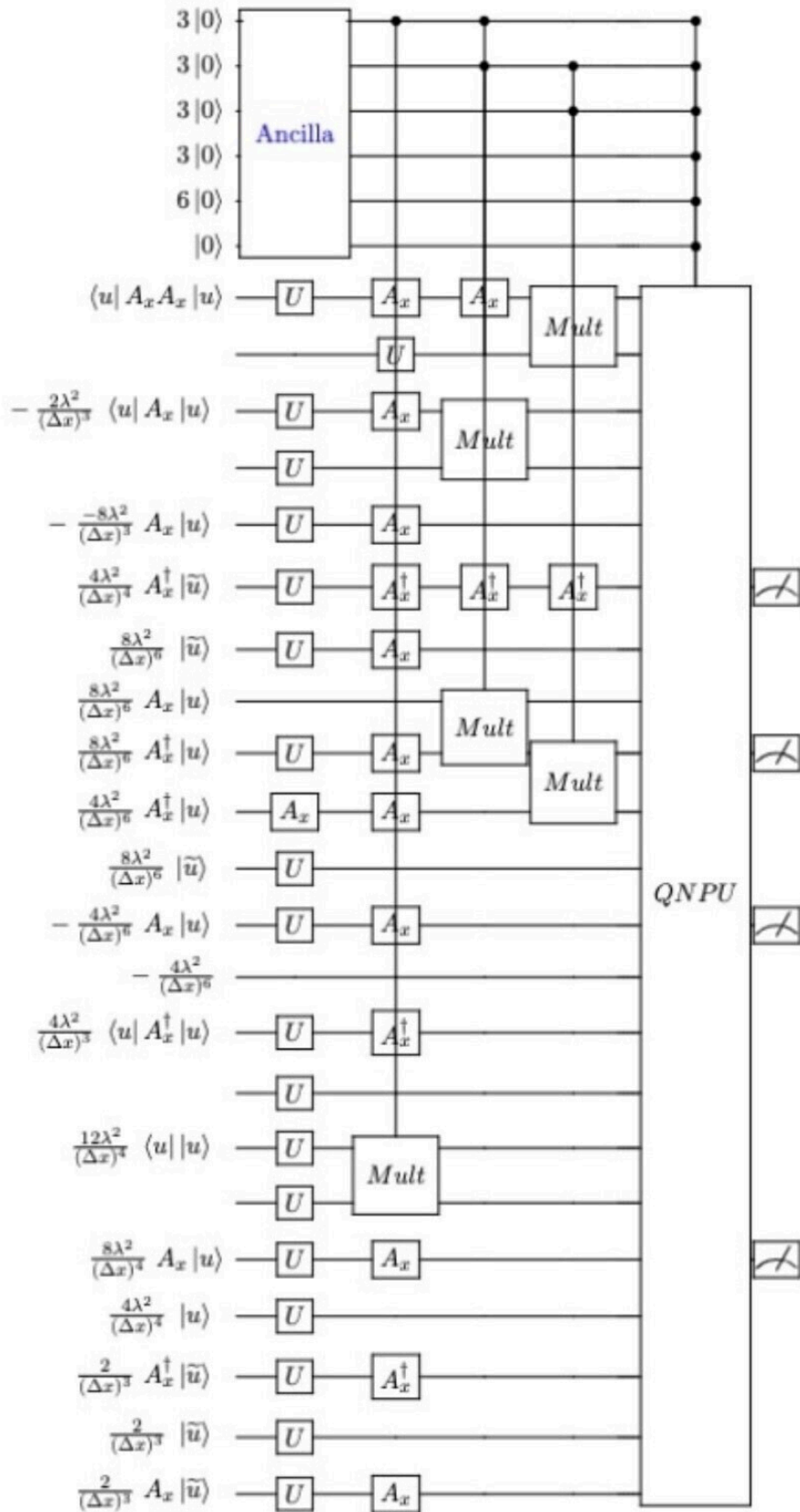


Figure 83: First portion of the quantum circuit diagram for the Camassa-Holm variational quantum algorithm. Quantum registers are depicted above for solutions obtained for the Camassa-Holm equation.

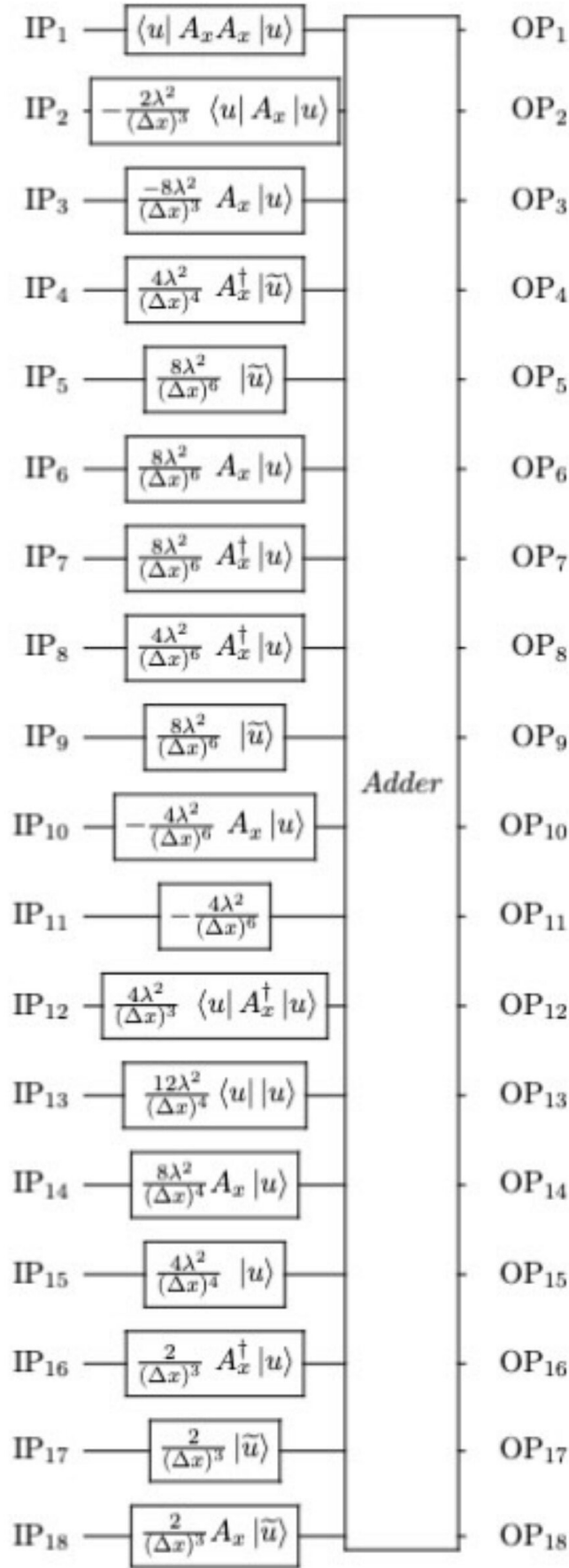


Figure 84: *First portion of the QNPU for the Camassa-Holm variational quantum algorithm.* Quantum registers are depicted above from input ports numbered 1 through 18.

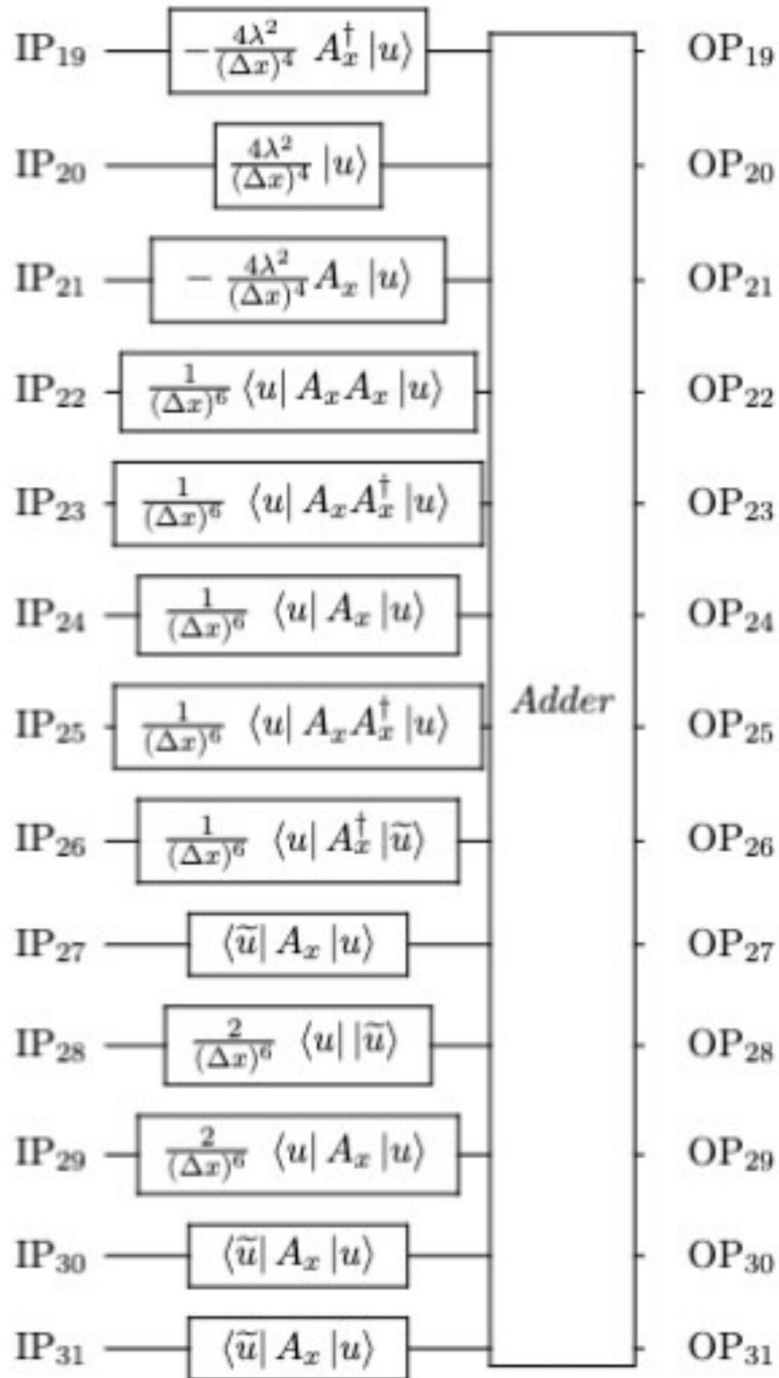


Figure 85: *Second portion of the QNPU for the Camassa-Holm variational quantum algorithm.* Quantum registers are depicted above from input ports numbered 19 through 31.

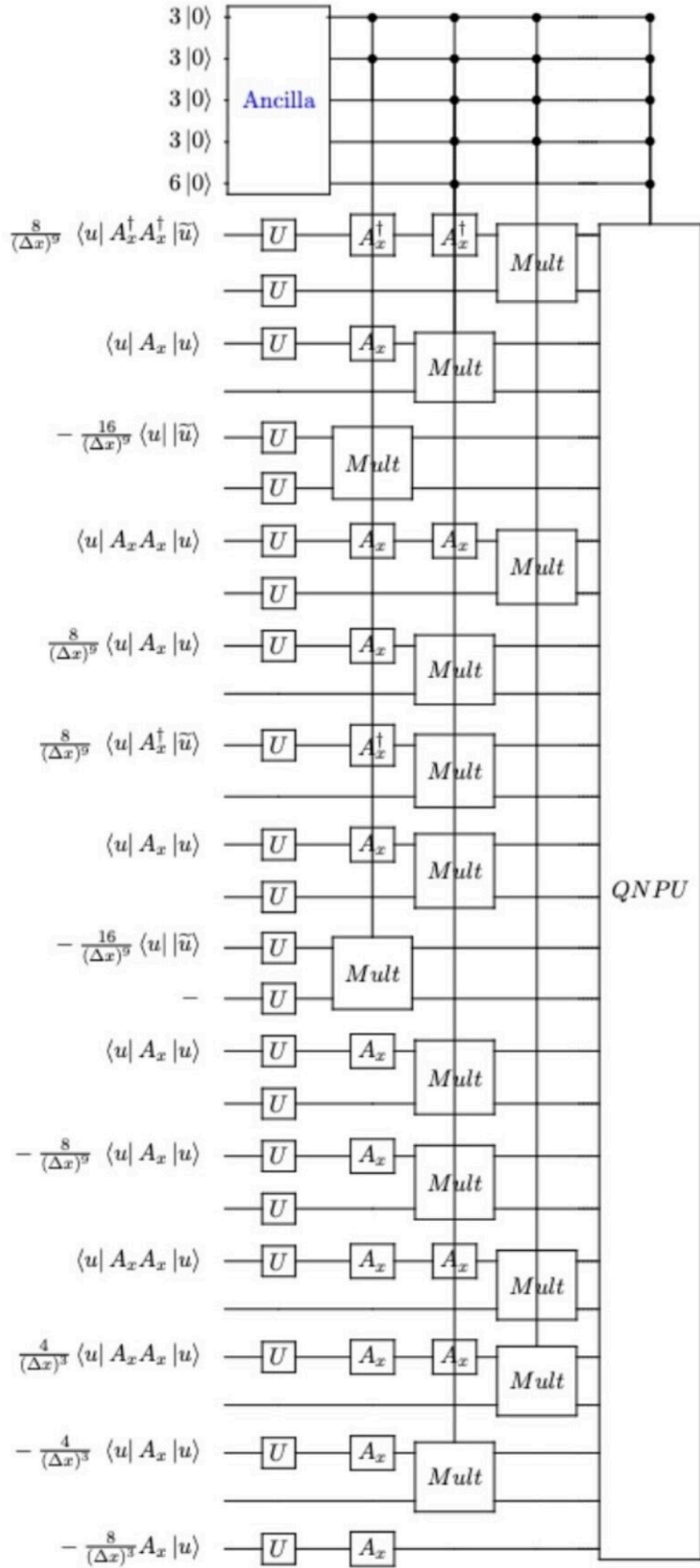


Figure 86: *Second portion of the quantum circuit for the Camassa-Holm variational quantum algorithm. Another portion of the quantum circuit compiled in Cirq for solution approximations is provided above.*

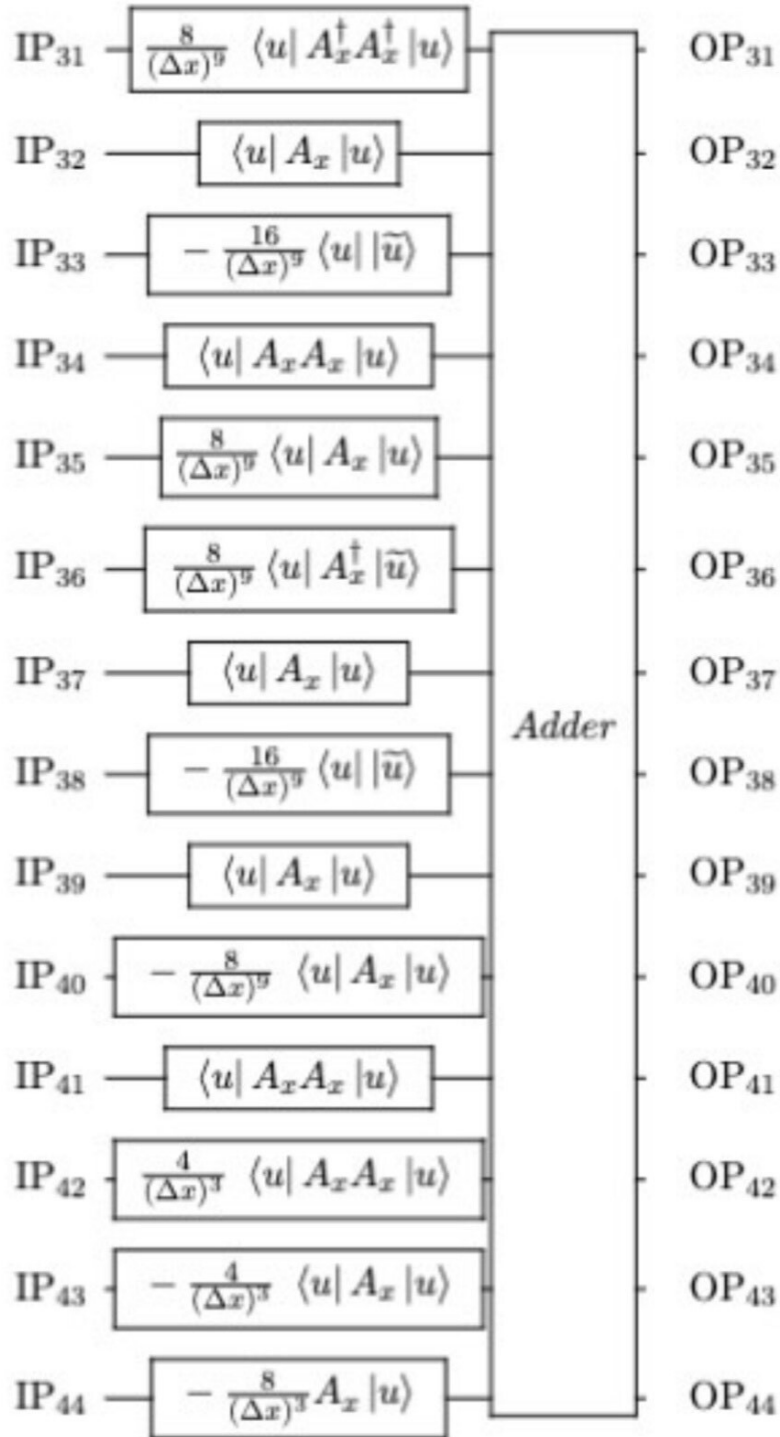


Figure 87: *Third portion of the QNPU for the Camassa-Holm variational quantum algorithm.* Quantum registers are depicted above from input ports numbered 31 through 44.

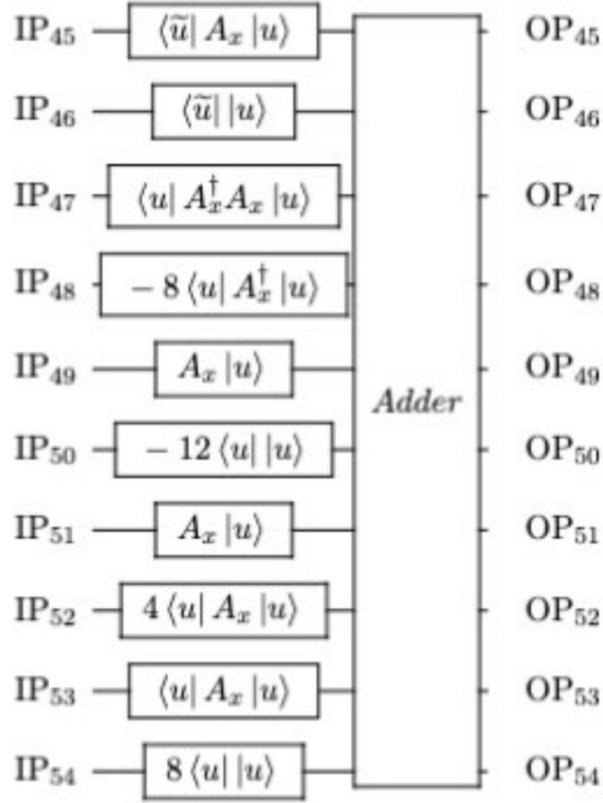


Figure 88: *Fourth portion of the QNPU for the Camssa-Holm variational quantum algorithm.* Quantum registers are depicted above from input ports numbered 45 through 54.

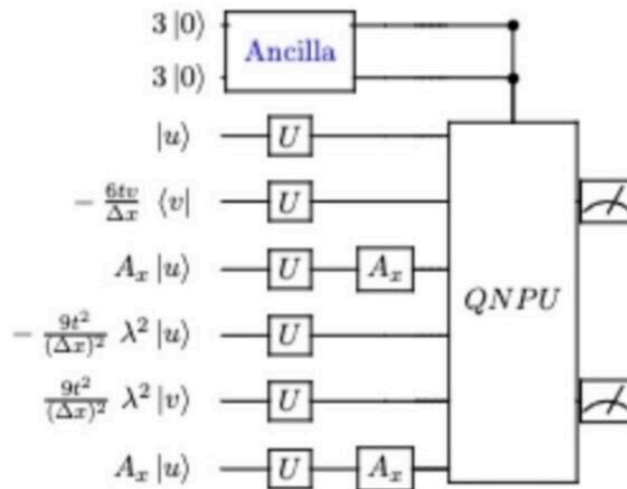


Figure 89: *Quantum circuit for the first equation of the DSW system.* Time-evolved nonlinearities in the quantum circuit above include terms from the first cost function of the system that is optimized.

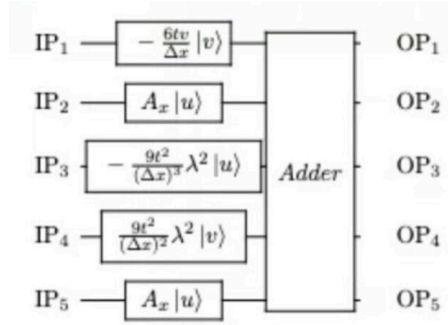


Figure 90: *DSW QNPU for the first equation of the system.* In the portion of the QNPU displayed above, input ports labeled from 1 to 5 are displayed.

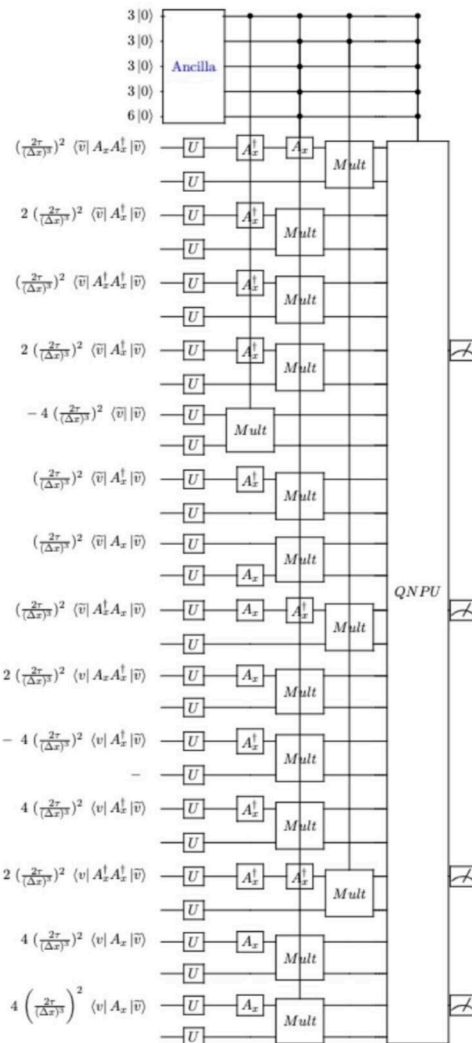


Figure 91: *First portion of the quantum circuit for the second equation of the DSW system.* Before IPs to the QNPU for the second equation of the DSW system, additional qubits are initialized for time evolution.

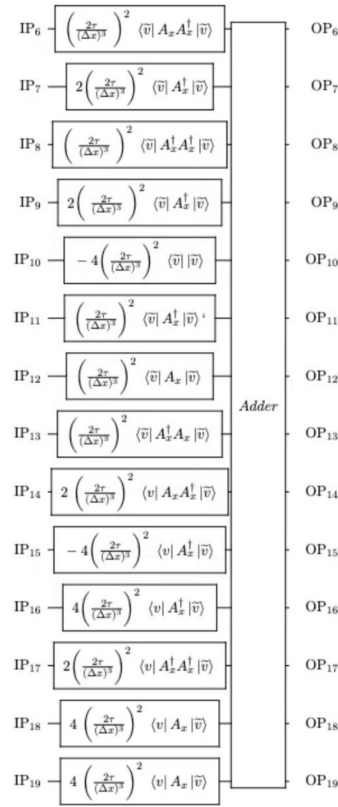


Figure 92: Quantum circuit for the QNPU of the second equation of the DSW system. Input ports labeled 6 through 18 are displayed above.

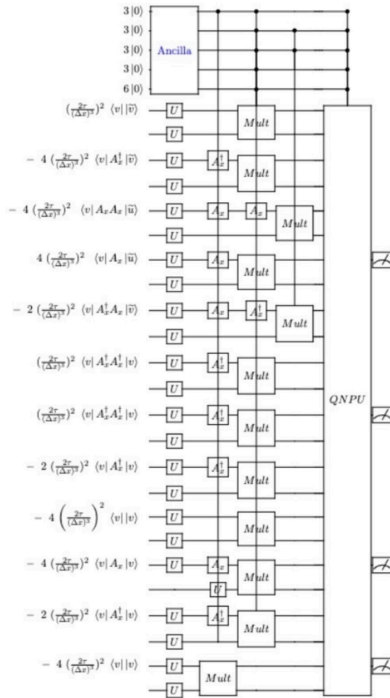


Figure 93: Second portion of the quantum circuit for the second equation of the DSW system. Additional quantum registers of the form indicated above are initialized.

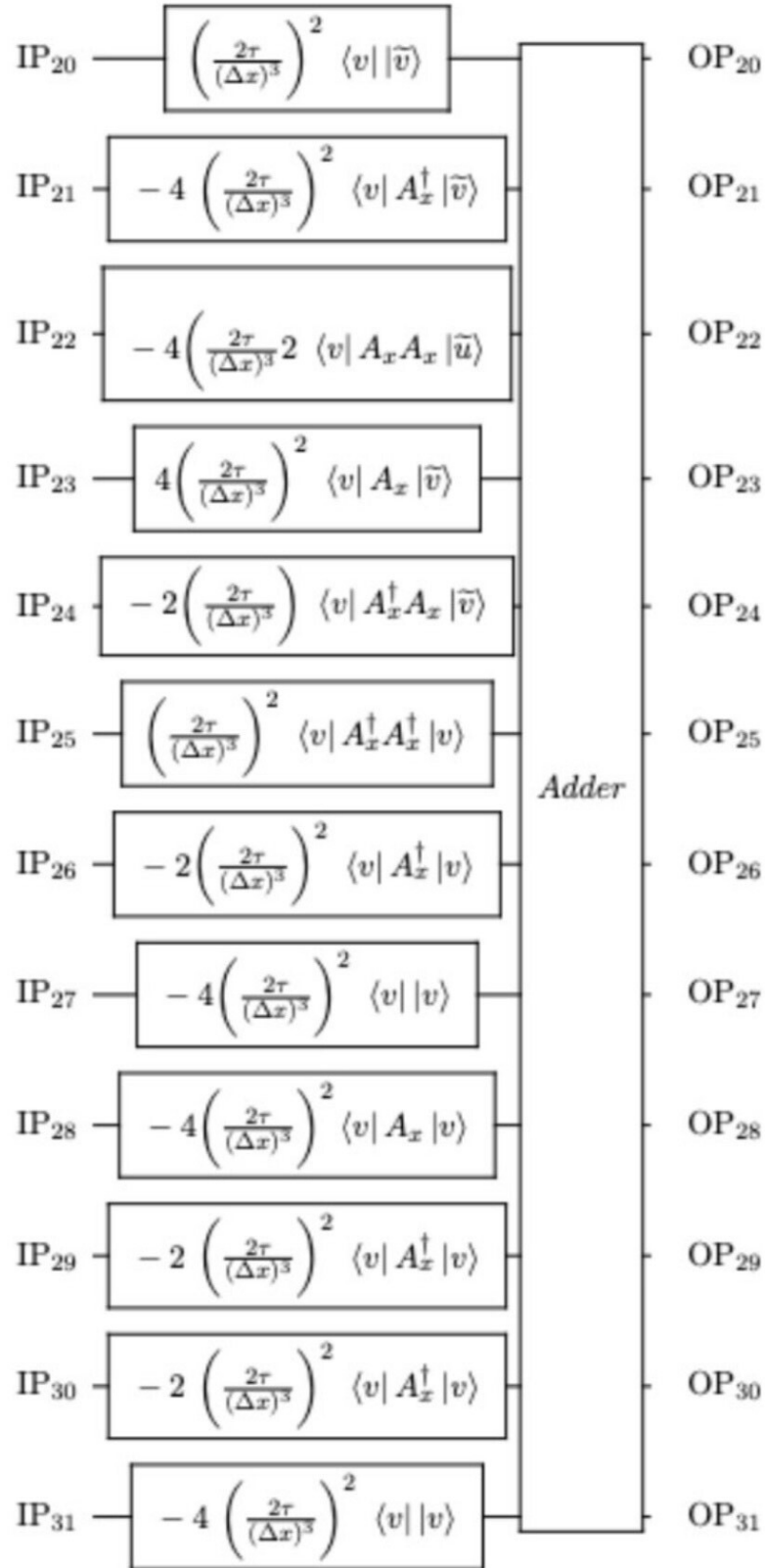


Figure 94: QNPU for the second equation of the DSW system. Input ports labeled 20 through 31 are displayed above.

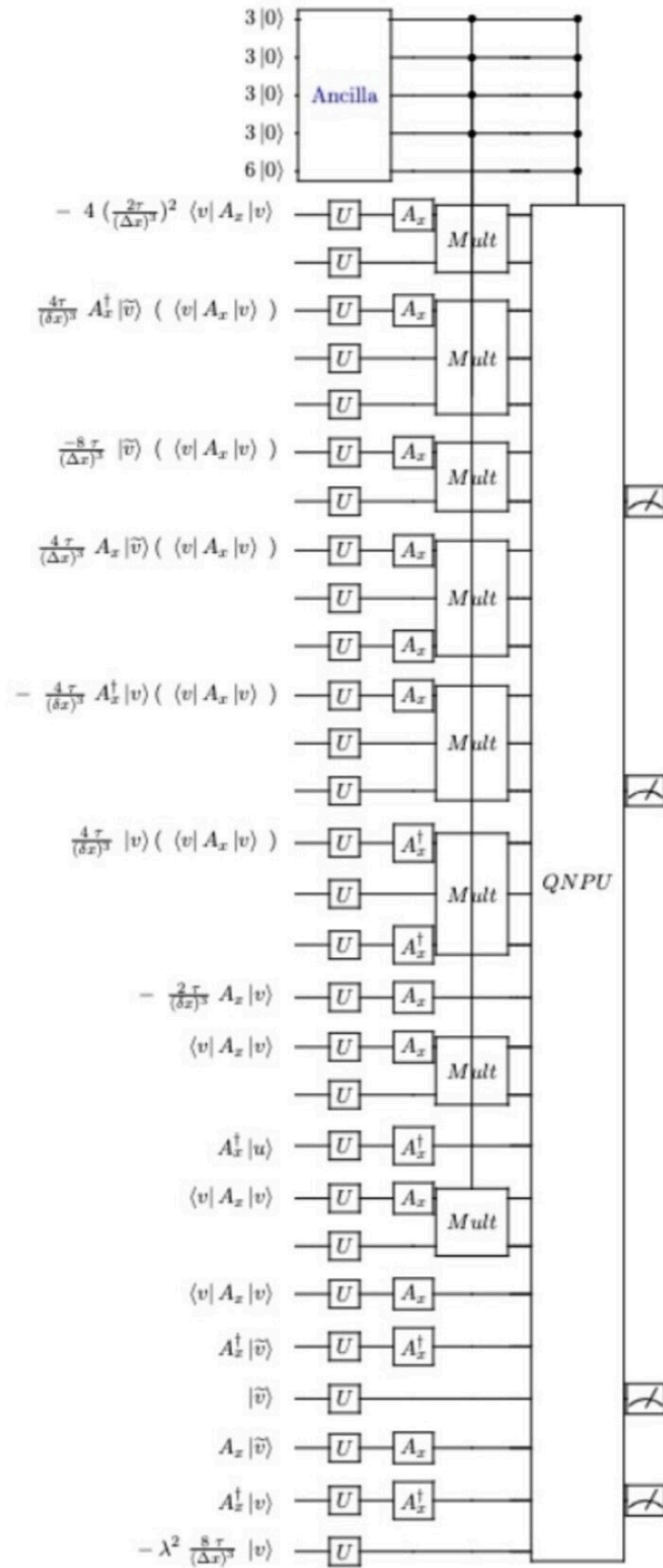


Figure 95: *Third portion of the quantum circuit for the second equation of the DSW system. Additional quantum registers of the form indicated above are initialized.*

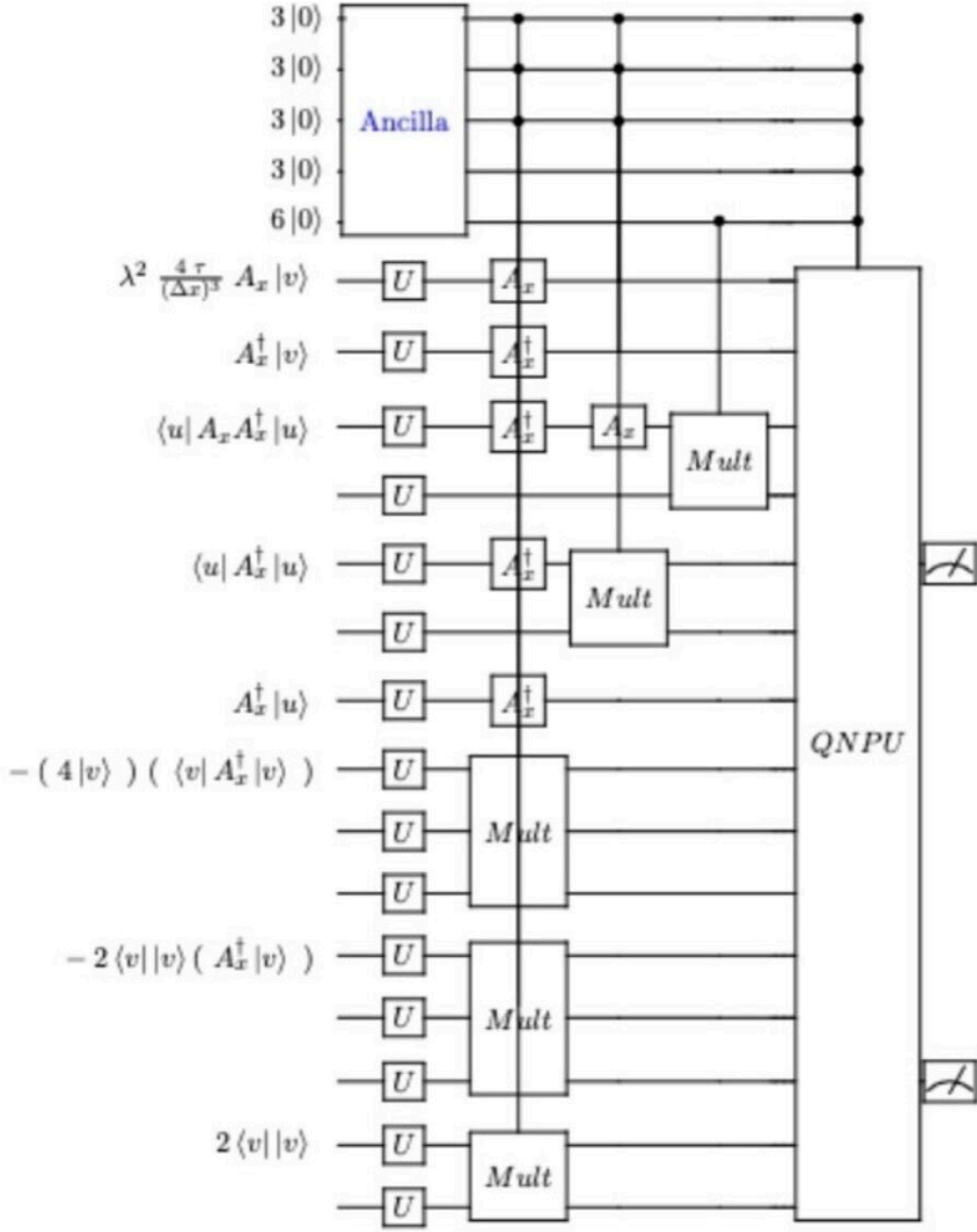


Figure 96: Fourth portion of the quantum circuit for the second equation of the DSW system. Additional quantum registers of the form indicated above are initialized.



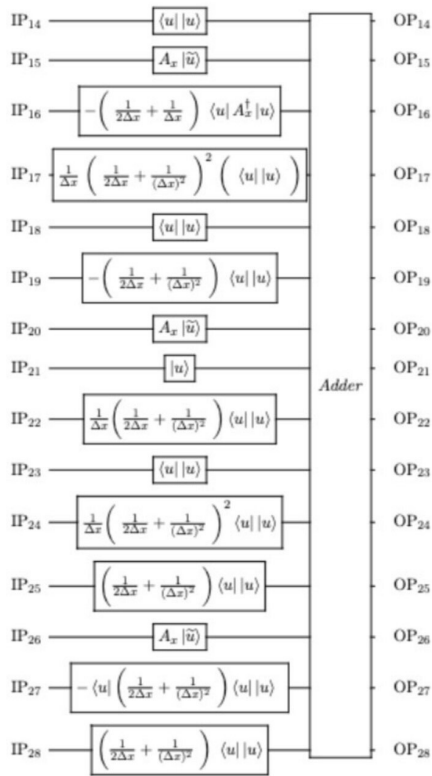


Figure 98: *First portion of the QNPU for the Hunter-Saxton equation.* Input ports labeled 14 through 28 are provided above.

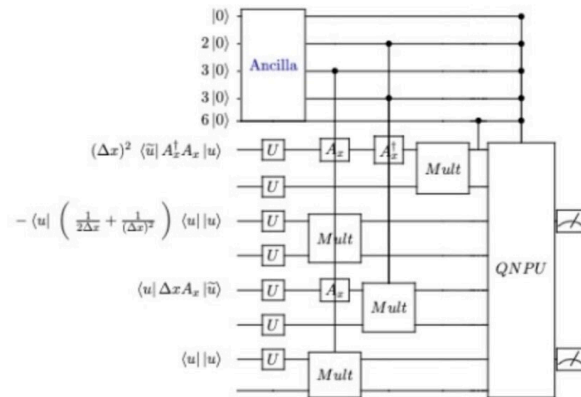


Figure 99: *Second portion of the quantum circuit for the Hunter-Saxton equation.* Quantum registers of the form indicated above are initialized.

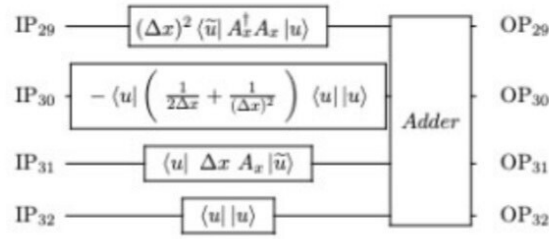


Figure 100: *Second portion of the QNPU for the Hunter-Saxton equation.* Input ports labeled 29 through 32 are provided above.

[7] Feng, W., Zhao, S-L, & Zhang, D-J. Exact solutions to lattice Boussinesq-type equations. *Journal of Nonlinear Mathematical Physics*, 19(4) (2012).

[8] Garay, R. & Zamboni-Rached, M. Exact analytical solutions of Maxwell's equations describing propagating nonparaxial electromagnetic beams. *Applied Optics*, DOI 136410/A0.53.004524 (2014).

[9] Grotto, F. & Pappalettera, U. Gaussian invariant measures and stationary solutions to 2D primitive equations arXiv: 2005.03339 (2020).

[10] Guzman, F.S. Introduction to numerical relativity through examples. *Revista Mexicana de Fisica* **53**(4) 78-93 (2007).

[11] Cresson, J. & Darses, S. Lagrangian Structure for the Stokes, Navier-Stokes and Euler Equations. arXiv: 0811.3286 (2008).

[12] Jayanthia, S. & Kavitha, T. A modified compact numerical algorithm to solve 2D Navier-Stokes equation, *Results in Applied Mathematics*, Volume 3, 2019, 100065, ISSN 2590-0374, <https://doi.org/10.1016/j.rinm.2019.100065>

[13] Liu, X-Z, & Yu, J. Symmetry Group Theorem of the Lin-Tsien Equation and Conservation Laws Relating to the Symmetry of the Equation. *Chinese Journal of Physics*, 51(6) (2013).

[14] MacCallum, Malcolm A.H. Exact solutions of Einstein's equations, *Scholarpedia* **8**(12):8585 (2013).

[15] Lubasch, M., et al. Variational quantum algorithms for nonlinear problems. *Phys Rev* **101** 010301 (2020).

[16] Nakaji, K. & Yamamoto, N. Expressibility of the alternating layered ansatz for quantum computation. arXiv: 2005.12537 (2020).

[17] Otarod, S. & Otarod, D. Analytical Solutions for Navier-Stokes Equations In Two Dimensions For Laminar Incompressible Flow. arXiv: physics/0609186v1 (2006).

[18] Theaker, K.A. and Van Gorder, R.A. Solutions to Force and Unforced Lin-Reissner-Tsien Equations for Transonic Gas Flows on Various Length Scales. *Communications in Theoretical Physics*, **67**(3): 309 (2017).

[19] Viladegut, A. and Chazot, O. Catalytic characterization in plasma wind tunnels under the influence of gaseous recombination. *Physics of Fluids* **34**, 027109 (2022).

[20] Yan, X. and Shu, C-W. Dissipative Numerical Methods for the Hunter-Saxton Equation. *Journal of Computational Mathematics*, **28**(5): 606-620 (2010).

[21] Zhu, R. & Zhu, X. Three-dimensional Navier-Stokes equations driven by space-time white noise. arXiv: 1406.0047 (2014).